E-Racer

Final Report

AE3200 Design Synthesis Exercise

25th of June, 2024

Group 26

Faculty of Aerospace Engineering

TU Delft

This page is intentionally left blank.

E-Racer

Final Report

by

Group 26

Student Name	Student Number
Olivier Buurman	5271010
Leon Dybioch	5251184
Jorge Gasch Chanfreut	5518849
Mariska Marree	5552168
Joost Meinesz	5310059
Ashton Michaud	5478693
Roeland Oosterveld	5546052
Kiki van der Sluis	5528747
Geronimo Tjon-A-Meeuw	5068738
Sava Zamfirescu	5465885

Version	Amendment	Date
2.0	Final Version	25/6/2024

Tutor:	Alexander in ‘t Veld
Coaches:	Adrian Grille Guerra, Ran Tao
External Expert:	Ricardo van der Pluijm, NLR
Course:	AE3200 Design Synthesis Exercise
Institution:	Delft University of Technology
Place:	Faculty of Aerospace Engineering, Delft

TU Delft

Nomenclature

Abbreviations

Abbreviation	Definition
A	Analysis
AC	Accept
ATC	Air Traffic Control
ATEX	Atmosphere Explosives
ATM	Air Traffic Management
AVL	Athena Vortex Lattice
BoP	Balance of Plant
CAN	Controlled Area Network
CAS	Calibrated Airspeed
CFD	Computational Fluid Dynamics
CG	Centre of Gravity
CID	Current Interrupt Device
ConOps	Concept Operations
COTS	Commerical Off The Shelf
D	Demonstration
DADC	Digital Air Data Computer
DC	Direct Current
DCI	Decompression Illness
DoF	Degree of Freedom
DSE	Design Synthesis Exercise
EFIS	Electronic Flight Display System
EoL	End-of-Life
EoM	Equation of Motion
EU	European Union
FAA	Federal Aviation Administration
FEM	Finite Element Method
HF	High Frequency
HHV	Higher Heating Value
I	Inspection
IAS	Indicated Airspeed
ISA	International Standard Atmosphere
ISSR	Ice Super Saturated Region
KCAS	Calibrated Airspeed in Knots
Li-S	Lithium Sulfur
LOF	Lift-Off
NAA	National Aeronautics Association
NASA	National Aeronautics and Space Administration
NLR	Royal Netherlands Aerospace Centre
MERRA-2	Modern-Era Retrospective analysis for Research and Applications version 2
MAC	Mean Aerodynamic Chord
MCDA	Multi-Criteria Decisions Analysis
MTOW	Maximum Take-Off Weight
MTOM	Maximum Take-Off Mass
ND	Navigation Display
NDT	Non-Destructive Testing
OEW	Operational Empty Weight
PCM	Phase Changing Material
PDU	Power Distribution Unit
PEM	Proton Exchange Membrane
PFD	Primary Flight Display
PTC	Positive Thermal Coefficient
RD	Review of Design
RL	Reduce Likelihood
RI	Reduce Impact
ROC	Rate of climb
ROD	Rate of descent
RPM	Revolutions Per Minute
SWOT	Strengths, Weaknesses, Opportunities, and Threats
T	Testing
TAS	True Airspeed
TO	Take-Off
TPR	Third Party Risk
TRL	Technology Readiness Level
US	United States of America
VHF	Very High Frequency
VFR	Visual Flight Rules
VLM	Vortex Lattice Method
VOC	Volatile Organics Compound
WSM	Weighted Sum Model

Symbols

Symbol	Definition	Unit
$A_{cross-section}$	Cross-sectional area	$[m^2]$
A_{str}	Stringer area	$[m^2]$
AR	Aspect ratio	[-]
a_p	Width of rectangular plate	$[m]$
a	Acceleration	$[m/s^2]$
$a_{centripetal}$	Centripetal Acceleration	$[m/s^2]$
ac_{aft}	Aerodynamic centre of aft wing	[-]
ac_{fw}	Aerodynamic centre of forward wing	[-]
a_{cruise}	Cruise speed of sound	$[m/s]$
B_i	Boom area	$[m^2]$
b	Span	$[m]$
b_p	Width of plate	$[m]$
b_r	Rudder Span	$[m]$
b_{rect}	Height of rectangular plate	$[m]$
b_v	Vertical stabiliser span	$[m]$
C_{aft}	Chord of aft wing	$[m]$
C_{d_0}	zero-lift drag coefficient airfoil	[-]
C_{d_y}	Coefficient of side drag of aircraft	[-]
C_D	Drag coefficient	[-]
C_{D_0}	Zero-lift drag coefficient	[-]
C_L	Lift coefficient	[-]
$C_{L_{cruise}}$	Lift coefficient during cruise	[-]
$C_{L_{landing}}$	Lift coefficient during landing	[-]
$C_{L_{TO}}$	Lift coefficient at take-Off	[-]
$C_{L_{max}}$	Maximum lift coefficient	[-]
C_{l_p}	Stability derivative	[-]
C_{l_r}	Stability derivative	[-]
C_{l_α}	Lift curve slope of airfoil	$[1/rad]$
$C_{l_{\alpha v]}}$	Slope of vertical stabiliser lift curve	$[1/rad]$
C_{l_β}	Stability derivative	[-]
$C_{l_{\delta_\alpha}}$	Control derivative	[-]
C_{m_0}	Zero-lift moment coefficient	[-]
C_{m_q}	Stability derivative	[-]
C_{m_u}	Stability derivative	[-]
C_{m_α}	Stability derivative	[-]
$C_{m_{\dot{\alpha}}}$	Stability derivative	[-]
C_{m_δ}	Elevator effectiveness	[-]
C_{n_0}	Stability derivative	[-]
C_{n_p}	Stability derivative	[-]
C_{n_r}	Stability derivative	[-]
C_{n_β}	Stability derivative	[-]
$C_{n_{\dot{\beta}}}$	Stability derivative	[-]
$C_{n_{\delta_r}}$	Control derivative	[-]
C_{X_0}	Stability derivative	[-]
C_{X_u}	Stability derivative	[-]
C_{X_α}	Stability derivative	[-]
C_{X_δ}	Control derivative	[-]
C_{Y_p}	Stability derivative	[-]
C_{Y_r}	Stability derivative	[-]
C_{Y_β}	Stability derivative	[-]
$C_{Y_{\dot{\beta}}}$	Stability derivative	[-]
$C_{Y_{\delta_r}}$	Control derivative	[-]
C_{Z_0}	Stability derivative	[-]
C_{Z_q}	Stability derivative	[-]
C_{Z_u}	Stability derivative	[-]
C_{Z_α}	Stability derivative	[-]
C_{Z_δ}	Control derivative	[-]
$C_{Z_{\dot{\alpha}}}$	Stability derivative	[-]
c	Average chord	$[m]$
c_a	Aileron chord	$[m]$
c_e	Elevator chord	$[m]$
c_f	Flap chord	$[m]$
c_{fw}	Chord of forward wing	$[m]$
c_p	Specific heat	$[kJ/(kg \cdot K)]$
c_r	Root chord	$[m]$
c_t	Tip chord	$[m]$
$c(y)$	chord function w.r.t. span	[-]
D	Drag	$[N]$
D_{ae}	Aerodynamic Drag	$[N]$
D_{aft}	Drag of aft wing	$[N]$
D_b	Asymmetric non-dimensional differential operator	[-]
d_c	X-distance between centroid and centre of gravity	$[m]$
D_c	Symmetric non-dimensional differential operator	[-]
D_{fw}	Drag of forward wing	$[N]$
D_g	Drag due to ground resistance	$[N]$
e	Oswald efficiency factor	[-]
E	E-modulus	$[Pa]$
E_a	Energy Available	$[MJ]$
E_{climb}	Energy needed for climb	$[MJ]$
E_{cruise}	Energy needed for cruise	$[MJ]$
$E_{descent}$	Energy needed for descent	$[MJ]$
E_{loiter}	Energy needed for loiter	$[MJ]$
F_w	Side force caused by wind	$[N]$
g	Gravitational Acceleration	$[m/s^2]$
$\dot{h}$	altitude gradient	$[m/s]$
$h_{approach}$	Approach height	$[m]$
h_{cruise}	Cruise height/altitude	$[m]$
h_{screen}	Screen height	$[m]$
I	Moment of inertia	$[m^4]$
K_X^2	Product of inertia	[-]
K_Y^2	Product of inertia	[-]
K_Z^2	Product of inertia	[-]
K_{XZ}^2	Product of inertia	[-]
k	Thermal conductivity	$[kW/(m \cdot K)]$
L	Characteristic length	$[m]$
L_e	Stiffener Length	$[m]$
L	Lift	$[N]$

L_{aft}	Lift of aft wing	[N]
L_{fw}	Lift of forward wing	[N]
L_{TO}	Lift at take-off	[N]
M	Moment	[Nm]
M^*	Technology factor	[-]
M_{dd}	Drag divergence Mach number	[-]
M_{eff}	Effective Mach number	[-]
M_{tip}	Mach number at propeller blade tip	[-]
M_W	Wing mass	[-]
m	Mass	[kg]
$m_{hydrogen}$	Mass of hydrogen	[kg]
$\dot{m}$	Mass flow	[kg/s]
N_a	Maximum yawing moment	[Nm]
Nu	Nusselt number	[-]
n_{TO}	Load factor for take-off	[-]
n_z	Load factor	[-]
P	Power	[W]
P_a	Power available	[W]
P_{bat}	Battery power	[W]
P_i	Shear force carried by boom i	[N]
P_{normal}	Normal force	[N]
Pr	Prandtl number	[-]
P_{req}	Power required	[W]
p	Roll rate	[$^\circ/s$]
p	Pressure	[Pa]
Re	Reynolds number	[-]
R_{TO}	take-off arc length	[m]
$R_{landing}$	Landing arc length	[m]
Re_x	Reynolds number at point along airfoil	[-]
r	Radius of the propeller	[m]
r_{fus}	Radius of the fuselage	[m]
$\dot{Q}$	Heat flow	[kW]
q	Shear flow	[N/m]
$\bar{q}$	Dynamic pressure	[N/m^2]
$\dot{q}_{cond}$	Specific heat conduction	[kW/m^2]
S	Wing surface area	[m^2]
S	Stroke length	[m]
S_s	Projected area of aircraft on the XZ plane	[m^2]
S_v	Vertical tailplane area	[m^2]
S_y	Shear force in y-direction	[N]
t	Thickness	[m]
t/c	Thickness-to-chord ratio	[-]
t_D	Skin thickness	[mm]
T	Thrust	[N]
T_p	Temperature	[$^\circ C$]
T_{in}	Inlet temperature	[$^\circ C$]
T_L	Drag one engine inoperative	[N]
$\hat{u}$	Normalised airspeed	[m/s]
V	Velocity	[m/s]
$\dot{V}$	Velocity gradient	[m/s^2]
$V_{approach}$	Velocity during approach	[m/s]
V_{cruise}	Cruise velocity	[m/s]
V_f	Landing velocity	[m/s]
V_{LOF}	Velocity at lift-off	[m/s]
V_{max}	Maximum velocity	[m/s]
V_R	Speed at rotation	[m/s]
V_{rot}	Rotational tip speed	[m/s]
V_{sink}	Sink velocity	[m/s]
V_t	Total velocity	[m/s]
$\bar{V}_v$	Vertical tailplane volume	[-]
V_w	Crosswind velocity	[m/s]
V_y	Vertical velocity	[m/s]
v	Poisson's ratio	[-]
W	Weight	[N]
W/S	Wing loading	[N/m^2]
x	Position along airfoil	[m]
$\dot{x}$	Horizontal distance gradient	[m/s]
$x_{ac_{aft}}$	X-location of aft a.c.	[m]
$x_{ac_{fw}}$	X-location of forward a.c.	[m]
x_{CG}	X-location of CG	[m]
x_{mg}	X-location of rotation point around main gear	[m]
x_{prop}	X-location of propeller	[m]
y_t	Y-distance between centre of gravity and propeller	[m]
$z_{ac_{aft}}$	Z-location of aft a.c.	[m]
z_{CG}	Z-location of CG	[m]
z_{mg}	Z-location of rotation point around main gear	[m]
z_{prop}	Z-location of propeller	[m]
α	Angle of attack	[rad]
α_r	Height-to-width ratio	[-]
β	Side slip angle	[rad]
$\delta(x)$	Boundary layer thickness	[m]
δ_a	Aileron deflection	[rad]
δ_e	Elevator deflection	[rad]
δ_r	Rudder deflection	[rad]
ΔT	Temperature difference	[$^\circ C$]
η	Efficiency	[-]
η_{bat}	Battery efficiency	[-]
η_{fc}	Fuel cell efficiency	[-]
η_{motor}	Motor efficiency	[-]
η_{mc}	Motor controller efficiency	[-]
η_{prop}	Propeller efficiency	[-]
η_v	Dynamic pressure ratio	[-]
θ	Roll rate	[rad]
$\ddot{\theta}$	angular acceleration	[deg/s^2]
λ	Taper ratio	[-]
$\Lambda_{c/2}$	Half chord sweep	[$^\circ$]
$\Lambda_{c/4}$	Quarter chord sweep	[$^\circ$]
ρ	Density	[kg/m^3]
ρ_g	Radius of gyration	[m]
μ	Dynamic viscosity	[$kg/(m \cdot s)$]
μ_b	Asymmetric non-dimensional mass	[-]
$\mu_b r$	Brake coefficient	[-]
μ_c	symmetric non-dimensional mass	[-]
μ_f	Roll friction coefficient	[-]

μ_g	Ground resistance coefficient	[-]
μ_p	Propeller efficiency	[-]
ν	Poisson ratio	[-]
ν_k	Kinematic viscosity	[m^2/s]
ϕ_p	Propeller pitch angle	[°]
φ_p	Propeller sweep angle	[°]
σ	Normal stress	[Pa]
σ_y	Yield stress	[Pa]
σ_{cc}	Crippling stress	[Pa]
σ_c	Crab angle	[rad]
τ	Shear stress	[MPa]
τ_a	Aileron effectiveness	[-]
τ_r	Rudder effectiveness	[-]
γ	Flight path angle	[°]

Executive Overview

The Pulitzer Air Race originated in the 1920s. The race was organised by the National Aeronautic Association (NAA) and sponsored by the journalist named Ralph Pulitzer. Their objective was to promote the development of high-performance aircraft and to promote general aviation. The race featured Pylon races and cross-country races where the fastest plane would be crowned the winner. The races served as a testing ground for experimental designs, particularly by the American Army and Navy, significantly propelling the development of fighter aircraft during that period. More recently, the NAA plans to use the idea of the Pulitzer Air Race of the 1920s to accelerate the development of electric and zero-emission aviation, especially high-performance, medium-range electric aviation by organising a modern version of the race: the Pulitzer Electric Aircraft Air Race. The race spans over four days and covers a distance of 1,000 nautical miles (1,852 km), from Eppley Airfield in Omaha, Nebraska, to Dare County Regional Airport in Manteo, North Carolina. The winner is determined by the fastest speed calculated from cumulative flight time, excluding ground maintenance, charging, or overnight stops.

The Royal Netherlands Aerospace Centre (NLR) has seen an opportunity in the upcoming Pulitzer race and wants to participate in developing a sustainable electric aircraft. Consequently, Delft University of Technology has been approached to deliver a proposal for a design that can participate in the Pulitzer Electric Aircraft Air Race.

Project Objectives

To this end, a mission need statement and project objective statement have been established. These are presented below. In addition, other project objectives have been set, emphasising a sustainable aircraft design, able to compete in and win the race, providing valuable experience to the team, and opening opportunities for researching and improving advanced technology.

Mission Need Statement: *"The design will win the Pulitzer Electric Aircraft Air Race."*

Project Objective Statement: *"Provide a winning design for the Pulitzer Electric Aircraft Air Race within a budget of €900,000, by 10 students in 10 weeks."*

Requirements & Constraints

Requirements were created to identify the aircraft design limitations. The requirements stem from stakeholders and potential competitors, identified in a market analysis, and are translated into technical requirements imposed on the design. Also, the main competitor that served as a source of inspiration was the Sirius Business Jet[1]. These led to the identification of driving and key requirements for this mission, presented in Table 8.

Table 8: Key and driving requirements

ID	Key Requirement Description	Stakeholder/Mission ID
ER-MIS-NAA-01.01	The aircraft shall be heavier than air.	**ER-STK-NAA-01**
ER-MIS-NAA-01.02	The aircraft shall be zero-emission.	**ER-STK-NAA-01**
ER-SYS-NAA-01.02.01	The aircraft shall use an electrical propulsion system.	**ER-MIS-NAA-01.02**
ER-MIS-AIRP-01.01	The aircraft shall be able to use the County Regional Airport, Manteo, North Carolina, US.	**ER-STK-AIRP-01**
ER-MIS-AIRP-01.02	The aircraft shall be able to use the Eppley Airfield, Omaha, Nebraska, US.	**ER-STK-AIRP-01**
ER-MIS-NLR-01.02	The aircraft shall be able to travel 1,000 nautical miles within four days.	**ER-STK-NLR-01**
ID	**Driving Requirement Description**	**Stakeholder/Mission ID**
ER-MIS-NAA-01.05	The aircraft shall be able to obtain a special airworthiness certificate in the experimental category with the purpose of air racing.	**ER-STK-NAA-01**
ER-MIS-NLR-01.01	The aircraft shall be able to win the Pulitzer Electric Aircraft Race.	**ER-STK-NLR-01**
ER-MIS-NLR-03.01	The aircraft shall be producible within a budget of €900,000	**ER-STK-NLR-03**
ER-NLR-TECH-CRU-1	The aircraft shall travel at a minimum average speed of 145 [m/s].	**ER-MIS-NLR-01.01**
ER-NAA-TECH-CRU-2	The aircraft shall have a minimum range of 200 [km].	**ER-MIS-NLR-01.01**

[1] `https://siriusjet.com/sirius-jet/sirius-business-jet/` [Accessed on 06-05-2024]

Aerodynamics, Stability, and Control

Using a vortex lattice model, the aircraft was modelled and optimised. From this, a wing planform was obtained, which minimised the drag and was both statically and dynamically stable. Subsequently, the control surfaces of the aircraft could be determined. The results of the control surfaces and the wing design can be seen in Figure 1.

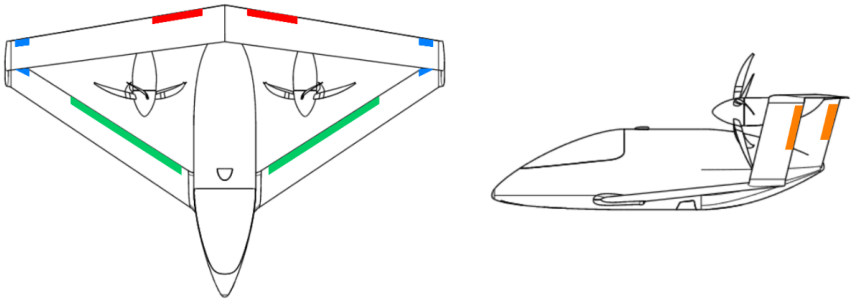

Figure 1: Control surfaces on aircraft. Blue surfaces are ailerons, red are elevators, green are flaps, and orange are rudders

Power and Propulsion

The propellers were sized using the Vortex Lattice Method (VLM). These can be seen in Figure 2. A motor was then sized, which required a continuous power of almost 80 [kW]. A battery system was also designed, containing a high-voltage and low-voltage battery pack. This has been done with an emphasis on safety. This resulted in a high-voltage battery with an energy capacity close to 15 [kWh], while the low-voltage battery has a capacity of 1.1 [kWh]. Both of these batteries are lithium-sulfur batteries. Next, a fuel cell was sized, providing an output power of 230 [kW], and to operate it accordingly, an air compressor was selected. A fuel tank, able to carry 30 [kg] of liquid hydrogen was necessary and was also designed, leading to a tank mass of 70 [kg]. Finally, a cooling system was put into place, to keep all electronics and the fuel cell on board at a safe operating temperature. A wing heat exchanger was the result of this process.

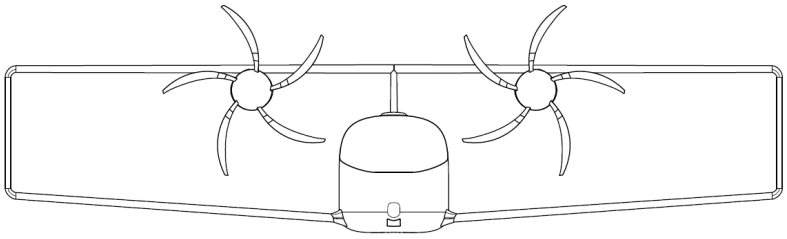

Figure 2: Front view of the aircraft showing the two counter-rotating propellers

Structures & Materials

The fuselage structure was designed based on the required contents of the aircraft and the loads it would have to withstand; these loads were identified after constructing a V-N diagram. From this, it was found that buckling and pressurisation were the 2 most critical load cases. Next, the material for the aircraft was determined using a trade-off. The criteria for this trade-off were weight, cost, and carbon footprint. This resulted in the selection of aluminium 7075 T6. A retractable landing gear system was then designed with the conventional layout of one nose landing gear and two main landing gears. The wingbox was then designed based on the loads experienced by the wing, with a second material trade-off being performed based on the same criteria. The wingbox material selected was also aluminium 7075 T6. Lastly, it was found that the total fuselage structure would have a mass of 120 [kg], while the wing system has a total mass of 186 [kg].

Flight Performance

Since the aircraft is designed to participate in an air race, its performance is crucial. To estimate the performance, two simulation models have been developed. First, an energy-based point analysis model was created to estimate optimal flight conditions. Next, a flight path simulation was made, which estimates the performance over the entire flight profile based on the Equations of Motion (EoM). This model was used as the main tool to estimate the final

performance of the aircraft. Lastly, a weather model was made to estimate the effect of weather conditions on the flight performance of the design. The final performance parameters are summarised in the Table 9.

Table 9: Output parameters of flight path model

Output parameter	Value	Unit	Description
Total possible range	2,291	km	This range represents the total potential distance the aircraft can fly with the implemented fly strategy
Average velocity	149.38	m/s	The average velocity with which aircraft completes the race.
Race time	206.41	min	The race time represents the amount of time the aircraft takes to complete 1,850 [km]
Cruise altitude	12.50	km	The altitude the aircraft cruises at
Take-off distance (dry)	1,544	m	The required length of the take-off runway in dry conditions
Take-off distance (wet)	1,689	m	The required length of the take-off runway in wet conditions
Landing distance (dry)	763	m	The required length of the landing runway in dry conditions
Landing distance (wet)	1,364	m	The required length of the landing runway in wet conditions
Cruise velocity	163.11	m/s	The velocity during cruise

Final Design

A render of the final design can be seen in Figure 3. Additionally, final geometric parameters for the aircraft were determined and are shown in Table 10 and Table 11. Additionally, the mass of the aircraft was found to be 1,162.51 [kg], with the propulsion making up the largest part of the weight.

Table 10: Final geometric parameters of the wings

Front Wing		Rear Wing	
Surface Area	4.29 [m^2]	Surface Area	4.29 [m^2]
Aspect Ratio	12.96	Aspect Ratio	12.96
Wingspan	7.46 [m]	Wingspan	7.46 [m]
MAC	0.58 [m]	MAC	0.58 [m]
Quarter Chord Sweep	33.50 [°]	Quarter Chord Sweep	-8.10 [°]
Taper Ratio	0.80	Taper Ratio	0.80
Dihedral	4.00 [°]	Dihedral	0.00 [°]
Incidence	2.30 [°]	Incidence	0.00 [°]
Airfoil	OAF128	Airfoil	OAF128

Table 11: Final geometric parameters of the fuselage and propeller

Fuselage		Propeller	
Length	4.7 [m]	No. Propellers	2
Height	1.2 [m]	No. Blades	5
Width	1.1 [m]	Diameter	1.8 [m]

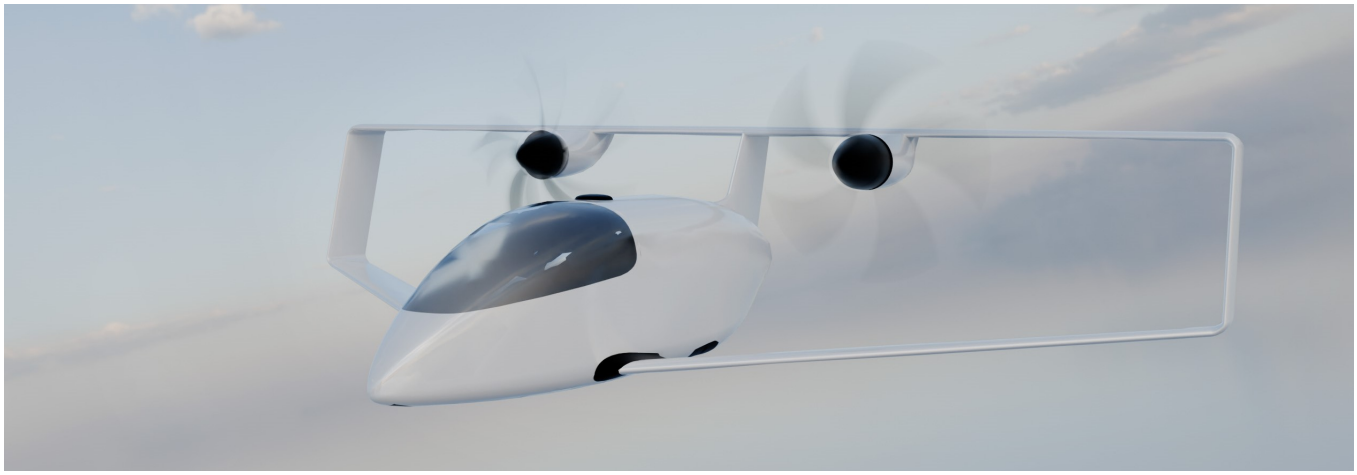

Figure 3: Final Design Render

Operations & Logistics

The aircraft will be disassembled and transported by truck to Eppley Airfield in Omaha. Here, the aircraft will be re-assembled and pre-flight operations will be performed to be ready for the race. The aircraft will then complete the race distance and post-flight operations will then take place. The personnel required for the smooth running of this mission can be divided into four professions: aerospace engineers, aircraft mechanics, electrical engineers, and a pilot. Three different teams can be distinguished: the transport team; the monitoring team, consisting of two aerospace engineers who will plan the best race strategy and monitor the aircraft's performance during the race; and a team of two mechanics and an electrical engineer who will assemble, repair, maintain, and disassemble the aircraft.

Sustainability

Three pillars of sustainability were investigated: environmental, social, and economic. These were all considered important for this report. Firstly, the environmental sustainability of the hydrogen system, batteries, structures, and end-of-life was investigated. From this, it was found that environmental sustainability is mainly dependent on the power grid used to both charge the battery and produce the hydrogen. Further, methods can be used to diminish the negative impact of the aircraft on the environment such as recycling, in particular during the end of life. Secondly, the social sustainability of the aircraft was investigated. The main negative impacts come from noise and pollution during manufacturing and the main positive impact comes from the advancement of environmentally friendly technology. Lastly, economic sustainability was determined. This led to the conclusion that the recyclability of the aircraft is crucial for resale value. Furthermore, partnerships with other companies have been considered and are determined to be crucial for sustainability in this aspect. The partnerships would reduce financial strain on the budget.

Cost Breakdown

After the design, the cost of each component was calculated, as well as costs for all manufacturing, testing, and all other labour that would be required. The components alone, add up to €444,455. All costs combined for design, components, manufacturing, testing, certification, and operations lead to a total cost of €897,709, Including a margin of %10 that is added as a contingency. The budget provided by the client, the NLR, was increased to €900,000, which means that the project is within the budget. Nevertheless, various methods to reduce costs were explored, which could reduce the total cost to €773,983, or €663,983 when reducing the fuel cell power.

Table of Contents

1. Introduction

The reduction of carbon emissions is a central theme in the transport industry nowadays; this also holds for the aviation industry. Currently, the aviation industry is responsible for 2.5% of the world's carbon emissions and this is predicted to rise if no changes are made[1] [1]. In recent years, electric propulsion has been considered a viable replacement for combustion engines. The drawback of electric propulsion is that the relevant technologies such as batteries and electric motors are not sufficiently mature. Therefore, electric propulsion performance is not yet at the same level as regular combustion engine performance [2]. Furthermore, one of the main drawbacks of zero-emission aviation is the limited range of these aircraft due to limited energy storage capabilities. Major improvements in this area are required before this technology can be used to replace existing combustion engine aircraft. To accelerate the development of high-performance electric aircraft, the National Aviation Authority (NAA) has planned to bring back the Pulitzer Air Race for zero-emission electric-powered aircraft.

The Pulitzer Air Race is an event that originated in the 1920s. The race was organised to promote the development of high-performance aircraft and was mostly used by the American Army to experiment with new designs. This race greatly influenced fighter plane designs[2] [3]. Similarly, the NAA is using the idea of the 1920s Pulitzer Air Race to help accelerate the development of electric aircraft in 2024, by organising a modern version of it: the Pulitzer Electric Aircraft Air Race.

This project, the E-Racer, aims to develop a design that can participate in and win the Pulitzer Electric Aircraft Air Race. It has been brought forth by the Netherlands Aerospace Centre (NLR) to promote the development of electric aircraft. Furthermore, the team established a project objective statement as follows: "Provide a winning design for the Pulitzer Electric Aircraft Air Race within a budget of €900,000, by 10 students in 10 weeks". During the analysis of different concepts, it was found that a hydrogen Prandtl plane would be the most optimal. Therefore, this report aims to present the final design of this aircraft. Furthermore, the design process will also be highlighted, showing the decisions and steps taken to arrive at the final design. Finally, the effects of the final design on several aspects such as manufacturing, operations, sustainability, and risk will be investigated and presented.

Firstly, the project objectives are outlined in Chapter 2, which provide a foundation for the whole project. Then, the market analysis is presented in Chapter 3, which entails the investigation of stakeholders and potential competitors. Subsequently, the functions of the product are analysed and shown in Chapter 4. This provides a starting point for the requirement generation. The final requirements and constraints for the aircraft are presented in Chapter 5. To select a winner configuration from five different possible design concepts, their strength and their weaknesses are assessed by conducting a trade-off. This process is summarised in Chapter 6.

The chosen concept was worked out further; this resulted in a preliminary design, presented in Chapter 7. A detailed design of the aircraft, including the design of various subsystems, is then explained. This design process and results for the different subsystems are also presented. First, the aerodynamics of the aircraft will be discussed in Chapter 8, followed by the stability and control in Chapter 9. Next, the propulsion system will be discussed in Chapter 10. Lastly, the design of the structural subsystems is presented in Chapter 11. Once all subsystem details are explained, the performance of the design will be analysed using a numerical simulation. This will result in an optimal race strategy, which will be explained in Chapter 12. Once the aircraft systems and safety systems are defined in Chapter 13 and Chapter 14 respectively, the final design parameters are then summarised in Chapter 15. The design is eventually verified and validated. This process is outlined in Chapter 16.

The design is then assessed on several different aspects. Firstly, the manufacturing and maintenance procedures for the aircraft, are presented in Chapter 17. Secondly, the operations and logistics will be explained in Chapter 18. Furthermore, the sustainability of the aircraft is analysed in Chapter 19. The technical risks of the product have been assessed and these are presented in Chapter 20. Finally, the future steps and the resource allocation for these steps will be outlined in Chapter 21. After this, the cost breakdown is presented in Chapter 22.

[1] `https://ourworldindata.org/global-aviation-emissions` [Accessed on 02-05-2024]

[2] `https://www.usni.org/magazines/proceedings/1959/september/pulitzer-races-1920-1925` [Accessed on 02-05-2024]

2. Project Objectives

This chapter is intended to help the reader understand the purpose of designing and building the aircraft. It gives a brief overview of the mission and project objectives.

This project aims to deliver an electric aircraft to win the Pulitzer Electric Aircraft Race, a 1,000 nautical mile race, between Eppley Airfield in Omaha and Dare County Regional Airport in Manteo. The mission need statement is presented below, followed by the project objective statement derived from it.

Mission Need Statement: *"The design will win the Pulitzer Electric Aircraft Air Race."*

Project Objective Statement: *"Provide a winning design for the Pulitzer Electric Aircraft Air Race within a budget of €900,000, by 10 students in 10 weeks."*

Alongside winning the Pulitzer Electric Aircraft Race within the given budget, there are other secondary objectives for this project. First, four relevant topics are discussed, and then, the project objectives are identified.

1. Sustainability

Sustainability is an important subject in all engineering disciplines in today's world. As future engineers, the team wants to contribute to advancing environmental sustainability in the aviation industry. Therefore, the project includes sustainability development strategies in the design process on environmental, social, and economic sustainability.

2. Technological Improvement

Expanding on the sustainability note, an important way to increase sustainability is to strive for technological advancements, especially in zero-emission aviation. Promoting that development is the main reason for organising the Pulitzer Electric Aircraft Race. Hence, the project evolves around technological improvement to a certain extent. In order to ensure this, near-future technology is used in the design of the propulsion system. 'Advancing technology' refers to all systems that support a zero-emission propulsion system.

3. Performance

In addition, the product is intended to compete in a race with the goal of winning. The objective of the race is to cover 1,000 nautical miles with the lowest air time possible. This means a high average speed, high climb and descent rate and low take-off and landing time.

4. Experience

Beyond the design objectives, this project aims to provide the team with valuable experience in managing a larger project, promoting the development of team skills, increasing technical expertise, and gaining organisational insights. Based on these considerations, the project objectives are defined and listed below.

Objectives

- Provide an aircraft design that can compete in the Pulitzer Electric Aircraft Race.
- Include sustainability strategies in the design for all phases of the product life.
- Provide a zero-emissions aircraft design.
- Include 'advancing technology' in the design of the aircraft.
- Provide a design that fits an optimal performance envelope for a given competitive race strategy.
- Acquire knowledge and gain experience as a team.

3. Market Analysis

Before any design can be realised, it is important to know what is expected of the system. These relevant expectations and needs are obtained from the stakeholders. It is also important to know what the current position is in the relevant market. This, together with a stakeholder analysis gives an extensive overview of the market and its needs. This chapter presents the market analysis and elaborates upon the used method. First, the stakeholders are discussed in Section 3.1. Following the stakeholder discussion, Section 3.2 presents the analysis of the current market position.

3.1. Stakeholders

A stakeholder is an individual or organisation that influences or is influenced by the project. Their interests may be positively or negatively affected by the execution or successful completion of the mission at hand. All stakeholders must be identified from the very beginning of the project as the need to meet their expectations and requirements has a major impact on the design of the aircraft. The identified stakeholders and their influence are presented in Table 3.1.

Table 3.1: Stakeholder Analysis

Nr.	Stakeholder	Description	Influence	Interest	Key/non-key
1	TU Delft	Includes programme and course coordinators as well as technical assistants, but especially the tutor, coaches and the external expert who came up with the project idea and created a team of students to tackle this challenge. They provide guidance and have an overview of the project's progress in order to deliver a successful final detailed design of an aircraft.	Low	High	Key
2	Royal Netherlands Aerospace Centre (NLR)	This organisation is the project client and states important requirements that have to be met. They took the first step in deciding to participate in the Pulitzer Electric Aircraft Race. This entity provides the funds and possesses the resources to turn the final aircraft design into a reality.	High	High	Key
3	National Aeronautic Association (NAA)	Dedicated to the promotion of the art, sport and science of aviation in the United States. They organise the competition and dictate the rules, procedures, and regulations of the race.	High	Low	Non-key
4	Federal Aviation Administration (FAA)	Oversees civil aviation, United States commercial space transportation, air traffic control, navigation systems, and aviation safety programs, ensuring a safe National Airspace System. They are in charge of certifying the aircraft before it can fly the race in the U.S.	High	Low	Non-key
5	Airports in between and including Omaha and Kitty Hawk	They will be affected by the race and will most likely have to change their commercial flight operations to accommodate this additional flow of aircraft over their airspace and on their ground operations.	High	Low	Non-key
6	Custom part manufacturers	This stakeholder is influenced by this project because their business will receive financial compensation after delivering the requested parts. These custom parts will have to be accurately produced, otherwise, they can negatively affect the performance of the aircraft.	High	Low	Non-key
7	Commercial off the shelf (COTS) part suppliers	This stakeholder is affected by the project because the company is compensated when the requested components are delivered. The project could be compromised by the delivery of these parts if they are defective or delayed.	Low	Low	Non-key
8	Pilot	This individual will risk their life to test and fly the aircraft during the race. Their skill set and flying ability will affect the result of the race.	Low	High	Key

9	The project group	This team composed of 10 people will participate in the design process of the aircraft. Their engineering skills will be put to the test as they design a winning aircraft.	High	High	Key
10	Society	Society as a whole will be affected by the development of sustainable technologies for the purpose of the race as well as the urban populations in between and including Omaha and Kitty Hawk, who will experience the race overhead.	Low	Low	Non-key

The stakeholders that have been identified can be categorised into four categories based on their interests and influence on the project outcome. These are described below:

1. Keep satisfied: This type of stakeholder has a high interest in the project but their influence is rather limited.
2. Manage closely: This group represents the stakeholders with the highest interest and influence on the project.
3. Monitor: This last category includes the stakeholders with a small influence and interest in the project.
4. Keep informed: This group includes the stakeholders with a non-negligible influence but their interest in the project is small.

These stakeholders can now be placed on a stakeholder map, also known as an interest-influence graph. This is shown in Figure 3.1.

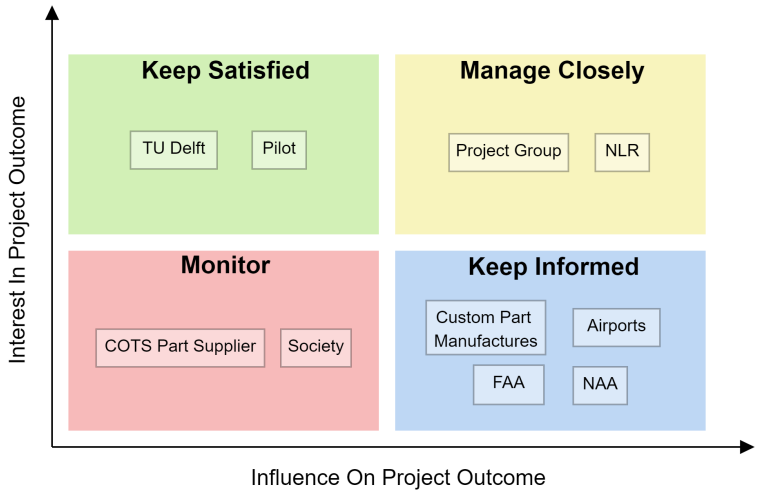

Figure 3.1: Stakeholder map of the project

The stakeholders can be classified as key or non-key by looking at the stakeholder map. This is done to identify the most important stakeholders versus the stakeholders that only have a passive effect on the project. In Figure 3.1, the key stakeholders are shown in the top two categories, ”keep satisfied” and ”manage closely”, while the other two categories indicate the non-key stakeholders.

The pilot is considered to have a high interest in the project as they will be flying the aircraft. However, if the pilot’s influence during the design process itself is taken into account, it will not be as high as that of other stakeholders placed in the yellow box. So the pilot’s influence is considered to be low. Additionally, TU Delft is considered to be a key stakeholder because this institution accommodates the project team throughout the design process. Their influence on the project is lower but non-negligible compared to the ”manage closely” category.

The stakeholders that reside in the bottom two categories of Figure 3.1 are considered non-key stakeholders. These stakeholders have low interest in the project because the E-Racer design does not have a direct impact on them. Furthermore, the ”keep informed” category deserves some additional attention. Their influence on the project is still significant since these stakeholders have regulations the system must adhere to. These regulations are necessary

to comply with for the E-Racer to be operable. However, the services/regulations provided by the four stakeholders in this category are not directly targeted at this project in particular but are aimed at the market in general.

3.2. Position in Market

By analysing the market position of this design, specific requirements can be identified at a later stage. This section identifies the market segments and competitors and conducts a Strengths, Weaknesses, Opportunities, and Threats (SWOT) analysis. It must be noted that the E-Racer design will be in a novel branch within the aviation industry. For this reason, it has proven difficult to give an overview of the direct market related to the design. To still be able to perform an informative analysis regarding the market, closely related industries have been considered as well. Furthermore, the goal of this market analysis is not to analyse the commercial opportunities in the market; it is rather an analysis of the currently available technologies that are related to zero-emission aviation and the performance of current zero-emission aircraft.

3.2.1. Market Segments & Competitors

Electric aircraft designed for the sole purpose of racing other aircraft is a very niche market. Before identifying the market segments and competitors, it is worth defining what the market is for the context of this mission. Since this project is about the participation of an aircraft in a competition that still has to be organised for the first time, there is no mature market involved. The mission is to win the race, so the competitive environment itself can be seen as the market in this analysis. The following market segments and corresponding potential competitors have been recognised:

- **Electric Aircraft Racing Segment:** Design and racing teams specialising in electric aircraft competitions, such as Nordic Air Racing Team or Team Bandit Racing. This market segment is the only direct competition to the E-Racer because it is the common goal in this market segment to participate in and win electric aircraft races.
- **General Electric Aircraft Segment:** Organisations that utilise their resources for the development of electric aircraft technologies applied to various purposes such as transportation, recreation, and surveillance are also considered competitors. The reason for this is that these companies possess technologies and expertise that can be used to create an aircraft that can compete in the Pulitzer Electric Aircraft Air Race. Some examples of these include companies like Airbus or Boeing.
- **Renewable Energy and Sustainability Segment:** Companies specialising in renewable energy solutions and sustainability technologies, like Tesla or ZeroAvia. These companies have been identified as competitors because of their expertise in renewable energy, which is needed for zero-emission aviation. While Tesla is not necessarily developing electric aircraft, they do develop electric vehicles, which means that Tesla could be a potential competitor in the development of new batteries. Additionally, Tesla or similar companies could also start the development of electric aircraft. A partnership with one of these companies can result in the development of a design that can compete in the Pulitzer Electric Aircraft Air Race.

It must be noted that the participants have not been made public. Therefore the market analysis looked at aircraft that fit the race description and rules as competitors.

3.2.2. Current or Near Future Electrically Powered Aircraft

In Section 3.2.1, related market segments were discussed. In this section, some of the current or near future electrically powered aircraft will be discussed. However, the term ”near future” must be discussed first. For this project, the use of technology in the design must be at a level of technical maturity such that the design can be produced between 2025 and 2030 [4]. Therefore, when discussing current or near future electrically powered aircraft, aircraft that have already flown or will fly before 2030 are considered. Below, some of these aircraft are listed.

- **Pipistrel Velis Electro:** It uses batteries of 22 [kWh] total and has a cruise speed of 90 [kts] calibrated airspeed (CAS) at 35 [kW]. At this speed, it has an endurance of 50 [min] and consequently a range of 139 [km]. Its maximum take-off weight (MTOW) is 600 [km] and a max power of 57.6 [kW]. It is also currently the only certified electric aircraft[1].
- **Flight Design F2e:** It also uses batteries and has a cruise speed of 85 calibrated airspeed in knots (KCAS) at 30 [kW]. At this speed, it has a range of 100 [min] and a range of 370 [km]. It has an MTOM of 1,000 [kg] and a max power of about 94.3 [kW]. Finally, it is currently in the process of certification and building of a prototype[2].

[1] `https://www.pipistrel-aircraft.com/products/velis-electro/` [Accessed on 04-05-2024]
[2] `https://flightdesign.com/flightdesignf2e` [Accessed on 04-05-2024]

- **H2Fly Hy4:** It uses liquid hydrogen, but no cruise speed or power specifications could be found. It is stated that it has a range of 1,500 [km]. It is already flying but no information on possible certification could be found[3].
- **Aerodelft Phoenix:** It will also use liquid hydrogen, have an endurance of 2 [hrs], and a range of 400 [km]. Its max fuel cell power will be 125 [kW] and it will be able to carry 6 [kg] of liquid hydrogen. The first flight is planned for 2026[4].
- **Sirius Business Jet:** This is an electric-powered VTOL aircraft. It will use liquid hydrogen, and have a cruise speed of 280 [kts] and a range of 1,850 [km]. It will have 28 electric fans with 1 [kN] peak thrust each. It is set to fly for the first time in 2025 and expected to be certified by the end of 2027[5].
- **Beta Technologies CX300:** It uses batteries and has a range of 621 [km]. The MTOM is 2,926 [kg] and is planned to be certified by 2025[6].

3.2.3. Mission SWOT Analysis

Since it is not known what competitors will participate in the competition, it is also difficult to predict what kind of designs might appear in the race and what their performance will be. However, a general SWOT analysis of the full project in the context of the mission and its outcome can still be performed. The SWOT analysis is presented in Table 3.2 and it describes the aspects of all the elements of the mission and the project.

Table 3.2: Mission SWOT analysis

	Helpful	**Harmful**
Internal	• Increased safety due to backup system implementation • Team cohesion • Use of university facilities • Operational independence due to lack of corporate governance	• Limited budget • Limited development time • Lack of expertise • Lack of experience • Limited workforce
External	• Advancing technology • New experimental data • Partnership potential	• Strong competitors • Technology immaturity • Regulation changes

3.2.4. Result of Market Analysis

The market research carried out shows that there are almost no certified, fully operational electric aircraft available today; the Pipistrel Velis Electro serves as an example. However, the performance of this aircraft has been deemed too low to be considered a competitor in the Pulitzer electric aircraft race.

Nevertheless, the Sirius business jet has been identified as the primary source of inspiration as the main competitor for this project. The jet can participate in the Pulitzer race without the need to change anything in its design. The performance levels of these aircraft are thereby used as a study case and can be translated to requirements on the performance of the E-Racer itself. The following requirement has been identified from the market analysis: the E-racer shall have an average cruise speed of at least 145 m/s. This is based on the specifications of the Sirius Business jet.

[3] https://www.h2fly.de/2023/09/07/h2fly-and-partners-complete-worlds-first-piloted-flight-of-liquid-hydrogen-powered-electric-a [Accessed on 04-05-2024]

[4] https://aerodelft.nl/project-phoenix/ [Accessed on 04-05-2024]

[5] https://siriusjet.com/sirius-jet/sirius-business-jet/ [Accessed on 06-05-2024]

[6] https://aviationweek.com/aerospace/advanced-air-mobility/beta-technologies-cx300-0 [Accessed on 06-05-2024]

4. Functional Analysis

This chapter aims to present the functional analysis performed to get an overview of the system's functions. In Section 4.1, the interconnections among various mission elements are elaborated upon. Section 4.2 presents the Functional Flow Diagram, describing the order and interdependencies of functions within the system, and the Functional Breakdown Structure of the required functions of the mission.

4.1. Mission Architecture

Before the functions of the product can be defined it is important to investigate the architecture of the mission. This defines the elements that make up the mission. Furthermore, the mission concept also needs to be investigated as this defines the relations between elements and how they will satisfy customer needs.

In the context of this project, the mission is to win the Pulitzer Electric Aircraft Air Race. The subject of this mission is the race itself as, during the mission, data on the performance and outcome of the race will be gathered. The main segments of the mission architecture are the ground, air, and strategy segments. Within these segments, different elements are identified, which are shown in the white boxes. Within a segment, all elements relate to each other. All segments and elements are shown in Figure 4.1. In the ground segment, there are the authorities such as FAA and NAA, the airports and the communication channels, which are the ground team and air traffic management (ATM). The pilot is in the air segment and talks to ATM. Additionally, the aircraft platform and the aircraft instruments are in the air segment. In the team segment, there is the recharging and refuelling, which is done at the airports. The strategy team talks to the ground team, to determine the best strategy if conditions change during the race. They also talk to the pilot to get their opinion and relate the strategy.

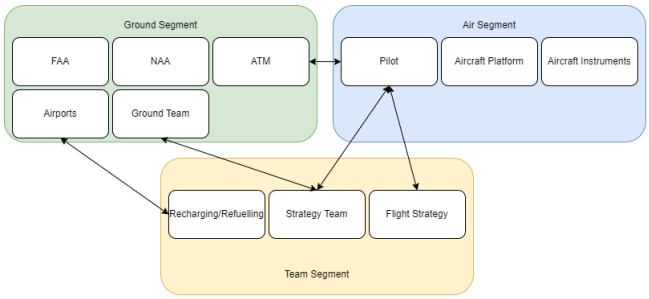

Figure 4.1: E-Racer Mission Architecture

4.2. Functional Flow Diagram & Functional Breakdown Structure

In order to identify the operational sequence of the system's functions, a Functional Flow Diagram (FFD) is developed. In the FFD, functions are broken down into three levels. On top, in the dark grey section, an overview of the first-level functions of the system is presented, where the first function is to produce the system, and the second function is to test and certify. The operation of the system follows afterwards. Performing maintenance is between operations. The last function is to follow the end-of-life procedure. These top-level functions are further broken down and shown in the lighter grey sections. Within the third-level functions, presented in orange boxes, hardware allocation is specified where possible. This allocation is particularly assigned to functions directly associated with a specific system component. For instance, "Start Electrical System" is attributed to the electrical system. This alignment helps to clarify the responsibilities of technical departments. Parallel functions are shown in combination with an AND or OR statement, indicating whether both conditions must be met or if either suffices. Throughout the flow diagram, some states/choices are shown in diamond-shaped boxes, denoting states or choices that may influence subsequent functions. Also, only functions that are either directly related or performed by the product are included in the FFD. That is the reason why the "Operate the System" function is the most detailed, as this is where the aircraft carries out the most tasks, as opposed to, for example, the design part, where the aircraft itself does not execute as many functions.

The Functional Breakdown Structure (FBS) is a breakdown of all functions that the system has to perform to fulfil the mission. The FBS shows the same functions as the FFD in a simplified way and is broken down into the same three levels. The main objective is to win the Pulitzer Race which is shown in purple. The top-level functions are shown in the green boxes. The Functional Breakdown Structure does not only show functions related to operating the aircraft but also functions related to production, certification, maintenance, and end-of-life. Second- and third-level requirements are given in the blue and orange boxes, respectively. Additionally, indices are assigned to the functions, which are consistent with the Functional Flow Diagram.

Functional Flow Diagram

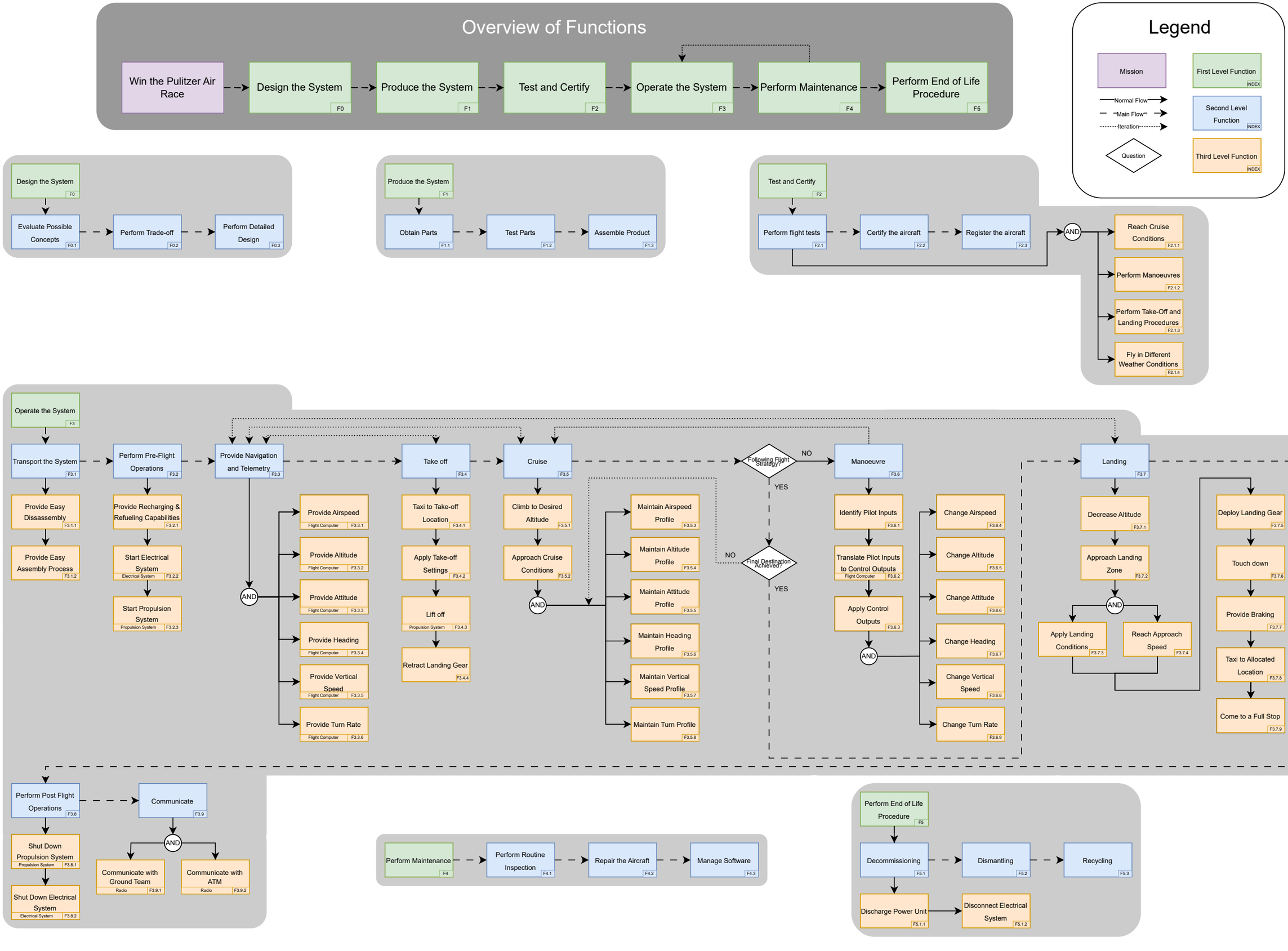

Functional Breakdown Structure

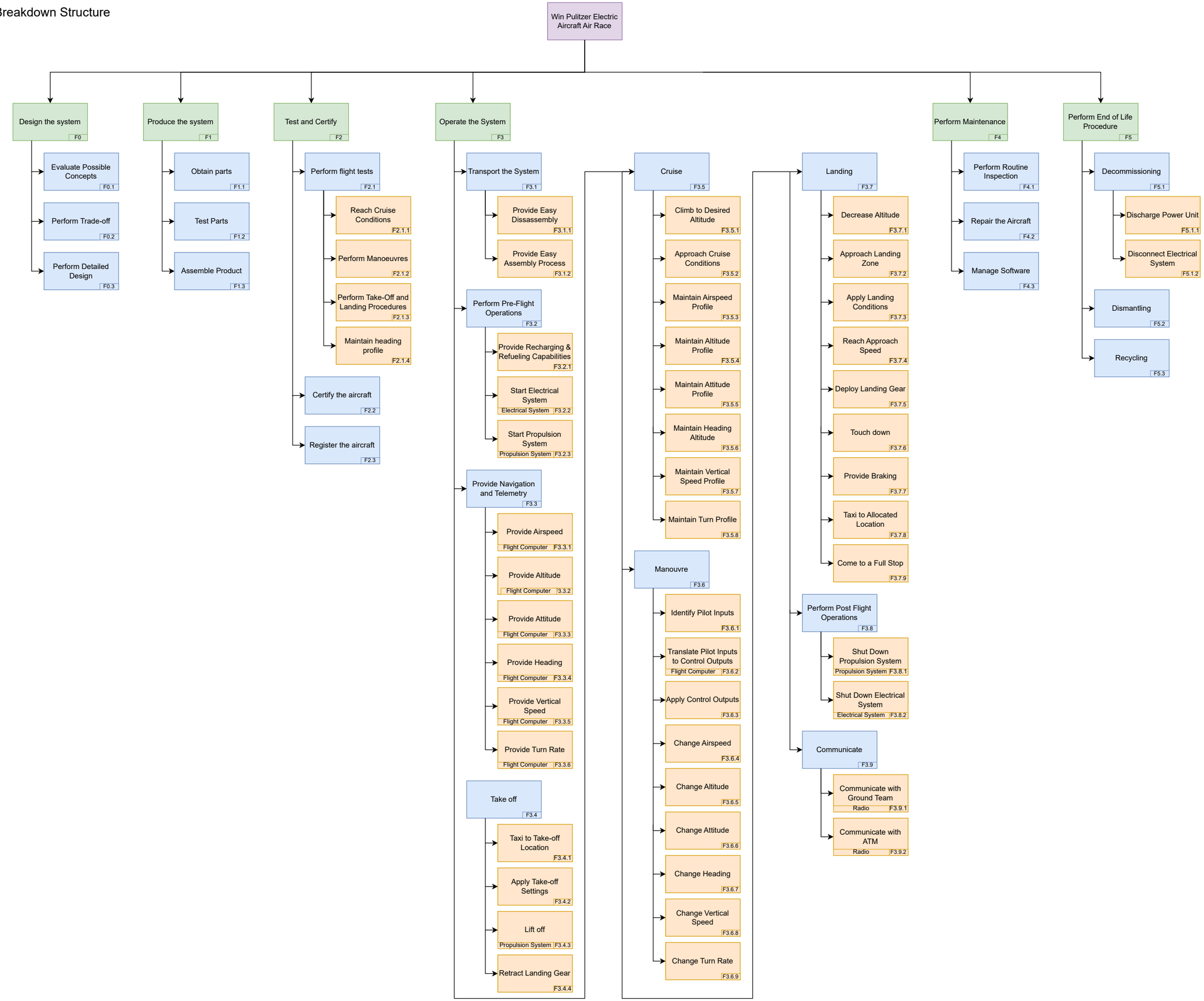

5. Requirements & Constraints

Every design must adhere to imposed requirements and will be limited by certain constraints. There are different sources for the requirements and constraints. In this chapter, these requirements and constraints are analysed and discussed. In Section 5.1 the different types of constraints on the design process are discussed. While Section 5.2 discusses the stakeholders as well as their requirements which will be translated into the mission requirements.

5.1. Constraints

Establishing constraints is an important step in keeping track of the project, both financially and in terms of time. To this end, both financial and labour budgets are determined and time constraints are established.

5.1.1. Financial Budget

In order to determine how the budget is split, it is important to decide where the budget will go between the beginning of the project and the final product. Initially, the budget is split into two parts. Firstly, a labour budget is determined. This budget will be used during the design phase of the project and will be discussed in Section 5.1.2. Secondly, there is a production budget. This includes the price of the components including commercial-off-the-shelf (COTS) and custom parts, delivery of parts, and assembly. For this project, the production budget is given as €900,000, which is the entirety of the financial budget. No financial engineering budget is allocated to this project.

5.1.2. Engineering Budget

The engineering budget is used to give an overview of how the human resources within the organisation are allocated and the costs of these resources. This budget takes into account the total available working hours during the whole project. The project spans over 10 weeks, and the project team will work 5 days a week. Each working day consists of 8 working hours. During the project, a team of 10 students are working on the design. After excluding 240 hours (3 days) due to holidays, this leads to a total of 3,760 available working hours for the entire project.

5.1.3. Time Constraints

In order to have a detailed overview of the time constraints, they have been divided into two groups: the ones of the design itself, which include the deadlines set by the DSE Organising Committee, and the time constraints of all the processes that follow after the completion of the design in order to have a certified aircraft that can compete in the Pulitzer Race.

The deadlines set by the DSE Organising Committee constrained the design as these timeframes limited the amount of time that could be spent on particular phases of the design process, such as the preliminary design of the concepts, the trade-off phase, and the detailed design itself. This directly impacted the level of detail that could be achieved in each of the phases. Secondly, to prepare the aircraft for the competition, activities such as production, certification and logistics are time constraints that need to be met to produce a fully finished product. These timeframes depend on the date of the Pulitzer Race.

5.2. Requirements

In order to create a design that will satisfy every party involved in the project, it is important to identify requirements. This helps remove ambiguity around the project, ensuring everyone knows what is being designed and that the design aligns with what each stakeholder desires. In order to differentiate between requirements, they are assigned IDs. All IDs will start with ER, which indicates it is part of the E-Racer project. This will be followed by STK (Stakeholder), MIS (mission), or SYS (system) to indicate the level of the requirement. An abbreviation for the stakeholder is then given and finally, a series of numbers is used for traceability, with each lower-level requirement inheriting the numbers from the requirement it is derived from.

5.2.1. Stakeholder Requirements

The first step towards determining all requirements is identifying stakeholder requirements. For every stakeholder determined in Section 3.1, requirements based on their desired outcome of the design have been determined. They are listed below.

Stakeholder 1: Technical University Delft (TUD)

- **ER-STK-TUD-01**: A design of the product concurrent with the other stakeholder requirements shall be provided

by June 19th 2024.

- **ER-STK-NAA-02**: The design of the aircraft shall take sustainability in mind.

Stakeholder 2: Royal Netherlands Aerospace Centre (NLR)

- **ER-STK-NLR-01**: The aircraft, when produced, shall be able to win the Pulitzer Electric Aircraft Air Race.
- **ER-STK-NLR-02**: The technology involved with the aircraft shall be available now or in the near future (2025-2030).
- **ER-STK-NLR-03**: The aircraft shall be produced with a provided budget of €900,000.
- **ER-STK-NLR-03**: The aircraft shall be certifiable.
- **ER-STK-NLR-05**: Systems and components shall be COTS as much as possible.
- **ER-STK-NLR-06**: At least one additional safety system shall be in place.
- **ER-STK-NLR-07**: The aircraft shall enable maintenance on the aircraft.
- **ER-STK-NLR-08**: The aircraft shall enable necessary ground operations.

Stakeholder 3: National Aeronautic Association (NAA)

- **ER-STK-NAA-01**: The aircraft shall comply with the race rules as provided by NAA.

Stakeholder 4: Federal Aviation Administration (FAA)

- **ER-STK-FAA-01**: The aircraft shall comply with relevant regulations as provided by the FAA.

Stakeholder 5: Airports (AIRP)

- **ER-STK-AIRP-01**: The aircraft shall be capable of safely operating in available airports.

Stakeholder 6: Custom part manufacturers (CPM)

- **ER-STK-CPM-01**: The custom aircraft components shall be producible.

Stakeholder 7: COTS part suppliers (COTS)

- **ER-STK-COTS-01**: The aircraft design shall allow easy integration of COTS parts into the design.

Stakeholder 8: Pilot (PIL)

- **ER-STK-PIL-01**: The aircraft shall provide a comfortable experience for the pilot.
- **ER-STK-PIL-02**: The aircraft shall provide communication capabilities for the pilot.
- **ER-STK-PIL-03**: The aircraft shall provide measurements of essential flight parameters to the pilot.

Stakeholder 9: The project group (G26)

- **ER-STK-G26-01**: The design of the product shall be related to the field of aerospace engineering.

Stakeholder 10: Society (SOC)

- **ER-STK-SOC-01**: The development of the aircraft shall increase the sustainability of air transportation.
- **ER-STK-SOC-02**: The aircraft shall not produce high noise levels that can disturb people on the ground.
- **ER-STK-SOC-03**: The aircraft shall not endanger any people or their property.

5.2.2. Mission requirements

Since stakeholder requirements can be unclear, mission requirements are created based on stakeholder requirements in order to clarify their impact on the design.

The mission requirements that must be met can be found in Table 5.1. In this table, the mission requirement's ID is given in the left column, the requirement is written out in the middle and finally, the ID of the stakeholder requirement from which this mission requirement was derived is given in the third column. Furthermore, a distinction has been made between key, killer, and driving requirements. The key requirements have been presented in Table 5.1 with a red text colour, while the driving requirements have been indicated with a blue text colour. The killer requirements had been identified and afterwards discussed at the baseline review, which resulted in a change of perspective and

not considering those requirements as killers anymore. Therefore, there are no killer requirements present in the project.

Table 5.1: Mission requirements

ER-MIS-NLR-01.01	The aircraft shall be able to win the Pulitzer Electric Aircraft Race.	**ER-STK-NLR-01**
ER-MIS-NLR-01.02	The aircraft shall be able to travel 1,000 nautical miles within four days.	**ER-STK-NLR-01**
ER-MIS-NLR-02.01	The technology involved with the aircraft shall be available by the year 2030.	**ER-STK-NLR-02**
ER-MIS-NLR-03.01	The aircraft shall be producible within a budget of €900,000.	**ER-STK-NLR-03**
ER-MIS-NLR-06.01	The aircraft shall be equipped with at least one additional safety system.	**ER-STK-NLR-06**
ER-MIS-NAA-01.01	The aircraft shall be heavier than air.	**ER-STK-NAA-01**
ER-MIS-NAA-01.02	The aircraft shall be zero-emission.	**ER-STK-NAA-01**
ER-MIS-NAA-01.05	The aircraft shall be able to obtain a special airworthiness certificate in the experimental category with the purpose of air racing.	**ER-STK-NAA-01**
ER-MIS-NAA-01.06	The aircraft shall be operated by a human pilot.	**ER-STK-NAA-01**
ER-MIS-AIRP-01.01	The aircraft shall be able to use the County Regional Airport, Manteo, North Carolina, US.	**ER-STK-AIRP-01**
ER-MIS-AIRP-01.02	The aircraft shall be able to use the Eppley Airfield, Omaha, Nebraska, US.	**ER-STK-AIRP-01**
ER-MIS-SOC-01.01	The aircraft shall provide test data for electrical propulsion aviation.	**ER-STK-SOC-01**

5.2.3. System Requirements

Having created the requirements discovery tree with the flow-down of requirements, system requirements may now be derived. System requirements are more technical, which allows them to be more usable during the design phase, as they lead the design. The system requirements for the design are shown in Table 5.2. Once again, red and blue indicators are used for key and driving requirements, respectively. The ID for the system requirements and the requirements themselves can be found in the first and second column respectively, while the ID of the mission requirement that the system requirement is based on can be found in the third column.

Table 5.2: System requirements

Indicator	System Requirement	Higher Level Related Requirement
ER-SOC-CON-SUS-1.1	The aircraft shall have a maximum fly-over perceived noise level of 89 dB.	**ER-STK-SOC-02**
ER-SOC-CON-SUS-1.2.1	The aircraft shall not emit harmful compounds.	**ER-STK-SOC-03**
ER-SOC-CON-SUS-1.2.2	Damaging compounds that are part of the aircraft shall be clearly indicated.	**ER-STK-SOC-03**
ER-TUD-CON-SUS-2.1	A partnership shall be used to develop the powertrain.	**ER-STK-TUD-02**
ER-NLR-CON-SAF-1	The aircraft shall have a reliability of 99% to successfully complete the race.	**ER-MIS-NLR-06.01**
ER-NLR-CON-SAF-2.1	The aircraft shall protect the pilot against a fire for 4 minutes.	**ER-MIS-NLR-06.01**
ER-NLR-CON-SAF-2.2	The aircraft shall prevent crashing into populated areas.	**ER-MIS-NLR-06.01**
ER-NAA-CON-REG-1.1.1	The aircraft shall derive its lift mainly from aerodynamic forces.	**ER-MIS-NAA-01.01**
ER-NAA-CON-REG-1.2	The aircraft shall not emit carbon dioxide.	**ER-MIS-NAA-01.02**
ER-NAA-CON-REG-1.3	The aircraft shall use an electrical propulsion system.	**ER-MIS-NAA-01.02**
ER-NAA-CON-REG-1.5.1	The aircraft shall provide breathable air to the pilot.	**ER-MIS-NAA-01.06**
ER-NAA-CON-REG-1.6	The aircraft shall be equipped with a GPS sensor.	**ER-STK-NAA-01**
ER-NAA-CON-REG-1.7	The aircraft shall fly in day Visual Meteorological Conditions.	**ER-STK-NAA-01**
ER-NLR-CON-RES-1.2.1	The design shall use a COTS engine.	**ER-STK-NLR-05**

ER-NLR-CON-RES-1.2.2	The design shall use COTS battery cells.	**ER-STK-NLR-05**
ER-NLR-CON-RES-1.2.3	The design shall be producible between 2025 and 2030.	**ER-MIS-NLR-01.02**
ER-PIL-TECH-NAV-1.1	The aircraft shall be able to measure altitude.	**ER-STK-PIL-03**
ER-PIL-TECH-NAV-1.2	The aircraft shall be able to measure airspeed.	**ER-STK-PIL-03**
ER-PIL-TECH-NAV-1.3	The aircraft shall be able to determine its location.	**ER-STK-PIL-03**
ER-PIL-TECH-NAV-1.4	The aircraft shall be able to measure internal vehicle states.	**ER-STK-PIL-03**
ER-PIL-TECH-NAV-1.4.1	The aircraft shall be able to measure energy storage levels.	**ER-STK-PIL-03**
ER-PIL-TECH-NAV-1.4.2	The aircraft shall be able to measure power output levels.	**ER-STK-PIL-03**
ER-PIL-TECH-NAV-1.4.3	The aircraft shall be able to measure temperature of powertrain.	**ER-STK-PIL-03**
ER-PIL-TECH-NAV-2.1	The aircraft shall be able to display the determined flight route.	**ER-STK-PIL-03**
ER-PIL-TECH-NAV-2.2	The aircraft shall be able to display the measured data.	**ER-STK-PIL-03**
ER-SOC-TECH-NAV-3	The aircraft shall be able to store the measurements taken during flight.	**ER-MIS-SOC-01.01**
ER-NLR-TECH-GOP-1.1	The aircraft shall be able to be refueled at all landing sites.	**ER-MIS-NLR-01.01**
ER-NLR-TECH-GOP-1.2	The aircraft shall be able to be refueled in 7 hours and 10 minutes or less.	**ER-MIS-NLR-01.01**
ER-PIL-TECH-GOP-2.1	The aircraft shall provide an entrance for the pilot.	**ER-STK-PIL-01**
ER-NLR-TECH-GOP-2.2	The aircraft shall enable access for regular maintenance.	**ER-STK-NLR-07**
ER-NLR-TECH-GOP-2.2.1	The aircraft shall enable access to check the landing gear.	**ER-STK-NLR-07**
ER-NLR-TECH-GOP-2.2.2	The aircraft shall enable access to check the powertrain.	**ER-STK-NLR-07**
ER-NLR-TECH-GOP-2.2.3	The aircraft shall enable access to check the control actuators.	**ER-STK-NLR-07**
ER-NLR-TECH-GOP-3.1	The aircraft shall be able to manoeuvre on the ground without tipping over.	**ER-STK-NLR-08**
ER-NLR-TECH-GOP-3.2	The aircraft shall be able to move from the hangar to the take-off location.	**ER-STK-NLR-08**
ER-PIL-TECH-COM-1	The aircraft shall enable the pilot to communicate with the ground team.	**ER-STK-PIL-02**
ER-PIL-TECH-COM-2	The aircraft shall enable the pilot to communicate with air traffic management.	**ER-STK-PIL-02**
ER-PIL-TECH-COM-3	The aircraft shall enable the pilot to communicate with other planes.	**ER-STK-PIL-02**
ER-NLR-TECH-CRU-1	The aircraft shall have a minimum cruise speed of 145 [m/s].	**ER-MIS-NLR-01.01**
ER-NLR-TECH-CRU-1.1	The aicraft shall have a continuous power-to-weight ratio of at least 8.1 [W/N].	**ER-MIS-NLR-01.01**
ER-FAA-TECH-CRU-1.2	The aircraft shall have a minimum cruise altitude of 10.000 [ft].	**ER-STK-FAA-01**
ER-NAA-TECH-CRU-2	The aircraft shall have a minimum range of 200 [km].	**ER-MIS-NLR-01.01**
ER-NLR-TECH-CRU-2.1	The aircraft shall have a maximum lift-to-drag ratio of at least 18:1.	**ER-MIS-NLR-01.01**
ER-FAA-TECH-FLM-1.1	The aircraft shall be able to withstand a load factor of 3.8.	**ER-MIS-FAA-01.01**
ER-NLR-TECH-FLM-2.1	The aircraft shall have a peak power-to-weight ratio of 10 [W/N].	**ER-MIS-NLR-01.01**
ER-AIRP-TECH-FLM-2.2	The aircraft shall have a maximum take-off distance of 2000 [m].	**ER-MIS-AIRP-01.01**
ER-AIRP-TECH-FLM-3.1	The aircraft shall have a maximum landing distance of 1000 [m].	**ER-MIS-AIRP-01.02**
ER-NLR-TECH-FLM-4.1	The aircraft shall be able to achieve a minimum climb rate of 5 [m/s].	**ER-MIS-NLR-01.01**
ER-FAA-TECH-FLM-4.2	The aircraft shall be able to achieve a minimum climb angle of 4 degrees.	**ER-MIS-FAA-01.01**
ER-PIL-TECH-CON-1.1.1	The aircraft shall be trimmable.	**ER-STK-PIL-01**
ER-PIL-TECH-CON-1.1.2	The lateral stick forces shall be at most 140 [N].	**ER-STK-PIL-01**
ER-PIL-TECH-CON-1.1.3	The longitudinal stick forces shall be at most 400 [N].	**ER-STK-PIL-01**
ER-PIL-TECH-CON-1.1.4	The pedal forces shall be at most 1500 [N].	**ER-STK-PIL-01**
ER-PIL-TECH-CON-1.2.1	The stick deflection angle shall be at most 45 degrees.	**ER-STK-PIL-01**
ER-PIL-TECH-CON-1.2.2	The stick deflection travel shall be at most 30 [cm].	**ER-STK-PIL-01**
ER-FAA-TECH-CON-2.1.1	The control accelerations shall not be larger than 1.1799 [rad/s^2] in pitch.	**ER-MIS-FAA-01.01**
ER-FAA-TECH-CON-2.2.1	The aircraft shall be statically stable.	**ER-MIS-FAA-01.01**
ER-FAA-TECH-CON-2.2.2	The aircraft shall be dynamically stable in the short period.	**ER-MIS-FAA-01.01**
ER-FAA-TECH-CON-2.2.3	The aircraft shall be dynamically stable in the dutch roll.	**ER-MIS-FAA-01.01**
ER-NLR-TECH-PPR-1.1	The aircraft shall structurally support the pilot.	**ER-MIS-NLR-01.01**

ER-NLR-TECH-PPR-1.2	The aircraft shall maintain its aerodynamic shape.	**ER-MIS-NLR-01.01**
ER-FAA-TECH-PPR-1.3	The structure shall not be damaged under ultimate loads.	**ER-MIS-FAA-01.01**
ER-AIRP-TECH-PPR-2	The aircraft shall have maximum wingspan of 40 [m].	**ER-STK-AIRP-01**
ER-NLR-TECH-PPR-3	The aircraft shall have a maximum mass of 1,200 [kg].	**ER-MIS-NLR-01.01**

A number of these requirements require an explanation as to how they were determined and these will be explained below. Other requirements that flow directly from stakeholders, race rules and regulations are not included. As mentioned before, for the structures and flight performance, FAA FAR 23 regulations will be used, since these should not be different from ”normal” aircraft. Most of the requirements with the FAA as a stakeholder follow directly from either the FAR 23 regulations or general rules for flight in the United States.

ER-SOC-CON-SUS-1.1 This requirement follows from ER-STK-SOC-02 which discusses high noise levels and their possibility to disturb people on the ground. To make this a specific requirement the Code of Federal Regulations was used[1]. This states that the fly-over perceived noise can be 89 dB maximum. Where perceived noise takes frequencies and variations into account next to the amplitude, this should make the value more relevant for actual disturbance to people.

ER-NLR-CON-SAF-1 This requirement considers the reliability of the aircraft. Since the mission need statement concerns a winning design for the Pulitzer electric aircraft race, there is not really any room for the aircraft to be unreliable. Consequently, it was decided along with the client to set a reliability of 99%; the definition of reliability in this case refers to the event of starting and finishing the race with the same airframe and propulsion system.

ER-NLR-CON-SAF-2.1 The main risk and TBD time of this requirement depends very heavily on the type of vehicle that will be designed, therefore they are not yet specified.

ER-NLR-TECH-GOP-1.2 The strategy is not clear yet, but by using the the minimum range of 200 km from ER-NAA-TECH-CRU-2 and the cruise speed of 145 m/s from ER-NLR-TECH-CRU-1 a maximum charge/refuel time can be set. This time was calculated to be 7 hours and 10 minutes, this would be quite close and stressful so hopefully it will be less.

ER-NLR-TECH-CRU-1 This requirement follows from the market analysis, The Sirius Business Jet has a cruise speed of 144.44 m/s. The design needs to be able to go faster, so it should have a higher cruise speed. Therefore the minimum cruise speed was set at 145 m/s.

ER-NLR-TECH-CRU-1.1 The value for this requirement follows from the minimum cruise speed from ER-NLR-TECH-CRU-1 and the lift-to-drag ratio from ER-NLR-TECH-CRU-2.1.

ER-FAA-TECH-CRU-1.2 This requirement follows from the speed restrictions at different altitudes by the FAA and requirement ER-NLR-TECH-CRU-1, it is not allowed to fly above 250 kts below 10,000 feet[2]. Since the minimum cruise speed is 145 m/s, the minimum cruise altitude must be 10,000 feet.

ER-NAA-TECH-CRU-2 This requirement comes from the NAA which advised a minimum range of 200 km[3]

ER-NLR-TECH-CRU-2.1 In general, for small aircraft the lift-to-drag ratio can be assumed to be between 14 and 18 [5]. However, electric aircraft have a considerably higher lift-to-drag ratio as their energy fraction is higher. Wolleswinkel found that an electrical aircraft could have a lift-to-drag ratio of 20 [5]. This does consider regional aircraft with passengers, so therefore a lift-to-drag ratio of 18 is set.

ER-NLR-TECH-CRU-2.2 This requirement still needs to be finalised, but it requires knowledge that will be gained during the midterm phase.

ER-NLR-TECH-FLM-1.2 Even though no regulatory requirements could be found it was considered important to have a requirement on the turn rate. It was decided to set the requirement to a standard turn which is a full 360°turn in 2 minutes[4] leading to 3 [$^\circ/s$].

[1] https://www.ecfr.gov/current/title-14/chapter-I/subchapter-C/part-36 [Accessed on 13-05-2024]

[2] https://www.ecfr.gov/current/title-14/chapter-I/subchapter-F/part-91/subpart-B/subject-group-ECFRe4c59b5f5506932/section-91.117 [Accessed on 13-05-2024]

[3] https://naa.aero/wp-content/uploads/2023/04/Pulitzer-Race-Pre-Registration-Information.pdf [Accessed on 08-05-2024]

[4] https://airplaneacademy.com/radius-of-standard-and-non-standard-rate-turns/ [Accessed on 13-05-2024]

ER-AIRP-TECH-FLM-2.2 & ER-NAA-TECH-FLM-3.1 The maximum take-off distance was taken as the starting airport runway length and the same for the landing distance at the finish airport. It is possible that the final race strategy requires one or multiple extra stop(s). In this case these requirements could be changed to allow for landings and take-offs at these airports.

ER-NLR-TECH-FLM-4.1 The rate of climb is once again heavily dependent on strategy since a strategy that requires more take-offs and landings needs a larger rate of climb to get back to cruising altitude.

ER-PIL-TECH-CON-1.1.2 - 1.1.4 These requirements were determined such that the pilot will physically be able to control the aircraft. This means that the control forces are limited which has been determined by the Psychological Corporation [6].

ER-FAA-TECH-FLM-4.2 and ER-FAA-TECH-CON-2.2.1 - 2.2.3 These requirements stem from the FAR 23 regulations from the FAA [5].

ER-NLR-TECH-PPR-2 Even though there are no real regulations for the maximum width of an aircraft, there are limitations by the airports themselves, this gives a limit of 40 [m][6]. It must again be noted that this depends on strategy in the same way as the maximum take-off and landing distances.

ER-NLR-TECH-PPR-3 The maximum aircraft mass was set due to the limited budget and as a result of an approximate weight breakdown of each of the components of the aircraft. This value has been verified during the detailed design phase.

[5] https://www.ecfr.gov/current/title-14/chapter-I/subchapter-C/part-23?toc=1 [Accessed on 13-05-2024]
[6] https://www.aopa.org/destinations/airports/KOMA/details[Accessedon13-05-2024]

6. Trade-Off Summary

After the requirements for the design have been established, the possible solutions can be investigated. First, the different design options were generated and pruned to determine feasible options which led to the concepts shown in Section 6.1. Then, a trade-off method was established and performed on the concepts as discussed in Section 6.2. A sensitivity analysis on the trade-off was performed, which is discussed in Section 6.3. Finally, a final choice could be made which will be explained in Section 6.4.

6.1. Design Concepts

To come up with feasible concepts, three major differentiators were identified. These consisted of energy source, lift generation configuration, and propulsion unit. For these differentiators, driven by requirements, a number of potential design options were identified. The different design options were then combined into full concepts which resulted in the concepts shown in Table 6.1. Furthermore, a visual representation of each concept is also shown in Figure 6.1.

Table 6.1: Proposed full concepts

Concept	Configuration	Energy Source	Propulsion
Electric conventional aircraft	Conventional	Battery	Unducted propeller
Hydrogen conventional aircraft	Conventional	Hydrogen/Batteries	Propeller
Electrical flying wing	Flying wing	Battery	Propeller
Hydrogen Prandtl plane	Multiwing	Hydrogen/Batteries	Propeller
Hybrid VTOL aircraft	Lifting propulsion + Lifting surface	Hydrogen/Batteries	Propeller

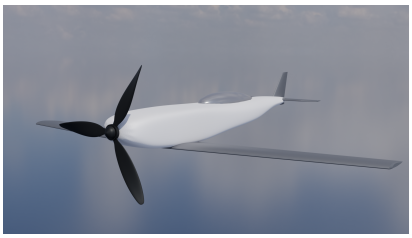

(a) Conventional electric

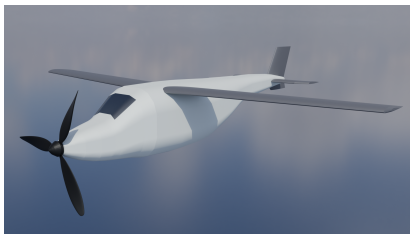

(b) Conventional hydrogen

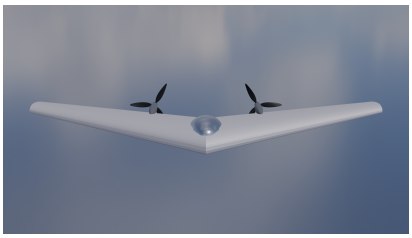

(c) Flying wing electric

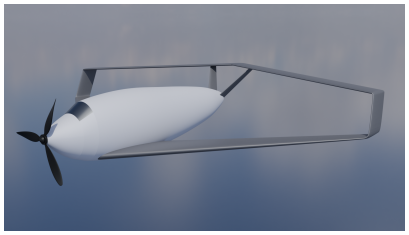

(d) Prandtl plane hydrogen

(e) VTOL hybrid

Figure 6.1: Visual representation of concepts

The concepts were generated from the design options such that all potentially successful combinations were present. One combination that might seem to be left out is a hydrogen-powered flying wing. However, for the flying wing, due to the small size of the aircraft, it was found that too little volume would be present in the aircraft to take enough hydrogen to be competitive with the other hydrogen-powered concepts.

Then, each concept was worked out in more detail and analysed to estimate its performance during the race. The analysis was split into different technical aspects: Aerodynamics, flight performance, weight estimations, energy budgets, and cost breakdown. The basis for each analysis was a literature review of the methods and parameters used. The goal for each evaluation was to provide preliminary values on characteristic parameters that were needed in the trade-off process, which follows after this conceptual analysis phase. The final values for each parameter are shown in Table 6.2.

Table 6.2: Overview of parameters for each concept

	Conventional Electric	Conventional Hydrogen	Flying Wing	Hydrogen Prandtl	Hybrid VTOL
Average speed $[m/s]$	117	154	125	159	147
Range $[km]$	268	1906	264	1910	970
Number of stops [-]	7	0	7	0	1
Time to finish race $[min]$	338	200	247	197	212
Take-off mass $[kg]$	1042	750	1300	741	913
Amount of hydrogen $[kg]$	0	22.5	0	21.7	13.3
Battery mass $[kg]$	482	34	511	34	185

6.2. Trade-Off Method

The decision was made to use the Weighted Sum Model (WSM), which is a Multi-Criteria Decision Analysis (MCDA) method as a trade-off method. This meant that different criteria and their weights needed to be defined. From high-level requirements and differences between the concepts, four different criteria were determined. These are shown and explained below.

- **Flight Time:** The mission of this project is to design an aircraft that can win the Pulitzer electric aircraft race. Therefore, the time the concept takes to finish the race is crucial. As it is of such importance for the mission, it has a weight of 60%.
- **Ground Logistics:** Ground logistics can greatly complicate the actual mission of the race and, furthermore, can affect the chances of winning the race. More stops required means that either more chargers need to be placed or that refuelling needs to take place more often. Thus, it is preferable to make the least numbers of stops. This criterion has a weight of 15%.
- **Design Complexity:** One of the top-level requirements is that the design shall have a reliability of finishing the race of 0.99. This is a stringent requirement and it was therefore important to represent this requirement in a criterion as well. It was decided to assess the concepts on design complexity. This includes the number of different systems and parts. The complexity of the mechanisms required is considered, as well as the technology readiness of the concepts as these were believed to highly influence the reliability of the concepts. This criterion received a weight of 15%.
- **Sustainability:** Lastly, the sustainability of the concepts was determined to be of importance as well. The aircraft will be zero-emissions during the mission as per requirements. However, emissions can have other sources as well such as indirect emissions from generating electricity or hydrogen as well as embedded emissions in the materials used. These emissions will be assessed for the different concepts. This criterion has a weight of 10%.

The data from Table 6.1 was used to grade the different concepts which can be summarised in the trade-off summary table shown in Table 6.3.

Table 6.3: Summary of the concept trade-off

	Flight Time 60%	Ground Logistics 15%	Design Complexity 15%	Sustain-ability 10%	Total Score
Conventional Electric	1	1	5	2	1.7
Conventional Hydrogen	4	4	4	5	4.1
Flying Wing	2	1	3	1	1.9
Hydrogen Prandtl Plane	4	4	3	5	3.95
Hybrid VTOL	3	3	3	2	2.85

6.3. Sensitivity Analysis

From the trade-off summary table, it can be seen that the two concepts perform very similarly, more explicitly the hydrogen conventional and hydrogen Prandtl plane. Furthermore, the determination of the weights of the criteria and the grades were partially subjective. Lastly, the flight time criterion had a substantially higher weight than any of the other criteria. Therefore, to increase confidence in the results and to investigate the potential effect that these choices have on the outcome, a sensitivity analysis was made.

It was decided to vary both the weights and the grades of the different concepts and to determine the final scores for the concepts for all these scenarios. The weights were varied by 0%, 5%, or 10% such that all weights add up to 100%. The grades were varied up or down by 1 full point. The result can be summarised in the boxplot shown in Figure 6.2, which shows the distribution of the final scores for the different concepts. Furthermore, the overlap of the distribution of the hydrogen conventional and hydrogen Prandtl plane is also shown in Figure 6.3.

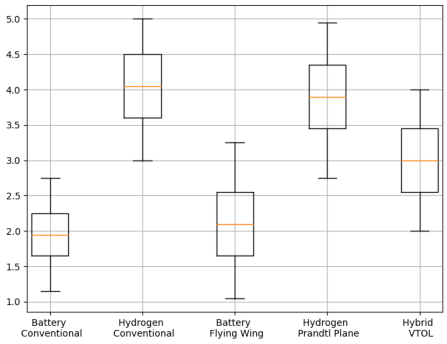

Figure 6.2: Distribution of final scores per concept based on changes in weight and grades

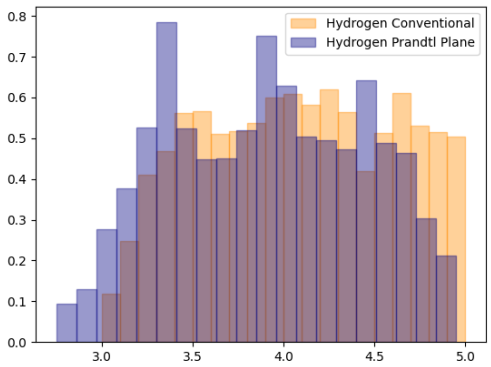

Figure 6.3: Overlap of two winning concepts

From Figure 6.2, it can be seen that, even when changing weights and grades, the conventional hydrogen and conventional Prandtl plane perform similarly and better than the other concepts. Furthermore, the overlap between the distribution of these concepts, shown in Figure 6.3, is large as well. Therefore, a choice between these concepts cannot be based on the trade-off alone. The choice of the final concepts will be discussed in Section 6.4

6.4. Final Choice

As mentioned before, no final concept could be chosen based on the trade-off. The sensitivity analysis ensured good confidence in the trade-off criteria weights. This means that a choice has to be made based on something else but, due to their similarities, this cannot be done based on the requirements. However, two areas were determined where the Prandtl plane has an advantage: the spirit of the race and optimisation potential.

The Spirit of the Race

Even though both concepts should be able to win the Pulitzer Electric Aircraft Air Race, the idea of the race is to push innovation. Even though the idea behind the Prandtl plane is a hundred years old by now, due to the conservative nature of the aviation industry, it is still a novel concept with no full-scale plane built to date. From research done on the Prandtl plane, it is also clear that it has many advantages, mainly focused on a reduction of induced drag and weight. Therefore, the team deems the Prandtl plane to be significantly more innovative compared to the conventional hydrogen-powered plane.

Optimisation Potential

Secondly, it is worth noting that the conceptual design of the Prandtl plane is conservative since the structural weight is nearly identical to an equivalent conventional aircraft, but it could be up to 36% lighter [7]. This was done intentionally since there are no equations specifically for a small box-wing aircraft, so the most conservative option was considered. This means that there is room for improvement during detailed design.

Chosen Concept

These reasons were also discussed with the tutor of the project and the NLR who approved the decision made by the team. Therefore, the Prandtl plane was chosen and its design will be used as the basis of the detailed design phase.

7. Preliminary Design

In order to start the detailed design of the subsystems of the aircraft, an initial starting point is required. Therefore, a preliminary design of the aircraft is performed. This process was partially done before the trade-off as information on the design was required for the trade-off. After the trade-off, the preliminary design of the Prandtl plane was further refined to provide a good starting point for the detailed design phase. The preliminary design process will first be explained in Section 7.1. Then, the relations between the different subsystems of the aircraft will be shown in Section 7.2.

7.1. Preliminary Design of Prandtl Plane

In the preliminary design phase, the aerodynamic parameters are estimated first, mostly from literature. This provides a base for the wing planform of the aircraft. Next, some initial propulsion parameters are estimated. Then, a weight estimation can be done by estimating the mass of the wing and other subsystems. After the mass estimation, the wing loading of the aircraft can be found, by placing some limits on the take-off, climb, cruise, and landing performance of the aircraft. Finally, the initial design is presented.

7.1.1. Aerodynamic Parameters

To begin the preliminary design of the aircraft, some designs for Prandtl planes were found, from which estimates for some initial aerodynamic and geometric parameters can be made. The maximum clean lift coefficient, the Oswald efficiency factor, and the zero-lift drag coefficient are used to create the power and wing loading diagram, as well as to analyse the performance of the aircraft. The maximum clean lift coefficient of the aircraft was found by comparing it to a smaller aircraft design. Also, it is important to mention that the aspect ratio (AR) is considered for the total surface area of the wings and not for each wing. The results of this analysis are shown in Table 7.1 and Table 7.2.

Table 7.1: Preliminary aerodynamic parameters

Parameter	Value	Unit
AR [8]	6.25	-
e [9]	1.24	-
C_{D0} [10]	0.016	-
C_{Lmax} [11]	1.4	-

Table 7.2: Wing planform parameters for wing weight estimation

Parameter	Value	Unit
$\Lambda_{c/4,front}$	25	$^\circ$
$\Lambda_{c/4,aft}$	-11	$^\circ$
λ	0.35	$-$
t/c	0.118	$-$

7.1.2. Propulsion parameters

For the propulsion system, some parameters need to be estimated as well. Firstly, the different components of the propulsion system need to be clear. As mentioned before, the energy source will be hydrogen. However, a small battery will be present for peak performance, during climb for example, and to compensate for the fuel cell's slow response time when throttling. The hydrogen system itself consists of a liquid hydrogen tank, a fuel cell, the hydrogen itself, and the tubing. For the preliminary design, the tubing will be neglected. However, a margin will be used in the weight estimation to account for it. Next to the fuel system, an electric motor and propeller will be present to provide thrust. The propulsion parameters required are shown in Table 7.3. The values were found during the literature study performed.

Table 7.3: Preliminary propulsion parameters

Parameter	Value	Unit
Propeller efficiency [12]	0.8	-
Motor efficiency	0.9	-
Battery discharge efficiency	0.9	-
Battery specific energy	270	Wh/kg
Hydrogen specific energy[1]	120	MJ/kg
Fuel cell specific power [13]	1.6	kW/kg
Fuel cell efficiency[2]	0.5	-
Gravimetric Storage Density Liquid Hydrogen Tank[3]	0.3	-
Payload (pilot + margin)	100	kg

7.1.3. Weight Estimation

The weight estimation method consisted of two different options: either for some components specific COTS component weights were found or, for others, weight estimation relations were used. The required weight relations regarding the powertrain are already listed in Table 7.3. However, the wing of a Prandtl plane is unique. Fortunately,

Equation 7.1 is provided for calculating the wing mass of a box-wing aircraft [14].

$$M_W = 0.028 \left[\frac{b \cdot S}{cos\Lambda_{c/4}} \left(\frac{1+2\lambda}{3+3\lambda} \right) \left(\frac{n_z \cdot MTOM}{S} \right)^{0.3} \left(\frac{V_{max}}{t/c} \right)^{0.5} \right]^{0.9} \tag{7.1}$$

Here M_W is the wing mass of either the top or bottom wing. For the total wing mass, the mass of both wings has to be added. S, b, and V_{max} are the total wing surface area, the total wingspan, and the maximum velocity respectively. The maximum velocity is equal to 193 $[m/s]$, based on the limit set on the maximum Mach number for the design. $\Lambda_{c/4}$ is the wing sweep of either the front or rear wing, depending on which wing mass is being calculated. n_z is the load factor, λ is the taper ratio for the wing and, finally, t/c is the thickness-to-chord ratio. The final Maximum Take-off Mass (MTOM) resulting from the weight estimation is 740.9 $[kg]$ after iteration.

7.1.4. Initial Sizing

To start the actual design of the aircraft, the wing and power loading diagram need to be generated, which was based on a method from Raymer [15]. This shows, based on certain requirements regarding stall speed, landing and take-off distance, cruise speed, rate of climb, and climb gradient values, what combinations of wing and power loading would result in a satisfactory design. Some additional parameters and performance requirements are required to generate the diagram. These are shown in Table 7.4 and are at this stage of the design based on FAR 23 requirements. Using all of these parameters together with the assumption of constant weight, Figure 7.1 can be created.

Table 7.4: Wing and power loading diagram parameters

Parameter	Value	Unit
Stall Speed	31.8	m/s
Take-Off Distance	2000	m
Landing Distance	1000	m
Cruise Speed	145	m/s
Climb Rate	10	m/s
Climb Angle	4	°

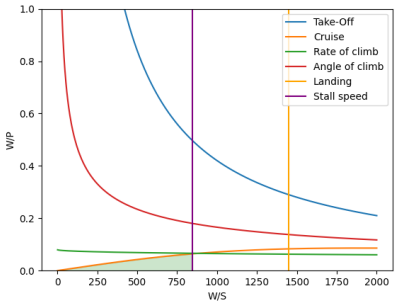

Figure 7.1: Initial power and wing loading diagram Prandtl plane

7.1.5. Further Design Steps

From Figure 7.1, the wing and power loading can be obtained. These were determined to be 845 $[N/m^2]$ and 0.0642 $[N/W]$ respectively as the top right corner of the design space was chosen as the design point. These values are determined by the intersection point between the orange line for the cruise and the purple line for stall speed, which are limiting for this case. The desired point is located at the top right corner of the green-shaded area; this area denotes the allowed values for wing and power loadings defined by the different situations outlined in the diagram.

The next step was to determine the MTOM and, since iterations would be performed to come up with the final mass, it was decided to use 800 $[kg]$ as the starting point. This has been established from similarly sized aircraft. However, no other hydrogen aircraft exist and therefore it can be assumed to be a rough estimation. Based on this mass, the mass of different aircraft components will be generated and iterated to find a final preliminary MTOM. Additionally, the power fraction used will be 0.8. This power fraction states how much of the take-off power is used at cruise, 1 would be the same power throughout the flight. This parameter is important since the fuel cell power requirement will be based on cruise conditions and, for the difference between the take-off (and climb power), a battery will be used.

Finally, the parameters for Equation 7.1 need to be determined. These are the sweep angle of the front and rear wing, the taper ratio, the maximum velocity, and the thickness-to-chord ratio. These will be determined by looking at other Prandtl plane concepts. The sweep angles were gathered, together with the taper ratio and thickness to chord ratio [8, 11]. The results are presented in Table 7.2.

A flight performance computer program was created and used to assess the performance of the aircraft and to provide a new estimate of the required power. From this, it was clear that a continuous power of 115 $[kW]$ - 120 $[kW]$ should suffice. The Emrax 268[4] was chosen as a motor. It has a continuous power of 117 $[kW]$, a peak power of 210 $[kW]$,

[4] `https://emrax.com/wp-content/uploads/2024/02/EMRAX_268_datasheet_v1.5.pdf` [Accessed on 22-05-2024]

and a mass of 22.3 [kg]. The motor needs to be combined with a motor controller, for this, a XAP motor controller was used[5]. It has a mass of 2.5 [kg] and a cost of €900. Lastly, a Diamond DA 40(XL) propeller is used, which has a mass of 21 [kg][6]. Then, from Vittorio et al. [16], the fuselage weight adjusted for the used MTOM is 128 [kg]. Additionally, a structural penalty of 30 [kg] was added, since the methods used for the Prandtl plane are not intended for such a small plane. Finally, a margin of 100 kg was used in the mass breakdown in case of unpredictable errors in the estimations. These extra 130 [kg] added to the MTOM were a design choice made by the team.

Table 7.5: Optimal flight parameters for the Prandtl plane

Parameter	Value	Unit
Maximum Power Output	145	kW
Number of Stops	0	-
Range	1910	km
Average Speed	159	m/s
Cruise Altitude	12.5	km
Time to Finish Race	194	min

Finally, all the information was in place to perform iterations. These started with the analysis from the flight performance program, then the mass of the energy system was updated, and lastly, the wing mass was updated. This cycle was performed multiple times until convergence was achieved. It was quickly realised that it would be possible to fly the entire race in one go, therefore this was then selected as the desired strategy. The result of the optimal strategy is presented in Table 7.5.

7.1.6. Final Design

After the iterations converged on a MTOM, the final design parameters are obtained and can be seen in Table 7.6. From this table, it can be seen that the MTOM decreased from its starting point by quite a significant margin.

Table 7.6: Final design parameters for the hydrogen Prandtl plane concept

Parameter	Value	Unit
MTOM	740.9	kg
Wing Mass	158	kg
Battery Mass	33.7	kg
Hydrogen Tank Mass	50.6	kg
Fuel Cell Mass	73.1	kg
Hydrogen Mass	21.7	kg
Hydrogen Energy	1300	MJ
Battery Capacity	9.1	kWh
Continuous Power	117	kW
Peak Power	145	kW
Wing Surface Area	8.6	m^2
Wingspan	7.33	m

7.2. N2 Chart

Before starting the subsystem designs, it is important to investigate the interdependencies between the different subsystems. These are put into an N2 chart as shown in Figure 7.2. The main systems are placed on the diagonal, from which outputs and inputs are determined. The outputs of a certain system are placed horizontally from that system. A given input for a system is placed vertically above or below it. This diagram gives an overview of possible design loops and dependencies of various systems in the design. Furthermore, it also shows which subsystems are most critical, meaning that it has the most influence on other subsystems. These subsystems require additional attention and should be designed as soon as possible. From the diagram, it can be seen that aerodynamics, the airframe, and the propulsion system are the most critical subsystems.

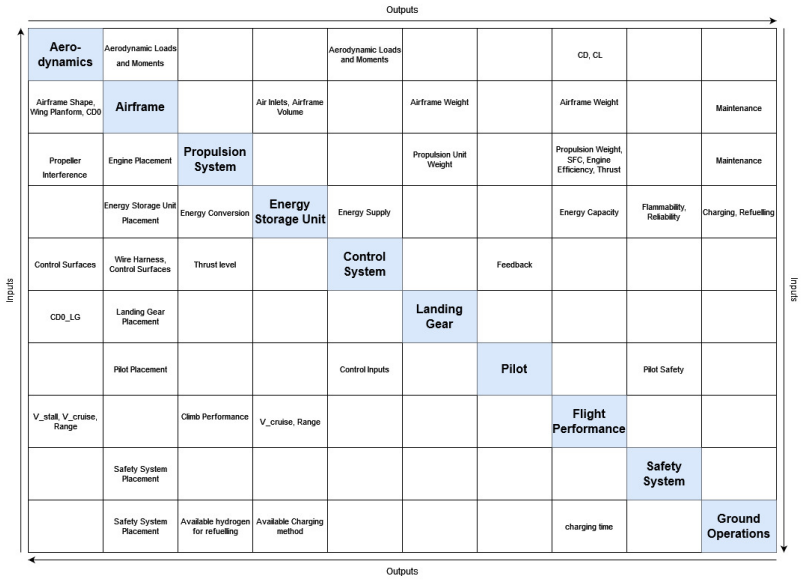

Figure 7.2: Subsystem N2 Chart

[5] https://store.xap.fr/en/22480-product.html [Accessed on 16-05-2024]
[6] https://hartzellprop.com/wp-content/uploads/COMPOSITE-DIAMOND-DA40XL.pdf [Accessed on 22-05-2024]

8. Aerodynamics

Aerodynamics is very important for the evolution of the design, as this is the department where the wings of the aircraft are sized to minimise the drag, making it the most efficient possible. In order to accurately analyse the drag, a literature study was first performed, with the results being discussed in Section 8.1. Following this, the method for obtaining the initial planform of the wing is explained in Section 8.2. The iteration process to obtain more accurate and better results is described in Section 8.3. The stall characteristics of the aircraft are then discussed in Section 8.4. Afterwards, the verification and validation of the procedures are discussed in Section 8.5. Finally, the final wing planform is presented in Section 8.6.

8.1. Literature Study

Determining all parameters relevant to the aerodynamics of an aircraft is a crucial part of the design. Therefore, an extensive literature study is needed to ensure a good understanding of the topic.

8.1.1. Aerodynamic Parameters

In order to determine the process for obtaining the aerodynamic properties of the aircraft, a literature study is performed. During this, research regarding the design of a similar Prandtl plane is found and it will be discussed.

The first aircraft that is investigated during this literature study is the amphibious Prandtl plane, IDINTOS [17]. While it is slower and a bit smaller than the E-Racer, as well as being able to land on water, the process for designing the aircraft is deemed to be usable on the aircraft designed in this report.

To determine the aerodynamic properties of the amphibious aircraft, a certain process was followed [18]. First, an optimisation-based design process is performed with their in-house code. After this, a computational fluid dynamics (CFD) analysis is performed to obtain aerodynamic parameters. Then, a towing tank test happens, which is used to determine take-off performance. Next, wind tunnel tests occur, before a scaled model of the aircraft is flown. For all steps following the CFD analysis, a scaled model is needed, making these steps significantly more challenging considering the schedule and the budget.

During the design optimisation process of IDINTOS, a vortex lattice method, namely Athena Vortex Lattice (AVL), is used to find estimates for the parasite drag, with an operational empty weight (OEW) found from an empty weight model with constant surface density for fuselage and wing [18]. The stall speed is estimated from the lift coefficient.

For the CFD analysis, various flight conditions must be investigated. For the amphibious aircraft, three are analysed [18]. The first one, water take-off, is not relevant for the E-Racer. However, the other two, high-speed and low-speed flight, will need to be performed in the analysis.

8.1.2. Wing Parameters

During literature, it was found that the two wings of typical Prandtl designs have equal surface area [19, 20, 21]. Therefore, it was decided to divide the total wing area equally between the forward and aft wings.

The quarter chord sweep angles of the initial planform design of the two wings have been decided using a similar Prandtl design [8]. Also, in general, Prandtl designs have negative sweep for the aft wing and positive sweep for the forward wing [11]. Thus, the initial quarter chord sweep angle of the forward wing is equal to 25 [$^\circ$], and the quarter chord sweep angle of the aft wing is equal to -11 [$^\circ$].

Similarly, for the dihedral angles of the initial planform design, it was decided to choose a dihedral of 6 [$^\circ$] for the forward wing and a dihedral of -2 [$^\circ$] for the aft wing [11].

8.2. Initial Planform Design

The method presented by Torenbeek [22] is used for the initial platform design. First, the taper ratio is calculated from the quarter chord sweep angle obtained from the literature study using Equation 8.1. It should be noted that this design method states that sweep is not needed below a cruise speed of 0.7 Mach. However, the Prandtl plane configuration requires sweep on both wings, in order to be able to effectively connect them. From the taper ratio, the root chord and tip chord lengths can be obtained by using Equation 8.2 and Equation 8.3. Here, $\Lambda_{c/4}$ is the quarter chord sweep, S is the wing area, and b is the span. The sweep angles used in the calculations are taken from Section 8.1.2. Also, it is important to mention that the total surface area suffered a minor change with respect

to the values in Table 7.6, as the mass of the aircraft decreased to 715 [kg]. Therefore, with the same wing loading, the new surface area is equal to 8.3 [m^2].

$$\lambda = 0.2(2 - \Lambda_{c/4}) \quad (8.1) \qquad c_r = \frac{2 \cdot S}{(1+\lambda)b} \quad (8.2) \qquad c_t = \lambda \cdot c_r \quad (8.3)$$

Next, the length of the mean aerodynamic chord (MAC) can be obtained from Equation 8.5. Additionally, with Equation 8.6, the location of the MAC along the wing is calculated.

$$\tan(\Lambda_n) = \tan(\Lambda_m) - \frac{4}{A}(n-m)\frac{1-\lambda}{1+\lambda} \quad (8.4)$$

$$MAC = c_r \cdot \frac{2}{3} \cdot \frac{1+\lambda+\lambda^2}{1+\lambda} \quad (8.5) \qquad y = \frac{b}{2} \cdot \frac{c_r - MAC}{c_r - c_t} \quad (8.6)$$

In order to find the thickness-to-chord ratio of the airfoil, the lift coefficient is required and can be calculated using Equation 8.8. To find the dynamic pressure for finding the lift coefficient, Equation 8.7 is used. The density is obtained by assuming an altitude of 12,500 $[m]$, which results in a density of 0.2354 [kg/m^3][1]. Moreover, the leading edge sweep and half-chord sweep can be calculated by using Equation 8.4 and afterwards can be put in Equation 8.9 to obtain the thickness-to-chord ratio. M^* is the technology factor defined by Torenbeek and is equal to 0.935. M_{dd} is the drag divergence Mach number. The drag divergence Mach number is assumed to be 0.03 bigger than the maximum Mach number at cruise, which is equal to 0.55 at this altitude [22]. This assumption is used only for the initial planform design.

$$\bar{q} = \frac{1}{2} \cdot \rho \cdot V^2 \quad (8.7) \qquad C_L = \frac{W}{\bar{q} \cdot S} \quad (8.8)$$

$$\left(\frac{t}{c}\right) = \min\left(\frac{(\cos\Lambda_{c/2})^3 \cdot (M^* - M_{dd} \cdot \cos\Lambda_{c/2}) - 0.115 \cdot C_L^{1.5}}{(\cos\Lambda_{c/2})^2}, 0.18\right) \quad (8.9)$$

The initial wing parameters calculated with these formulae are shown in Table 8.1.

Table 8.1: Initial wing parameters of the forward and aft wing

Forward wing								
Wing Parameter	**Value**	**Unit**	**Wing Parameter**	**Value**	**Unit**	**Wing Parameter**	**Value**	**Unit**
Quarter chord sweep	25	°	Root chord	0.86	m	Span	7.33	m
Leading edge sweep	27.5	°	Tip chord	0.27	m	Aspect ratio	12.96	–
Taper ratio	0.31	–	t/c	0.18	–	Surface area	4.15	m^2
MAC	0.62	m	Dihedral	6	°	y-location MAC	1.49	m
Aft wing								
Wing Parameter	**Value**	**Unit**	**Wing Parameter**	**Value**	Unit	**Wing Parameter**	**Value**	Unit
Quarter chord sweep	-11	°	Root chord	0.79	m	Span	7.33	m
Leading edge sweep	-7.5	°	Tip chord	0.35	m	Aspect ratio	12.96	–
Taper ratio	0.44	–	t/c	0.18	–	Surface area	4.15	m^2
MAC	0.6	m	Dihedral	-2	°	y-location MAC	1.58	m

8.3. Optimising Wing Planform

The wing planform was optimised by doing two main iterations. The first iteration was to optimise the wing planform such that drag is minimised. The goal of the second iteration was to design the wing planform to be stable, while not sacrificing too much drag.

8.3.1. First iteration

With the initial parameters calculated, a model of the aircraft could now be used in a vortex lattice method (VLM) model. It was decided that AVL would be used for this, as this was found to be the most commonly used tool in papers studying similar aircraft, as explained in Section 8.1.1. In order to also simulate the fuselage, it was modelled as a horizontal and a vertical plane. The size of these was initially estimated based on the packaging of all required items in the fuselage.

[1] `https://www.engineeringtoolbox.com/international-standard-atmosphere-d_985.html` [Accessed on 03-06-2024]

The goal of this model is to minimise drag during cruise, as this takes up the largest amount of time during the flight. Firstly, possible airfoils for the aircraft were found. These airfoils were obtained from TU Delft's database[2]. The airfoils were tested for minimum drag with the requirement that their thickness must be between 11% and 18% thickness to chord ratio. These numbers were chosen to limit the amount of airfoils to be tested, with thinner airfoils considered to not be large enough to carry anything in the wing and larger airfoils considered to cause too much drag. After testing all the airfoils on the aircraft, giving both wings the same airfoil, 20 airfoils were found that gave the lowest drag for the same conditions. From this, the NACA M12 airfoil was selected. This process is done multiple times throughout the design when new planform parameters are obtained.

Once the airfoil was selected, the parameters of the wing planform were iterated. When iterating these, minimising drag and increasing stability were considered important. As spiral stability is given by the AVL program and no information on the centre of gravity (CG) was known at that moment, increasing this was found to be the clearest initial indicator for stability. Firstly, the sweep of both wings was varied. It was found that for the front wing, increasing sweep increased drag, however also provided more spiral stability. For the aft wing, making the sweep more negative decreased drag, while it didn't have a proportional relationship with spiral stability. Next, the dihedral of both wings was varied. For the front wing, increasing dihedral tended to give more drag, but it also showed good improvement for the spiral stability. Meanwhile, making the dihedral more negative on the aft wing had negative effects on both drag and spiral stability. After this, the taper ratio of both wings was tested. Increasing the taper ratio of the front wing improved spiral stability while having a varying effect on drag. For the back wing, increasing the taper ratio decreased spiral stability while having a minimal effect on drag. Following this, the twist of each wing was tested. For both, it was found that increasing twist had a very negative effect on drag, while slightly improving stability. Next, the vertical and horizontal distance between the two wings was varied. Increasing vertical distance had a positive effect on both drag and stability. However, the unknown negative effects on the structure were deemed to be too great to ignore. Increasing horizontal distance had no effect on drag, while spiral stability was increasing. After this, the span of both wings was varied, keeping the total surface area of the wings the same. This greatly increased stability while having a varying effect on drag. Finally, the incidence angle of the two wings was varied. However, it was found that this would increase stability while increasing drag.

8.3.2. Second iteration

While the first iteration focused on minimising drag, with stability being analysed only based on the spiral stability, as mentioned in Section 8.3.1, the second iteration included the position of the centre of gravity into account, as more in-depth analysis into stability was required. Also, at this point of the detailed design, some estimation of the position of the CG was made available by the Structures department. Therefore, the wing planform parameters such as sweep and taper ratio were once again iterated, with the main focus on being stable at the given CG, with drag often being sacrificed to this end. The methods for checking stability are further discussed in Chapter 9. At the end of this iteration, the best 20 airfoils previously analysed in Section 8.3.1 were checked again and it was observed that the OAF128 airfoil[3] performed better than the others in terms of both drag and stability.

8.4. Stall

One of the flaws with the AVL software is that it does not predict stall, as it considers a linear lift coefficient slope for all angles. Prandtl planes are prone to stall in one of two ways. Firstly, one of the wings can stall individually due to too high of an angle of attack. Secondly, the front wing will create a wake and, at high angles of attack, the back wing can be located in this wake. If this happens, the aft wing will provide less lift, causing a severe increase in the angle of attack.

For the first case, the stall angle of the airfoil is used as an estimate for the wing, which is a conservative estimate. For high Reynolds numbers, which the aircraft wing will be subjected to, the OAF 128 airfoil will stall at around 15 [°] angle of attack. Due to the selected incidence angle on the front wing of 2.6 [°], the stall angle of attack of the aircraft is 12.4 [°]. Furthermore, a precaution taken to prevent complete stalling of the aircraft in this case is having a greater incidence angle on the front wing than on the aft wing. If the maximum angle of attack is exceeded, the forward wing will stall first. Due to the severe decrease in lift on the front wing, the angle of attack will greatly decrease as the lift on the aft wing has not changed. This will prevent the full stall from occurring. Furthermore, the stall of the wing across the span can have an effect on the aircraft, however, the wing is assumed to stall spontaneously, with further analysis possible on this.

The second case for the aircraft stall, the wake, is considered to be less important. Due to the short length of the

[2] https://aerodynamics.lr.tudelft.nl/cgi-bin/afCDb [Accessed on 03-06-2024]
[3] https://aerodynamics.lr.tudelft.nl/cgi-bin/afCDb?oaf128 [Accessed on 03-06-2024]

fuselage and the significant height difference between the two wings, the angle between the line caused by the most forward part of the front wing and the most aft part of the aft wing and the body of the aircraft is 24 [°]. As the maximum angle of attack of the aircraft is 12.4 [°], this case of stall is considered to not be driving.

8.5. Verification and Validation

To confirm the results of the AVL program are usable for this project, verification and validation procedures are performed. As this program was not written in-house, it was possible to find a validation procedure that has already been performed on the software [23]. As explained by Pereira R. L. [23], using software such as AVL, Tornado[4] or Panair[5] is the best way of getting the most accurate results. In the case of this project, only one was used due to time constraints. However, Pereira also says that while AVL becomes very unreliable at transonic flows, anything below a speed of 0.7 Mach returns reliable results. Due to the E-Racer's lower Mach of 0.55, the software is viable. The data shown by Pereira proves that the program is functional for non-transonic aircraft, which leads to the conclusion that using it to model the aircraft is a valid option.

One possible room for error while using the AVL software comes from the way the model is created. As the coordinates of various parts of the aircraft need to be written into the program, it can be easy to make mistakes throughout the file, in particular when changing the parameters of the wing planform. To avoid this, verifying the model is found to be useful. This was done by loading a visual representation of the aircraft in the program and rotating it in order to find any errors in the location of aircraft parts.

A second possible error could arise from the type of aircraft being designed. As the Prandtl plane is an unconventional aircraft configuration, there could be inaccuracies occurring. However, as it has been used in other papers, as stated in Section 8.1, it is considered to be valid here.

8.6. Final Wing Planform

The final wing planform is obtained after the second iteration converges, such that all stability parameters and drag have been manually optimised, based on the values given by the other departments. Some values include the hydrogen mass and tank position, in order to obtain the distance the CG varies, the initial position of the CG when the hydrogen tank is full, or the required lift coefficient based on the speed, mass, and altitude during cruise.

Also, it should be noted that, based on the final wing planform, the aircraft has to cruise at an angle of attack of 2 [°] in order to achieve the desired lift coefficient of 0.3632. As seen from Table 8.2, the lift coefficients of the two wings sum up to only 0.3594. This is because the fuselage also has a contribution to the lift coefficient, which is equal to 0.0038, which is not considered representative, because of the way the fuselage has been rendered in the AVL.

8.6.1. Final Aerodynamic Parameters

After iteration for both drag and stability, the wing planform returns the parameters presented in Table 8.2. After the optimisation, it was determined that it was best for both wings to have the same surface area, as this was beneficial for stability. Therefore, the only difference between the two wings is the sweep, dihedral, and incidence angle.

Table 8.2: Final wing parameters of the forward and aft wing

Forward wing								
Wing Parameter	**Value**	**Unit**	**Wing Parameter**	**Value**	**Unit**	**Wing Parameter**	**Value**	**Unit**
Quarter chord sweep	33.5	°	Root chord	0.64	m	Span	7.46	m
Leading edge sweep	34.1	°	Tip chord	0.51	m	Aspect ratio	12.96	–
Taper ratio	0.80	–	t/c	0.128	–	Surface area	4.29	m^2
MAC	0.58	m	Dihedral	4	°	$C_{L_{cruise}}$	0.2416	–
y-location MAC	1.79	m	Incidence	2.6	°	Twist	0	°
Aft wing								
Wing Parameter	**Value**	**Unit**	**Wing Parameter**	**Value**	**Unit**	**Wing Parameter**	**Value**	**Unit**
Quarter chord sweep	-8.1	°	Root chord	0.64	m	Span	7.46	m
Leading edge sweep	-7.1	°	Tip chord	0.51	m	Aspect ratio	12.96	–
Taper ratio	0.80	–	t/c	0.128	–	Surface area	4.29	m^2
MAC	0.58	m	Dihedral	0	°	$C_{L_{cruise}}$	0.1178	–
y-location MAC	1.79	m	Incidence	0	°	Twist	0	°

Furthermore, the parameters for the vertical stabilisers of the aircraft are presented in Table 8.3. These stabilisers

[4] `https://tornado.redhammer.se/index.php/about` [Accessed on 12-06-2024]
[5] `https://www.pdas.com/panair.html` [Accessed on 12-06-2024]

were mostly designed to connect the wings and to connect the fuselage to the wings. The two side stabilisers are the same and are thus only given once in the table.

Table 8.3: Final stabiliser parameters for the middle and side stabilisers

Middle Stabiliser								
Parameter	**Value**	**Unit**	**Parameter**	**Value**	**Unit**	**Parameter**	**Value**	**Unit**
Quarter chord sweep	8.56	°	Root chord	0.480	m	Height/Span	1.02	m
Leading edge sweep	13.0	°	Tip chord	0.320	m	Aspect ratio	2.51	–
MAC	0.405	m	Taper ratio	0.667	–			
Side Stabiliser								
Parameter	**Value**	**Unit**	**Parameter**	**Value**	**Unit**	**Parameter**	**Value**	**Unit**
Quarter chord sweep	4.61	°	Root chord	0.511	m	Height/Span	1.23	m
Leading edge sweep	4.61	°	Tip chord	0.511	m	Aspect ratio	2.41	–
MAC	0.511	m	Taper ratio	1.0	–			

Finally, the model created by the AVL program using the final parameters is presented in Figure 8.1.

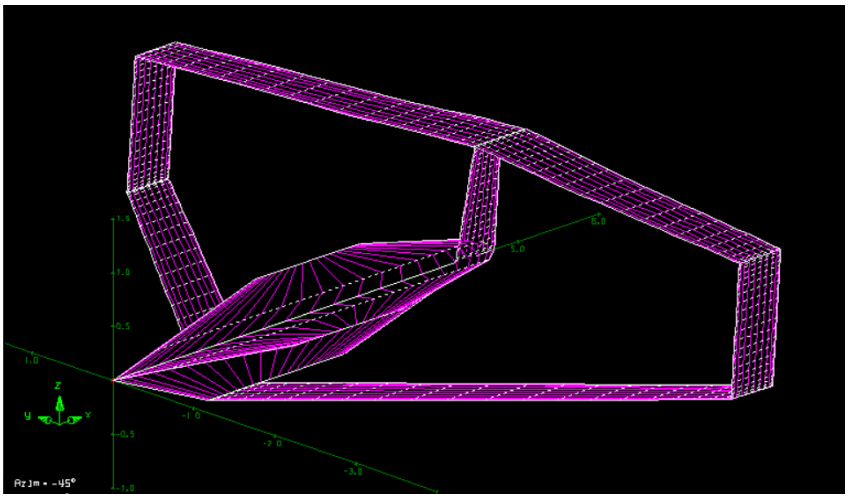

Figure 8.1: Model created by AVL

8.6.2. Lift & Drag Polars

Finalising the planform design means that the lift and drag polars of the whole aircraft can be constructed using the AVL software. The angles of attack that have been considered are between -12 [°] and 12 [°], as more extreme angles would most likely stall the aircraft, something that is not modelled within AVL, as mentioned in Section 8.4. The lift and drag polars are shown in Figure 8.2. Also, it is important to mention that these plots are made for cruise conditions only, as the cruise represents the biggest part of the flight mission.

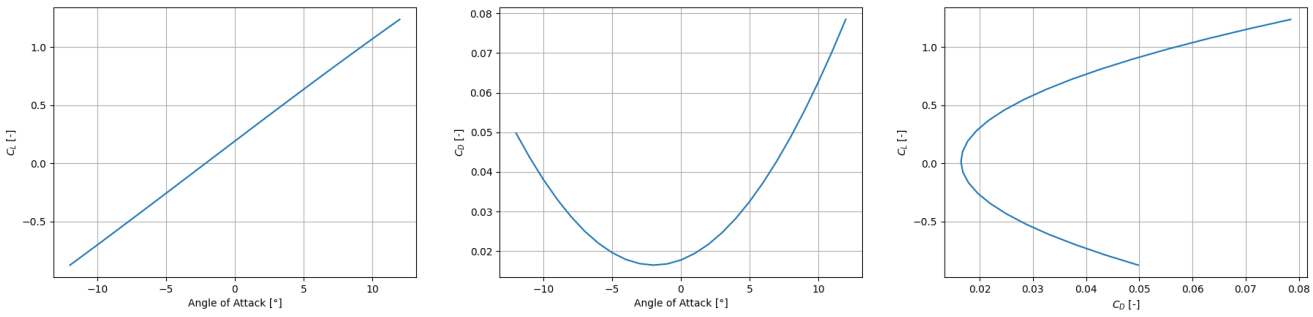

(a) C_L vs. angle of attack **(b)** C_D vs. angle of attack **(c)** C_L vs. C_D

Figure 8.2: Lift and drag polars

9. Stability & Control

Stability and control are crucial to the aircraft's functionality. Not being stable could lead to the aircraft losing control due to small disturbances or requiring expensive alternative solutions, such as an autopilot, while low controllability can lead to failure to complete the mission. This chapter will focus on ensuring the aircraft is both stable and controllable. To this end, the aircraft is first tested for moment equilibrium during cruise in Section 9.1, then for stability in Section 9.2. Finally, to ensure controllability, control surfaces are sized for the aircraft in Section 9.3.

9.1. Moment Equilibrium

Determining moment equilibrium was a crucial factor in determining the lift distribution across the two wings. While an equal lift provided by both wings is considered optimal for aircraft efficiency [20], this is seen as impossible for the moment equilibrium, due to the position of the centre of gravity. However, it was still decided to get as close to this goal as was deemed possible for this aircraft without having a negative impact on drag. A visual representation of the free body diagram of the aircraft that has been used in the analysis of moment equilibrium is shown in Figure 9.1.

To determine the percentage of lift that can be carried by each wing, moment calculations are performed on the aircraft during cruise, as this is the longest flight phase and hence the most important for an efficient flight. Since the moments are taken around the centre of gravity, the forces causing moments are: the lift provided by each wing, the drag on each wing, and the thrust at the propeller. A moment is also provided by the zero lift moment coefficient C_{m_0} acting on the aircraft, which is positive in order to have a trimmable aircraft [19]. This gives Equation 9.1. Here, all variables are defined in Figure 9.1, except for V which is the airspeed, ρ the density, S the wing surface area, and $\bar{c}$ the average chord length.

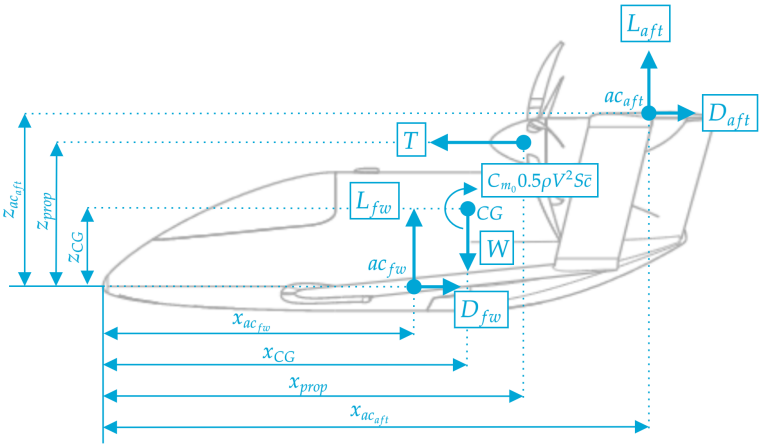

Figure 9.1: Free Body Diagram

$$L_{fw}\left(x_{cg}-x_{ac_{fw}}\right)+L_{aft}\left(x_{cg}-x_{ac_{aft}}\right)+D_{fw}\left(z_{cg}-z_{ac_{fw}}\right)+ D_{aft}\left(z_{cg}-z_{ac_{aft}}\right)+T\left(z_{prop}-z_{cg}\right)+C_{m_0}\frac{1}{2}\rho V^2 S\bar{c}=0 \tag{9.1}$$

The lift on the front wing, the drag on the aft wing, and the zero-lift moment coefficient provide a positive moment, while the lift on the aft wing, the drag on the front wing, and the thrust provide a negative moment.

The two forces with the greatest impact on the moment equation are the lift forces, as they are much greater than the other forces. Hence, to maximise the efficiency of the aircraft, it is ideal to have the CG as far aft as possible. This will minimise the moment arm for the aft wing while maximising the moment arm for the forward wing.

Based on the position of the hydrogen tank with respect to the centre of gravity and the amount of hydrogen used for the mission, the range the centre of gravity will vary throughout the flight is calculated. The most forward and most aft CG can then be used for the moment calculations. While the elevator can be used to trim the aircraft for moment equilibrium, having a small deflection would allow for the least drag. To this end, the aircraft should have a moment of zero at the middle of the range of CG.

The wing planform is first changed to find an optimal position for the CG and the aerodynamic centre of each wing. Once the desired lift distribution can be achieved, the incidence angle is varied. This causes changes to the lift distribution across the two wings as well as the zero lift moment coefficient. The two incidence angles are iterated until the aircraft has moment equilibrium for the average CG location, which can then be trimmed throughout the flight to have moment equilibrium at the most forward and aft CG. The most aft CG occurs at full tank. This is 3.0

[m]. The most forward centre of gravity location is considered to be at 2.91 [m], as the consumption of hydrogen produces a 9 [cm] shift in CG location.

9.2. Stability

Stability refers to the behaviour of the aircraft as a response to disturbances. This is investigated in two ways. Firstly, the stability coefficients of the aircraft will be investigated in order to determine static stability, then the eigenmotions will be simulated to determine dynamic stability.

9.2.1. Static Stability

The stability coefficients of an aircraft can be used to see its response to a change in roll rate, yaw rate, pitch rate, angle of attack, or sideslip. These coefficients are outputted from the AVL software, allowing them to easily be identified and investigated. For static stability, there are requirements on the signs of some stability coefficients [24].

The first three coefficients show how force in the Y direction, rolling moment, and yawing moment change with respect to the sideslip angle. The first coefficient, C_{Y_β}, is usually negative. The second, C_{l_β}, should be negative for a stable aircraft. The third, C_{n_β} should be positive for a stable aircraft. The next three coefficients show how force in the Y direction, rolling moment, and yawing moment vary with respect to a change in roll rate. The first coefficient, C_{Y_p}, is usually small and negative. The second, C_{l_p}, is often negative. The third coefficient, C_{n_p}, is usually negative. The last three coefficients show how force in the Y direction, rolling moment, and yawing moment differ with respect to a change in yaw rate. The first coefficient, C_{Y_r}, is usually small and positive. The second, C_{l_r}, is often positive. The third coefficient, C_{n_r}, is usually negative.

Another important coefficient is C_{m_α} and involves the neutral point. For static longitudinal stability, the neutral point must be behind the centre of gravity with respect to the nose, such that C_{m_α} is negative [19]. This would mean that an increase in the angle of attack would generate a stabilising pitch-down moment. While this was closely monitored, it was found that the stability coefficients were more constraining than the neutral point, and hence the neutral point was never a driving requirement. In the final design, the aircraft has coefficients of the correct sign up to a CG location of 3.06 [m] from the nose. This ensures lateral static stability up until this point and gives a margin of 5% of the sum of the average chords with respect to the most aft CG, 3.0 [m]. Furthermore, the neutral point, which must be behind the centre of gravity, is not limiting as it is at 3.47 [m].

The values for the coefficients outputted by the AVL program can be seen in Table 9.1.

Table 9.1: Stability coefficients of the E-Racer

Stability Parameters												
C_{X_u}	-0.03	C_{Z_0}	-0.17	C_{X_α}	-0.09	$C_{Z_{\dot\alpha}}$	-1.28	C_{l_β}	-0.10	C_{l_r}	0.12	C_{l_p}	-0.59
C_{Z_u}	-0.09	C_{Z_q}	0.00	C_{Z_α}	-0.09	$C_{m_{\dot\alpha}}$	-4.34	C_{n_β}	0.01	C_{n_r}	-0.06	C_{n_p}	-0.59
C_{m_u}	-0.08	C_{m_q}	-12.76	C_{m_α}	-2.07			C_{Y_β}	-0.97	C_{Y_r}	0.26	C_{Y_p}	-0.01

Of the values in the table that were previously discussed, all parameters are the correct sign, despite some being small. However, while C_{l_r} is the correct sign, it is not as small as was expected. It should be noted that vertical stabilisers have a positive contribution on the coefficient. Since the Prandtl plane has three vertical stabilisers, it follows that the coefficient would no longer be small.

Furthermore, two values in the table were not outputted by the AVL program, being $C_{m_{\dot\alpha}}$ and $C_{Z_{\dot\alpha}}$. To obtain these, other aircraft were looked at and an average of available data was taken [24]. While this does provide an initial estimate for these values, it is unsure how accurate these results are. Hence, the stability of the aircraft, which is most affected by the changing of these parameters, was checked at differing values. It was found to be stable for a large range of both these parameters, and the estimation was hence found to be reasonable.

Finally, the symmetric non-dimenional mass, μ_c, the asymmetric non-dimensional mass, μ_b, and the products of inertia, K_X^2, K_Y^2, K_Z^2. and K_{xz}^2, can be found using Equation 9.2-9.7. The moments of inertia I_{xx}, I_{yy}, I_{zz} are obtained from the model of the aircraft constructed by the Structures department.

$$\mu_c = \frac{m}{\rho S c} \quad (9.2) \qquad \mu_b = \frac{m}{\rho S b} \quad (9.3) \qquad K_X^2 = \frac{I_{xx}}{mb^2} \quad (9.4)$$

$$K_Y^2 = \frac{I_{yy}}{mb^2} \quad (9.5) \qquad K_Z^2 = \frac{I_{zz}}{mb^2} \quad (9.6) \qquad K_{xz}^2 = \frac{I_{xz}}{mb^2} \quad (9.7)$$

9.2.2. Dynamic Stability

In order to assess the dynamic stability of the aircraft, the equations of motion were used to find the eigenvalues of the aircraft. Two values not present in Table 9.1 are necessary for the solving of the equations of motion. Firstly, $C_{n_{\dot{\beta}}}$ is assumed to be zero as the aspect ratio of the wings is considered to be large [24]. Next, $C_{Y_{\dot{\beta}}}$ is also assumed to be zero, as it is considered to be negligible when compared to the non-dimensional mass.

Symmetric equation of motion

The full symmetric equations of motion are shown in Equation 9.8 [24]. These equations of motion are used to determine the stability in the short period and phugoid motion.

$$\begin{bmatrix} C_{X_u} - 2\mu_c D_c & C_{X_\alpha} & C_{Z_0} & C_{X_q} \\ C_{z_u} & C_{Z_\alpha} + (C_{Z_{\dot{\alpha}}} - 2\mu_c)D_c & -C_{X_0} & C_{Z_q} + 2\mu_c \\ 0 & 0 & -D_c & 1 \\ C_{m_u} & C_{m_\alpha} + C_{m_{\dot{\alpha}}} D_c & 0 & C_{m_q} - 2\mu_c K_Y^2 D_c \end{bmatrix} \begin{bmatrix} \hat{u} \\ \alpha \\ \theta \\ \frac{q\bar{c}}{V} \end{bmatrix} = \begin{bmatrix} -C_{X_\delta} \\ -C_{Z_\delta} \\ 0 \\ -C_{m_\delta} \end{bmatrix} \delta_e \tag{9.8}$$

Asymmetric Equations of Motion

The equations of motion for asymmetric motion can be used to check for stability in the asymmetric eigenmotions. These are the Dutch roll, aperiodic roll and spiral. The equations can be seen in Equation 9.9.

$$\begin{bmatrix} C_{Y_\beta} + (C_{Y_{\dot{\beta}}} - 2\mu_b)D_b & C_L & C_{Y_p} & C_{Y_r} - 4\mu_b \\ 0 & -\frac{1}{2}D_b & 1 & 0 \\ C_{l_\beta} & 0 & C_{l_p} - 4\mu_b K_X^2 D_b & C_{l_r} + 4\mu_b K_{XZ} D_b \\ C_{n_\beta} + C_{n_{\dot{\beta}}} D_b & 0 & C_{n_p} + 4\mu_b K_{XZ} D_b & C_{n_r} - 4\mu_b K_Z^2 D_b \end{bmatrix} \begin{bmatrix} \beta \\ \varphi \\ \frac{pb}{2V} \\ \frac{rb}{2V} \end{bmatrix} = \begin{bmatrix} -C_{Y_{\delta_a}} \\ 0 \\ -C_{l_{\delta_a}} \\ -C_{n_{\delta_a}} \end{bmatrix} \delta_a + \begin{bmatrix} -C_{Y_{\delta_r}} \\ 0 \\ -C_{l_{\delta_r}} \\ -C_{n_{\delta_r}} \end{bmatrix} \delta_r \tag{9.9}$$

Eigenvalues

After considering the matrices, the eigenvalues can be calculated by finding the characteristic equations and applying the quadratic formula, as described in [24]. This results in the eigenvalues given in Table 9.2. From these eigenvalues, it can be concluded that the aircraft is stable in all eigenmotions, although for the phugoid and spiral motion, the aircraft is barely stable. The eigenvalues of eigenmotions are given in Table 9.2.

Table 9.2: Non-dimensional eigenvalues of each eigenmotion

	Eigenvalue	Stability
Short period	-2.0489324±7.78037652j	Stable
Phugoid	-0.00320908±0.06637981j	Stable
Aperiodic roll	-2.2143064236	Stable
Dutch roll	-0.18140553±1.4562472j	Stable
Spiral	-0.0403012779	Stable

9.3. Control Surfaces

Sizing control surfaces based on critical cases allows the aircraft to be controllable throughout all phases of the mission. For the placement of each control surface, it was decided to keep them separate. This is done since the highest efficiency for each surface happens at different locations. For the ailerons, they should be as far as possible from the centre of gravity in the spanwise direction, leading to them being on the tips of the wings. Next, for the elevators, the ideal position is as far away from the centre of gravity along the fuselage. Due to the sweep of the wings, this occurs closest to the fuselage. Finally, the rudder must be placed on a vertical surface, with the only available space being the middle and side stabilisers.

9.3.1. Aileron Sizing

In order to begin with the sizing of the ailerons, a roll rate for maximum deflection has to be decided upon. This is done by using the value given by a class I aircraft, which is represented by a small and light aircraft, category B, as the flight mission includes climb, cruise, loiter, and descent, and level 3 because the worst flying quality level can be considered as turning is not crucial in achieving the mission [25]. Therefore, the aircraft must be able to roll 60 [°] in 3.4 seconds, which would equal a constant roll rate of $p \approx 17.65$ [$^\circ/s$].

In order to check if the target roll rate is achieved, different parameters in Equation 9.10 will be iterated [26]. Those parameters are the spanwise start and end position and the chord ratio with respect to the wing of the aileron.

$$p = -\frac{C_{l_{\delta a}}}{C_{l_p}} \cdot \delta_a \cdot \frac{2V}{b} \tag{9.10}$$

$$\tau_a = 1.129 \cdot \left(\frac{C_a}{C}\right)^{0.4044} - 0.1772 \tag{9.11}$$

The maximum deflection angles have been decided based on values from similar aircraft [26]. Therefore, the maximum deflection angles are equal to ± 20 [°]. However, the maximum deflection during flight is assumed to be equal to only 75% of that, which means that $\delta_a \pm 15$ [°] will be used in the analysis. This is because the ailerons stretch during the flight, therefore reducing the effective deflection. Also, stall velocity has been used in the calculation in order to achieve the required roll rate at the most critical velocity, which is equal to 40 $[m/s]$.

In order to obtain the aileron control derivative $C_{l_{\delta a}}$ and the roll damping coefficient C_{l_p}, Equation 9.12 and Equation 9.13 are used [26].

$$C_{l_{\delta_a}} = \frac{2 \cdot c_{l_\alpha} \cdot \tau_a}{S_{ref} \cdot b} \int_{b_1}^{b_2} y \cdot c(y) dy \tag{9.12}$$

$$C_{l_p} = -\frac{4 \cdot (c_{l_\alpha} + c_{d_0})}{S_{ref} \cdot b^2} \int_0^{b/2} y^2 \cdot c(y) dy \tag{9.13}$$

In Equation 9.12 and Equation 9.13, c_{l_α} and c_{d_0} are the airfoil's 2D lift curve slope and drag coefficient, which are known as the airfoil used is the OAF128[1]. Also, S_{ref} represents the area in $[m^2]$ of the wing enclosed by the spanwise start (b_1) and end (b_2) positions in $[m]$ of the aileron. It is also important to mention that $c(y)$ is the chord function with respect to the span. Also, the symbol for aileron effectiveness is τ_a and it is computed using Equation 9.11, where it only depends on the chord ratio of the aileron C_a/C.

As the Prandtl plane has two main wings, it was observed that the surface of the ailerons required to perform the roll rate mentioned above would be smaller if the ailerons were sized on both wings. This is because more area would be concentrated close to the tips of both wings, which allows it to be further away from the centre of gravity. This would result in a greater moment arm. That is the main reason why the size of the ailerons is smaller than other conventional aircraft, as worse roll rate requirements are used and having two wings allows for more area towards the tip [26].

As the wings have the same taper ratio, surface area, and wingspan, the ailerons are considered to be the same size on both wings. In order to calculate the total roll rate of the ailerons, the sum of the roll rate of each pair of ailerons is needed.

Therefore, after optimising ailerons to achieve the required roll rate with the smallest possible area in order to save weight, the final size of the ailerons is shown in Table 9.4. Also, it is important to mention that further analysis is required for different conditions, such as the one-engine operative situation. Additionally, more investigation can be performed on the interaction between the wings, when the ailerons are deployed.

9.3.2. Elevator & Flap Sizing

The elevator sizing is done by partially following the method described by Al-Shamma, Orman et al. [27], which uses the moment around the landing gear at take-off to size the elevators. It was decided to have a maximum deflection of ± 25 [°] for the elevators. First, the linear acceleration is calculated by using the equation of motion presented as Equation 9.14, where the friction force is calculated by assuming a friction coefficient of 0.04. Then, the lift for take-off can be calculated by using Equation 9.15. The total lift is provided by the front and aft wing.

$$T - D - \mu_f(W - L_{TO}) = ma \tag{9.14}$$

$$L = C_L \frac{1}{2} \rho V_R^2 S = L_{fw} + L_{aft} \tag{9.15}$$

Here T is the thrust, D is the drag, μ_f is the roll friction coefficient, L_{TO} is the lift at take-off, m the mass, and a the acceleration. Furthermore, V_R is the speed at rotation. Next, all moments are calculated around the point of rotation, which is the point where the landing gear touches the ground. For the CG location, the most aft CG location was used. The angular acceleration at take-off, $\ddot{\theta}$, was decided to be 10 $[deg/s^2]$ [27]. Afterwards, the desired lift distribution between the two wings was found, such that the moment in Equation 9.16 was as close to zero as possible, where x_{mg} and z_{mg} are the x and z locations of the rotation point, respectively, and I_{yy} is the moment of inertia about the y-axis.

$$\begin{aligned} M = W(x_{CG_{fw}} - x_{mg}) + L_{fw}(x_{ac_{fw}} - x_{mg}) + L_{aft}(x_{ac_{aft}} - x_{mg}) + D_{fw}(z_{ac_{fw}} - z_{mg}) \\ + D_{aft}(z_{ac_{aft}} - z_{mg}) + T(z_{prop} - z_{mg}) + ma(z_{CG} - z_{mg}) = I_{yy}\ddot{\theta} \end{aligned} \tag{9.16}$$

Then, an initial size for the elevator is chosen. The ratio between the chord of the elevator and the chord of the aft wing c_e/c_{aft} is chosen to be 0.2, as there are important systems that are placed in the wing. Furthermore, the stall

[1] http://airfoiltools.com/airfoil/details?airfoil=oaf128-il

angle decreases with an increase in c_e/c_{aft} [27]. Additionally, the span of the elevators was iterated using AVL, in order to achieve the lift distribution that satisfies the desired lift distribution, while still providing the C_L needed for lift-off. It was then found that, with a deflection of ± 25 [°], it was not possible to only have elevators on the back wing, as the angle of attack needed to provide enough lift would be higher than the stall angle. Therefore, at this point, it was decided to add plain flaps to the front wing.

The implementation of flaps was done in the same way. A ratio between the chord of the flap and the chord of the forward wing (C_f/C_{fw}) of 0.2 was used, for the same reasons as stated before. Next, the span and deflection of the flaps and the span of the elevators were iterated in AVL, until the desired lift distribution and C_L were achieved, at an acceptable angle of attack that would not result in the aircraft stalling.

Table 9.3: Flap and elevator deflections per flight phase

Flight Phase	Flap Deflection	Elevator Deflection
Take-off	25 [°]	-20 [°]
Climb	25 [°]	12 [°]
Cruise	0 [°]	0 [°]
Approach	47 [°]	4 [°]

Take-off was assumed to be limiting for the first estimation of the elevator size. To verify this assumption, climb, cruise, and landing were also considered by using the same method where the moment was then taken around the centre of gravity. It was determined that the flap size was limited by landing, while the elevator size was limited by climb. This resulted in flaps from 0.2 to 0.7 of the span. Elevators, which include trim tabs, are placed from 0.1 to 0.33 of the span. The deflections needed for each of the flight phases are shown in Table 9.3.

9.3.3. Rudder Sizing

In order to size the rudders, it is important to know the critical conditions of the aircraft. For this design, these are chosen to be landing with cross-winds and flying with one propeller inoperative [28]. For the first case, landing with cross-winds of 20 [kts] seemed to be a reasonable goal as per regulations [29]. Using the method as described by Al-Shamma, Omran et al. [28], an initial estimate for the size of the rudder was decided. This was chosen from other aircraft for which the information was available [30]. This gave an initial estimate for size ratios C_r/C_v = 0.32 for the chord and b_r/b_v = 0.87 for the span. The total speed of the aircraft was then found using a landing speed V_f of 40 [m/s] and the crosswinds V_w found earlier with Equation 9.17.

Next, the projected area of the aircraft on the XZ plane S_s, as well as its centroid, are found and used to determine the force caused by the wind, as well as where it acts. The distance between the centre of gravity and the centroid is then determined to find the moment caused by the wind. The side force caused by the wind can finally be found with Equation 9.18. In this equation, C_{d_y} is the side drag of the aircraft, which often lies in the range of 0.55 to 0.8, with a value of 0.8 being used in this report to represent the worst wind force. Additionally, the sideslip β angle can be calculated using Equation 9.19.

$$V_t = \sqrt{V_f^2 + V_w^2} \qquad (9.17) \qquad F_w = \frac{1}{2}\rho V_w^2 S_s C_{d_y} \qquad (9.18) \qquad \beta = \arctan(\frac{V_w}{V_f}) \qquad (9.19)$$

Next, the stability parameters C_{n_β} and C_{y_β} need to be known. While these could be obtained through equations, it was decided to take these from the VLM model which has been created as this was deemed more accurate.

From the rudder size, the rudder angle of attack effectiveness can be determined using Equation 9.11. Following this, some necessary control derivatives $C_{n_{\delta r}}$ and $C_{Y_{\delta r}}$ can be calculated with Equation 9.20 and Equation 9.21.

$$C_{n_{\delta r}} = -C_{l_{\alpha_v}} \bar{V}_v \eta_v \tau_r \frac{b_r}{b_v} \qquad (9.20) \qquad C_{y_{\delta_r}} = C_{l_{\alpha_v}} \eta_v \tau_r \frac{b_r S_v}{b_v S} \qquad (9.21)$$

Where $\bar{V}_v$ is the vertical tailplane volume, η_v is the dynamic pressure ratio, and τ_r is the rudder effectiveness. This is assumed to be the same as the dynamic pressure ratio for a horizontal tail. The standard for this is between 0.85 and 0.95 [31], so a value of 0.9 was selected.

Finally, the rudder deflection and the crab angle, σ_c, are calculated with the rudder needing to be resized if the deflection is found to be greater than 30 [°]. The equations used to find the rudder deflection δ_r and the crab angle σ are Equation 9.22 and Equation 9.23.

$$\frac{1}{2}\rho V_t^2 S b \left(C_{n_0} + C_{n_\beta}(\beta - \sigma_c) + C_{n_{\delta r}}\delta_r\right) + F_w d_c \cos\sigma = 0 \qquad (9.22)$$

$$\frac{1}{2}\rho V_w^2 S_s C_{d_y} - \bar{q} S \left(C_{y_0} + C_{Y_\beta}(\beta - \sigma_c) + C_{y_{\delta_r}}\delta_r\right) = 0 \qquad (9.23)$$

Where d_c from Equation 9.22 indicates the distance in the x direction between the centroid and the centre of gravity.

The rudder deflection was found to meet the previously stated requirement, and hence the next case can then be investigated.

For this case, the minimum controllable speed of the aircraft must be determined. For an initial estimate, it is recommended for the aircraft to be functional at 80% of the stall speed [28]. Next, the maximum yawing moment can be calculated using Equation 9.24.

$$N_a = -T_L y_t \tag{9.24}$$

$$\delta_r = \frac{T_L y_t}{-\bar{q} S b C_{n_{\delta_r}}} \tag{9.25}$$

In Equation 9.24, T_L is the drag with one engine inoperative, which is equal to the drag of the aircraft, while y_t is the distance in the y direction between the centre of gravity and propeller.

The rudder deflection is then calculated using Equation 9.25, where $\bar{q}$ is the dynamic pressure. It was found that for the given rudder size, the rudder deflection was too great. The rudder size was increased. However, it was found that the aircraft would require an all-moving tail in order to be operational with one propeller inoperative. Hence, it was decided to put rudders on all three vertical stabilisers, including the surfaces connecting the two wings. To size these, the three rudders were given the same size for simplicity. Relevant parameters such as vertical tail area and distance to the aerodynamic centre were then considered the weighted average based on area.

The moment required for the total aircraft is then divided by three and this moment is used to find the rudder deflection for each rudder. The rudders are resized until the rudder deflection is reasonable, 24.1 [°]. A lower number is chosen to account for assumptions made during the sizing procedure.

This led to all rudders having the same size relative to the vertical stabiliser they were attached to, with the numbers presented in Table 9.4.

9.3.4. Final Control Surfaces Sizes

After the calculations performed in Section 9.3, final values for control surface sizes and their maximum deflections are found. These numbers are presented in Table 9.4. All numbers in this table are given with respect to the surface they are placed on. A visual representation of the control surfaces is shown in Figure 9.2.

Table 9.4: Final parameters of the high lift devices and control surfaces

Aileron Parameter	**Value**	**Elevator Parameter**	**Value**
Start aileron ($a_1/(b/2)$)	0.9	Start elevator ($e_1/(b/2)$)	0.1
End aileron ($a_2/(b/2)$)	0.95	End elevator ($e_2/(b/2)$)	0.33
Aileron chord ratio (C_a/C)	0.23	Elevator chord ratio (C_e/C)	0.2
Maximum deflection (δ_a)	$\pm 20[^\circ]$	Maximum deflection (δ_e)	$\pm 25[^\circ]$
Flap Parameter	**Value**	**Rudder Parameter**	**Value**
Start flap ($f_1/(b/2)$)	0.2	Start rudder ($r_1/(b_v/2)$)	0.4
End flap ($f_2/(b/2)$)	0.7	End rudder ($r_2/(b_v/2)$)	0.9
Flap chord ratio (C_f/C)	0.2	Rudder chord ratio (C_r/C_v)	0.2
Maximum deflection (δ_f)	$60[^\circ]$	Maximum deflection (δ_r)	$\pm 30[^\circ]$

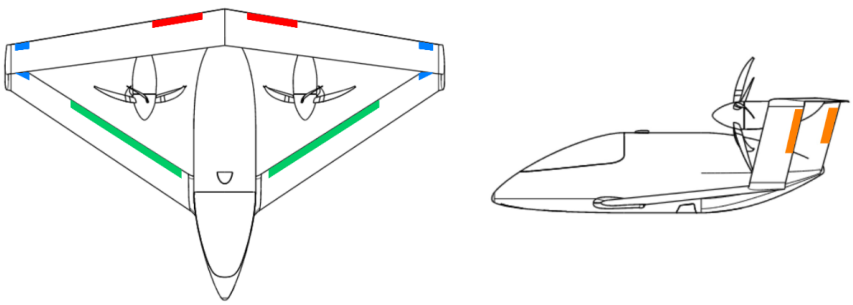

Figure 9.2: Control surfaces on aircraft. Blue surfaces are ailerons, red are elevators, green are flaps, and orange are rudders

10. Power & Propulsion

In order to propel the aircraft and power its systems, the power and propulsion system is designed. The aircraft primarily uses hydrogen for power, but batteries are used to provide additional power when required. This chapter aims to design a cohesive and effective power and propulsion system that meets the aircraft's operational needs. This chapter begins with the selection and performance analysis of a propeller in Section 10.1. Following this, the motor and its motor controller are selected in Section 10.2. With the batteries playing a significant role in the power system, a trade-off on the battery type is performed in Section 10.3. After selecting the appropriate battery type, the batteries on the aircraft are sized in Section 10.4, followed by the sizing of the capacitors in Section 10.5.

The aircraft is powered by hydrogen through the use of a fuel cell. In Section 10.6 the fuel cell and the additional air compressors are sized. Section 10.7 discusses the hydrogen tank design, followed by the design of the hydrogen tubing in Section 10.8. The cooling system is sized in Section 10.9, in which the cooling requirements are determined and the wing heat exchanger is sized. Finally, an overview of the electrical system is presented in Section 10.10, summarising how all components are interconnected.

10.1. Propeller Design

In order to propel the aircraft at altitudes up to 12,500 [m], this altitude cap is reasoned in Section 12.2, at a cruise velocity of 163 [m/s], the propeller has to be designed accordingly. This cruise altitude and velocity were found in the energy model, which will be elaborated upon in Section 12.2. Initially, research on COTS propellers was performed, but no suitable propellers were found to match the size and power requirements at this altitude. Therefore, a new propeller was designed. Various propeller design programs, including OpenProp, PropCalc, XROTOR and OpenVSP, were evaluated. OpenVSP emerged as the preferred tool. It offered greater flexibility in shape generation and provided more valuable output data for analysing the propeller performance compared to the other programs.

OpenVSP, also known as Open Vehicle Sketch Pad, is an open-source tool developed by NASA, allowing for the parametric design of aircraft and propellers[1]. Within OpenVSP, analyses can be performed on rotating propeller blades using VSPAERO. In VSPAERO, the Vortex Lattice Method (VLM) is used to solve for inviscid, irrotational and incompressible flow around the body [32]. Also, VSPAERO takes a compressibility correction factor into account to allow for compressible flow analysis [33]. Besides, a viscous correction is applied for lifting surfaces in VSPAERO. When comparing VSPAERO to another VLM solver, RoBIN, and a high fidelity CFD solver, OVERFLOW, it is deemed to be valuable in the conceptual and early design phases, where capturing the approximate solution quickly is of higher importance than obtaining a highly accurate solution [33]. VSPAERO was selected for its rapid turnaround time and its capability to model arbitrary geometries [34]. Besides, OpenVSP allows for both the design and analysis of propeller blades, making it an attractive program for estimating the propeller performance.

To design the propeller, a combination of OpenVSP and OpenProp were used. OpenProp allows for the optimisation of propellers in certain flight conditions, but cannot take into account the shock waves generated by high tip speeds [35]. Over 30 different propeller designs were created and analysed for cruise conditions. Variations across these designs involved adjustments in diameter, number of blades and propeller pitch angle. The propeller pitch angle ϕ_p, refers to the angle between the root chord line of the propeller blade and the plane of the propeller rotation. Changes in the chord length, twist, thickness, and sweep were defined and altered via a continuous function of the radius [36]. A maximum diameter was assumed to be 1.8 [m], with the propeller being placed on the rear wing. This was based on the initial sizing of the aircraft in CATIA. Placement on the front wing was not considered due to ground clearance, since only a propeller diameter of around 0.2 [m] would be possible. Placement at the rear of the fuselage would limit the diameter due to the required scrape angle.

To analyse the propeller in VSPAERO, the following parameters are put in: Mach number, free stream velocity, air density, Reynolds number, and the rotational speed of the propeller in revolutions per minute [rpm]. During cruise, the revolutions per minute are limited by the Mach number at the tips of the propeller blades. If the tip speed is near or greater than the speed of sound, shock waves will form on the propeller blades. This will increase the drag on the propeller, leading to a reduction in thrust [37]. Furthermore, the shock waves will lower the lift coefficient of the airfoil sections, causing an additional decrease in thrust. With this comes noise and, in order to maintain

[1] `https://openvsp.org/` [Accessed on 28-5-2024]

acceptable noise levels, it is recommended to limit the effective Mach number at the propeller blade tip to 0.85 [38]. This recommendation determines the rotational speed of the propeller and its diameter. To check if the chosen rotational speed and diameter result in tip speeds below this effective Mach number, Equation 10.1 is used [39].

$$V_{rot} = \frac{rpm \cdot r}{60 \cdot 2 \cdot \pi} \tag{10.1}$$

$$M_{tip} = \frac{\sqrt{V_{rot}^2 + V_{cruise}^2}}{a_{cruise}} \tag{10.2}$$

In Equation 10.1, V_{rot} is the rotational tip speed in $[m/s]$, rpm is the revolutions per minute of the propeller, and r is the radius of the propeller in $[m]$. The rotational tip speed is substituted in Equation 10.2, to calculate the Mach number at the tip. In Equation 10.2, M_{tip} is the Mach number at the tip, V_{cruise} being the cruise velocity in $[m/s]$, and a_{cruise} the speed of sound during cruise in $[m/s]$. The effective Mach number can be decreased using propeller sweep [22].

$$M_{eff} = M_{tip} \cdot \sqrt{cos(\varphi_p)} \tag{10.3}$$

With φ_p being the propeller sweep angle at the tip in [°]. Variations in the propeller sweep and revolutions per minute can be altered to meet the maximum Mach number at the tip of 0.85. A literature study has been performed to estimate the revolutions per minute for propeller aircraft cruising at high altitudes with similar speeds. It was found that typical values of the rotational speed lie between 800 and 3,000 $[rpm]$[2],[3] [40, 41, 42, 43].

After analysing the different propeller designs in OpenVSP, a five-bladed propeller with a diameter of 1.8 $[m]$ was chosen based on its relatively high efficiency during cruise. When cruising at 12,500 $[m]$ altitude, a propeller efficiency μ_p of 0.714 was found. This is achieved with a rotational speed of 2,500 $[rpm]$, propeller blade sweep of 40 [°], and a pitch angle of 27.4 [°]. Two propellers are required to meet the thrust requirement, and both are placed on the rear wing. The performance of this propeller has been analysed throughout the different phases of flight. To meet the thrust requirements at different altitudes, the propeller pitch angle ϕ_p, is altered accordingly. The thrust requirements stem from the performed flight path simulation, which will be elaborated upon in Section 12.3. For altitudes below 1,000 $[m]$, changing the propeller pitch was not enough, but an additional decrease in the rotational speed was required. The pitch angle varies from 0 to 27.4 [°] during the flight and the rotational speed varies from 2100 to 2500 $[rpm]$.

The propeller performance at different altitudes has been evaluated. The required thrust equalled the drag for these altitudes, simulating cruise conditions at different altitudes, with the goal of finding an optimal cruise altitude. In Figure 10.1, the propeller efficiency can be seen for a range of altitudes. A peak in propeller efficiency can be seen at an altitude of around 11,000 $[m]$. However, efficiency does not propel the aircraft, therefore a combination of both high efficiency and low power is preferred. As air density decreases with altitude, less power is required. This can be observed in Figure 10.2, in which the required power at one motor is shown for different altitudes. It can be seen that the required power reduces until an altitude of around 13,000 $[m]$. This sudden increase could be due to the decline of propeller efficiency from this altitude onwards. The lowest power is achieved between 11,500 $[m]$ and 12,500 $[m]$.

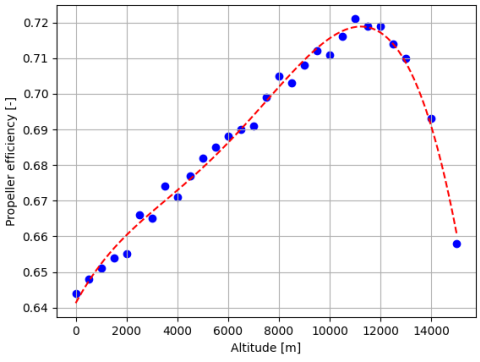

Figure 10.1: Propeller efficiency for increasing altitudes. Note that the y-axis starts at 0.64 [-], not at 0

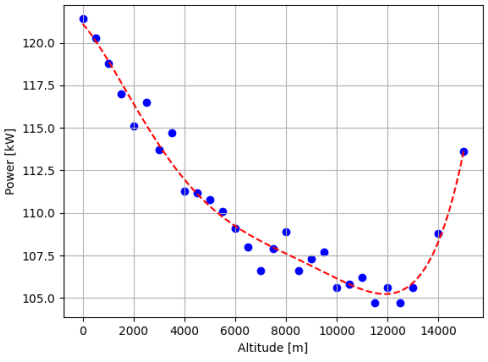

Figure 10.2: Motor power per propeller for increasing altitudes. Note that the y-axis starts at 105 kW, not at 0

[2] https://careers.rolls-royce.com/~/media/Files/R/Rolls-Royce/documents/careers/spirit-of-innovation-leaflet.pdf [Accessed on 24-5-2024]

[3] https://www.smithsonianmag.com/air-space-magazine/zwrrwwwbrzr-4846149/ [Accessed on 24-5-2024]

The two propellers are placed on the rear wing, and are counter-rotating. This is to balance the effects of torque and asymmetric loading (P-factor) [44]. The P-factor moves the centre of thrust in the direction of the downward moving propeller side, when flying at high angles of attack [44]. By using counter-rotating propellers, the torque generated by this effect is reduced. However, their respective rotation is still of importance. In case of a one-engine-inoperative situation, the moment arm is preferably as short as possible. Therefore, the following rotation of the propellers is chosen: when looking from the front of the aircraft, the left-hand propeller rotates clockwise and the right-hand propeller rotates counter-clockwise. This can also be seen in Figure 10.3. However, CFD analysis should be performed to understand the interference between the propeller and the wing. The rotating wake generated by the propeller influences the lift distribution on the wing. As the upward moving propeller blades locally increase the lift and drag, whilst the downward moving propeller generates the opposite effect [45]. Since OpenVSP does not take these effects into account, a detailed analysis using CFD would be recommended.

Typical difficulties encountered with piston engines to achieve counter-rotating propellers, such as adding a reversing gearbox or manufacturing a mirrored engine, are not found in electric motors. Generally, the same motor can operate in both directions [46]. However, a mirrored propeller would need to be manufactured. A propeller weight of 20 [kg] is estimated from existing propellers operating at a maximum of 2700 [rpm] [47]. Both propellers require propeller governors, to change the pitch angle during flight. Using the propeller governors, the motor can maintain a constant speed of 2500 [rpm] for the majority of the flight. Electrically activated propeller governors, with an accuracy of 0.1 [deg], were selected for this purpose[4]. The propeller governor can run on 24 [V] and weighs 7.4 [kg]. It is controlled through the low-voltage system, which will be explained in Section 10.10. A total feathering state can also be achieved with this pitch angle controller, reducing drag if the motor fails. In Figure 10.3, a front view of the aircraft is presented, showing the two five-bladed counter-rotating propellers. The propellers are shown in cruise condition with a pitch angle of 27.4 [°].

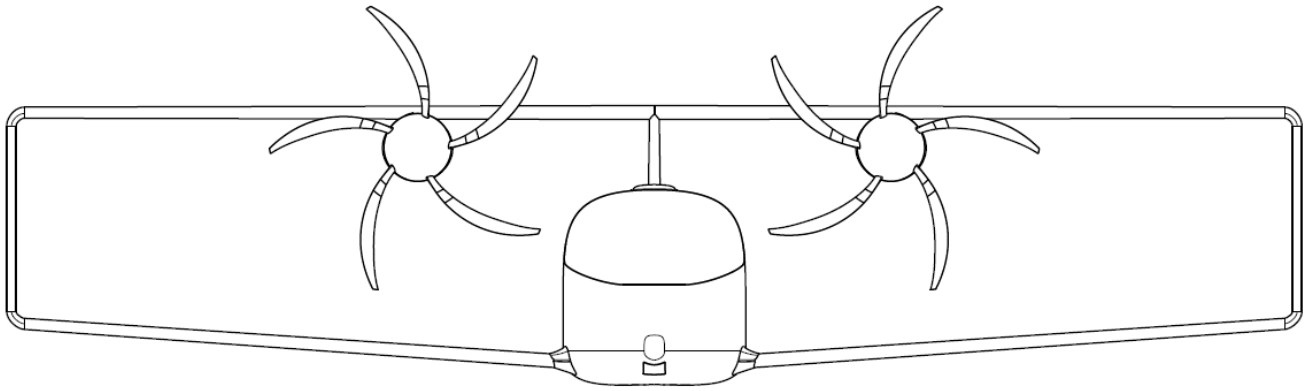

Figure 10.3: Front view of the aircraft showing the two counter-rotating propellers

10.2. Motor Selection

After the design of the propellers, the motors were sized to fit the required power and moment. To meet the thrust requirements from the flight path simulation (Section 12.3), a continuous power of 79.2 [kW] is required during cruise in combination with a moment of 303 [Nm]. A maximum power of 101 [kW] is reached during the climbing phase, with a moment of 385 [Nm]. For altitudes starting from 1,000 [m], the rotational speed of the propeller is constant at 2,500 [rpm]. The minimum rotational speed is 2100 [rpm] and is required during take-off. Motors across various motor suppliers and stacked motor options have been considered. The motor that fits the power and torque requirements the best, whilst being relatively light, is the EMRAX 348. It can deliver a continuous power of 110 [kW] and a torque of 410 [Nm], at 2,500 [rpm] with an efficiency of 96%[5]. The motor is operated at a Direct Current (DC) voltage of 600 [V], weighs 44 [kg], and is liquid-cooled.

The motor is controlled through a motor controller. The controller was chosen based on the motor requirements, such as the maximum continuous power and amperes. The Embenition MC110 2.0 motor controller was found to fit the

[4] `http://gr-engines.ru/en/catalog/propellers/5-blade-vpp` [Accessed on 12-6-2024]
[5] `https://emrax.com/e-motors/emrax-348/` [Accessed on 12-6-2024]

requirements best. It is in compliance with aviation standards DO-178C and DO254[6]. The motor controller allows for a maximum continuous power of 110 [kW]. During the flight, a maximum of 101 [kW] is achieved, therefore staying below the maximum limit. It can operate under an input voltage ranging from 65 to 800 [V]. The motor controller weighs 2.28 [kg]. As no efficiency is specified by Embenition, an efficiency of 98% is assumed, based on an existing motor controller from ZeroAvia[7]. The motor controller also allows for regenerative air braking with the propellers. This means that if the fuel cell were to fail or is switched off, the motor could generate electricity for the battery through the windmilling of the propeller. Yokota et. al [48] estimated that approximately 10% of the potential energy of the aircraft could be regenerated while descending. This energy could be used to charge the batteries and power onboard systems. Additionally, the negative thrust generated could be used as a substitute for conventional air brakes [49]. However, further analysis should be performed before this can be added to the flight strategy. This includes analysing the stability and aerodynamics of the aircraft when windmilling. Additionally, the exact amount of potential energy that can be converted should be further analysed.

10.3. Battery Design

An important part of the propulsion system is the design and layout of the batteries. The batteries are used to provide additional power during the climbing phase and enable quick power changes. To determine the battery design, the battery type needs to be determined first as many types of batteries exist. This will be done using a trade-off.

10.3.1. Battery Options

Firstly, a design options tree was created that investigates the different battery types, which is shown in Figure 10.4.

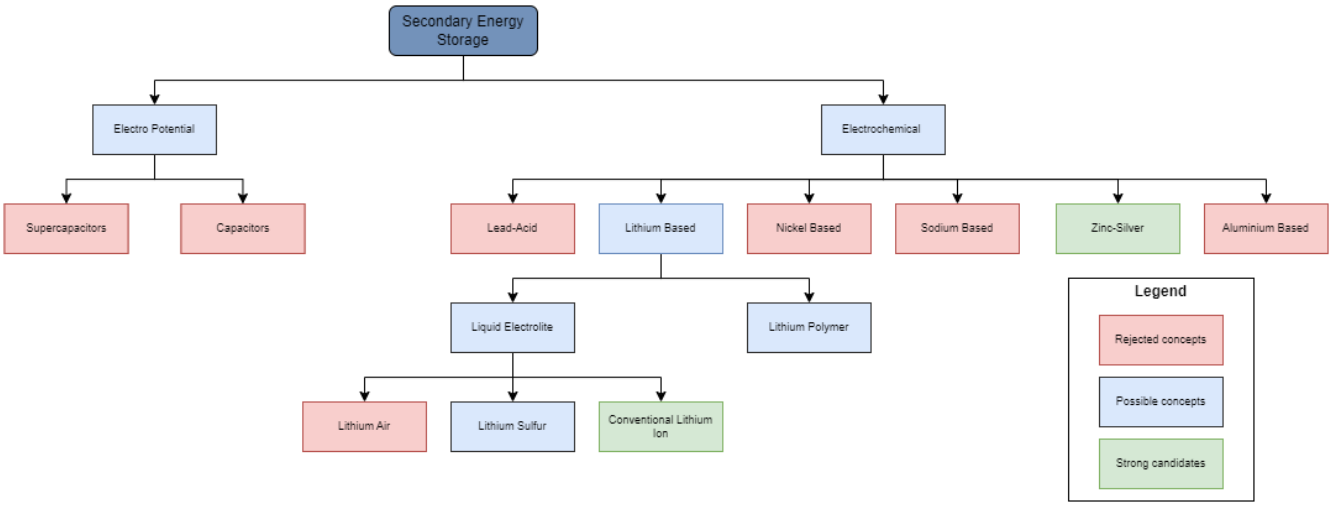

Figure 10.4: Design option tree on battery types

Figure 10.4 shows the pruned tree with the infeasible options shown in red. There are two main reasons for pruning: insufficient specific energy and technology readiness level (TRL). The reason that the focus is on specific energy instead of specific power, is that this design option tree is for a secondary energy source, not a part of the power management system. Then, the electro potential options were pruned first as they generally have too short of a discharge time, whereas for this application discharges in the range of minutes are required [50]. Section 12.3 will elaborate more on the required additional power during climb. But on average, a discharge power of 25.6 [kW] for 22 minutes is required during climb. From the electrochemical options, every battery except lithium and silver-based was pruned because of too low specific energy [51, 52, 53, 54]. Furthermore, lithium-air was pruned because of a too low TRL [55]. This results in four potential battery types that will enter the trade-off. It should be noted that zinc-silver and conventional lithium-ion batteries are considered strong candidates, as they have been used in aerospace applications before.

[6] https://www.embention.com/en/product/mc110/ [Accessed on 12-6-2024]
[7] https://zeroavia.com/wp-content/uploads/2024/05/Inverter-Single-Datasheet-3-digital.pdf [Accessed on 12-6-2024]

10.3.2. Battery Trade-Off

To determine the battery type to be used on the aircraft, a trade-off will be performed following the weighted sum model. This means that the criteria and their weight are determined, after which the battery types are scored on these criteria.

Criteria and Weights

For this application, weight is an important parameter. Furthermore, the battery should meet a certain energy storage capacity. This means that specific energy is an important aspect of the battery and is therefore a trade-off criterion. In addition, it was found that the two main differentiators between the battery types are safety and sustainability. These parameters are also of importance for the design and therefore included as trade criteria. Specific power was deemed of most importance for the design. Thus, the specific power received a weight of 50%. The safety and sustainability of the batteries were deemed of equal importance, and both have a weight of 25%.

Grading of Batteries

Firstly, the specific energy of the batteries was investigated. These values were found to differ a lot depending on the source used. The choice was made to use the most realistic values based on what has been achieved or what is expected to be achieved in the following couple of years. This resulted in the specific energies as shown in Table 10.1.

Table 10.1: Battery specific energy

Battery Type	Specific Energy [Wh/kg]
Lithium-ion	300 [56]
Lithium-Polymer	345 [57, 58]
Lithium-Sulfur	400 [59, 60]
Zinc-Silver	300 [61, 62]

Safety cannot be quantified and therefore is ranked qualitatively. Conventional lithium-ion batteries are generally safe, as they are used in billions of products today. However, certain intrinsic risks are present considering thermal runaway and abuse resistance (TEC-14-PR, Table 20.2. This leads to a safety grade of 3. Lithium-sulfur has the same intrinsic risks as lithium-ion batteries, however, their use has been limited which means this type of battery is less optimised to ensure safe use. It is generally stated that the safety of lithium-sulfur batteries is one of the areas where development is needed before widespread use[8]. Thus, lithium-sulfur batteries receive a 2 for safety. Lithium-polymer batteries do not use a liquid electrolyte thus leakage is not possible and thermal runaway risk is decreased[9]. Therefore, this is given a grade of 4. Lastly, the zinc-silver battery generally has a lower risk of thermal runaway and explosion than lithium-ion batteries. Furthermore, its components are also non-toxic. Thus, silver-zinc batteries receive a grade of 4 for safety.

Table 10.2: Battery production emissions

Battery Type	Production Emissions [kg/kWh]
Lithium-ion	139 [63]
Lithium-Polymer	98.5 [64]
Lithium-Sulfur	89.8 [65]
Zinc-Silver	-

Finally, the environmental impact of the different batteries is taken into account (SUS-01, Chapter 20, and can be estimated. A life cycle analysis approach has been taken to determine the $CO_2 - eq$, in $[kg]$, emissions during the production of the battery. This is shown in Table 10.2.

For the zinc-silver batteries, the environmental impact could not be found anywhere. However, generally, the literature states that they will be more environmentally friendly than lithium-ion batteries as fewer rare earth metals are required for their production[10]. Therefore, zinc-silver batteries are assigned a grade of 3 to be conservative.

The different types of batteries were graded with the parameters discussed in the previous paragraph. This can then be combined in a trade-off summary table, which is shown in Table 10.3.

Table 10.3: Battery trade-off summary table

Battery Type	Specific Energy	Safety	Sustainability	Score
Lithium-ion	3	3	1	2.6
Lithium-Polymer	4	4	4	4.0
Lithium-Sulfur	5	2	5	4.4
Zink-Silver	3	4	3	3.2

Table 10.3 shows that the lithium-sulfur battery is the winner of the trade-off and therefore, this will be used for the battery design. From prototype lithium-sulfur batteries, a maximum discharge and charge rate of 3C and 0.25C are

[8] https://www.tycorun.com/blogs/news/lithium-sulfur-battery-vs-lithium-ion-battery [Accessed on 27-05-2024]

[9] https://legendbatteries.com/blog/lithium-polymer-battery-vs-lithium-ion-battery-which-is-better [Accessed on 27-05-2024]

[10] https://www.ufinebattery.com/blog/what-is-the-difference-between-silver-zinc-battery-vs-lithium-ion-rechargeable/ [Accessed on 19-06-2024]

found [66]. Additionally, the pack density is calculated based on the Spirit of Innovation[11], in which the pack density is 67.5% the specific energy of the battery cell. The specific energy of the lithium-sulfur cell is 400 [Wh/kg], resulting in a pack density of 270 [Wh/kg] [59, 60].

10.3.3. Battery Safety

An important consideration for the battery design is battery safety. Lithium batteries, and thus lithium-sulfur have an inherent risk for thermal runaway (TECH-14-PR, Table 20.2). Some causes of thermal runaway are the following[12]:

1. Rapid or over-charging
2. Internal or external short circuit
3. High or low temperature environment
4. Moisture
5. Physical damage.

Considering the specific properties of the design, three of these causes are of main concern: short circuit, charging and temperature environment. Multiple measures will be taken to reduce the risks of thermal runaway concerning these causes. Furthermore, several other measures can be taken at a cell or circuit level to reduce the risk of thermal runaway. They include the following measures [67]:

- **Positive thermal coefficient (PTC) thermistors:** Thermistors are built into the battery to protect the single cell from excessive current by increasing its resistance with temperature. PTC characteristics are determined by the cell manufacturer to match the current and voltage of the cell itself.
- **PTC electrodes:** PTC thermistors are embedded in the cap of the cell, however, thermal runaway most likely occurs inside the cell. This can result in delayed activation of the PTC thermistors. Thus, the use of PTC electrodes inside the cell has shown great promise, where the current can be limited with increasing temperature inside the cell.
- **Pressure-responsive current interrupt devices (CIDs):** These serve to cut off the current from the batteries when the internal pressure reaches a specific preset value. This can protect the battery from thermal runaway in overcharging conditions.
- **Thermal fuse:** A thermal fuse made of a low melting point metal can be attached to the terminals of the cells. These will cut the current from the battery if the temperature reaches a dangerous level.
- **Safety vents:** Secondary safety vents can be installed, which will prevent battery explosion. This can be done by creating a weak spot in the battery case material such that it will rupture at that point without building up the pressure.
- **Battery management system (BMS):** This monitors the voltage, current, and temperature of the circuit. When they exceed a certain preset value, a transistor switch will be activated to disable circuits.

However, it was found that protection mechanisms at the cell level do not always guarantee protection against thermal runaway for multi-cell packs [67]. Thus, protection measures at pack level are investigated as well. Furthermore, these are of more importance for the design as the package design is directly influenced by the required capacity, while the cell design can only be influenced by choosing a certain COTS Li-S cell. The possible mitigation strategies include the following:

- **Thermal barriers:** By putting thermal barriers evenly spaced between different groups of cells, the potential thermal runaway of one cell can be contained, and the thermal runaway of the total battery pack can be avoided or delayed.
- **Phase changing materials (PCMs):** PCMs decrease the occurrence of thermal runaway by changing phase and thus through absorbing heat. This can help passively regulate the temperature of the battery depending on the type of PCM used.
- **Package structure design:** Ensuring that the package is designed such that ventilation can take place effectively. Furthermore, sufficient distance between groups of cells is required to allow for thermal barriers and PCMs.

From these different types of options to mitigate thermal runaway, a thermal runaway solution can be created. This will be based on the solutions used for the Spirit of Innovation outlined by Bingham et al. [68]. As previously mentioned,

[11] `https://evolito.aero/battery-solutions/` [Accessed on 19-6-2024]

[12] `www.emtez.co.uk/editorial/what-is-thermal-runaway-common-causes-and-how-to-prevent-it` [Accessed on 07-06-2024]

the cell will be acquired COTS. Thus, certain safety requirements can be set for the battery cell, which are listed below.

- A PTC thermistor will be present in the cell.
- PTC electrodes will be present in the cell.
- A CID will be present in the cell.

This ensures that on a cell level, the most effective protection measures are present. These will not be implemented directly in the design as the battery cells will be obtained COTS. However, these safety measures should be present in the chosen cell. The other protective strategies can be grouped into preventing, detecting, and reactive measures, which will be outlined.

The first step in mitigating is preventing thermal runaway. This will be done via two main strategies. Firstly, manufacturing defects can lead to internal short-cuts. Therefore, every cell is individually tested to determine its capacity and open-circuit voltage. Furthermore, all cells are tagged and labelled such that full traceability is possible. Secondly, a cooling system will be incorporated to ensure that the cells stay within their operative temperature. Specifically, a liquid cooling system is used, as will be explained in Section 10.9.

The second step in mitigation is detection, which is done by the BMS. To ensure that any potential thermal runaway is detected on time, the temperature of all cells is measured and monitored. Furthermore, each parallel connection is monitored for voltage to detect any spikes in voltage. Finally, the air inside the battery box is monitored for Volatile Organic Compounds (VOCs). This allows for the detection of early venting, which occurs prior to thermal runaway.

Lastly, reactive mitigation strategies are used to decrease the chance of thermal runaway when early signs have been detected, as well as to decrease the impact of potential cell thermal runaway. Firstly, if any signs of potential thermal runaway are detected, the choice can be made to shut off certain parts of the battery. This would then mean that the mission would need to be aborted. Secondly, a purge system will be included that is able to dilute the flammable gasses and oxygen of the battery to prevent the risk of explosion. Thirdly, sufficient spacing between cells is used to allow for effective venting of the cells. Furthermore, the cells will all face the same direction such that they can vent into a free volume. Finally, the battery will be located in the wing box, which is a main structural element and therefore, this should be protected from the heat created by a potential thermal runaway. The wing box will be made of aluminium, which loses strength at temperatures as low as 100 [$^\circ C$][13]. The choice was made to use an intumescent coating on the inside of the wing box, as it was found that this would be the most weight-effective and practical option for insulation against fire [69]. The mentioned pack-level safety measures add weight to the total weight of the battery. However, this weight is already included in the pack density of the battery as this is based on a battery pack with similar safety measures.

10.4. Battery Sizing

The trade-off resulted in lithium-sulfur batteries being used for the aircraft. The aircraft contains two batteries, one high-voltage and one low-voltage battery. The high-voltage battery aids the fuel cell in the climbing phase and allows for the starting up of the fuel cell. The low-voltage battery operates the relays of the high-voltage system before the fuel cell is started up.

The required discharge power of the high-voltage battery was found to be at least 26.5 [kW], which is based on the flight path simulation, this will be elaborated upon in Section 12.3. In which an average of 25.6 [kW] is used for 22 minutes during the climbing phase. Resulting in a battery capacity of 9.7 [kWh]. However, it was decided that a larger capacity was needed since flying with the batteries fully charged is not preferred. This is partially due to the fact that the batteries are used to take up part of possible excess power or power spikes together with the capacitors. Additionally, having fully drained batteries after the climb could pose problems if the fuel cell shuts down, as no power would be available to restart it. Therefore, the battery has been sized to have a capacity of 14.45 [kWh]. Considering a discharge efficiency of 0.9, this translates to 26 [kW] for 30 minutes. This margin would allow for the restarting of the fuel cell at cruise altitude. If the fuel cell does not restart and the fuel cell fails, there would be enough time to glide down from the cruise altitude. However, if such a failure occurs immediately after take-off, there is insufficient altitude to use. Therefore, the performance of the aircraft was analysed at screen-height (15.4 [m]) without accelerating or climbing. Using the method that will be described in Chapter 12, a drag was found of 350 [N]. The propeller simulation was performed and resulted in an efficiency of 0.526 [-] and a required power of 14.1 [kW] at the motor per motor. Taking into account the efficiencies of the motor, motor controller, and battery, this results

[13] https://www.xometry.com/resources/materials/7075-aluminum-alloy/ [Accessed on 10-06-2024]

in a required discharge power of 33.3 [kW]. With a battery capacity of 14.45 [kWh], the aircraft could fly at screen height 26 minutes, providing enough time to return to base.

The lithium-sulfur batteries have an estimated discharge and charge rate of 3C and 0.25C, respectively [66]. For a battery pack of 14.45 [kWh] having a discharge efficiency of 0.9, this results in a maximum discharge power of 39 [kW] and a maximum charging power of 3.25 [kW]. A maximum discharge power during the climb phase was found to be 34.5 [kW], staying below this limit. A charging power of 3 [kW] was chosen, and the batteries will be charged during the cruise phase of the flight. Charging the batteries during the cruise phase allows for the use of batteries in the descent phase. With a pack-specific energy of 270 [Wh/kg], a battery mass of 53.52 [kg] is found. The high-voltage batteries are located in the rear wing of the aircraft.

To operate the relays, the low-voltage system is used. In order to close the relays before the fuel cell is operating, a low-voltage battery is required. Additionally, in case the DC-DC converter fails, the low-voltage system would still provide power, allowing for the monitoring of the flight instruments and the operation of the relays, sensors, cooling system, hydrogen heating system and propeller governors. The low-voltage system runs at 4 [kW], and the low-voltage battery system has been sized to operate at 4 [kW] for 15 minutes. The same batteries were selected as used for the high-voltage battery, having a pack density of 270 [Wh/kg]. Resulting in a battery of 1.11 [kWh] taking into account a discharge efficiency of 0.9 [-]. The low-voltage battery weighs 4.12 [kg] and is located in the cockpit. But, if the high-voltage battery and the fuel cell were to fail, not all low-voltage systems have to be powered. This includes the pumps and heating element in the hydrogen tank. Turning these systems off would result in an estimated decrease of 3 [kW]. Of which 1.2 [kW] is due to the hydrogen heating element being turned off. This results in 1 [kW] of power required to power the necessary flight instruments and sensors. Taking into account a discharge efficiency of 0.9, the low-voltage system could deliver 1 [kW] of power for 60 minutes. According to the EASA regulation CS 25.1351(d), the required endurance of at least 60 minutes to provide power to essential flight instruments and systems [70]. With the current size of the low-voltage battery, this requirement is met. The current descent phase is estimated to take around 50 minutes, how this is determined will be elaborated upon in Chapter 12. With the current low-voltage capacity, the flight instruments and sensors could be powered for the entire descent. T

10.5. Capacitor Sizing

Capacitors are added for protection against voltage spikes. In addition, if a motor were to fail, the capacitors could quickly absorb current, while the fuel cell is powered down to a lower level. The batteries are also used for this and can be charged at 3 [kW], but the capacitors have significantly higher charging rates. It is assumed that the fuel cell requires 1 [s], to lower its power output [71]. With this in mind, the capacitors were sized. The required capacitance can be calculated using Equation 10.4 [72].

$$C = \frac{2 \cdot E}{V^2} \tag{10.4}$$

In Equation 10.4, C is the capacitance in [F], E is the energy stored in a parallel-plate capacitor in [J] and V is the voltage in [V]. The critical scenario was found to be when one motor or motor controller fails. Resulting in a sudden excess of power. From the fuel cell, without additional battery power, the motor controller could receive a maximum power of 93.5 [kW]. If a motor or motor controller were to fail, it is assumed that part of this excess power can be stored in the battery. The battery can be charged with 3 [kW], resulting in a power of 90.5 [kW] going to the capacitors for 1 [s]. Substituting this in Equation 10.4, in combination with a voltage of 600 [V], results in a required capacitance of 0.503 [F]. COTS capacitors with a voltage rating of 600 [V] were evaluated. A capacitor with a voltage rating of 600 [V] and capacitance of 6800 [μF] was selected due to its relatively high capacitance whilst weighing 0.22 [kg][14]. Dividing the total required capacitance, of 0.503 [F], by the capacitance of the individual capacitors, of 6800 [μF] results in a capacitor pack consisting of 74 capacitors. The capacitors have a total mass of 16.3 [kg].

10.6. Fuel Cell System Design

The beating heart of the plane is the fuel cell, it converts hydrogen with oxygen from the air into electricity with water as a byproduct. This section will deal with the sizing of the fuel cell as well as the sizing of the air compressor. That information can then be used to size the rest of the hydrogen system.

[14] https://nl.mouser.com/ProductDetail/EPCOS-TDK/B43720B8688M000?qs=W0yvOO0ixfFeZU0c%252BNhmrA%3D%3D [Accessed on 18-6-2024]

10.6.1. Fuel Cell Sizing

The key parameter for fuel cell sizing is the required power since fuel cells have a certain rated power. It was decided to size the fuel cell for the maximum continuous power and let the batteries deal with peak power demands. The continuous power required as given in Table 10.7 is 230 [kW], so the fuel cell should have a rated power equal to this value. One of the primary interests of sizing the fuel cell is to determine the mass. For this, the specific power will be used, Fly Zero [73] expects that in the near future a specific power for fuel cell systems of 2.0 [kW/kg] will be achieved. It is relevant to note that the fuel cell system includes the balance of the plant (BoP), so since this specific power is for fuel cell systems it includes the weight of the BoP. Using the power and the specific power, the mass was determined to be 115 [kg]. The other relevant fuel cell parameter is the efficiency, Fly Zero [73] expects this to be 60% in the near future.

Now the power and efficiency are known, the hydrogen consumption can be calculated. The unit for power is [kW] which is equivalent to [kJ/s], this can then be converted to mass flow using the energy density of hydrogen. The higher heating value (HHV) of hydrogen is 141.7 [MJ/kg][15]. The amount of chemical energy per second the fuel cell requires at rated power is 383.33 [kJ/s], this leads to a hydrogen consumption rate of 2.705 [g/s].

10.6.2. Air Compressor Sizing

Even though an air compressor is already present in the fuel cell BoP, it cannot deal with the extremely low inlet pressures at cruising altitude. Ambient pressure at cruising altitude is 17.93 [kPa][16] and the required inlet pressure of the fuel cell air compressor is 37.65 [kPa][16],[17], this leads to a required pressure ratio of 2.1 during cruise.

There are two possible solutions to increase the pressure: using ram air and using a compressor. To determine whether ram air could achieve this pressure ratio, the dynamic pressure has to be calculated. The formula for the dynamic pressure is given by Equation 8.7, the density during cruise is 0.288 [kg/m^3][16], and the velocity is 163 [m/s]. This leads to a dynamic pressure of 3.826 [kPa], the total pressure of the flow at cruise is then 21.76 [kPa], which is not the required 37.65 [kPa]. Therefore, compressors are required to ensure the correct inlet pressure into the fuel cell air compressor, whilst maintaining the proper flow rate.

This flow rate can be calculated by using the hydrogen consumption rate and assuming that the fuel cell consumes oxygen in a stoichiometric ratio with the hydrogen. The stoichiometric ratio of hydrogen to oxygen is two to one. However, the mass flow rate first has to be converted to a molar flow rate. The molar masses of hydrogen and oxygen are 2.01568 [g/mol] and 31.9988 [g/mol] respectively[18]. This leads to a molar hydrogen flow rate of 1.342 [mol/s] and then a molar oxygen rate of 0.671 [mol/s]. The required oxygen mass flow rate is then 21.471 [g/s] and using that the oxygen percentage in air is 20.947%[19], the required air mass flow rate is 102.5 [g/s]. At cruise conditions, the density is 0.288 [kg/m^3] or 0.288 [g/L], which leads to a volumetric air flow rate of 355.9 [L/s] or 21,354 [L/min].

When investigating possible air compressors, it was discovered that for this scenario the volumetric flow rate is more limiting than the mass flow rate. The air compressor that came closest to the requirements was the Celeroton CT-3001[20] and its accompanying controller is the Celeroton CC-3001[21]. Two of these air compressors are required in parallel in order to meet the volumetric flow rate requirement. These have a combined mass of 68.6 [kg], a peak power consumption of 42 [kW], and an efficiency of 69%.

10.7. Hydrogen Tank Design

Now that the fuel cell has been sized, the tank can be sized, this will consist of two parts: determining the amount of hydrogen required and determining the size of the tank. In order to determine the amount of hydrogen, the hydrogen flow rate and time to complete the race can be used. The hydrogen flow rate has already been determined in Section 10.6.1, the time to complete the race can be estimated by using the race distance of 1,852,000 [m] and minimum average speed of 145 [m/s]. The maximum time to complete the race would then be 12,772 [s], but in the current strategy, the fuel cell is turned off for 36 [min] during descent. This means that the fuel cell running time is the aforementioned time minus 2,160 [s], which gives 10,612 [s]. Using the flow rate the required hydrogen mass was calculated to be 28.709 [kg], since this does not include any margins this was rounded up to 30 [kg]. It is also

[15] https://www.engineeringtoolbox.com/fuels-higher-calorific-values-d_169.html [Accessed on 14-06-2024]
[16] https://www.engineeringtoolbox.com/international-standard-atmosphere-d_985.html [Accessed on 12-06-2024]
[17] https://zeroavia.com/wp-content/uploads/2024/05/SuperStack-Datasheet-6-digital.pdf [Accessed on 17-06-2024]
[18] https://www.horizoneducational.com/what-s-the-molar-mass-of-hydrogen/t1496?currency=usd [Accessed on 14-06-2024]
[19] https://www.noaa.gov/jetstream/atmosphere [Accessed on 14-06-2024]
[20] https://www.celeroton.com/wp-content/uploads/Datasheet-CT-3001.pdf [Accessed on 17-06-2024]
[21] https://www.celeroton.com/wp-content/uploads/Datasheet-CC-3001.pdf [Accessed on 17-06-2024]

relevant to note that the flow rate used in this calculation is for full fuel cell power, however, that is not required at all times, so the aforementioned hydrogen mass is conservative

For the tank a gravimetric ratio of 30%[22] was used, this ratio expresses the ratio of the hydrogen to the combined hydrogen plus tank mass. Where the tank mass is for a vacuum insulated twin-walled tank. Since no COTS tank has been selected, internal pressure is not set, but a maximum pressure of 6 bar is used in other concepts [74]. The aforementioned gravimetric ratio leads to a hydrogen tank mass of 70 [kg]. It is relevant to note that there are two possibilities to extract hydrogen from a liquid hydrogen tank: liquid extraction or gaseous extraction. For liquid extraction, a pressure difference to force out the hydrogen has to be created, this could be done by a second hydrogen or helium pressure vessel or a cryogenic pump. For gaseous extraction, the hydrogen has to be boiled off quickly enough, this leads to the interesting scenario of placing a heating element in or on the liquid hydrogen tank. From these two scenarios, gaseous extraction is clearly the more simple one, since it only requires a heating element. The reason a heating element is used instead of a heat exchanger is that running cooling tubes in the vacuum layer of the tank makes it more complex again. They also create a path for heat to flow in when the fuel cell is not on requiring venting of hydrogen to release pressure, the heating element when turned off provides less of a path for heat flow. Using the latent heat of vaporisation and the flow rate, the power required by the heating element can be calculated. The latent heat of vaporisation of hydrogen is 446.06 [kJ/kg][23] and from Section 10.6.1 the flow rate is 2.705 [g/s], the heat energy required is then 1.207 [kW]. To remain conservative, the heat inflow from the environment is ignored, which means that an electric heating element of 1.207 [kW] or higher is necessary.

10.8. Hydrogen Tubing Design

The hydrogen tubing will be based on a report by P.C. de Boer on behalf of the NLR [74], their system was designed for a drone however the basic system lay-out should not be very different. Firstly, the equipment directly surrounding the tank will be discussed. This starts with the following safety equipment: a burst disk and a pressure relief device. These components are both passive, the burst disk simply bursts if the pressure gets too high whereas the pressure relief device consists of a spring mechanism to open at a certain pressure, however, it closes again when the pressure is low enough. The idea of both these devices is that they release the pressure before the tank itself could burst, as such they should be connected directly to the tank, without any possible obstructions in between. Then there is the liquid refuelling line, however, the external connection is still to be selected since that might depend on the hydrogen supplier. The final connection out of the tank is the gaseous extraction line, this then leads to what P.C. de Boer [74] describes as the conditioning system.

The conditioning system is the system in between the tank and the fuel cell and ensures that the hydrogen that arrives at the fuel cell is at the correct temperature and pressure. The first part of this system is a heat exchanger where some of the heat of the fuel cell is used in order to heat up the hydrogen to a temperature above 0 [$^\circ C$] [74]. In order to calculate the heat energy required for heating up the hydrogen, the simplified first law of thermodynamics for heat transfer is given by Mills [75]:

$$\dot{Q} = \dot{m} C_p \Delta T \tag{10.5}$$

Where $\dot{m}$ is the mass flow in [kg/s], C_p is the specific heat in [$kJ/(kg \cdot K)$], and finally ΔT is the temperature difference in [K] or [$^\circ C$]. The mass flow is given in Section 10.6.1 as 2.705 [g/s], the specific heat of hydrogen is 15.0608 [$kJ/(kg \cdot K)$][23] and the temperature difference is given as 270 [$^\circ C$] for a final temperature of roughly 20 [$^\circ C$]. The heat required is then 11.0 [kW], and the effect on the cooling will be discussed in Section 10.9. After the heat exchanger, there is both an electrical and manual vent valve to release hydrogen. Then, there is a valve to shut off the fuel flow and a pressure regulator to ensure the correct pressure going to the fuel cell. Finally, there is another pressure relief device, this one is to protect the fuel cell in case the pressure regulator fails or a pressure difference is formed due to the plane flying at different altitudes. All the tubing up to the valve should be vacuum jacketed to prevent air from liquefying on the tubes, the reason that this must be done until the valve is that during venting the fuel cell might not be running, so then no heat could be provided to the heat exchanger. The entire system described in this system has also been visualised in Figure 10.5.

[22] `https://newatlas.com/aircraft/hypoint-gtl-lightweight-liquid-hydrogen-tank/` [Accessed on 18-06-2024]
[23] `https://encyclopedia.airliquide.com/para-hydrogen#properties` [Accessed on 18-06-2024]

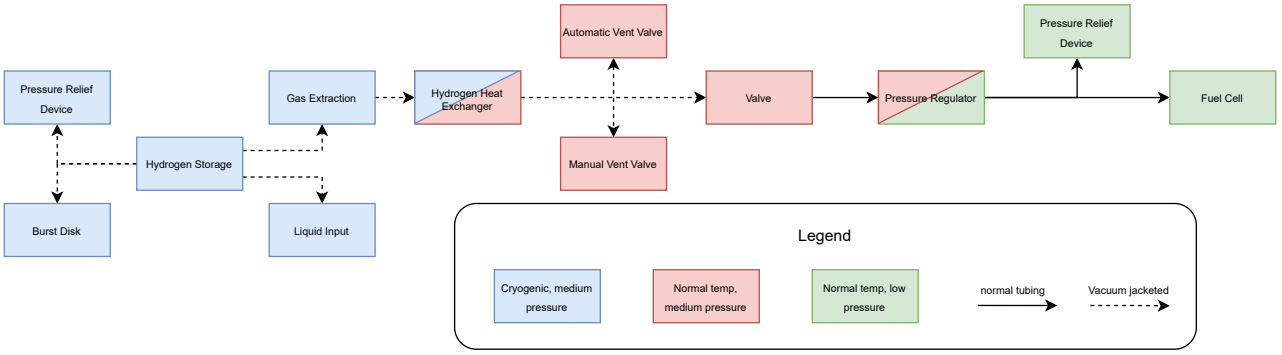

Figure 10.5: Hydrogen Block Diagram

10.9. Cooling Design

A less obvious but no less important part of the propulsion system is the cooling system. This is especially important for hydrogen fuel cell-powered planes since those have high cooling demands. However unlike traditional jet engines they cannot shed heat into their exhaust, so liquid cooling is required, here another innovative system is introduced: using the wing surface as heat exchanger area. Kellerman et. al. [76] showed that surface heat exchangers provide sufficient cooling capabilities for all hybrid electric medium to large aircraft which is the range they investigated. They also noted that smaller aircraft can dissipate more heat through their surfaces. However, they used nearly all of the aircraft surfaces, not just the wing surface. No papers were found that discussed the use of a wing heat exchanger for very small single-seater planes like the one designed in this report. Therefore, an analysis had to be performed to determine the cooling capacity of the Prandtl plane front wings. The front wings were chosen for their direct connection to the fuselage which allows for large coolant tubes which might be necessary due to the large fuel cell. Habermann et. al. [77] showed that the best location for a wing surface heat exchanger was in the lower forward part of the cross-section. They showed an increase of lift-to-drag ratio of 2.1% for a fully turbulent flow, in Section 10.9.2 it is shown that the flow is probably turbulent by the time it reaches the wingbox, which spans 20% to 60% of the chord. Therefore, the decision was made to place the wing heat exchanger on the bottom of the wingbox. To remain conservative, it was decided to neglect the aerodynamic effects of the heat exchanger. Another reason to neglect the aerodynamic effects is that the currently used AVL software cannot incorporate the effects in its simulation.

10.9.1. Analysis of Cooling Requirements

Firstly, the cooling requirements are determined, this is done by means of the power consumption and efficiencies. It is then assumed that all the waste power is rejected in the form of heat. The coolant temperature range of these heat sources is also important since they pose a limit on the coolant temperature range. In Table 10.4 the components that require cooling are shown with their heat flow ($\dot{Q}$) in [kW], inlet temperature (range) (T_{in}) in [$^{\circ}C$].

Table 10.4: Peak cooling requirements

Heat Source	$\dot{Q}$ [kW]	T_{in} [°C]
Fuel Cell	153.3	$\geq$20
Motor	8.417	$\leq$50
Motor Controller	4.294	$\leq$50
Battery	4.335	-
Air Compressor + Controller	14.49	-20 - 55

From the table it is obvious that the fuel cell is the primary heat source and will require by far the most cooling, it poses also the most strict requirements on its inlet temperature [78]. Using the values in the table the total cooling power is 184.87 [kW]. The outlet temperature depends on the position of the components within the cooling loops. The cooling loops were decided based on mainly on practicality, Figure 10.6 shows the different cooling loops.

As can be seen in Figure 10.6, there are three distinct cooling loops. There are also circles to represent a value for the mass flow rate (mX) in [kg/s] or for the temperature (TX) in [$^{\circ}C$] at specific points. The colours offer some slight indication of how the temperature changes, where blue is cold, red is hot, and purple is in between. The first one contains the fuel cell, the two air compressors with their controllers, and the hydrogen heat exchanger. This loop has a higher flow rate to accommodate the large amount of heat generated by the fuel cell, it is also noteworthy that the hydrogen heat exchanger heats up the hydrogen and therefore cools down the coolant. The second and third loops are identical and go to the two rear wings where the batteries, motor controllers, and motors are located. All three loops share the aforementioned wing heat exchanger and the same pump, although 2 are installed for redundancy.

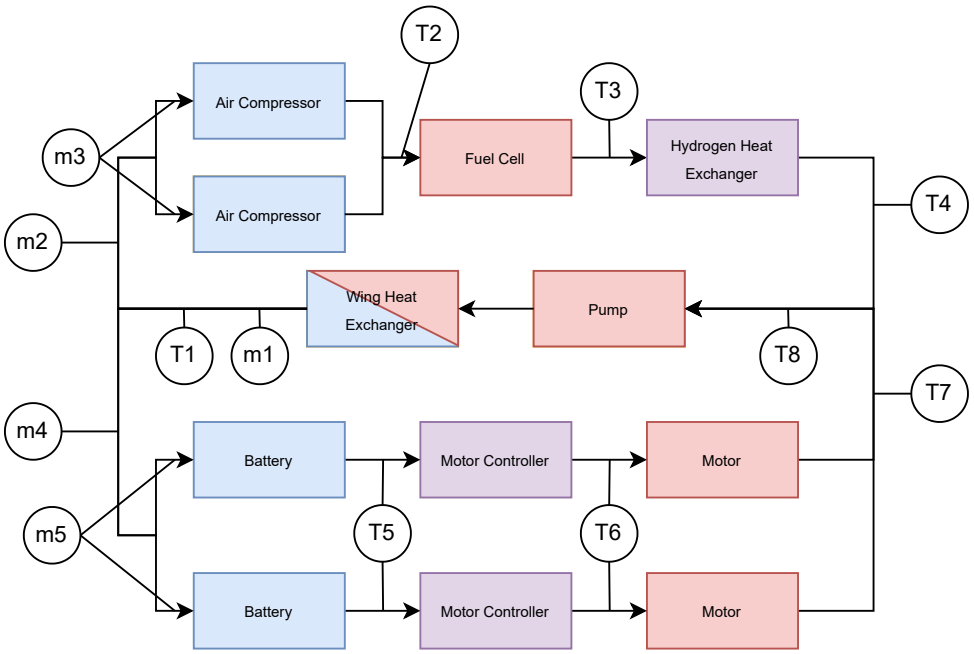

Figure 10.6: Cooling Block Diagram

In order to calculate the coolant mass flow from or temperature difference across components, Equation 10.5 can be used. The information that is still missing is the coolant itself and its specifications. Some components require a water-glycol mixture like the air compressor[20], it is also desired that the cooling does not freeze at the cruising altitude of 12,500 [m]. This leads to a required freezing point of -56 [$^{\circ}C$][24] or lower, the only water-glycol mixture that achieves that is a 70 to 30 ratio of glycol and water respectively[25],[26]. A linear expression between the specific heat and the temperature at a specific point (T_p) in [$^{\circ}C$] can be formulated[26], this is given in Equation 10.6.

$$c_p = \frac{583}{150,000} T_p + \frac{9,007}{3,000} \tag{10.6}$$

Now the temperatures and mass flow rates from Figure 10.6 can be calculated, these are shown in Table 10.5 and Table 10.6 respectively. For these calculations it was used that m3 was half of m2 and m5 was half of m4, m5 was limited by the motor to be at least 6 [L/min][5] or 0.111 [kg/s][26], and finally T1 was also set at 20 [$^{\circ}C$] from Table 10.4 and the fuel cell outlet temperature is 75 [$^{\circ}C$] so T3 was set to that value [78].

Table 10.5: Temperature at different points

Temperature point	T_p [°C]
T1	20.00
T2	29.41
T3	75.00
T4	71.68
T5	26.31
T6	32.52
T7	44.55
T8	66.79

Table 10.6: Mass flow rates at different points

Mass flow point	$\dot{m}$ [kg/s]
m1	1.231
m2	1.009
m3	0.504
m4	0.222
m5	0.111

[24] https://www.grc.nasa.gov/WWW/K-12/airplane/reynolds [Accessed on 12-06-2024]
[25] https://www.idrivesafely.com/defensive-driving/trending/coolant-vs-antifreeze-whats-difference [Accessed on 12-06-2024]
[26] https://www.engineeringtoolbox.com/ethylene-glycol-d_146.html [Accessed on 12-06-2024]

10.9.2. Wing Heat Exchanger Sizing

Now that all the cooling requirements are clear, the thermodynamics of the wing heat exchanger itself can be explored in more detail. This analysis depends heavily on the work done by Bahrami [79] on flat plate forced heat transfer. Even though this analysis is not intended for a wing, it is assumed that this analysis is accurate enough for the current stage of design.

The heat transfer from the wing comes in two forms conduction and convection, the ratio between convection and conduction is called the Nusselt Number. Since the convection itself is very difficult to calculate, the Nusselt Number and the heat conduction will be calculated and/or estimated in order to calculate the heat convection. Then both heat conduction and convection can be combined in order to estimate the total heat dissipation capabilities of the wing.

First, the heat conduction will be calculated using Fourier's Law, which gives Equation 10.7 [75].

$$\dot{q}_{cond} = \frac{k\Delta T}{t} \tag{10.7}$$

In Equation 10.7 $\dot{q}_{cond}$ is the specific heat transfer in $[kW/m^2]$, k is the thermal conductivity in $[kW/(m \cdot K)]$, and t is the thickness in $[m]$. The heat flow could then be calculated by multiplying the specific heat flow with the surface area. However, this will only be done at the end to verify that the wing surface area is large enough and to calculate the amount of wing surface area needed for the heat exchanger. The thermal conductivity of air at the cruising altitude and take-off altitude are $1.952 \cdot 10^{-5}$ $[kW/(m \cdot K)]$[16] and $2.534 \cdot 10^{-5}$ $[kW/(m \cdot K)]$[16] respectively. The temperature difference can be taken as the difference between the free stream air and the heat exchanger temperature which is T8 from Table 10.5. The ambient temperatures are -56 $[^{\circ}C]$[16] during cruise and roughly 20 $[^{\circ}C]$[27] at take-off. It is worth noting that an increase in temperature difference increases heat flow, so it could be relevant to take-off early in the morning. However, the temperature is really weather dependant, so this is something that will have to be decided during the race. Then only the thickness is still unknown. In order to find this thickness three more parameters have to be introduced: the boundary layer thickness, the thermal boundary layer thickness, and the Prandtl number.

The Prandtl number is the ratio between the boundary layer thickness and the thermal boundary layer thickness, it can be calculated by Equation 10.8[28].

$$Pr = \frac{\mu c_p}{k} \tag{10.8}$$

In Equation 10.8 the only new value is the μ which is the dynamic viscosity in $[kg/(m \cdot s)]$, these were found to be $1.4216 \cdot 10^{-5}$ $[kg/(m \cdot s)]$[16] and $1.7896 \cdot 10^{-5}$ $[kg/(m \cdot s)]$[16] for cruise and take-off respectively. The c_p in this formula is the specific heat for air since it does not change with higher altitudes but only with temperature[29], the specific heat of air at 1 $[bar]$ and cruise altitude temperature is then 1.007 $[kJ/(kg \cdot K)]$[30], for take-off the value is 1.006 $[kJ/(kg \cdot K)]$[30]. Using these values the Prandtl numbers for cruise and take-off are 0.733 and 0.710 respectively.

With the Prandtl numbers for the edge cases known, the boundary layer thicknesses should be found. However, firstly the Reynolds numbers should be determined, for this the kinematic viscosity is required next to the characteristic length and the velocity. The kinematic viscosities are $4.930 \cdot 10^{-5}$ $[m^2/s]$[16] and $1.461 \cdot 10^{-5}$ $[m^2/s]$[16] for cruise and take-off respectively, similarly the velocities are 163 $[m/s]$ in cruise and 53 $[m/s]$ for take-off. The characteristic length depends on the point of interest along the airfoil. However, since the transition point is of most interest, the critical Reynolds number can be used, which is $5 \cdot 10^5$ [80]. Using all this information, the transition points can be determined with the formula for the Reynolds number given in Equation 10.9 [80].

$$Re = \frac{VL}{\nu_k} \tag{10.9}$$

In Equation 10.9 Re is the Reynolds number, V is the velocity in $[m/s]$, L is the characteristic length in $[m]$, and ν is the kinematic viscosity in $[m^2/s]$. The characteristic lengths associated with transition are then 0.151 $[m]$ and 0.138 $[m]$ for cruise and take-off respectively. Since the heat exchanger is to be placed in the wingbox and the wingbox starts at 20% it can be assumed that the flow in already in the transition phase and getting turbulent. Therefore for

[27] https://weatherspark.com/m/9483/5/Average-Weather-in-May-in-Omaha-Nebraska-United-States [Accessed on 24-06-2024]

[28] https://www.engineeringtoolbox.com/air-prandtl-number-viscosity-heat-capacity-thermal-conductivity-d_2009.html [Accessed on 13-06-2024]

[29] https://www.engineeringtoolbox.com/air-specific-heat-various-pressures-d_1535.html [Accessed on 13-06-2024]

[30] https://www.engineeringtoolbox.com/air-specific-heat-capacity-d_705.html [Accessed on 13-06-2024]

the rest of this analysis turbulent flow over the heat exchanger is assumed. The thickness of a turbulent boundary layer was discussed by Schlichgting [81] and can be approximated by Equation 10.10.

$$\delta(x) \approx 0.37 \frac{x}{Re_x^{1/5}} \tag{10.10}$$

In Equation 10.10 δ is the boundary layer thickness in [m], x is the position along the airfoil in [m], and Re_x is the Reynolds number at that location. Using the aforementioned value of $5 \cdot 10^5$ for the Reynolds number would result in the smallest boundary layer thickness, resulting in a conservative approach. For cruise and take-off this then results in a boundary layer thickness of 3.269 [mm] and 3.209 [mm] respectively. Using the aforementioned Prandtl numbers the thermal boundary layer thicknesses were calculated to be 4.458 [mm] and 4.517 [mm] for cruise and take-off. The thermal boundary layer thickness can then be used as thickness t in Equation 10.7 to calculate the heat conduction. The heat conduction during cruise is then 0.5398 [kW/m^2] and during take-off it is 0.2625 [kW/m^2].

Finally, the Nusselt (Nu) number had to be calculated, this can be done with Equation 10.11 [79].

$$Nu = 0.037 Re^{4/5} Pr^{1/3} \tag{10.11}$$

Using Equation 10.11 the Nusselt numbers during cruise and take-off are 974.785 and 1038.828 respectively. Now all the relevant parameters have been calculated in order to calculate the heat convection. During cruise the heat convection is 526.23 [kW/m^2], which then leads to a total heat transfer of 526.77 [kW/m^2] during cruise. During take-off the heat convection is 271.66 [kW/m^2], this gives a total heat transfer during take-off of 272.93 [kW/m^2].

These values were considered to be optimistic, this was also confirmed by looking at the work performed by Kellerman et. al. [76]. Even though their graphs do not cover the size of the design discussed in this report, a rough estimate for an aircraft of this size would be roughly 500 [kW]. A possible reason for why these values are optimistic is that incompressible flow was assumed, this leads to friction and thus heat. However, there is room for a 2 [m^2] wing heat exchanger on the bottom of the wingbox, since the required cooling power is 184.87 [kW], this surface area should be enough.

10.9.3. Other Cooling Components

To finalise the cooling system, two important parts still have to be discussed: the pump and the tubes. The pump is fairly easy to size, since it mainly depends on flow rate, a 150 [L/min] pump was found[31], this pump has a power consumption of 120 [W] and a mass of 1.170 [kg]. Since the cooling system is a critical system and the mass is quite low, it was decided to use two pumps in order to have redundancy. The pump works with tube diameters in a range of 35 [mm] to 51 [mm][31], the motor with tubes with a diameter of 10 [mm][32]. Since no specific fuel cell has been selected, no specific tube diameters are known. However, to be conservative, it was chosen to use the largest diameter allowed by the pump for the fuel cell and heat exchangers. This means very roughly that 2 [m] of the 51 [mm] diameter tube is required and 25 [m] of the smaller 10 [mm] tube.

10.10. Electrical System Overview

After identifying the main components of the electrical system, an electrical block diagram has been established. Figure 10.7 presents the electrical block diagram. The boxes in red represent the high-voltage systems of 600 [V]. With the power distribution unit (PDU) serving as the central control unit for managing the power within the high-voltage network. For the low-voltage system, this is done through the switchgear, which serves to control, protect and isolate electrical circuits. Double arrows represent possible electric currents in both directions. This is the case for the batteries, both high and low-voltage, as well as the capacitors, fuel cell, and motors. The fuel cell requires power from the high-voltage battery to activate the air compressor. This is necessary to provide the required pressure for the fuel cell to begin its electrochemical reaction and generate power. Once the fuel cell is running, it can then operate continuously and generate its own power. The motors are able to regenerate power by windmilling. This can be done if the fuel cell is turned off and the battery is not fully charged. A possible scenario for this is if additional drag is required during the landing phase or if the batteries need to be charged during the descent. The 24 [V] system, indicated with blue boxes, powers the propeller governors, flight computer, flight instruments, data acquisition, and the fan. The propeller governors are powered through the flight computer, where they are controlled. The data acquisition consists of the sensors or measurement systems used in the aircraft. A more in-depth explanation of this will be provided in Chapter 14. A charging port is provided in the 24 [V] system, this can be used to charge

[31] https://races-shop.com/water-pumps/88339-davies-craig-universal-electric-water-pump-150l-min-10a.html [Accessed on 18-06-2024]

[32] https://emrax.com/wp-content/uploads/2022/11/Manual_1.4.pdf [Accessed on 18-06-2024]

both the low and high-voltage battery. Due to this, double arrows can be seen between the low-voltage switchgear, DC-DC converter, and the high-voltage PDU. The pumps and heating element of the fuel cell are operated at different voltages, which are 48 and 12 [V] respectively.

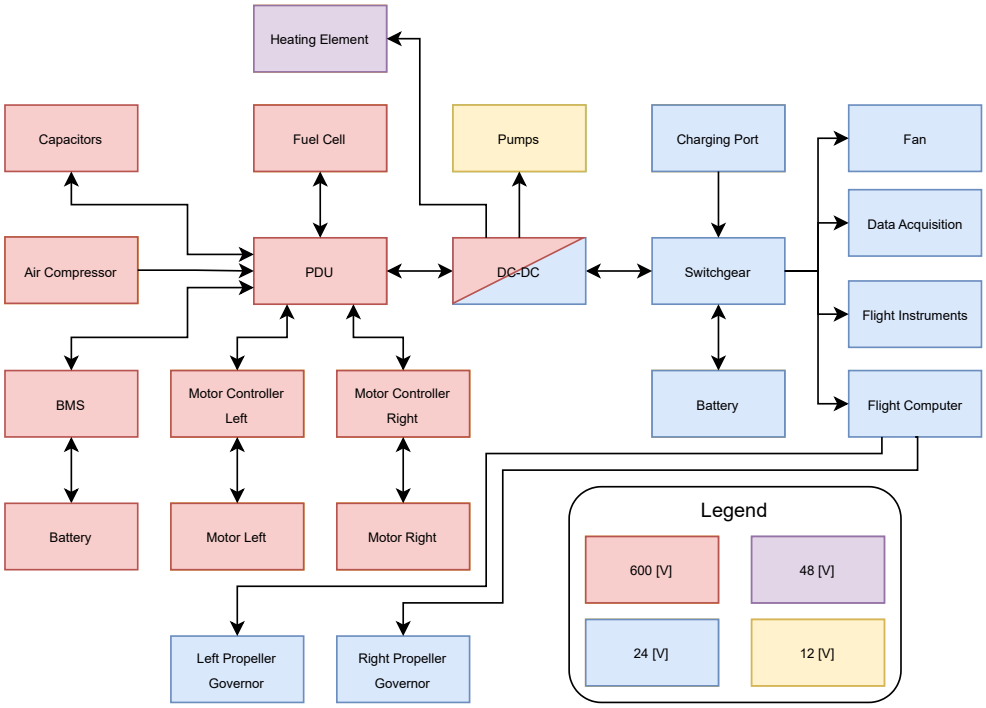

Figure 10.7: Electrical block diagram

With the power if the main components known, the appropriate electrical components, such as the wires and contactors. In Table 10.7, an overview of the power supplied and consumed during continuous and peak conditions is given. The continuous power is used during cruise, where the batteries are charged with excess power. It was found that the last part of the climb, above around 8,000 [m], was the most power-intensive flight phase. Therefore, the batteries are used to provide extra power. The power outputted by the battery varies, depending on the power required for climbing. A more detailed description of this process will be provided in Chapter 12. The battery can achieve a maximum discharge rate of 57 [A]. With the high-voltage system running at 600 [V], due to the chosen motor as mentioned in Section 10.2, a maximum power of 30.8 [kW] can be supplied when a discharge efficiency of 0.9 is taken into account. This is not reached with the current flight strategy, on average a power of 17.6 [kW] is used for 22 minutes. A maximum power of 26.5 [kW] is used for 16 seconds. Table 10.7 presents the peak power in case the batteries were discharged at their maximum rate since the wiring should be sized to handle these currents. With the current flight strategy, this maximum is not achieved but theoretically possible. Additionally, the component masses are shown. The high-voltage battery is mentioned twice, once when discharging and once when charging. This is the same battery, therefore the weight is only shown once. The low-voltage system has not been broken down in detail, but it contains elements such as the low-voltage battery, and avionics and provides energy to the sensors. A mass of 15 [kg] has been assumed, which includes the low-voltage battery mass.

Table 10.7: Overview of supplied and consumed power during continuous and peak conditions for different components and component mass

Component	Continuous power [kW]	Peak power [kW]	Mass [kg]
Fuel cell	230	230	115
High-voltage battery discharge	0	39	53.52
Electric motors	165	215.6	88
Motor controllers	3.37	4.4	5

Air compressor	42	42	68.6
High-voltage battery charging	3	0	-
Low-voltage system	4	4	15

With the peak power known, the electrical cables can be sized. The high-voltage system runs at a voltage of 600 [V], which is driven by the chosen motor. The type of electrical wire is partially dependent on the ampere, which can be calculated according to Equation 10.12 [72].

$$I = \frac{P}{V} \tag{10.12}$$

With I being the intensity in [A], P the power in [W] and V the voltage in [V]. Based on the calculated ampere, possible cables were selected. Copper cables were chosen with an allowable ampacity exceeding the ampere of the components. Ampacity describes the maximum current that can continuously carry, without exceeding the temperature rating of the cable [82]. The required length of the cables was estimated based on the CATIA model of the aircraft. With the length, material, and radius known, the cable efficiency can be calculated according to Equation 10.13 [72].

$$\mu_c = \frac{\rho \cdot L \cdot I_{peak}^2}{A \cdot P_{peak}} \tag{10.13}$$

Where μ_c is the dimensionless cable efficiency, ρ is the resistivity in [Ωm], L is the length of the cable in [m], A is the cross-sectional area in [m^2] and I_{peak} and P_{peak} are the ampere and power in peak respectively. For simplicity, it is assumed that the entire cross-sectional area A, is made out of copper, the strands that make up the cable are ignored. The resistivity, ρ, of copper is assumed to be $1.724 \cdot 10^{-8}$ [Ωm][33]. In Table 10.8, an overview is shown of the main parameters of the cable for specific components to or from the PDU. To power both motors, 2 cables of 6 meters are required. This cable spans from the PDU, to the motor controller to eventually the motor itself. But, it was sized on the ampere between the PDU and motor controller. This is slightly higher than between the motor controller and the motor due to the efficiency of the motor controller.

Table 10.8: Overview of sized cable parameters for individual components

PDU to/from	Peak power [kW]	Ampere [A]	Allowable ampacity [A]	Length [m]	Cable efficiency [-]
Fuel cell	230	383.3	430[34]	1.5	0.9999
Battery	39	65	75[35]	8	0.9991
Motor controller	110.54	184.24	260[36]	2x8	0.9997
Low-voltage system	4	6.67	20[37]	4	0.9998
Compressor	34	56.67	75[35]	4	0.9995
Capacitors	230	383.3	430[34]	1	0.9994

In Table 10.8, it can be seen that the cable efficiency is ranging between 0.9991 and 0.9999 [-], in further calculations an efficiency of 1 was assumed for the cables since the loss was deemed negligible. The high-voltage cables have a combined weight of 25.4 [kg][34],[35],[36],[37].

The PDU distributes energy and contains control, measurement, and protection equipment. It consists of relays, allowing for the control of the high-voltage circuit by low-voltage powered switches. The primary purpose of this is to protect the system from too high of a current or voltage and allow for the opening of the circuit when a short circuit is detected.

[33] https://www.engineeringtoolbox.com/copper-aluminum-conductor-resistance-d_1877.html [Accessed on 14-6-2024]
[34] https://www.awcwire.com/product/thhn-500-37 [Accessed on 14-6-2024]
[35] https://www.wireandcableyourway.com/6-awg-xlp-use-2-rhh-rhw-2-building-wire [Accessed on 14-6-2024]
[36] https://www.wireandcableyourway.com/4-0-awg-xlp-use-2-rhh-rhw-2-building-wire [Accessed on 14-6-2024]
[37] https://www.wireandcableyourway.com/12-awg-xlp-use-2-rhh-rhw-2-building-wire [Accessed on 14-6-2024]

As can be seen in the electrical block diagram, the aircraft system contains a low-voltage system. This system runs on multiple voltages and powers the cooling pumps, propeller governors, hydrogen tank heating, flight computer, avionics, and sensors. A DC-DC converter is used to convert the voltage level between the two systems. A COTS DC-DC converter from BrightLoop was selected, which is able to deliver a maximum power of 4.8 [kW][38], meeting the required 4 [kW]. It weighs 1.8 [kg] and can be liquid-cooled. It has four output ports which can operate at different output voltages. This comes in handy since the fuel cell heating system and the pumps operate at 48 and 12 [V] respectively, whilst the other systems operate at 24 [V].

[38] `https://brightloop.fr/products/hv-lv-dc-dc-converters/dcdc-mp-converters/` [Accessed on 14-6-2024]

11. Structures & Materials

The airframe of the aircraft provides structural support and enclosure for all the components and subsystems of the aircraft. Therefore it is crucial to the aircraft's existence and operations. This chapter focuses on the structural design of the fuselage, wings, and the landing gear. Firstly, relevant loads are determined in Section 11.1. This is followed by the design of the fuselage in Section 11.2 and material trade-off in Section 11.3. Landing gear design is then presented in Section 11.4. Lastly, wingbox design is shown in Section 11.5.

11.1. V-n Diagram

To determine the loads that the structure needs to withstand, the maximum load factor needs to be investigated. To determine the maximum load factor two V-n diagrams are generated: the manoeuvring V-n diagram and the gust V-n diagram. These are generated with FAR 23 requirements which dictate the minimum manoeuvring load factors as well as the gusts that aircraft may encounter. The choice has been made to adhere to these standards in this stage of the design based on two main factors. Firstly, a high reliability of 99% of finishing the race is required, which means that the aircraft should be able to perform in all kinds of different scenarios and thus, should survive considerable manoeuvring and gust loads. Secondly, the values from FAR 23 were specified such that the aircraft is sufficiently manoeuvrable. In this stage of the design, the exact manoeuvres required and thus the exact manoeuvring load factors have not yet been determined. Therefore, this method has been used as a starting point. In later design stages, the actual manoeuvring load factor can be determined. Using this approach, results in the V-n diagram shown in Figure 11.1.

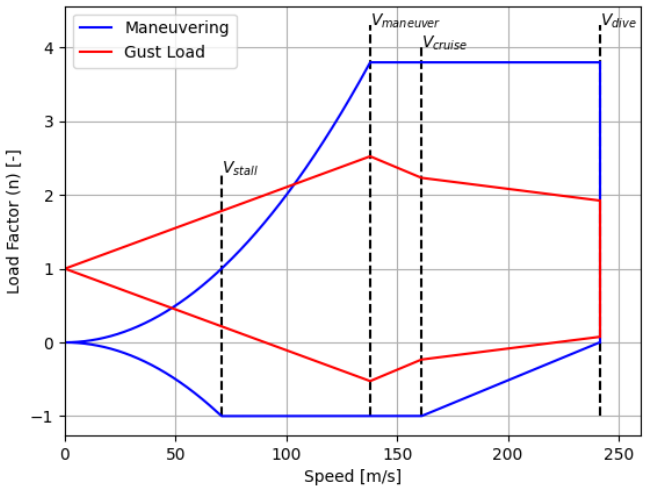

Figure 11.1: V-n diagram

Figure 11.1 was generated for cruise conditions and it shows that the limit load factor is 3.8. Furthermore, for structural design, the ultimate load factor is required. This is defined as $1.5 \cdot n_{limit}$ and is equal to 5.7[1].

11.2. Fuselage Structure

An important part of the structural design is the design of the fuselage. The fuselage is a complex structure that needs to support the other subsystems and to provide a load path for the aerodynamic forces. The design of the fuselage starts of with the packaging of the different subsystems to determine size and shape. Then, the loads on the fuselage are assessed. Finally, the loads will be used to determine an optimal fuselage design.

11.2.1. Fuselage Packaging

The method of determining the fuselage shape consists of different steps. First, the components that need to be placed inside are determined. Next, the components are put in a tight formation together with the pilot and a fuselage shape is fitted around it. However, a few important considerations need to be taken into account, namely:

- **Pilot position and visibility:** The pilot needs to be able to sit in the cockpit and operate the control systems, such as stick and pedals. Furthermore, sufficient visibility to safely operate the aircraft is needed. In this case, looking forward, the lowest visibility angle from the fuselage axis is 17 [°], which is equal to the landing angle of attack of 12 [°] and an additional 5 [°] to allow the pilot to see the runway during approach and touchdown.
- **Landing gear positioning:** Position of landing gear inside the fuselage is highly dependent on the required extended position. Furthermore, its attachment points and mechanisms have to be taken into account.
- **Wing attachments:** Wings need to transfer loads to the fuselage for the aircraft to fly. Therefore, the attach-

[1] `https://www.law.cornell.edu/cfr/text/14/23.2230` [Accessed on 06-06-2024]

ment points and structures need to be considered in the packaging of the fuselage.

Due to the above considerations and many interrelations with all of the aircraft subsystems, the fuselage packaging had to be determined iteratively. The final fuselage shape, the placement of components, and the pilot are shown in Figure 11.2.

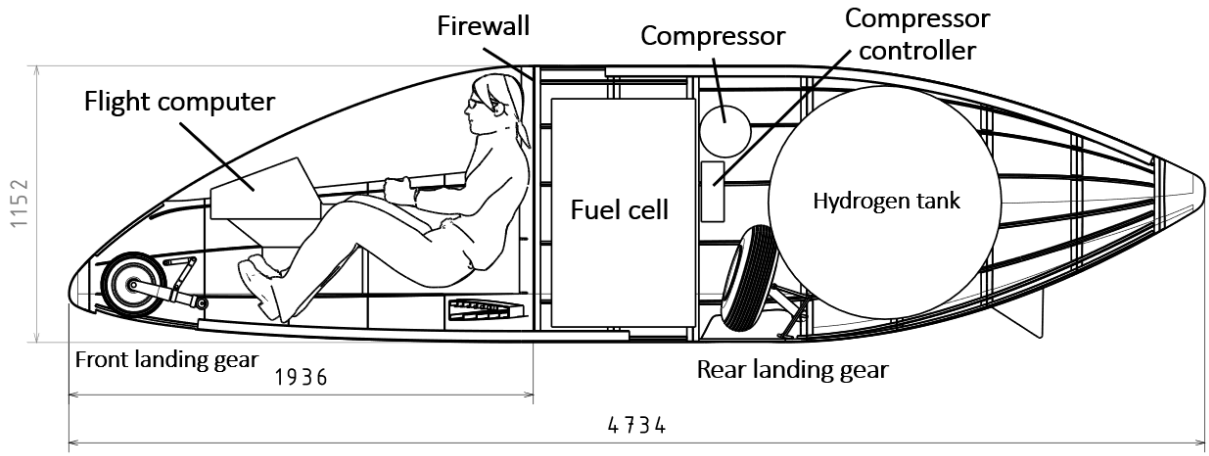

Figure 11.2: Packaging of components in the fuselage

The fuselage is split into two main sections: the cockpit and the rear compartment. The pilot sits in the cockpit, surrounded by the flight computer. It also features a canopy that may be opened to allow for access to the cockpit. All of the high-voltage and high energy components are placed in the rear part of the fuselage and separated from the cockpit with a firewall.

11.2.2. Fuselage Loads

There are a number of different loads that the fuselage will be subjected to. Firstly, the fuselage is subjected to the gravitational loads of its own weight and the weight of the subsystems within the fuselage. Furthermore, the fuselage needs to provide a load path between these gravitational loads and the lift generated by the wing. From the locations of the different subsystems in the fuselage as well as the aerodynamic forces on the wing, the shear force diagram could be generated. For this, the ultimate load factor has been used. The shear force diagram is shown in Figure 11.3.

From the shear force diagram and with the aerodynamic moments, the bending moment diagram could be generated, again the ultimate load factor was used. The bending moment diagram of the fuselage is shown in Figure 11.4.

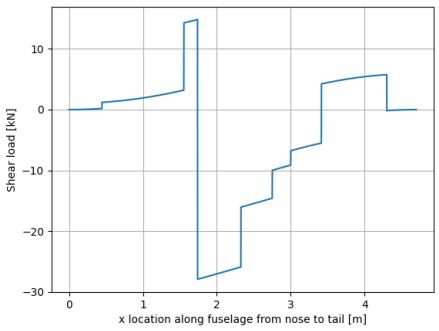

Figure 11.3: Shear force diagram of the fuselage

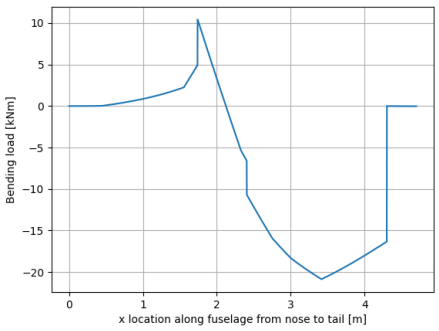

Figure 11.4: Bending moment diagram of the fuselage

The fuselage will also be subjected to normal forces due to the drag and the thrust. To estimate the maximum normal force the fuselage could be subjected to, the maximum thrust has been used. Together with the drag distribution between the front and the back, the normal force on the mid-section was estimated to be -988 [N], meaning that the

fuselage is in compression.

Finally, the fuselage will also be subjected to a torsional load due to the vertical tail. It should be noted that due to the box-wing design, the torsional loads on the fuselage will be significantly lower than for conventional aircraft as part of the torsion is carried by the box-wing. For the design of this aircraft, the torsional load is therefore neglected.

11.2.3. Fuselage Pressurisation

The aircraft needs to provide sufficient oxygen to the pilot. This can be done by either ensuring sufficient cockpit pressure or by providing the pilot with additional oxygen through an oxygen mask. It has been determined that providing additional oxygen would be the most cost-effective way as only one pilot would be on board. A more detailed analysis of the oxygen system is presented in Section 14.1. However, just providing additional oxygen is not sufficient. This is because exposure to the low pressure of high-altitude flight can result in Decompression Illness (DCI). The most common symptoms include pain in the joints, itching of the skin, and faintness. DCI can occur at altitudes as low as 8,000 [ft], however, the risk rises substantially between 21,200 and 22,500 [ft] [83]. It should also be noted that the pilot should not fly multiple times a day at high altitudes for extended periods as this can greatly increase the risk of DCI as well [83]. Thus, to ensure the pilot is safe and to minimise the risk of DCI the cockpit pressure will be at least equivalent to 21,000 [ft], which corresponds to 446 [hPa]. At the cruise altitude of 12,500 [km], the atmospheric pressure is 178 [hPa]. Thus, the cockpit needs to be able to provide a pressure differential of 268 [hPa].So, a combination of pressurisation and an oxygen mask will be used. The pressurisation is to reduce the risk of DCI. However, the cockpit altitude is to low to prevent hypoxia as well. Therefore, an oxygen mask will be used to provide additional oxygen to the pilot as this was considered to be the most weight-efficient solution.

The pressurisation of part of the fuselage introduces an additional loading case. The internal pressure will cause additional normal stresses in the skin and stringers in this part of the fuselage. Furthermore, the bulkheads themselves that seal off the pressurised part from the non-pressurised parts experience normal stress as well. The fuselage is not exactly circular or rectangular which makes the stress analysis more complex. Therefore, certain assumptions were required to provide an estimation. For the pressure bulkheads, the assumption can be made that it will either be circular or rectangular. This leads to equations Equation 11.1 and Equation 11.2 respectively[2],[3]. The equations that lead to the larger stress given the geometry is used for sizing the bulkheads.

$$\sigma = \frac{3(3+\nu)pr_{fus}^2}{8t^2} \tag{11.1}$$

$$\sigma = \frac{0.75pa_p^2}{t^2(1.61(\frac{a_p}{b})^3+1)} \tag{11.2}$$

Furthermore, the stress caused by the pressure in the fuselage section can be estimated with Equation 11.3 and Equation 11.4 for circular and rectangular fuselages respectively[4] [84]. It should be noted that the function for the rectangular cross-section incorporated a number of assumptions and simplifications, however, for an estimation it provides an acceptable estimate as it is used for a cross-section without stiffening while stiffeners will be incorporated.

$$\sigma = \frac{pr_{fus}}{t} \tag{11.3}$$

$$t_{skin} = \frac{b_{rect}}{\sqrt{3}}\sqrt{\frac{1+\alpha_r^3}{1+\alpha_r}}\sqrt{\frac{p}{\sigma_y}} \tag{11.4}$$

Lastly, it should be noted that a safety factor of 1.5 will be used when determining the stress from pressurisation [85].

11.2.4. Fuselage Design Method

The fuselage design will be based on a semi-monocoque structure. This means that the fuselage skin will be load-bearing. The skin will be supported by stringers and frames to transfer loads. An example of this can be seen in Figure 11.5. The loads mentioned in Section 11.2.2 can now be used to design the fuselage such that it can withstand all loads. From the loads, several load cases can be analysed which will be discussed in this section.

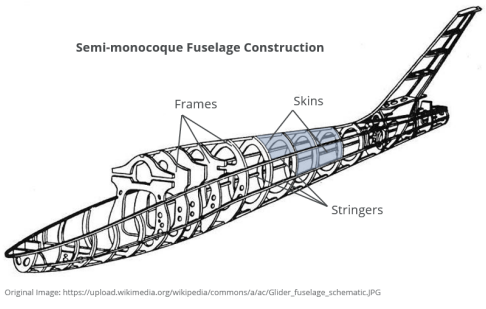

Figure 11.5: Example of semi-monocoque fuselage structure[5]

Bending and Normal Stress

The fuselage design needs to be able to withstand the maximum bending moment. As mentioned before, the fuselage structure will consist of a

[2] https://roymech.org/Useful_Tables/Mechanics/Plates.html [Accessed on 10-06-2024]

[3] https://structx.com/Plate_Formulas_001.html [Accessed on 10-06-2024]

[4] https://prod-edxapp.edx-cdn.org/assets/courseware/v1/05c38d4e1e39ee343aa454ccba35468c/asset-v1:DelftX+AEASM1x+1T2019+type@asset+block/chapter7.pdf [Accessed on 10-06-2024]

[5] https://aerotoolbox.com/fuselage-structure/[Accessed on 16-06-2024]

load-bearing skin and a number of stringers. To analyse the bending performance of the structure, the structure is idealised as shown in Figure 11.6.

In Figure 11.6, the dots represent the stringers with a particular cross-sectional area and the line represents the skin. The moment of inertia is estimated from the locations of the stringers and the skin geometry. The bending stress needs to be added to the normal stress which can be calculated using Equation 11.5 to find the total normal stress distribution.

$$\sigma = \frac{P_{normal}}{A} \tag{11.5}$$

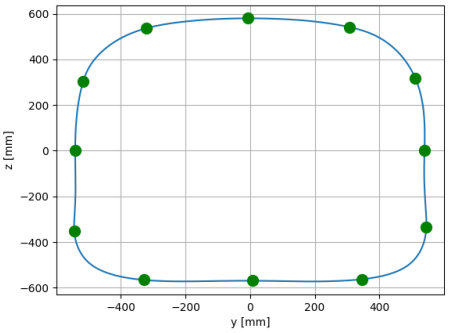

Figure 11.6: Example of idealised fuselage structure

Shear

The fuselage will also encounter shear forces as shown in Section 11.2.2. For this analysis, the same idealised structure as shown in Section 11.2.4 is used. This means that only the skin will carry the shear force. This shear force can be calculated by first determining the shear flow through the skin. The open shear flow will equal the total shear flow when the structure is "cut" at a point where the shear flow is zero, which has been done, thus, Equation 11.6 can be used to determine the shear flow in the skin sections.

$$\Delta q = -\frac{S_y}{I_{xx}} A_{stringer} y - \frac{S_x}{I_{yy}} A_{stringer} x \tag{11.6}$$

Panel Buckling

An important aspect of thin-walled structures is that buckling can occur. This can occur when a stiffened panel undergoes compression. Buckling is a highly complex failure mode and partial buckling of the skin might not be considered a failure at all. However, a simplified approach is taken here. To be conservative, the choice has been made that any buckling will be considered a failure of the structure. Therefore, the structure should be designed such that no buckling will occur under ultimate loads. This means that any post-buckling strength is not taken into account. Furthermore, it is assumed that the top and bottom of the fuselage have straight stiffened panels under the maximum normal stress depending on the load case. As can be seen from the fuselage cross-section shown in Figure 11.6 this is a close approximation. There are many different methods for determining the critical buckling strength of a stiffened panel. For a high-level estimation, the following method is used:

Firstly, the crippling strength of the stringer used has been calculated with Equation 11.7 and Equation 11.8.

$$\frac{\sigma_{cc}^i}{\sigma_y} = \alpha\left[\frac{C\pi^2 E}{\sigma_y 12(1-\nu^2)}\left(\frac{t}{b}\right)^2\right]^{1-n} \tag{11.7}$$

$$\sigma_{cc} = \frac{\Sigma \sigma_{cc}^i A_i}{\Sigma A_i} \tag{11.8}$$

Where α and n are 0.8 and 0.6 respectively for aluminium, which will be the material used as will be discussed in Section 11.3. Then, the buckling stress of the stringer can be determined using the Johnson-Euler column curves determined by Equation 11.9 and Equation 11.10.

$$\sigma_{cr} = \sigma_{cc}\left[1 - \frac{\sigma_{cc}(L_e/\rho)^2}{4\pi^2 E}\right] \tag{11.9}$$

$$\sigma_{cr} = \frac{\pi^2 E}{(L_e/\rho)^2} \tag{11.10}$$

This can then be used to determine the effective skin width, $2w_e$, as shown in Equation 11.11. Now, the skin buckling stress can be calculated using Equation 11.12.

$$2w_e = t\sqrt{\frac{C\pi^2}{12(1-\nu^2)}}\sqrt{\frac{E}{\sigma_{cr_s tringer}}} \tag{11.11}$$

$$\sigma_{cr} = C\frac{\pi^2 E}{12(1-\nu^2)}\left(\frac{t}{b_p}\right)^2 \tag{11.12}$$

Finally, the buckling stress of the stiffened panel can be calculated using Equation 11.13.

$$\sigma_{cc_{panel}} = \frac{\Sigma \sigma_{cc}^i A_i}{\Sigma A_i} \tag{11.13}$$

11.3. Material Trade-Off & Final Fuselage Design

An important part of the structural design is the determination of the material that will be used. This design consists of two major parts for which the material will be determined independently. These are the fuselage and the wing. The material to be used will be determined using a trade-off following the WSM.

11.3.1. Material Options

Firstly, the potential material options need to be explored. For this purpose, a design options tree has been created, that shows typical materials used in the aviation industry today, shown in Figure 11.7 [86].

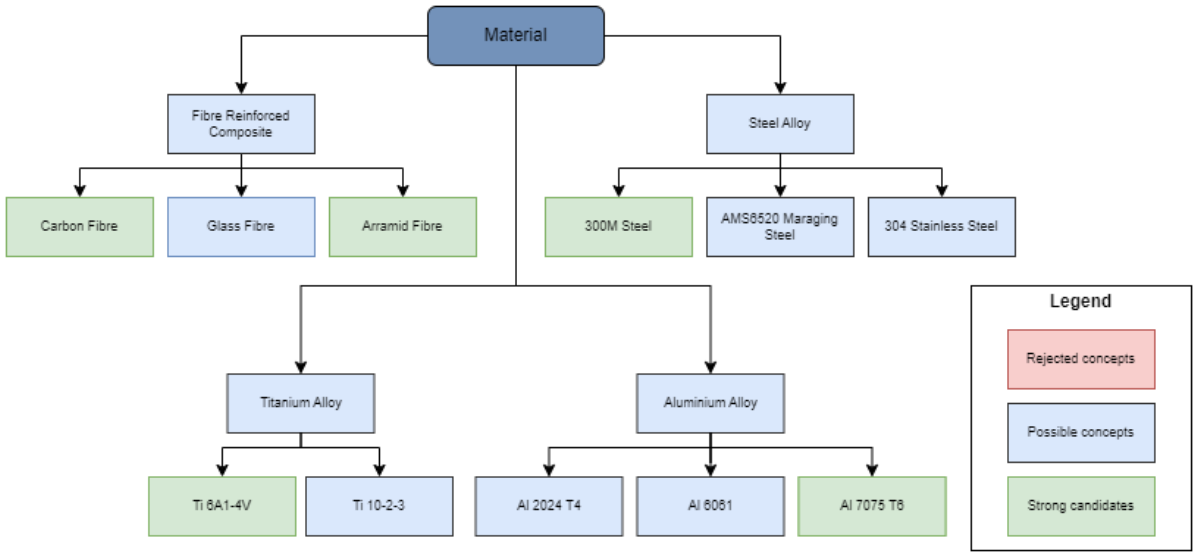

Figure 11.7: Design options tree of material types

In Figure 11.7, certain materials are shown as green as they are found to be the best materials within their category considering their mechanical properties. An assumption has been made that within the categories variables like cost, sustainability, and density would not vary too much, therefore the best of each category could be chosen based on their mechanical properties. These materials will be entering the material trade-off. To determine the performance of the materials, their properties are required. These are shown in Table 11.1.

Table 11.1: Material properties

Material	Tensile Yield Strenght [MPa]	Shear Yield Strenght [MPa]	E-Modulus [GPa]	Shear Modulus [GPa]	Density [g/cm^3]
Carbon fibre composite[6] [87]	673	65.6	46.45	4.2	1.8
Aramid fibre composite[6] [87]	380	46	29.3	1.7	1.4
Aluminium 7075 T6[7]	503	331	71.7	26.9	2.81
Steel 300M[8]	1550	1100	205	80	7.87
Ti 6A1-4V[9]	880	550	113.8	44	4.43

11.3.2. Trade-Criteria

For the material trade-off, three criteria are of importance: weight of the final structure, cost, and sustainability. For this mission in particular, weight is highly important as it has a high impact on the final performance. This will be assessed by estimating the weight of the structure in question if it was made of that material. This criterion was assigned a weight of 50 %.

[6] https://performance-composites.com/carbonfibre/mechanicalproperties_2.asp [Accessed on 04-06-2024]
[7] https://asm.matweb.com/search/SpecificMaterial.asp?bassnum=ma7075t6 [Accessed on 04-06-2024]
[8] https://www.azom.com/article.aspx?ArticleID=6671 [Accessed on 04-06-2024]
[9] https://asm.matweb.com/search/SpecificMaterial.asp?bassnum=mtp641 [Accessed on 04-06-2024]

Cost is the second most important parameter as it is a driving requirement, which has been determined in the preliminary stage. Cost includes both the raw material cost and the manufacturing cost. This is based on an estimation from statistics and literature. The cost criteria has a weight of 30%.

Lastly, from the sustainable development strategy it has been found that the material used would have a large impact on total embedded emissions. Therefore, the sustainability of the material will be assessed as well. This includes emissions caused during the full life cycle of the material type. This criterion has a weight of 20%.

11.3.3. Grading of Materials

With the criteria determined, the different materials can be graded with respect to these criteria. Each material is assigned a grade from 1-5 depending on its performance with respect to the criteria. The grading of the materials is discussed in this section.

Weight Criteria

As mentioned before, the weight criterion is dependent on the structure that the material is used for. In this case, both the wings and fuselage structure are assessed separately. The method described in Section 11.2.4 has been used to estimate the mass required for the structure depending on the material properties. Here, the weight for the fuselage will be discussed, in Section 11.5.3 the weight for the wingbox will be discussed. From initial sizing estimates, it was found that the buckling failure mode would be most critical for the fuselage, thus, the fuselage designs for the different materials are created using only this failure mode in mind. It should be noted that this weight estimation has been done in the early stages of the design and therefore, the values of the stringers and weight vary significantly from the final design of the fuselage. Furthermore, for all designs, the same stringer size and geometry is used. Lastly, the amount of stringers is determined by the stringer spacing required for the most critical part of the fuselage. This results in the following designs for the different materials, shown in Table 11.2.

Table 11.2: Fuselage design properties per material

Material	Skin Thickness [mm]	Amount of Stringers	Weight [g/cm]	Grade
Carbon fibre composite	0.52	42	71	5
Aramid fibre composite	0.58	45	61	5
Aluminium 7075 T6	0.48	38	102	4
Steel 300M	0.39	31	232	1
Ti 6A1-4V	0.45	34	147	3

On this criteria, the grading is done relatively as a lower weight is always more beneficial. The following grading rules have been determined:

- **1 - Unacceptable:** >2225 [g/cm]
- **2 - Undesirable:** 175 - 225 [g/cm]
- **3 - Acceptable:** 125 - 175 [g/cm]
- **4 - Good:** 75-125 [g/cm]
- **5 - Excellent:** <75 [g/cm]

Cost Criteria

The cost criteria consist of two main parts. The cost of the raw material and the cost of manufacturing when using the material. During the literature review, information was found on the total cost of these materials for a manufactured beam. Therefore, this has been used as a representation of the cost of the different materials. This is shown in Table 11.3 [88]. Again, relative scoring is used, with the following grading rules:

Table 11.3: Raw material cost

Material	Raw Material Cost [$/kg]	Grade
Carbon fibre composite	90	1
Aramid fibre composite	80	1
Aluminium 7075 T6	8.4	5
Steel 300M	12	5
Ti 6A1-4V	66.1	2

- **1 - Unacceptable:** >75 [$\$/kg$]
- **2 - Undesirable:** 55 - 75 [$\$/kg$]
- **3 - Acceptable:** 35 - 55 [$\$/kg$]
- **4 - Good:** 15-35 [$\$/kg$]
- **5 - Excellent:** <15 [$\$/kg$]

Sustainability Criteria

To determine the sustainability of the different materials, a life cycle analysis approach is used. This means that the emissions caused throughout the entire production of the material are summed up to determine the life-cycle emissions in $CO_{2_{eq}}$. From literature, the values for embedded emission per material are found, which are shown in Table 11.4.

Table 11.4: Material carbon footprint

Material	$CO_{2_{eq}}$ Footprint [kg/kg]	Grade
Carbon fibre composite [89, 90]	29	2
Aramid fibre composite [91]	17	3
Aluminium 7075 T6 [92]	12.7	4
Steel 300M [93]	2	5
Ti 6A1-4V [94]	50	1

From this, a relative scoring can be made as there are no requirements on embedded emissions. Thus the following grading rules have been defined:

- **1 - Unacceptable:** >35 $[CO_2 - eqkg/kg]$
- **2 - Undesirable:** 25 - 35 $[CO_2 - eqkg/kg]$
- **3 - Acceptable:** 15 - 25 $[CO_2 - eqkg/kg]$
- **4 - Good:** 5 - 15 $[CO_2 - eqkg/kg]$
- **5 - Excellent:** <5 $[CO_2 - eqkg/kg]$

Which results in the grading for the materials shown in Table 11.4.

11.3.4. Trade-Summary Table

The criteria weights together with the grading for the different concepts can be summarised in a trade-summary table. This is shown for the fuselage material in Table 11.5.

Table 11.5: Material trade-off summary table

Material	Weight	Cost	Sustainability	Total
Carbon fibre composite	4	1	2	2.7
Aramid fibre composite	5	1	3	3.4
Aluminium 7075 T6	4	5	4	4.3
Steel 300M	1	5	5	3.0
Ti 6A1-4V	3	2	1	2.3

From Table 11.5, it can be seen that Aluminum 7075 is the clear winner and therefore, this is used as the material for the fuselage. The material selection for the wing is discussed further in Table 11.10.

11.3.5. Sensitivity Analysis

When performing a trade-off, it is important to determine the sensitivity of the trade-off method. For the specific trade-off, relative grading has been used, which is generally subjective as the grade boundaries are chosen subjectively. Furthermore, the weights of the different criteria are also subjectively based on what is considered the most important aspect of the material selection.

Thus, a sensitivity analysis has been performed which varied the weights of the criteria by +-10% and +-5%, such that the total of the weights is 100%. Furthermore, the grades for the materials were also changed with +-1 or 0. This resulted in the following final score distribution as shown in Figure 11.8.

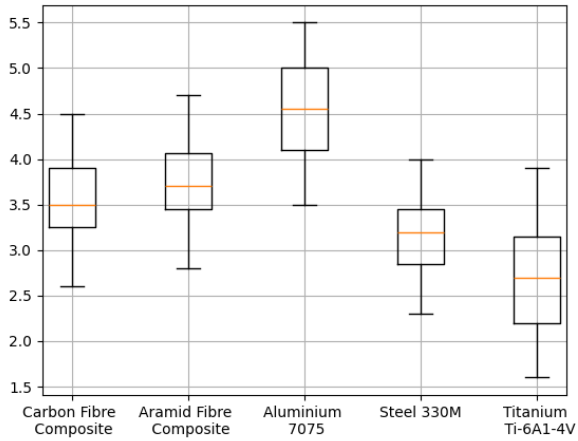

Figure 11.8: Box plot of score distribution for different materials

In Figure 11.8, it can be seen that there is an overlap between the different materials. Specifically, the winner of the trade-off, aluminium 7075 shows considerable overlap with both composite materials. However, the interquartile range of aluminium is fully disconnected from any other interquartile range which gives sufficient confi-

dence that the winner of the trade-off is only slightly impacted by the subjectivity of the grades and the criteria weights and thus, that aluminium 7075 is the clear winner of this trade-off.

11.3.6. Fuselage Design

The formulas presented in Section 11.2.4 can now be used to create a fuselage design. As mentioned before, the fuselage structure will be made up of skin and stiffening elements such as stringers and frames. The fuselage is not allowed to yield in any particular load case including combined loading. Therefore, to generate a design it is useful to initially investigate which failure mode might be most critical. During this investigation, it has been found that buckling would be the most critical failure mode considering the normal stress.

An important parameter influencing the design is the stringer shape. It has been found that a Z-stringer is the most used and most efficient stringer [86]. Therefore, the choice has been made to use this stringer type as well. Considering that skin buckling has been determined to be critical, it is more beneficial to use more small stringers than fewer big stringers. Therefore, the stringer geometry shown in Figure 11.9 has been chosen, with a thickness of 1 [mm].

To start the design, firstly, the frame spacing has been set to be 0.33 [m]. For normal commercial aircraft, the frame spacing is generally set to be around 0.5 [m] [95]. However, due to the size of this aircraft and the buckling constraints, it has been found that the aforementioned spacing was better suited to this design. The frame design was based on a T cross-section, and the dimensions were based on standard sizes of frames, as analysing the loads on the frames would require a Finite Element Method (FEM) analysis [86]. The frame geometry is shown in Figure 11.10, where the frame has a thickness of 2 [mm].

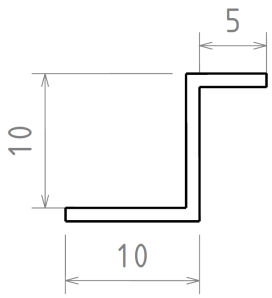

Figure 11.9: Stringer geometry

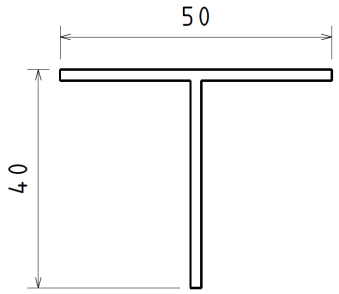

Figure 11.10: Frame geometry

Then, the skin thickness and amount of stringers were varied to find the most lightweight combination meeting the buckling load. The buckling load has been determined from the combined maximum normal and bending stresses present in the mid-fuselage section. For this analysis, a minimum skin thickness of 0.4 [mm] has been set as this has been found to be the minimum thickness an aluminium-7075 skin needs to have to carry shear loads [96]. This resulted in a skin thickness of 0.4 [mm] and a total of 16 stringers for the mid-fuselage section. Finally, the design needs to be checked with respect to the other failure modes/load cases. The results of this analysis are shown in Table 11.6.

Table 11.6: Stresses and safety factors for different load cases

Failure Mode	Maximum Allowable Stress [MPa]	Maximum Stress [MPa]	Safety Factor [-]
Buckling	36.9	30.75	1.2
Normal yield	500	30.75	16.3
Shear yield	207	7.2	28.8

As can be seen in Table 11.6, the buckling criteria is in fact most critical, as all the other load cases do not approach failure. It can also be seen, that for the other load cases, the safety factor is very high. This is mainly due to the limit set by the minimum practical skin thickness as otherwise the skin thickness could be further decreased to decrease the mass of the fuselage. It should be noted that the analytical approach to the fuselage is not very accurate and therefore additional analysis such as the FEM need to be used to get a more accurate sizing of the fuselage structure. A start on process has been made for the verification of the design and is shown in Section 11.3.8.

However, the fuselage does not only consist of the midsection, therefore, both the nose and the aft section needed to be designed as well. For the nose section, pressurisation has been found to be the most critical. The equations in Section 11.2.3 are used to determine the required thickness of the fuselage skin in this section. It has been found that a skin thickness of 3.1 [mm] is required for a rectangular fuselage and less than 0.1 [mm] for a circular fuselage. This difference is substantial, however, the effect of the complex in-between fuselage shape that has been chosen cannot be assessed at this point. Therefore, the worst case is taken as a preliminary estimate as a conservative approach. Furthermore, the back bulkhead will also act as a firewall, which is explained further in Chapter 14. Thus, the decision has been made to create this bulkhead/firewall from 300M steel instead of aluminium due to its superior thermal performance. Again, the method in Section 11.2.3 is used to determine that the thickness of the firewall should be 11.6 [mm] based on the largest thickness found in the circular and rectangular estimations. However, as this is a relatively simple part, the decision has been made to analyse this with the FEM. Using this method, it has been found that the bulkhead could be substantially thinner and only needed to be 1.2 [mm]. The resultant stresses in the bulkhead are shown in Figure 11.11. The mass of the firewall is equal to 10.1 [kg] and is considered part of the safety systems' mass in Table 15.7 instead of in the fuselage structure's mass.

The front bulkhead will have a complex shape due to the nose gear placement. To determine the geometry for this bulkhead has been deemed outside the scope of this report. Furthermore, to limit the additional loads on the skin, a structural beam will be placed between the front wingbox, the nose landing gear, and the mid-section fuselage frames. An additional structural beam will be placed at the connection of the vertical stabiliser as this will be used to distribute the loads from the aft wing across several frames.

For the aft section, the most important part is the cutout caused by the main landing gear. To accommodate this, cut-out frames will be placed on either side of the cutout. Furthermore, additional stringers will be placed to provide additional strength and stiffening. With the full fuselage structure determined, the weight breakdown can be determined. This can be seen in Table 11.7.

Table 11.7: Weight breakdown of fuselage structure

Component	Mass [kg]
Stringers	3.9
Frames	29.1
Beams	6.7
Skin	40.9
Canopy	8.5
Contingency margin	30.9
Total fuselage mass	**120.0**

It should be noted that the weight breakdown shown in Table 11.7 is incomplete. Additional weight needs to be taken into account for joining materials, such as rivets as well as the support structure for the different subsystems. Therefore, for the weight breakdown of the entire aircraft, a total fuselage structural mass of 120 [kg] is used, which includes a margin of 35%. Which is 10% for the joining methods employed and 25% for additional structure to support the subsystems [97].

11.3.7. Canopy Design

The canopy of the cockpit is also considered a part of the structure. The design of this canopy consists of a number of steps. Firstly, the dimensions and geometry of the canopy needed to be determined. This has been determined by the packaging of the pilot and the fuselage as well as the visibility required for the pilot.

Such canopy designs are generally made of monolithic or laminated acrylics and polycarbonates[10]. It should be noted that the limiting design constraints for canopies and windshields are bird strike and pressurisation loads. Therefore, a strong and impact-resistant material is beneficial. Polycarbonates perform better than acrylics with respect to these parameters and therefore, it has been chosen to use a polycarbonate canopy. Finally, it has been found that laminated canopies perform better than monolithic for the same thickness [98] using solvent bonding between the laminates. It has been found that a thickness of 4 [mm] is sufficient to resist bird strike, thus this will be used for the design [98].

11.3.8. Verification

Since the fuselage has been designed, mostly using simplified analytical formulas, it has been decided to perform a structural numerical analysis to verify the design under design loads. Initially, it was planned to perform a simulation of a full fuselage assembly, including the skin, canopy, stringers, frames, and beams. However, after numerous attempts, it has been found that this model would be computationally intensive and the available computational resources would not allow the analysis to be performed in an acceptable timeframe. Therefore, in the end, a simplified model has been simulated.

To verify the fuselage, FEM analysis offered by Ansys has been utilised. The simplified model of the fuselage consists

[10] `https://www.dsiac.org/wp-content/uploads/2018/02/2175747_STI_Document.pdf` [Accessed on 09-06-2024]

of skin coupled with frames and stringers that represent its middle section and it is illustrated in Figure 11.12. The most critical loads in the structure were the bending loads due to lift provided by the wings, and therefore, only those were simulated, which allows for saving computing resources by only having half of the fuselage and applying symmetry boundary conditions in the analysis.

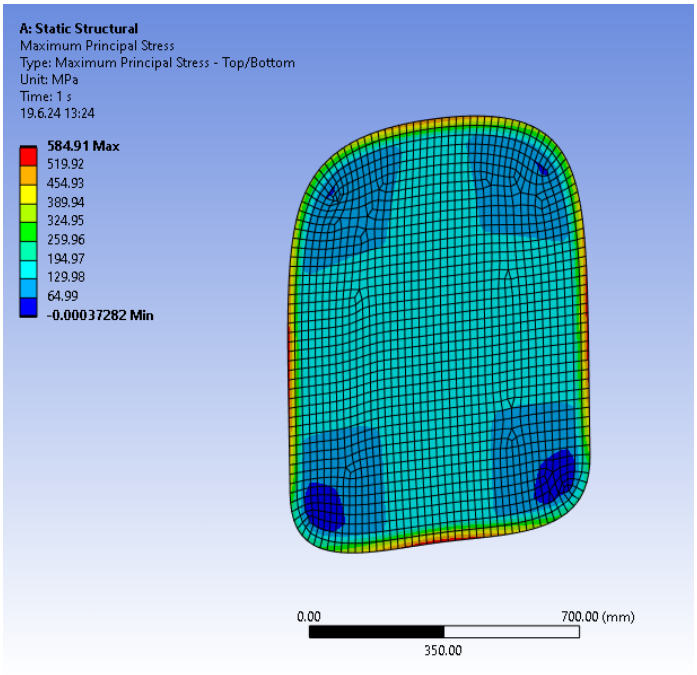

Figure 11.11: Maximum stresses in the firewall

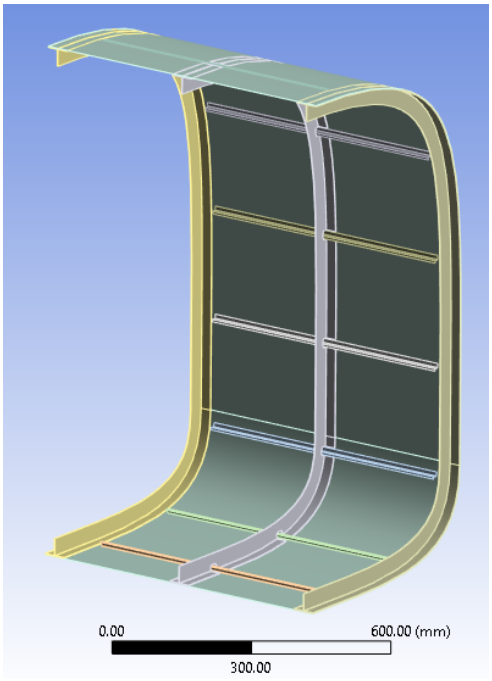

Figure 11.12: Fuselage section used in FEM analysis

In the model, the front side of the fuselage section is fixed in space and to the middle, a symmetry boundary condition is applied to mimic the presence of the other half of the fuselage. To simulate bending loads, a maximum design bending moment is applied to the rear side of the fuselage section. Buckling has been deemed to be the limiting failure mode of the fuselage, and as such the eigenvalue buckling simulation has been run. The visualisation of the results of this analysis is shown in Figure 11.13.

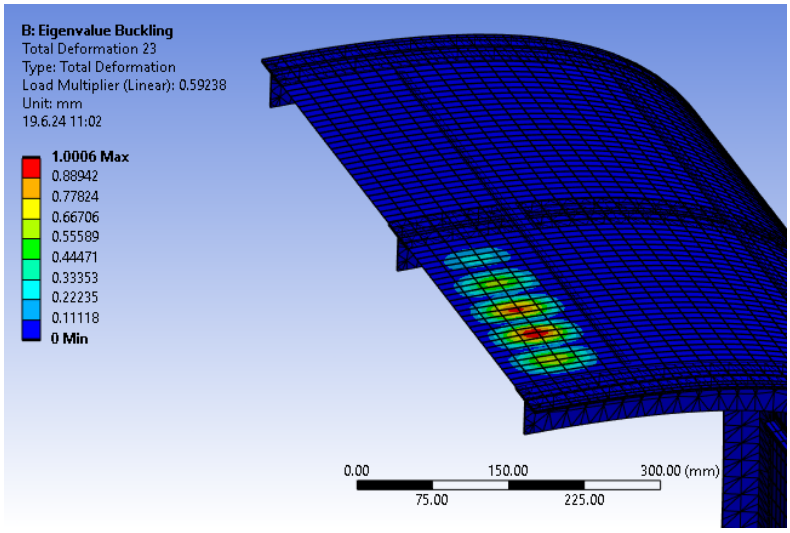

Figure 11.13: Results of buckling FEM analysis

The numerical analysis indicates that the first occurring buckling mode is the buckling of the skin at the top of the fuselage. This confirms the expected behaviour, since the top of the fuselage is subjected to compression during bending and the extreme stresses should occur at the maximum vertical distance from the fuselage axis. However, the load at which this buckling occurs is determined to be equal to 59 % of the design load. This means that the fuselage design might not withstand the required loads. This discrepancy could not be analysed in more depth due to time constraints, but a possible recommendation to fix this issue might be to increase the critical skin buckling stress. As can be seen in Equation 11.12, this stress is proportional to the term $\left(\frac{t}{b}\right)^2$. Since the original design is expected to buckle at around 59 % of the load, a 70 % increase of this term should suffice to satisfy the requirement. The exemplar changes that could be made to the design is increasing the skin thickness by 30 % or decreasing the spacing between the stringers by 23 %. Those changes, however, are just estimates and they might not guarantee the necessary strength. For this reason, a more detailed analysis of this matter must be

performed before the plane can be flown.

11.4. Landing Gear Design

The landing gear is an essential part of the structure as well. It determines the ground handling manoeuvring capabilities and requires additional support structure as well. To design the landing gear, multiple criteria need to be taken into account which are discussed in the following subsections.

Firstly, however, the landing gear configuration needs to be determined. Considering the size of the aircraft three configurations were possible: conventional, tricycle and bicycle. The bicycle configuration needs additional wheels on the wings and is generally considered a last resort. Therefore, this has not been chosen. Secondly, the conventional configuration requires the centre of gravity to be located far forward to ensure that no undesirable ground-looping tendencies are present. During initial estimations, it was found that the centre of gravity would be located near the middle of the fuselage and thus this configuration is not feasible either. This leaves the tricycle configuration, which is the chosen configuration.

11.4.1. Landing Gear Position

Firstly, the landing gear position is determined using three main sizing angles. These ensure that during ground manoeuvres, no parts of the plane except the landing gear touch the ground and that no tip-over will occur. The 2 most important limitation angles are shown for this design in Figure 11.14.

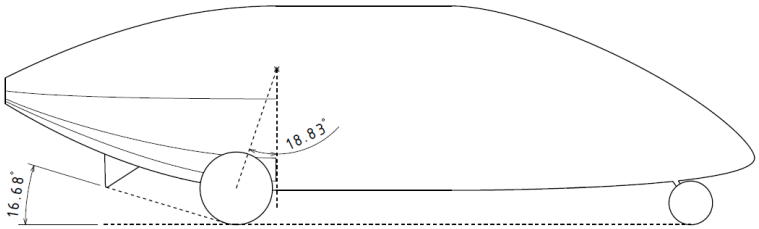

Figure 11.14: Landing gear design

To keep the landing gear size as small as possible the main landing gear is placed on the edge of the limitation lines. The location of the front landing gear has been determined by the available space in the fuselage and thus, put all the way at the front.

11.4.2. Tyre Sizing

To size the tyres, an approach based on statistics has been used [99]. This resulted in the parameters for the main and the nose wheel as shown in Table 11.8.

Table 11.8: Main and nose wheel parameters

Parameter	Main Wheel	Nose Wheel	Unit
Rim Diameter	20	12	cm
Tyre Diameter	40.5	24.3	cm
Tyre Width	13	7.8	cm
Mass Tyres	2.6	0.55	kg
Mas Wheel	7.9	2.9	kg

11.4.3. Shock Absorption

An important function of the landing gear is shock absorption. The landing gear should absorb the shock of the initial touch-down such that this shock is not transferred to the rest of the aircraft and the pilot. Thus, shock absorbers are required. There are several different types of shock absorbers, however, for this design, it has been decided to use an oleo-pneumatic shock absorber. This is the most used shock absorber in the industry both for its high absorbing efficiency and its low weight. It is more complex than other options but due to its extensive use, it has a high reliability [86]. For the oleo absorber the stroke length can be determined using [100]:

$$S = \frac{V_{sink}^2/2g + (1 - K - Nn_t)S_t}{Nn_s + K - 1} \tag{11.14}$$

Where for K, S_t, n_t, n_s and N values based on literature were used [100]. The sink velocity has been determined using the approach speed and angle. This results in a stroke length of 12.3 [cm], which holds for both the nose gear and the main gear.

11.4.4. Landing Gear Retraction

Now that the landing gear location and size have been determined, the retraction mechanism can be designed. Firstly, the storage locations have been determined using available space in the fuselage and rotation mechanisms. Secondly, the strut length can be determined by finding the minimum of the fuselage to hub distance and the stroke length. Then, by using the required extended and retracted positions the extraction mechanism can be determined. The nose gear will be retracted forwardly, which is a conventional mechanism as shown in Figure 11.15.

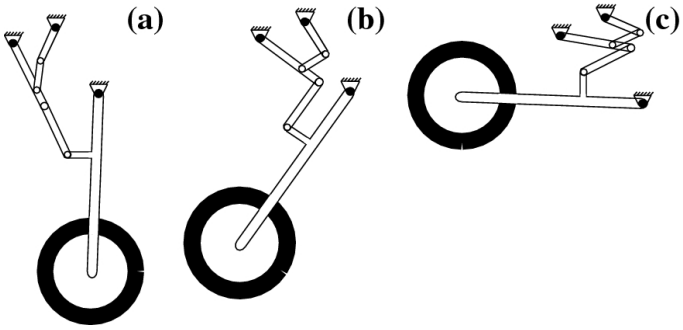

Figure 11.15: Nose landing gear retraction mechanism [101]

This will result in the required retracted and extended location of the nose wheel. The main landing gear retraction mechanism is more complicated as its retracted and extended locations are very specific. Furthermore, generally main landing gear folds sideways, whereas in this mechanism it folds both forward and sideways, meaning that the rotation axis is not strictly horizontal or vertical. Still, a similar mechanism as shown in Figure 11.15 can be used here as well, but the modification was required to meet the larger required rotation angle.

11.5. Wingbox Design

The wingbox is a crucial structural component of an aircraft wing. It serves as the primary load-bearing structure, resisting bending, torsional, and shear forces encountered during flight. The wingbox is composed of spars, webs, stringers, ribs, and skin, forming a rigid framework that provides both strength and rigidity to the wing.

The design and analysis of a wingbox are critical to ensuring the structural integrity and safety of an aircraft. This section outlines the methodology employed to design an idealised wingbox structure, calculate the stresses and critical buckling loads, and optimise the design for different materials. The simplified 'boom' type analysis approach facilitates a first-order design by reducing the complexity of the wingbox structure. The analysis also incorporates the effects of taper and material properties to ensure a robust and lightweight design. The following subsections detail the idealised structure, stress calculations, loading conditions, optimisation process, and final design verification. This comprehensive approach ensures that the wingbox meets all safety requirements while optimising for weight and material efficiency.

11.5.1. Method

Idealised structure

As the wingbox consists of multiple components such as spars, webs, stringers, ribs, and skin, the analysis of the wingbox can become quite complex. In order to make a first-order design, the complex structure is idealised into a more simple model. This simplification is a 'boom' type analysis from T. Megson [102]. As the cross-sectional area of the stringers, spars, and flanges is relatively small compared to the complete section the variation of stress across a stringer would be small [102]. Also, the difference between the stringer centroid and skin is small enough to assume constant direct stress [102]. Furthermore, it is also assumed that the booms carry all normal stresses, and the skin only carries shear stresses. Hence, the surrounding skin area is added to a boom and the skin thickness is zero. The boom area, B, can be calculated with the following formulas [102].

$$B_1 = \frac{t_D b}{6} \cdot (2 + \frac{\sigma_2}{\sigma_1}) \tag{11.15}$$

$$B_2 = \frac{t_D b}{6} \cdot (2 + \frac{\sigma_1}{\sigma_2}) \tag{11.16}$$

Here t_D is the thickness of the skin, b is the width of the section which is in this case the stringers spacing, and σ_i is the normal stress in boom 'i'. For pure axial stress the ratio $\frac{\sigma_1}{\sigma_2}$ would be zero, in case of a pure bending moment this would be -1. With this idealisation, the position of the stringers can be determined using the contour of the airfoil as a function of the number of stringers on the top and bottom. The wingbox configuration is optimised for weight while still being able to carry all required loads. It has been found that the wingbox needs to consist of four corner stringers, 7 top stringers equally spaced between the top corner stringers, and 4 bottom stringers equally spaced between the bottom corner stringers. Furthermore, Figure 11.16 shows the conventions used with respect to the coordinate system. Figure 11.17 shows the boom representation of the sheet.

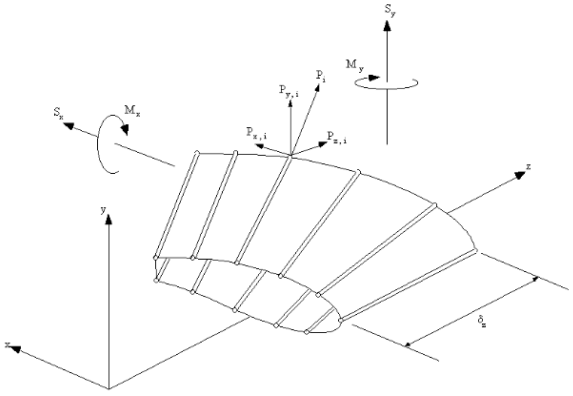

Figure 11.16: Wingbox coordinate conventions

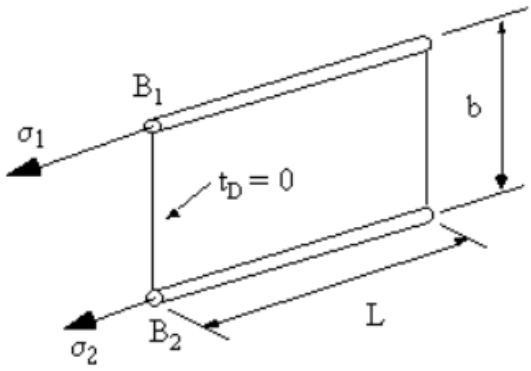

Figure 11.17: Boom representation of sheet

Stresses

The loading distribution in the wing induces a shear stress in the wingbox. This shear stress should be below the allowable maximum shear stress. To determine the shear stress, the shear flow is calculated. The effect of taper is also accounted for, as the effect on shear stresses is considerable with taper present in a beam [102]. From [102], the following formulas can be used to calculate the shear force in the web with the effect of taper considered:

$$S_{x,w} = S_x - \sum_{n=1}^{n} P_{z,i} \frac{\delta x_i}{\delta z} \tag{11.17}$$

$$S_{y,w} = S_y - \sum_{n=1}^{n} P_{z,i} \frac{\delta y_i}{\delta z} \tag{11.18}$$

Where $\frac{\delta x_i}{\delta z}$ is the taper in x-direction, $\frac{\delta y_i}{\delta z}$ represents the taper in y-direction, S_x and S_y are the shear forces in x and y direction respectively. Where $P_{z,i}$ represents the normal force carried by a boom, this is defined below [102]:

$$P_{z,i} = \sigma_{z,i} B_i \tag{11.19}$$

To determine the total shear flow in the section, the shear flow of the open section q_s is added to the shear flow of the closed section $q_{s,0}$.

The shear stress in the wingbox for a closed section for an idealised boom structure is defined as [102]:

$$q_s = q_{s,0} - \frac{S_{w,y}}{I_{xx}} \sum_{i=1}^{n} B_i y_i - \frac{S_{w,x}}{I_{yy}} \sum_{i=1}^{n} B_i x_i \tag{11.20}$$

As the shear flow is constant between boom sections there is a 'jump' of shear stress in a given boom, this jump can be expressed as [102]:

$$\Delta q_i = -\frac{S_y}{I_{xx}} B_i y_i - \frac{S_x}{I_{yy}} B_i x_i \tag{11.21}$$

To determine $q_{s,0}$, to account for the closed section shear the formula below can be used [102]:

$$q_{s,0} = \frac{T}{2A_{cross-section}} \tag{11.22}$$

Where T is the torque around the z-axis of the beam.Next to shear stresses, normal stresses are also present in the wingbox mainly induced by the lift force imposing a moment, M_x, on the wingbox. A general formula for moment-induced stress can be used [102].

$$\sigma_z = \frac{M_x(I_{yy}y - I_{xy}x)}{I_{xx}I_{yy} - I_{xy}^2} + \frac{M_y(I_{xx}x - I_{xy}y)}{I_{xx}I_{yy} - I_{xy}^2} \tag{11.23}$$

Where $I_x x$ and $I_y y$ are the moments of the area around the x and y axis respectively. Also, M_x and M_y are the moments on the wingbox around the x and y axis respectively.

Next to staying below the yield stress of the material, critical buckling loads are also considered. The most critical buckling case has been found to be [102]:

$$\sigma_{cr,buckling} = \frac{k\pi^2 E}{12(1-v^2)}(\frac{t}{b_p})^2 \tag{11.24}$$

Here, k is the buckling coefficient, which depends on the clamping conditions of the section. For this analysis, it is assumed the section is simply supported at the edges which gives the most critical k of 4. Furthermore, E is the E-modulus of the material, v the Poisson's ratio, t the sheet thickness, and b_p is the width of the plate which is the stringer spacing in this case.

11.5.2. Loading

The simulations performed during the aerodynamic analysis resulted in a span-wise distribution of lift coefficients and quarter-chord moment coefficients. The moment about the z-axis, T, can be obtained by multiplying the forces in both directions, S_y and S_x, with the dynamic pressure and the wing surface area. The moment around the y-axis, M_y, and x-axis, M_x, of a section located at z-distance from the root can be obtained by taking the shear force of the section multiplied with z. As can be seen in Figure 11.1, the maximum load factor of the aircraft is 3.8. A safety factor of 1.2 has been added to the ultimate safety factor of 1.5. This results in a maximum load factor of 6.84, and a minimum load factor of -1.8 which have been used in the analysis of the wingbox.

11.5.3. Trade-Off and Optimisation

With the method described above, the model can be utilised for material selection and optimisation. Optimisation has been performed by running the model for a range of inputs making all possible combinations. The inputs for the model are listed below.

- sheet thickness, t_D
- stringer area, A_{str}
- number of top stringers, n_{top}
- number of bottom stringers, n_{bottom}

By adjusting the range of each input, an optimal design could be determined for a given material. However, a material still has to be chosen. Different materials have been considered, and using their various properties the optimisation was able to run multiple times. Different materials have been considered, which are tabulated in Table 11.9, along with their properties and the estimated wingbox weight. The properties shown in the table are the E-modulus E, the yield stress σ_{yield}, maximum shear stress τ_{max}, Poisson ratio, and the density ρ. The values are taken from Table 11.1. The output, the wingbox mass, has been highlighted.

Table 11.9: Wingbox results for different materials

Material	Total Mass [kg]	E [GPa]	σ_{yield} [MPa]	τ_{max} [MPa]	Poisson [-]	ρ [kg/m^3]
Carbon Fibre Composite	**145.68**	46.45	673	65.6	0.27	1800
Arramid Fibre	**135.22**	49.25	380	46	0.27	1400
Aluminium 7075 T6	**146.37**	71.1	503	331	0.33	2810
Steel 300M	**300.97**	205	1586	1190	0.28	7870
Ti6A1	**201.72**	114	880	550	0.342	4430

With these results a trade-off with the same setup as in Section 11.3.3 could be performed. Scores are given for the mass of the wingbox, cost, and sustainability. The results of the trade-off are tabulated in Table 11.10. In addition, a sensitivity analysis was performed where the weights and scores were changed by $\pm$ 10%. The results are presented in a boxplot, Figure 11.18 .

Table 11.10: Trade-off wingbox material

Material	Mass	Cost	Sustainability	Score
Carbon fibre	4	1	2	2.7
Arramid fibre	5	1	3	3.4
Aluminium	4	5	4	4.3
Steel 300M	1	5	5	3
Ti 6A1-4V	3	2	1	2.3

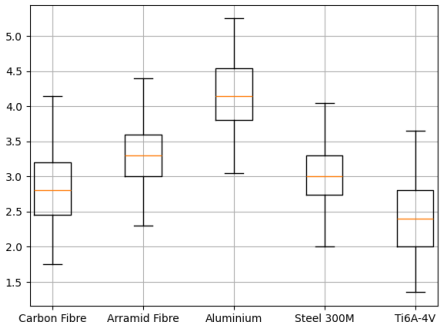

Figure 11.18: Sensitivity analysis wingbox material

11.5.4. Final Design

The final design of the wingbox is summarised in Table 11.11 below. The top row shows the front wing, which refers to the backward sweeping wing connected to the fuselage of the aircraft. The second row shows the aft wing, which refers to the forward sweeping wing connected at the vertical stabiliser. In the table, the safety factors for both yield stress and maximum shear stress are shown for a load factor of 5.6, which is the maximum load factor of 3.8 with only the ultimate safety factor applied of 1.5. The results show that the safety factor of 1.2 is met. Next to the number of stringers, stringers area, and sheet thickness, the skin thickness and wing mass are also included in the table.

Table 11.11: Final design wingbox results

Wing	n_{up}	n_{bot}	A_{str} [mm^2]	t_D [mm]	mass [kg]
Front wing	7	4	80	1.9	34.85
Aft wing	7	4	50	1.5	38.55
Skin	-	-	-	1.0	24.0
Side stabilisers	-	-	-	1.0	10.0
Vertical stabiliser	-	-	-	1.0	5.0

11.5.5. Verification

To verify the code, a number of tests will be performed where the initialisation of the booms, shear and direct stresses, safety factors, and optimisation will be verified.

To verify how the code interprets the number of stringers correctly, two cases are visualised where the airfoil is plotted with the stringers and corner stringers scattered in the same graph, which should verify whether the stringers are placed correctly along the airfoil. The first case consists of zero stringers on the top as well as on the bottom of the airfoil, this verifies whether the program correctly handles the corner stringers. This can be seen in Figure 11.19. In addition, the actual design case is also visualised, which consists of 7 top stringers (excluding 2 corner stringers) and 4 bottom stringers (excluding 2 corner stringers) as shown below in Figure 11.20.

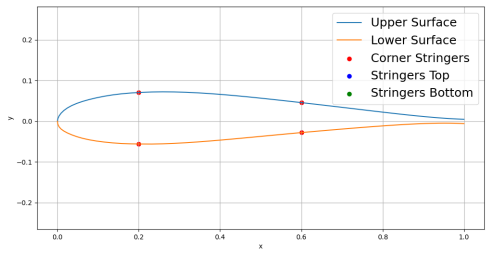

Figure 11.19: Stringers initialisation case 1

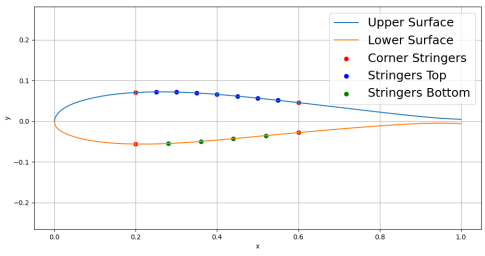

Figure 11.20: Stringers initialisation case 2

As the most critical cases have been identified the applied safety factor can be verified. An initial maximum loading case of 3.8 from the loading diagram has been taken, which has been increased with an ultimate safety factor of 1.5 and an additional safety factor of 1.2. For each failure mode a Safety Factor is computed, which is defined below:

$$SafetyFactor = \frac{Critical_{stress}}{Actual_{stress}} \tag{11.25}$$

The critical stress is defined as the stress at which the component fails. The actual stress is calculated by applying the ultimate safety factor of 1.5 to the applied loads on the wingbox. Since the yield stress and shear stress vary over the crosssection, the maximum possible value for both stresses is taken to obtain the lowest safety factor in the wing. The safety factors for maximum shear stress and yield stress are listed below for both the front and aft wings, for both types of maximum stresses.

- Safety Factor front wing (σ_{yield}): 1.34
- Safety Factor aft wing (σ_{yield}): 2.14
- Safety Factor front wing (τ_{max}): 6.80
- Safety Factor aft wing (τ_{max}): 7.82

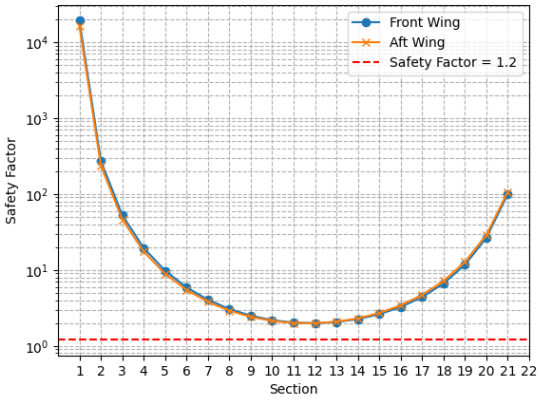

Figure 11.21: Safety Factor for buckling

For buckling, a spanwise analysis has been used where the wing is divided into 22 sections. Each section has an individual safety factor as the critical buckling stress varies over the wing.

The results are plotted in Figure 11.21. The lowest value of the safety factor is 1.99 at section 12 of the wing, which is at 1.99 [m] from the root. Also, section 22 is not included as the stresses at the tip are zero giving an infinite safety factor. The applied safety factor of 1.2 is highlighted in the graph, showing no values below this line means the design passes the buckling verification. A decreasing area which lowers the actual stress, is indicated in the graph with an initial decrease. After a critical point the stringer spacing is decreased to such an extent its effect on the critical stress is bigger than the decreased area on the actual stress, leading to an increase in safety factor again.

Lastly, the optimisation process is verified by plotting the weight of the wingbox as a function of sheet thickness and stringer area in a heatmap. The heatmap shown in Figure 11.22 shows the optimisation space of the front wing, whereas Figure 11.23 describes the aft wing. Where the graphs show white, the design does not meet the loading requirements. From the figures, both designs can be verified as the previously mentioned final design has the lowest weight while still complying with the loading requirements set.

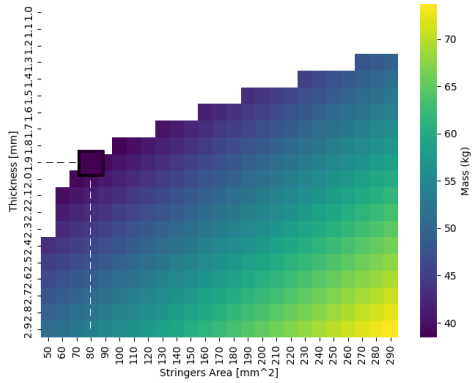

Figure 11.22: Mass optimisation heatmap: front wing

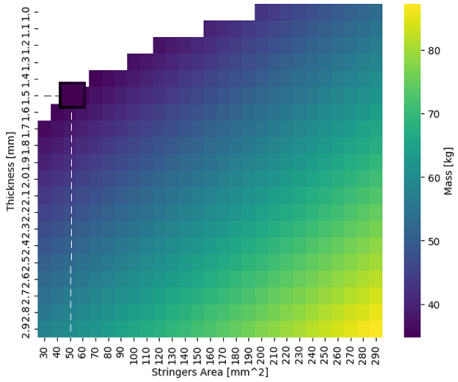

Figure 11.23: Mass optimisation heatmap: aft wing

11.5.6. Final Note

One of the Prandtl plane's advantages in theory should be that the structural weight, of the wing in particular, has the potential of being lower compared to conventional aircraft with the same aerodynamic performance. However, determining the gain in structural efficiency is left out of the scope of this project. This has been due to two main reasons. The first one is the limited amount of time within this project. To more accurately estimate the structural efficiency a significant amount of structural analysis would have to be performed, both more detailed and more extensive than resources in this project have allowed. Secondly, it has been found there is limited research available concerning the structural efficiency and analysis of the Prandtl plane's wing structure, this can be seen as a knowledge gap within the aviation industry.

12. Flight Performance Analysis

The goal of the E-Racer is to participate in and win the Pulitzer Electric Aircraft Air Race. Due to the competitive nature of racing, the aircraft's performance plays a crucial role. The performance of the design should thus be investigated and a flight strategy should be developed to optimise the aircraft's race performance. In this project, simulation has been used as the main tool to evaluate the performance, since actual flight tests are not within the scope of the DSE. Two simulation models have been developed with different goals, these are an energy model and a flight path model. Further, a data analysis tool is created which is the weather model.

This chapter aims to elaborate further on each model. To start, the assumptions for each simulation model have been stated in Section 12.1. This is followed by a discussion on the energy model in Section 12.2. Section 12.3 elaborates upon the flight path simulation. The weather model is the topic in Section 12.4. Lastly, in Section 12.5 the verification and validation procedures on the simulation tools will be explained.

12.1. Simulation Assumptions

Assumptions have been made to simplify the computations necessary to estimate the aircraft's performance. These assumptions have been carefully chosen such that the results are still at the desired accuracy level while minimising computational time. In this section, the used assumptions are explained. The consequences of these assumptions are also elaborated upon. First, the general assumptions for the 2 simulation models are listed, after which additional assumptions used in the two different models are also listed in the dedicated subsection.

12.1.1. General Assumptions

The general assumptions used by the 2 simulation models are listed below:

1. **3 Degrees of Freedom (DoF):** The model simulates the aircraft in a 2-dimensional frame, meaning that 3 DoF are used instead of 6 in a full 3-dimensional simulation. The lateral motion is thereby neglected.
2. **No wind:** The model neglects wind contributions. A separate model has been made to analyse the weather conditions and is discussed in Section 12.4.
3. **Point mass representation:** The aircraft has been modelled as a point mass, meaning that the rotational dynamics have been neglected. Only six DoF simulations account for the rotational dynamics and they are typically only used for short, single manoeuvres thus this simplification has been accepted [103].
4. **Flat Earth:** This assumption has 2 implied effects. first, the curvilinear motion the aircraft experiences, in reality, is modelled as a rectilinear motion thus neglecting the centripetal force to the earth. This can be done because the gravitational acceleration is orders of magnitude larger than the centripetal acceleration. Next, the ellipsoidal shape of the earth on the kinematic coordinates within the simulation is neglected [104].
5. **Non-Rotating Earth:** This means that the Earth-fixed reference system becomes an Inertial system. This neglects the Coriolis acceleration. Over a long period of time this may lead to a significant error [104].
6. **Airfields lie on a straight line:** The starting point and finish line of the race has been used as references and the trajectory has been modelled as a straight line between these 2 points. This means that possible deviation from this straight line is not taken into account instead a margin has been added to the design range to account for possible deviations.
7. **Constant aircraft mass:** It has been assumed that the aircraft weight stays the same over the entire flight mission, although hydrogen is used as fuel. The weight of the hydrogen is estimated to be 2.5% of the total aircraft weight and thus the change in weight can be neglected.
8. **Gravitational acceleration (g) is constant:** The gravitational acceleration has been modeled as constant. In reality, the gravitational acceleration decreases over altitude. with the formula on slide 70 in [105] the gravitational acceleration can be calculated. At sea level, g is 9.80665 [m/s^2]. while at an altitude of 15 [km], g is 9.76068 [m/s^2]. The difference is equal to 4.5% and thus can be safely ignored.
9. **Quadratic drag estimation:** In the performance model a quadratic drag estimation is assumed.
10. **Atmosphere according to ISA:** Atmosphere considered is assumed to be International Standard Atmosphere (ISA).

11. **Compressibility effects are neglected:** A maximum Mach number is imposed on the design of 0.65. This is done to avoid the critical mach number where compressibility effects play a crucial role. By doing this the effects of compressibility are minimised and are considered to be negligible.

12.1.2. Energy Model Assumptions

The assumptions used only by the energy model simulation are stated below.

1. **No cable loss:** As this model is used to provide a preliminary energy budget for making the main requirements cable efficiency is neglected for now. Resulting in a cable efficiency, η_{cable}, of 100%
2. **Small angle approximation:** For climb phase the small angle approximation is used for the climb angle. This assumption is often considered to applicable to angles under 0.26 [rad][1]. To decrease the effect of the small angle approximation a limit was set to 0.2 [rad] reducing the induced error to less than 2%.

12.1.3. Flight Path Model

The assumptions used only by the flight path simulation are listed below.

1. **Constant Propeller Efficiency**: The model utilises a constant propeller efficiency. This is not the case in reality, therefore an analysis was done on the variation of the propeller efficiency, shown in Section 10.1. It is found that the variation is limited to 10% of the max value over the entire mission profile and thus this assumption is accepted.
2. **Changes in pitch are instantaneous:** The change in pitch is considered to happen instantaneously except for lift-off and landing phases, where the pitch angle plays a crucial role. This assumption is considered valid since the time to change the pitch is very small compared to the flight time.
3. **Instantenous change in thrust:** The power for the propeller is supplied by a PEM fuel cell. Sun et al. state in [106] that the reaction time for this type of fuel cell can be estimated to be less than 5 seconds and therefore this assumption is considered valid.

12.2. Point Analysis: Energy Model

In order to give a first estimation of the flight performance an energy model of the flight mission was constructed where the flight envelope can be simulated. The goal of the model is to provide swift iteration opportunities with other departments as flight performance is connected to all departments. First the methods used will be discussed after which the results are shown.

12.2.1. Method

The model consists of various flight phases, which are climb, cruise, descent, and loiter. The energy available for these phases are the sum of energy carried by the hydrogen on board and the battery capacity. With this model, the performance of the aircraft can be optimised and a strategy can be determined. The model has proved to be useful mainly for iterative purposes with the propulsion department for the sizing of hydrogen tank and battery system, as a quick estimation can be made whether the aircraft meets the main mission requirements.

As mentioned, the total flight mission is determined by analysing different phases during the mission. Each phase is discussed below.

Climbing Phase

During the climb phase of the aircraft the small angle approximation is used, this leads to the following formula [107]:

$$P_{req} = W \cdot \sqrt{\frac{W}{S}\frac{2}{\rho}\frac{C_D^2}{C_L^3} cos^3(\gamma)} \tag{12.1}$$

Where P_{req} is the power required, $\frac{W}{S}$ is the wing loading, ρ the density, C_D is the drag coefficient, C_L is the lift coefficient, and γ is the climb angle. Further, the available power, P_a, is known as this is the power to be used during the climb. The rate of climb, ROC, can then be formulated [107].

$$ROC = \frac{P_a - P_{req}}{W} = V \cdot sin(\gamma) \tag{12.2}$$

[1] https://study.com/academy/lesson/small-angle-approximation-formula-examples.html

Which is equal to the velocity of the aircraft, V, times the sine of the climb angle. For a given cruise altitude to which the aircraft has to climb the energy used during this climb phase can be determined. From the ROC the horizontal speed can be obtained.

Cruise Phase

During cruise the aircraft is assumed to have a straight, steady, and level flight. This means thrust and drag are equal, resulting in the following equations [107].

$$C_D = C_{D_0} + \frac{C_L^2}{\pi ARe} \quad (12.3) \qquad P_{req} = D \cdot V = T \cdot V \quad (12.4) \qquad D = C_D \frac{1}{2} \rho V^2 S \quad (12.5)$$

In these equations, C_{D_0} is the zero lift drag, C_L the lift coefficient, AR the aspect ratio of the aircraft, e is the Oswald efficiency, P_{req} is the required power, D the drag, T is thrust and S is the surface area of the wings.

Combing and rewriting Equation 12.4 and Equation 12.5 gives,

$$V = \sqrt[3]{\frac{P_{req}}{C_D \frac{1}{2} \rho S}} \quad (12.6)$$

Descent Phase

After the cruise phase the aircraft has used all its energy and will descend without much hydrogen power on board, only a charged battery for landing and a small amount of hydrogen which can be used for loiter and emergency situations.

Again from Ruijgrok [107],

$$tan(\gamma) = \frac{C_D}{C_L} \quad (12.7)$$

Substituting the quadratic drag formula, Equation 12.3, gives the lift coefficient, C_L.

Then from Ruijgrok [107] the Rate of Descent (ROD) can be calculated:

$$ROD = \sqrt{\frac{W}{S} \frac{2}{\rho} \frac{C_D^2}{C_L^3} cos^3(\gamma)} \quad (12.8)$$

The efficiencies, η, in the design are also taken into account. Starting with hydrogen energy the fuel cell converts this to electrical energy, η_{fuel_cell}. After which the motor converts the electrical energy to rotational energy, η_{motor}. Further, the propeller operates at a certain efficiency, this efficiency, η_{prop} has been analysed by the propulsion department in Section 10.1. The results are shown in Figure 10.1 and Figure 10.2.

- η_{bat} = 0.9
- η_{fc} = 0.5
- η_{motor} = 0.9
- η_{prop} = See Section 10.1

12.2.2. Results

With these energy relations and efficiencies defined for the aircraft, the performance can be modelled. Using the model, optimisation strategies can be explored.

First, the relation between cruise altitude, climb power and cruise power is visualised. In Figure 12.1 the cruise power is set to a value of 175 [kW], while the simulation is run for a varying climb power and altitude. The result is a heatmap showing the average speed for a combination of cruise altitude and climb power. Also, the number of stops needed to complete the race is plotted in a grid on top of the heatmap. It has to be noted that for some combination of climb power and altitude, the aircraft does not meet the cruise altitude as the fuel runs out before it does. In the graph this is plotted as an average speed of 100 [m/s], to maintain a relevant bar scale. Also, the number of stops is indicated by an 'X'. Figure 12.2 uses the same approach but varies cruise power and uses a constant climb power of 225 [kW]. These figures can be used to understand the relation between the power ratios and flight strategy. As can be seen, both higher power and altitude result in a higher average speed.

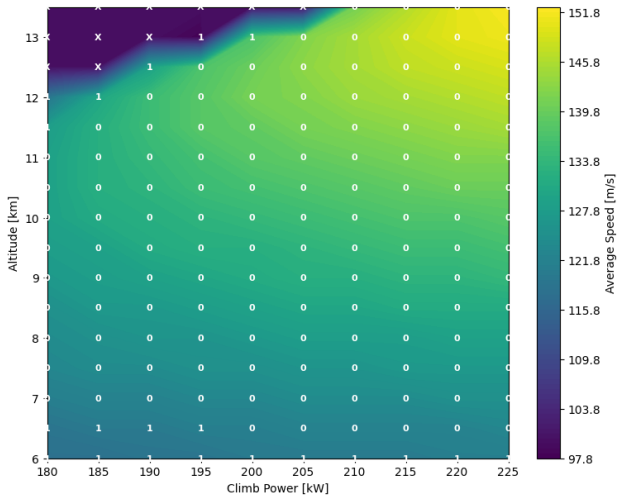

Figure 12.1: Heatmap of average speed vs altitude and climb power with stops

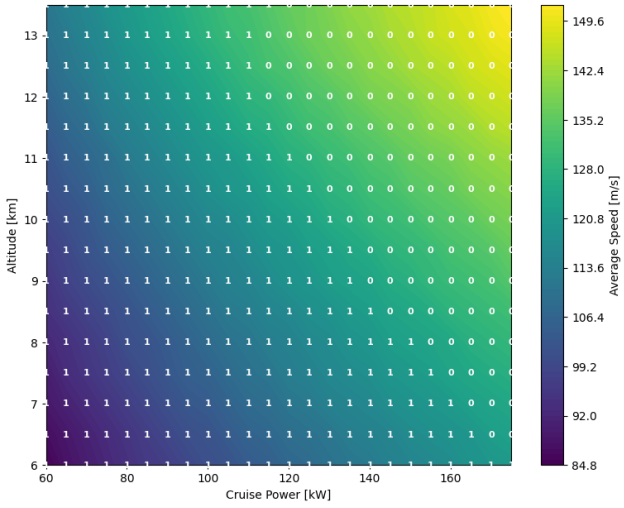

Figure 12.2: Heatmap of average speed vs altitude and cruise power with stops

Now the relation between altitude, cruise power, and climb power is visualised, an optimisation can be performed. The model is run for different values of cruise power, climb power, altitude, and climb angle. From Figure 12.1 and Figure 12.2 it can be seen that there are possibilities for a maximum of 175 [kW] cruise power and a maximum of 225 [kW] climb power where the average speed requirement can be met. A power system with motors, a fuel cell and batteries was designed in Chapter 10 which can deliver a constant power of 175 [kW] by the fuel cell and 225 [kW] for some time during the climb by also using the batteries, which is why the cruise power range and climb power range have been limited to 175 [kW] and 225 [kW] respectively.

Table 12.1: Results of energy budget optimisation

Parameter	Value	Unit
Number of Stops	0	-
Average Speed	150	m/s
Range	2117	km
Cruise Power	175	kW
Climb Power	225	kW
Climb Angle	11.46	deg
Altitude	12.5	km
Cruise Speed	167	m/s

After iterating between several departments a decision was made to set the cruise altitude at 12.5 kilometers. The iteration is a combination of the affect of different departments on the aircraft design, where flight performance is provided an optimal strategy for the highest cruise altitude, propulsion has to design for a higher climb power at this altitude, increasing the weight significantly. Also, the propeller sacrifices performance at sea level as its design is optimised for the cruise altitude. Furthermore, conditions for the pilot will be more critical at higher altitude as oxygen systems might have to be installed. Next to that, the pilot's safety is also affected as there is a limit on the altitude at which the pilot can 'evacuate' the aircraft and still use a parachute. After iterations between the departments, 12,5 [km] was found to be a high enough altitude for flight performance with respect to the race requirements set, yet still an acceptable altitude for the above mentioned effects.

Furthermore, the assumption is made for a small angle approximation for the climb angle. This assumption imposes a maximum climb angle of 0.2 [rad]. With these limits installed an optimisation is run where all combination of the inputs is analysed, with the best performing option being the upper limits of all input. Which is expected, as the heatmaps suggested this earlier. The range of input is listed below:

- Cruise Power: [100 [kW] - 175 [kW]]
- Climb Power: [150 [kW] - 225 [kW]]
- Altitude: [5 [km] - 12.5 [km]]
- Climb angle: [0 [rad] - 0.2 [rad]]

The result of the optimisation is tabulated in Table 12.1.

12.3. Flight Path Simulation

With the main subsystems sized, a 2-dimensional path simulation was developed during the detailed design stage to accurately estimate the aircraft's performance during the entire mission profile. This simulation model extends the energy model discussed in Section 12.2, which attempts to identify the optimal flight profile with point-performance analysis in contrast with the path analysis used in this simulation.

12.3.1. Input Parameters

To simulate the desired design, several parameters have to be given as input. The required inputs are summarised in Table 12.2.

Table 12.2: Input parameters of flight path model

Input parameter	Symbol	Unit
Cruise altitude	h_{cruise}	m
Aspect ratio	AR	-
Zero-lift drag coefficient	C_{D_0}	-
Oswald efficiency factor	e	-
Maximum power output for batteries	$P_{battery_{max}}$	KW
Power available for fuelcell	P_a	KW
Energy available	E_a	MJ
Aircraft Mass	m	Kg
Lift coefficient zero angle of attack	C_{L_0}	-
Lift-curve gradient	$C_{L-\alpha}$	-
Desired cruise velocity	V_{cruise}	m/s
Wingspan	b	M
Wing surface area	S	m^2
Hydrogen mass	$M_{hydrogen}$	Kg
Battery energy capacity	$E_{battery}$	MJ
Ground resistance	μ_g	-
Motor efficiency	η_{motor}	-
Motor controller efficiency	η_{mc}	-
Propeller efficiency	η_{prop}	-
Fuelcell efficiency	η_{fc}	-
Battery efficiency	η_{bat}	-
Brake resistance	μ_{br}	-

12.3.2. Description of Flight Path Simulation

A generic flight profile consists of different phases. On a high level, these phases are: *Take-Off*, *Climb*, *Cruise*, *Descent*, and *Landing*. Each of these phases can be divided into smaller phases. To increase the accuracy of the simulation, these lower-level phases have been taken into account and are given below:

- Take-off ground run
- Take-off rotation run
- Take-off initial climb out
- Unsteady climb to 3,048 [m] (10,000 ft)
- Horizontal acceleration at 3,048 [m] (10,000 ft)
- Constant indicated airspeed climb to cruise altitude
- Horizontal acceleration to cruise speed
- Steady cruise
- Descent at constant indicated airspeed to approach altitude
- Deceleration to approach speed
- Steady descent at approach speed to screen height
- Flare manoeuvre
- Landing ground run

Simplified Equations of Motion have been used to model each phase. A general derivation of the Equations of Motion was explained by Vinh [108]. The simplified equations of motion that have been used are given in Equation 12.9:

$$\begin{bmatrix} \dot{h} \\ \dot{V} \\ \dot{x} \end{bmatrix} = \begin{bmatrix} V \cdot \sin\gamma \\ \frac{1}{m} \cdot \{T - D_{ae} - D_{gd} - g\sin\gamma\} \\ V \cdot \cos\gamma \end{bmatrix} \tag{12.9}$$

In this equation, D_{ae} is the aerodynamic drag, and D_{gd} is the ground drag. The EoM forms the basis of the simulation model since these govern the behaviour of the time-stepping simulation.

Apart from these EoM, several other formulas have been used in the model. Especially, during the Take-Off phase, Constant IAS climb and descent phases, and Landing phase, several additional equations are needed. Also, it must be stated that the simulation takes into account performance limits such as stall and power limitations.

The drag is modeled with Equation 12.5, with the drag coefficient being modeled with Equation 12.3. The lift is modeled with Equation 12.10

$$L = 0.5 \cdot C_L \cdot \rho \cdot S \cdot V^2 \tag{12.10}$$

Take-Off

The complete procedure that describes the take-off phase can be found in [109]. Changes have been made to this approach to facilitate design decisions. The TO has been simulated as a curvilinear motion along an arc. The radius of this arc, R_{TO}, can be found with Equation 12.11, in this equation, the desired load factor during the TO, n_{TO} has been incorporated. Using this radius, the centripetal acceleration, $a_{centripetal_{TO}}$, can be calculated using Equation 12.12.

$$R_{TO} = \frac{V_{LOF}^2}{(n_{TO} - 1) \cdot g} \tag{12.11}$$

$$a_{centripetal_{TO}} = \frac{V_{LOF}^2}{R_{TO}} \tag{12.12}$$

From these equations, V_{LOF} is the lift-off velocity. Lastly, the lift-coefficient necessary to be able to obtain $a_{centripetal_{TO}}$, $C_{L_{TO}}$ needs to be calculated. This can be done with Equation 12.13.

$$C_{L_{TO}} = \frac{m \cdot a_{centripetal_{TO}} + W - L}{0.5 \cdot \rho S \cdot V_{LOF}^2} \tag{12.13}$$

It must be noted that the take-off performance is mostly influenced by the load factor during take-off. The load factor has been chosen such that the take-off parameters are realistic and optimal to minimise time.

Constant Indicated Airspeed Climb & Descent

The constant indicated airspeed (IAS) climb and descent procedures are based on steady conditions with respect to the IAS. The true airspeed (TAS), during these phases, is actually increasing, and thus unsteady conditions need to be used with respect to TAS. The simulation only uses TAS as an input and output and thus the proper change in velocity over altitude needs to be incorporated. A small inspection is made to investigate how the TAS changes over altitude for a constant IAS.

The TAS is now known at the altitudes within the height regime, which represents $\frac{dv}{dh}$, the required acceleration can be calculated using Equation 12.14 with $\frac{\partial h}{\partial t} = V\sin(\gamma)$. It must be noted that $\frac{\partial h}{\partial t}$ is positive for climb and negative during descent.

$$\frac{dv}{dt} = \frac{\partial v}{\partial h} \cdot \frac{\partial h}{\partial t} \tag{12.14}$$

Landing

The Landing phase follows the same mechanics as the Take-Off phase. The only difference lies in the fact that the aircraft goes down in landing and needs to go up in take-off.

Equation 12.11, Equation 12.12, and Equation 12.13 can also be used during this phase if V_{LOF} is replaced with $V_{Approach}$ and the take-off load factor is replaced with the load factor during landing

The capture conditions approach, as proposed by Vinh [108], was used in the simulation tool. This approach has been simplified, to make the implementation possible within the given timeframe. This approach uses several conditions to switch from one phase to another. Only after the capture condition has been reached, the switch to another phase is made.

The capture conditions for every low-level phase are summarised in Table 12.3.

Table 12.3: The capture conditions for each low-level phase

Phase	Capture Condition	Description
Take-Off ground run	$V = V_{rot}$	The ground run begins from a standstill and ends when the airplane reaches the velocity at which rotation can be initiated (V_{rot})
Take-Off rotation run	$N = 0$	The rotational ground run ends when enough lift is generated to take off, this happens at V_{LOF}
Take-Off climb-out	$h = h_{screen} = 15.2[m]$	The take-off phase officially ends when the airplane reaches the screen height, h_{screen}, after this climb starts
Unsteady Climb to 10.000 [ft]	$h = 10,000$ [ft]	In this phase the airplane accelerates while climbing to 10.000 [ft]
Horizontal acceleration during climb	$V = V_{max_{horizontal}}$	The airplane accelerates at this attitude to the velocity where lift equals weight in clean configuration ($V_{max_{horizontal}}$)
Constant IAS climb to cruise altitude	$h = h_{cruise}$	Constant Indicated Airspeed climb is employed to minimise the time required to climb
Horizontal acceleration to cruise velocity	$V = V_{cruise}$	The airplane speeds up to the desired cruise velocity
Steady cruise	$E_{cruise} = 0$	The cruise phase ends when the hydrogen fuel dedicated to it depletes
Descent at constant indicated airspeed to approach altitude	$h = h_{approach}$	Constant IAS descent is used to maintain a high velocity while minimising the descent time
Deacceleration to approach speed	$V = V_{approach}$	The aircraft reduces the velocity during horizontal flight to reach the approach speed
Steady descent at approach speed to screen height	$h = h_{screen}$	Steady descent is followed to keep the airplane at the approach speed.
Flare manoeuvre	$h = 0$	Flare is employed to minimise the loads on the landing gear during the loading
Landing ground run	$V = 0$	The airplane uses several braking techniques to make the aircraft stop to a standstill

12.3.3. Results of the Flight Path Simulation

The results of the flight path simulation have been summarised in Table 12.4.

Table 12.4: Output parameters of flight path model

Output parameter	Value	Unit	Description
Total possible range	2291	km	This range represents the total potential distance the aircraft can fly with the implemented fly strategy
Average Velocity	149.38	m/s	The average velocity that the aircraft completes the race.
Race time	206.41	min	The race time represents the amount of time the aircraft takes to complete 1850 km
Cruise Altitude	12.5	km	The altitude the aircraft cruises at
Take-Off distance (dry)	1,544	m	The required length of the take-off runway in dry conditions
Take-off distance (wet)	1,689	m	The required length of the take-off runway in wet conditions
Landing distance (dry)	763	m	The required length of the landing runway in dry conditions
Landing distance (wet)	1,364	m	The required length of the landing runway in wet conditions
Cruise velocity	163.11	m/s	The velocity during cruise

12.4. Weather Model

To account for the impact of the weather on the performance of the aircraft (RAC-04, Table 20.2), a weather model has been developed. This model does not simulate the weather, rather it analyses the weather history in the area of the race.

12.4.1. Description of the Weather Model

This weather model uses data from the National Aeronautics and Space Administration's (NASA) Modern-Era Retrospective analysis for Research and Applications version 2 database (MERRA-2)[2]. The MERRA-2 database stores atmospheric data based on latitude and longitude. Within this atmospheric data, wind velocities and wind directions based on altitude are present and have been used as the main parameters of interest for analysis.

The considered area is based on the starting point, Eppley Airfield (longitude: -95 [°] 53 [′] 37.19 [”], latitude: 41 [°] 18 [′] 7.20 [”]), and the finish line, Dare Country Regional Airport (longitude: -75 [°] 41 [′] 26.39 [”], latitude: 35 [°] 55 [′] 4.79 [”]). Based on these coördinates and the resolution of the MERRA-2 database which is 0.625 [°] x 0.5 [°] [110], an inspection area ranging from -97 [°] to -73 [°] longitude and 43 [°] to 33 [°] latitude. This inspection area takes into consideration 2 [°] more in each direction to have a better indication of the weather behaviour in the surrounding area of the race.

The MERRA-2 database contains instantaneous values and average values for the parameters of interest. Since the goal is to have a good indication of the overall behaviour of the weather in the area, the time-averaged values have been used for analysis. The parameters have been averaged out over a time span of a month at 42 different altitude levels, based on the pressure. For analysis, only the first 24 pressure levels have been used since these correspond to the flight regime, the aircraft aims to fly in.

To keep the data as relevant as possible, only the month May 2023 have been investigated. The reason for choosing these specific months is that the 2023 Pulitzer Air Race was supposed to be scheduled for May 2023. It is thus highly likely that the same will be used in another year.

The MERRA-2 database saves data at specified times. For the use case within this project, the relevant data is captured at 6:00, 9:00 and 12:00, 15:00, and 18:00 The data shown in this rapport only concerns the 12:00 timestamp data. This time has been chosen because it is in the middle of the timeframe that the aircraft is allowed to fly in.

12.4.2. Results of Weather Analysis

The model analyses the wind speed and direction at the 24 relevant pressure levels. First, the original data is visualised in a heat map at the pressure level closest to the cruise altitude, this pressure level corresponds to an altitude of 11783 [m]. From this heat map, the wind velocity at localised points can be seen along the trajectory between the starting and finish points. An upper and lower limit on the wind velocity can be obtained. With these limits, an estimation of the wind speed during the cruise phase can be made. The wind velocities have been visualised in Figure 12.3.

To accompany Figure 12.3, arrow plots have been made from the data, to show the average wind direction at the altitude closest (11,783 [m]) to the cruise altitude. The results have been visualised in Figure 12.4.

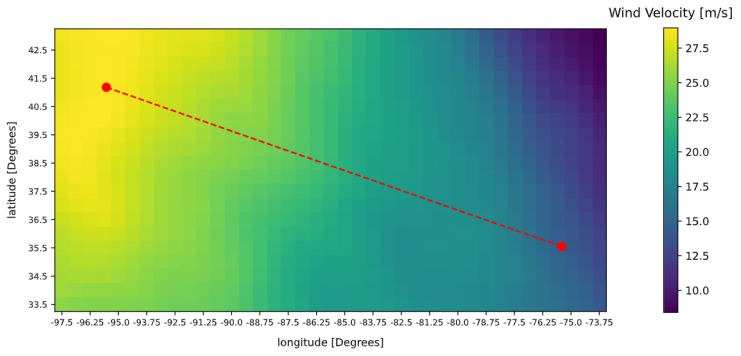

Figure 12.3: Average wind velocities, May 2023

[2] `https://gmao.gsfc.nasa.gov/reanalysis/MERRA-2/` [Accessed on 07-06-2024]

The wind velocity can be analysed relative to the trajectory of the race. In this analysis, the wind direction is shifted with the heading of the trajectory. This allows for the examination of the wind that is parallel with the flight trajectory and a component that is perpendicular to it.

From Figure 12.3, it was seen the aircraft typically will experience a tailwind and a cross-wind component. For further analysis, the cross-wind component has been neglected since the flight path Model does not take into account the lateral motion. The fact that the wind velocities are positive in Figure 12.3 indicates that there will be a tailwind.

In addition, it can be seen that a higher tailwind can be obtained if a slight deviation from the straight line is followed. The relative advantage of deviating from a straight line to the gain in tailwind velocity requires a more detailed analysis since this has been left out of the simulation model due to the timeframe of the project.

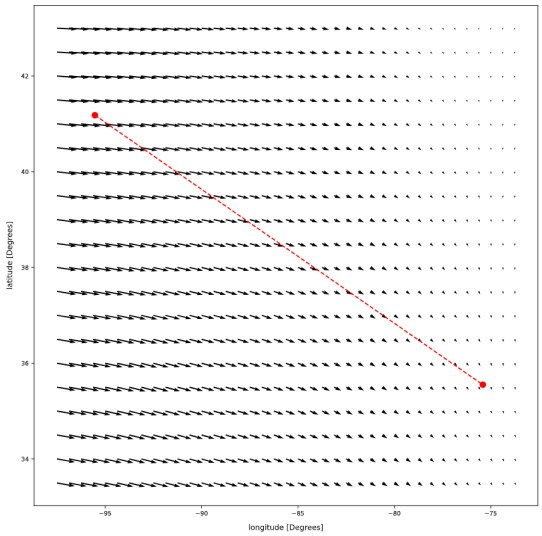

Figure 12.4: Average wind directions, May 2023

It can also be seen that if the weather follows this average trend, then the aircraft would experience a tailwind with a large velocity, which would improve the race time significantly. However, it can be assumed that this would affect competing teams in a similar way and therefore analysing the effect of wind on race time is not helpful. The effect of wind on the range, however, is of interest for the potential race strategy. A small case study has been performed to estimate the aircraft performance's behaviour with different velocities of headwind and tailwind.

Table 12.5: Variation of range in different wind conditions

	Case: Headwind		Case: Tailwind	
Wind Velocity [m/s]	**Range [km]**	**% of initial range**	**Range [km]**	**% of initial range**
5	2216	96.70	2367	103.29
10	2140	93.42	2442	106.58
15	2065	90.12	2518	109.88
20	1990	86.80	2593	113.17
25	1914	83.54	2669	116.46
30	1839	80.24	2744	119.75
35	1763	76.95	2820	123.05

From Table 12.5 it can be seen that the aircraft's range decreases significantly with headwind. If the headwind reaches an average velocity of 35 $[m/s]$ then the aircraft will not be able to make the race distance in 1 go. If this wind condition is present it is advised to fly lower to avoid the larger wind velocities or fly towards the south where more tailwind is present. It must be stated that this case study was performed with the assumption that the inspected wind velocities would be applied throughout the entire flight. In practice, this will not be the case since the wind velocities at lower attitudes are also smaller and thus this case study shows conservative values.

12.5. Verification of Flight Performance Tools

To ensure that the developed tools are working as expected, verification is performed. This section aims to elaborate on that process.

Validation of the simulation tools is also a necessity. This has been done by validating the assumptions used in the models. This is discussed in Section 12.1.

12.5.1. Energy Model

The Python script uses a class called 'Aircraft' where the basic parameters of the aircraft are defined such as weight, wing surface area, Oswald efficiency factor, and more. The class is initialised with a cruise altitude, cruise power, climb power, and climb angle. Using different aircraft objects, flight phases can be simulated. To verify the model, the flight phases have been verified first, starting with climb.

The climb phase was run for different values of climb power and altitude ranging from zero to significantly higher

values than the mission requires. In Table 12.6 the results are tabulated, with the output of the code in the energy used during climb, E_{climb}. A too low climb power results in an error 'Not sufficient power' which is expected. Also, the energy used in the climb phases scales linearly with the climb power available, this can also be expected from the equation provided in Section 12.2. Therefore, the model passes this test.

Table 12.6: Climb phase verification

		Climb power [kW]			
		0	50	200	500
Altitude [m]	0	'Not sufficient power'	'Not sufficient power'	1.3 [MJ]	3.24 [MJ]
	5,000	'Not sufficient power'	'Not sufficient power'	131 [MJ]	323.5 [MJ]
	10,000	'Not sufficient power'	'Not sufficient power'	325.5 [MJ]	156.7 [MJ]
	50,000	'Not sufficient power'	'Not sufficient power'	'Too high alt.'	'Too high alt.'

Similar tests have been performed for cruise, descent, and loiter phases. A more global test is performed by simulating a number of flights for varying altitude. For each flight the energy in each flight phase will be subtracted from the total available amount of energy in the aircraft. This makes sure the model using the amount of energy available and is not overestimating the performance of the aircraft. The results are tabulated in Table 12.7.

Table 12.7: Energy verification

Altitude [m]	**Sum of energy**	**E_{climb} [MJ]**	**E_{cruise} [MJ]**	**$E_{descent}$ [MJ]**	**E_{loiter} [MJ]**
0	-1.043e-13	1.4	1455.1	0.0	28.5
1,000	-1.043e-13	21.9	1434.6	0.0	28.5
10,000	-1.043e-13	267.9	1188.5	0.0	28.5
20,000	-1.043e-13	'Too high alt.'	'No prop simulation at this alt.'	0.0	28.5

As can be seen, the energy sums up to zero in all cases, which verifies the aircraft uses all energy available. In addition, the program prints for climb and cruise phase a message when an altitude is not possible. The loiter phase is constant for all altitudes as this is not influenced by altitude due to the requirement being set to 15 minutes loiter time at an altitude of 500 [m].

12.5.2. Flight Path Model

In the verification procedure of the flight path model, Unit tests have been implemented to test the behaviour of the simulation to limit cases of the inputs. These tests have been summarised in Table 12.8.

Table 12.8: Unit tests of the flight performance model

ID	**Input**	**Expected**	**Actual**	**Result**
FPM-UT-01	$m = 0$	Error	Error	Pass
FPM-UT-02	$AR = 0$	Error	Error	Pass
FPM-UT-03	$C_{D_0} = 0$	Error	Error	Pass
FPM-UT-04	$e = 0$	Error	Error	Pass
FPM-UT-05	$M_{hydrogen} = 0$	Error	Error	Pass
FPM-UT-06	$C_{L_{cruise}} = 0$	Error	Error	Pass
FPM-UT-07	$C_{L_{TO}} = 0$	Error	Error	Pass
FPM-UT-08	$C_{L_{landing}} = 0$	Error	Error	Pass
FPM-UT-09	$S = 0$	Error	Error	Pass
FPM-UT-10	$b = 0$	Error	Error	Pass

System tests have also been implemented to verify the behaviour of the simulation to variation in inputs. These tests have been summarised in Table 12.9.

Table 12.9: System tests of the flight performance model

ID	Input	Expected	Actual	Result
FPM-ST-01	Increasing $M_{hydrogen}$	Total range increasing	Total range increasing	Pass
FPM-ST-02	Increasing P_a	Total time decreasing	Total time decreasing	Pass
FPM-ST-03	Increasing m	Total time increasing	Total time increasing	Pass
FPM-ST-04	Increasing A	Total time decreasing	Total time decreasing	Pass
FPM-ST-05	Increasing C_{D_0}	Total time increasing	Total time increasing	Pass
FPM-ST-06	Increasing e	Total time decreasing	Total time decreasing	Pass
FPM-ST-07	Increasing S	Total time decreasing	Total time decreasing	Pass
FPM-ST-08	Decreasing h_{cruise}	Total time decreasing	Total time decreasing	Pass

As can be seen, all tests have passed, leading to correct code.

13. Aircraft Systems

In this chapter, all aircraft systems are outlined. In Section 13.1, all avionic systems that will be in the aircraft are discussed. Then, in Section 13.2, all hardware and software needed in the aircraft, and their connections are shown.

13.1. Avionics

The avionics of an aircraft concern the electronics that are present in the aircraft. Therefore it is a broad subsystem that entails a number of different components. The different parts of the avionics will be handled in the following subsections.

13.1.1. Air Data

An important part of the avionics system is the air data system. This is the system that gathers and handles information from the air. This will provide crucial information to the pilot. The following sensors that are part of the air data system will be included in the aircraft. These are mainly based on the instruments that are required for Visual Flight Reference (VFR) flight[1].

- **Static Pressure Sensor:** A pressure sensor measures the static pressure outside the aircraft. Using the ISA, the altitude can then be determined. However, when the atmosphere is not equal to the ISA, the measured altitude is not equal to the true altitude. Therefore, reference altitudes are defined to ensure no ambiguity in vertical separation.
- **Vertical Airspeed:** In modern aircraft the altitude rate is computed from vertical acceleration and the rate-of-change of pressure altitude.
- **Pitot Tube:** A pitot tube measures the total pressure of the incoming flow. Together with a measurement of the static pressure, the dynamic pressure can be calculated. When assuming sea-level density, the equivalent airspeed is computed from the dynamic pressure. For this specific mission, compressibility needs to be taken into account when computing the equivalent airspeed.
- **Air Temperature Sensing:** The static air temperature is required to convert the equivalent airspeed to true airspeed. First, the total air temperature is measured using a temperature probe. Then using the Mach number, the static air temperature can be computed.
- **Angle of Attack:** The angle of attack measurement is mainly used for a stall warning for the pilot. Furthermore, it provides the pilot with additional information about the aircraft. It is measured using a free rotation vane that will align itself with the incoming airflow, thus indicating the angle of attack.

It should be noted that an angle of attack vane is not required for VFR flight. However, the choice was made to add one nonetheless. This was done to ensure a reliable stall warning. Furthermore, this information can be used to further analyse the Prandtl plane configuration and therefore it was added for research purposes as well. The data gathered by all these different sensors will then be processed by a Digital Air Data Computer (DADC). These are smaller, lighter, more accurate, and cheaper than early-generation air data computers. The computational flow of the DADC is shown in Figure 13.1. It also shows that the Mach number can be determined from the properties already measured.

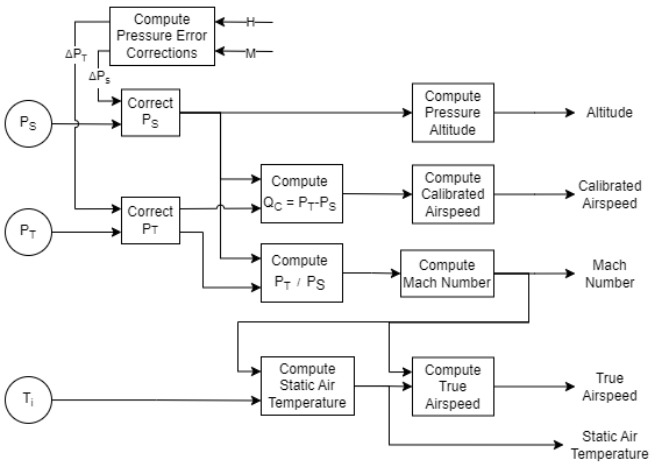

Figure 13.1: Computational process of DADC

13.1.2. Attitude & Navigation

The aircraft also needs to be able to determine its attitude and needs to provide a navigation system. This will be done using two types of main sensors.

- **Gyroscopes:** Gyroscopes will be on board to determine the attitude of the aircraft.

[1] https://www.law.cornell.edu/cfr/text/14/91.205 [Accessed on 18-06-2024]

- **GYROSYN compass:** A GYROSYN compass uses both a magnetometer and measurements from gyroscopes. This is done as gyroscopes on their own will have a drift leading to deficiencies and magnetometers have deficiencies during accelerations and turning. Using both the deficiencies of either option are counteracted.

The position of the aircraft can be determined using GPS/GNSS. Together with the attitude information, this can provide the pilot with enough information to navigate the aircraft to the final destination. It should be noted that both the gyroscopes and the GYROSYN compass are not required for VFR flight, however, it is deemed that this information will be useful for research on the behaviour of the Prandtl plane configuration and therefore, these will be included in the aircraft. It can also provide crucial information for testing, as the control and stability characteristics of the aircraft can be measured this way as well.

13.1.3. Communication

To ensure a successful mission, communication is key. This includes both communication with the ground team, as well as communication with Air Traffic Control (ATC) and other aircraft. This will be done using a radio communication system. Generally, Very High Frequency (VHF) and High Frequency (HF) radios are used. These radios can be acquired COTS and it was chosen to use the Air Com VHF-Radio from MillenAir as it is compact and relatively affordable[2].

13.1.4. Telemetry

During the race itself, it is also crucial that the ground team has access to the data of the aircraft. This will have two main purposes.

Firstly, it will provide additional safety. The ground team will be able to monitor the detailed data on the state of the aircraft as well as important parameters of the powertrain such as battery cell temperature, fuel cell temperature, hydrogen flow rate, and hydrogen content in the fuselage. Any deviations from nominal operation conditions can be identified as quickly as possible, and a correct approach can be determined by the ground team. This includes identifying potential thermal runaway of the batteries or potential leaks of the hydrogen system.

Secondly, the ground team will use this data to analyse potential strategy changes. If the winds change substantially, or there is bad weather at the landing airport, alternative flight profiles need to be determined. This requires detailed information on the aircraft, as these decisions can be influenced by parameters such as available fuel and the state of the high-voltage batteries. It is most efficient to send this directly to the ground team instead of communicating this data on the radio, as the pilot will also be busy controlling the aircraft. Thus, telemetry downlink ensures that the ground team has access to all the possible data of the aircraft such the mission can be carried out as efficiently and safely as possible. In essence, real-time data is required to ensure that the aircraft is used to the full limit of its capabilities.

To send the telemetry down to the ground station, radio communication cannot be used, as it is limited to line-of-sight communication. At the cruising altitude, this means the transmission range of VHF is only 320 $[km]$[3]. Thus, beyond line-of-sight communication is required, which means a relay is necessary. This is already a widely used technology in aircraft today, and therefore the choice was made to use this type of data connection as well. This also means that a COTS antenna can be used, which was chosen to be the AMT-700 antenna[4].

13.1.5. Cockpit Layout

For the cockpit, the choice was made to use an Electronic Flight Information System (EFIS) as it is cheaper, lighter, and more versatile than traditional electro-mechanical displays. The EFIS consists of several displays, which will be discussed in the following paragraphs.

Firstly, all main flight data will be displayed on the Primary Flight Display (PFD). An example of a PFD is shown in Figure 13.2. The second display that will be present is the Navigation Display (ND). This display has two different modes. In compass mode, the display shows a compass from which a heading can be read. In map mode, the display gives a bird's eye view of the flight plan. Therefore, it not only shows where the aircraft is headed but also shows the flight plan. The flight plan will include waypoints, directions, and airports. An example of the ND is shown in Figure 13.3.

[2] https://millenair.eu/product/air-com-vhf-radio-8-33khz-6w/ [Accessed on 14-06-2024]

[3] https://www.boldmethod.com/blog/lists/2024/03/9-things-you-never-knew-about-your-vhf-radio/ [Accessed on 14-06-2024]

[4] https://aerospace.honeywell.com/us/en/products-and-services/product/hardware-and-systems/satellite-communications/amt-700-antenna [Accessed on 14-06-2024]

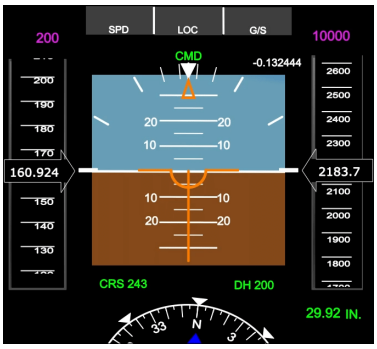

Figure 13.2: Example of primary flight display

Figure 13.3: Example of navigation display

Lastly, the EFIS can be controlled with manual input to change between different modes. Besides the EFIS, flight warning systems will also be present to warn the pilot of (potential) hazards. The following hazards will be incorporated into the flight warning systems.

- Ground Proximity
- Stall and Overspeed
- System Failures

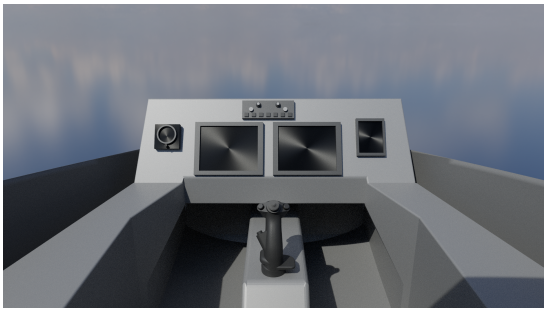

Figure 13.4: Cockpit layout

These different systems will be integrated into the cockpit. Generally, the choice was made to try to make the cockpit layout similar to other small aircraft, such that the pilot would be familiar with the locations of the different systems. However, the space allocated for the controls and displays was limited. This resulted in the cockpit layout shown in Figure 13.4.

Figure 13.4 shows the PFD, the ND as well as the radio on the left and an additional side display for communication with the ground team and aircraft data.

13.1.6. Avionics Diagram

The different components of the avionics system discussed in the previous subsections only show a part of the avionics. Other subsystems, such as the hydrogen system, the battery system, and the engine have their own respective sensors and inputs. These can all be combined and are shown in Figure 13.5.

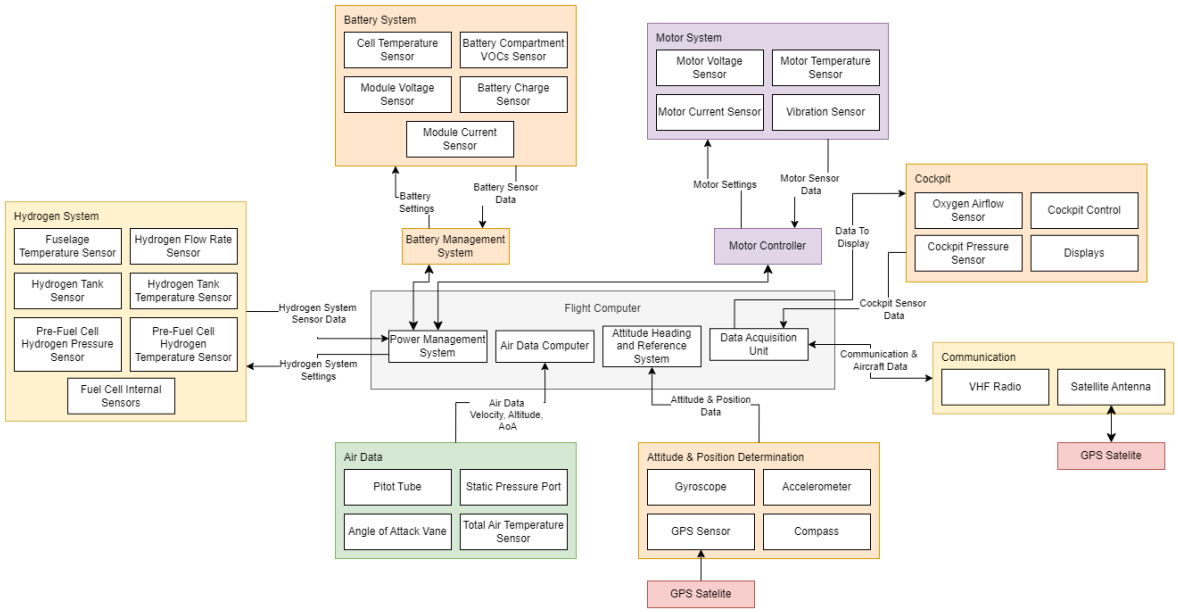

Figure 13.5: Data handling diagram

13.2. Hardware Software Block Diagram

In order to visualise the interactions between the subsystems of the aircraft, a hardware block diagram was created. The hardware-software block diagram is presented in Figure 13.6.

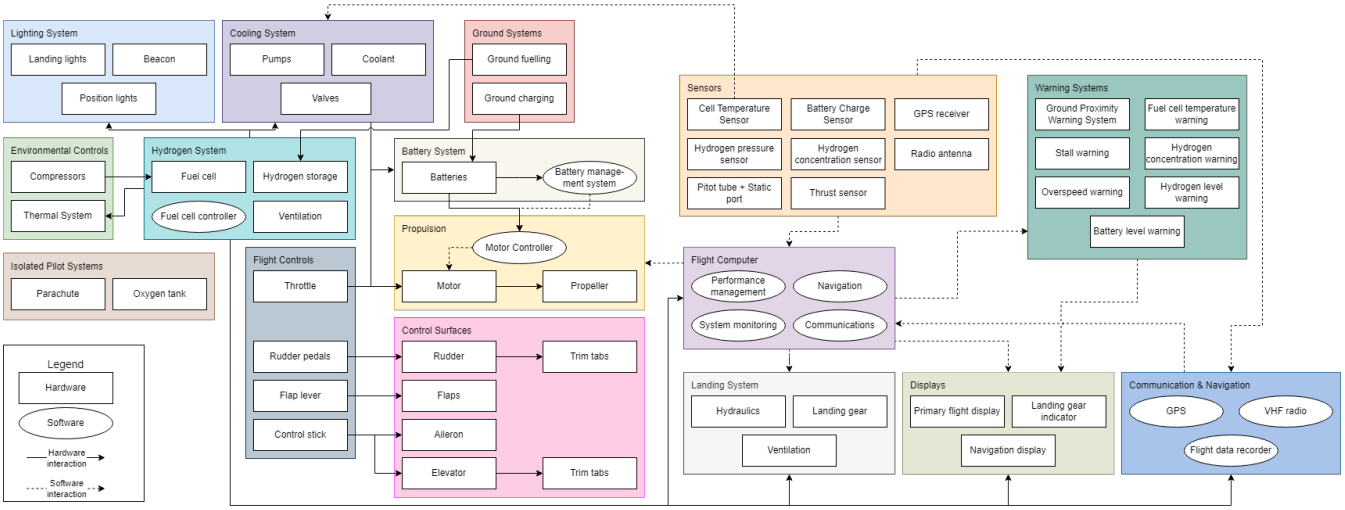

Figure 13.6: Hardware and software block diagram

In this diagram, the software and hardware connections between interactions can be seen. From this graph, the most central system is the hydrogen system. A lot of connections originate from this system, as all energy used outside of climb comes from the fuel cell. The other connections for this system are the ground fuelling, which fills the hydrogen storage, and the compressor, providing air at the correct pressure and flow rate to the fuel cell. The power provided to the propulsion system is compensated by the batteries for climb, there is communication between the battery management system and the motor controller, there is energy going from the ground charging to the batteries and the cooling system cools the battery system. The temperature sensor also provides information to the cooling system about the battery temperature. The cooling system also cools the motor of the propulsion system. From the flight controls, the throttle connects to the motor, while cables connect the rudder pedals, flap lever and control stick to their respective control surfaces. The flight computer is the most important software component of the aircraft, with most information going through it. Information from the sensors goes to the flight computer which then sends the information to the warning systems giving unusual results. Data from the flight computer goes to the hydraulics system in the landing system as well as the displays. Data from the sensors, notably the GPS receiver and the radio antenna, goes to the communication and navigation system which then goes back to the flight computer. Finally, there are two isolated systems controlled by the pilot, being the oxygen tank and the parachute.

14. Safety Systems

This section discusses the need and design of several safety systems in the aircraft. As the aircraft uses a novel energy source it is important to carefully consider the threats associated with the system. Next to preemptive measures, backup systems and safety procedures are also put into place to ensure maximum safety when a failure does occur. The chapter is divided into safety systems related to pilot safety in Section 14.1 and safety systems related to hydrogen and propulsion-associated threats in Section 14.2.

14.1. Pilot Safety

Pilot safety was identified as a need from the customer as NLR required an additional safety system that could help the pilot survive in the event of a failure. Initially, the option of an ejection seat was investigated. However, it was found that considering the pilot position and the aircraft's weight it was not possible to include such a system. To still give the pilot the option of getting out of the aircraft in case of an emergency he will be equipped with a parachute. The procedures for such a pilot exit will be discussed in the following paragraphs as it is not a straightforward action.

There are several limitations to jumping out of the aircraft with a parachute. These include altitude, speed, and possible exit methods. Firstly, the altitude is of concern as at high altitudes where the aircraft will be cruising, the pressure is low and there is not enough oxygen to breathe. Luckily, the pilot is already equipped with additional oxygen. To withstand the cold temperatures and the low pressure outside the aircraft the pilot will need to wear a special suit that will protect him from the environment. Still, the maximum altitude at which parachute jumps are generally done is 10,700 [m][1]. Thus, the plane will need to descend to at least this altitude, but lower would be preferable. Secondly, the speed while jumping out of the aircraft should be as low as possible. Generally, it was found that jumping out above a speed of 120 [mph] would not be safe. Thus, the aircraft would need to decelerate to close to stall speed depending on the altitude. Lastly, to provide a clear exit path the canopy must be ejected as opening the canopy would make it break off and potentially hit critical components like the rear wing or the propeller. Therefore, the canopy must be ejected upwards above the propellers and the rear wing such that a clear exit is possible without causing risk of additional damage to the aircraft.

Transitioning from cruise conditions to jumping conditions will take a significant amount of time as both altitude and speed need to be decreased. It was found that this will take approximately 4 minutes. Therefore, the other safety systems must be able to delay catastrophic failure for at least 4 minutes such that the pilot has time to jump out. The emergency procedures are elaborate and require certain specific conditions to be present in order to be successful. Still, this procedure has been deemed valuable as the only real addition to the design is a parachute. Therefore, the penalty is limited, while this procedure can potentially save the life of the pilot.

Lastly, as mentioned in Section 11.2.3, the pilot will require additional oxygen. It was found that an average person consumes 0.25 [L] pure oxygen per minute[2]. Thus, for the total flight time, 52 [L] of pure oxygen are required. However, when increasing activity oxygen consumption can increase significantly and therefore the choice was made to carry at least twice the amount of oxygen resulting in 104 [L] of oxygen. This will be stored in a small pressure tank at 110 bar, thus only a 1 [L] tank will be required, which is estimated to weigh no more than 5 [kg][3].

14.2. Hydrogen Safety

As has been identified in the risk analysis from Chapter 20, the hydrogen propulsion system introduces additional risks. Due to the small size of hydrogen atoms, leaks in the system are quite probable. Coupled with hydrogen's wide ignition range, which is a hydrogen concentration of between 4% and 75%[4], the risk of fire is substantial. Therefore, hydrogen safety systems are essential to mitigate the potential for fires or explosions. From Adler et al. [111] it is advised to install hydrogen leakage detection systems in areas where hydrogen build-up might occur. The risk is captured under the risk-ID as 'SAF-07' in Table 20.2.

[1] https://wnyskydiving.com/blog/what-is-halo-jumping/ [Accessed on 10-06-2024]

[2] https://www.britannica.com/science/human-respiratory-system/Interplay-of-respiration-circulation-and-metabolism [Accessed on 19-06-2024]

[3] https://hsgascylinders.en.made-in-china.com/product/GdxaJEZCgorK/China-1-Litre-ISO9809-0-15m3-150bar-37mn-Oxygen-Tank-Gas-Cyl
html [Accessed on 19-06-2024]

[4] https://h2tools.org/bestpractices/hydrogen-flames[Accessed on 10-06-2024]

The event of hydrogen build-up can be separated into two main risks: the first one being the direct safety of the pilot and the second one being the structure of the aircraft. Next to the large range of hydrogen concentration where fire can occur, the hydrogen also has a low explosion energy of 0.017 [mJ]. For each of these risks, several procedures and design features have been put into place and are discussed below.

14.2.1. Hydrogen Tank

From the risk analysis in Chapter 20, a failure of the hydrogen tank was identified (TEC-06-PR, Table 20.2). Therefore, the hydrogen tank utilised in the aircraft features a double-walled design, ensuring that even if the outer wall sustains damage, the integrity of the inner wall remains uncompromised. Although this is not a design choice made by the team[5], it is still important to consider this safety aspect. This ensures there will not be a hydrogen leak. In addition, leaks or damage in the inner wall will be contained within the outer wall of the tank. This makes the overall probability of leaks smaller increasing the safety. Furthermore, over-pressurisation of the hydrogen system with at least 0.2 bar will be applied to prevent ingress of foreign particles [112].

14.2.2. Sensors

In case a leak occurs, the level of hydrogen in the fuselage needs to be accurately measured. This way, it is possible for the pilot to take the necessary safety measures in order to prevent an accident. Therefore, an accurate sensor is needed in the fuselage, and the hydrogen concentration has to be communicated to the pilot. The sensor that has been chosen for this is an ATEX-certified sensor, with ATEX standing for Atmosphere Explosives. Electronics with this certification do not produce sparks or have failures that could ignite the hydrogen in case of a leak. In the aircraft, two Neohysens H_2 sensors will be used. This specific sensor is chosen, as it is lightweight, works at a high temperature range and has a Controlled Area Network (CAN) signal output[6]. Two sensors will be used for redundancy.

The placement of the sensor is crucial for detecting hydrogen build-ups. Since hydrogen is a lighter element, the build-up tends to occur at the top of the aircraft. Additionally, the aircraft often flies with a slight angle of attack, making the highest point at the front of the hydrogen compartment, near the firewall. Therefore, the sensors will be positioned at the top of the fuselage near the firewall, with one slightly to the left of the centre line and the other slightly to the right.

In addition to the hydrogen sensors, three temperature sensors will be placed in the hydrogen compartment too. The choice to use three sensors can be motivated by the scenario that if two sensors give different readings, there is no way of knowing which sensor to ignore, while the likelihood of two sensors failing at the same time is significantly lower, reducing the chance of false alarms. Providing the pilot with information on the temperature indicating if a fire is present will be crucial for safety procedures as a hydrogen fire in the aircraft is one of the most critical conditions for the structural integrity of the aircraft and the safety of the pilot. The sensor that will be used is the ATEX SMOOTH TUBE PROBE IP67, which has the following certification set by EU standards: TG8Ex Appendix N ° 2 to the certificate number FTZÚ 07 ATEX 0142X. The sensor will be operating between a range of -40 [$^{\circ}C$] to 230 [$^{\circ}C$].

From the thermodynamic analysis described in Section 10.9, the fuel cell operates at a temperature in the range of 70-90 [$^{\circ}C$], from this, a temperature of 200 [$^{\circ}C$] is set as a preliminary threshold to trigger a fire alarm. However, it should be noted that this threshold temperature should be iterated during the testing phase of the aircraft as there should be a proper balance between false alarms and detecting a firing as soon as possible. This balance should be established by performing tests to obtain data, from which the threshold can be determined.

14.2.3. Ventilation

Some hydrogen will always escape from the system when in flight but also while on the ground when the aircraft is stationary. This is why ventilation has to be added to the aircraft. The total size of the inlets and outlets should be 0.003 [m^2] per 1 [m^3] of volume. This will ensure that the hydrogen can be ventilated up to a volumetric concentration of about 1%[7]. Since the volume of the unpressurised part of the fuselage is 2 [m^3], the required outlet area is 0.006 [m^2]. Therefore, a hole with a 92 [mm] diameter is made on top of the aircraft, with a small cap to prevent water from going into the fuselage. Additionally, a fan is added to drive the hydrogen out, this is done such that ventilation is possible throughout all stages of the mission even when stationary on the ground. As the aircraft hydrogen compartment is not airtight, no inlet holes are needed. The fan that is used has a flow rate of 146 $[m^3/h]$[8].

[5] https://hyresponder.eu/wp-content/uploads/2021/06/Lecture-3-slides.pdf [Accessed on 24-06-2024]

[6] https://www.neohysens.de/en/produkte-und-services/hydrogen-sensoren-for-automotive/neo1xxxa-h2-sensoren[Accessed on 10-06-2024]

[7] https://h2tools.org/bestpractices/ventilation [Accessed on 10-06-2024]

[8] https://nl.rs-online.com/web/p/axial-fans/0251075?cm_mmc=NL-PLA-DS3A[Accessed on 11-06-2024]

As will be explained in Section 14.2.5, the critical percentage of hydrogen concentration is 1.2%. This means that a leak with a flow rate of up to 1.752 [m^3/h] can be supported by the fan. With respect to the placement of the fan, the same reasoning can be applied as in Section 14.2.2. Hence, the ventilation will be placed at the top of the aircraft just after the firewall. A potential additional vent for emergency in-flight use can be investigated in future design phases. This mainly depends on the risk of a hydrogen leak occurring as well as the weight and drag effects of such as panel.

14.2.4. Firewall

With a risk of fire (SAF-07, Table 20.2) in the hydrogen storage compartment which is placed right behind the pilot, a firewall is essential in ensuring safety for the pilot. The purpose of the separation system is to provide the pilot with time to position the aircraft for an escape opportunity (discussed further in Section 14.2.5). As for now, the objective is to maximise the time when the pilot is able to operate the aircraft. This will be done by providing a firewall between the pilot and the hydrogen compartment.

The material used for the firewall will be steel 300M, as this is a steel-based alloy which is used in the aviation industry frequently. Therefore, the material does not have to be tested[9]. Compared to aluminium, steel is a much better firewall due to the higher melting point[10]. This means that the firewall will fail after the structure of the aircraft as this consists of mainly aluminium parts. Giving the pilot maximum time to perform emergency procedures before the aircraft loses its structural integrity.

Estimating the time window for the pilot to safely exit or land the vehicle has proven to be difficult as the intensity of a potential fire is hard to model. However, the condition of a hydrogen fire in the aircraft has been deemed to be non-recoverable as the amount of hydrogen on board makes the fire inextinguishable [113]. Therefore, knowing the firewall will outperform the aircraft in case of a fire is sufficient for the design of the firewall itself as the aircraft fails before the pilot will not be able to operate the aircraft. However, for safety procedures, this introduces a challenge as a time estimate of the operating time of the aircraft in case of fire is difficult to estimate. In addition, the firewall has to withstand the pressure gradient from the pressurised cabin to the atmosphere. This is discussed in Section 11.3.6.

14.2.5. Procedures

Safety procedures to be executed during a hydrogen leak will be discussed below, with this case and that of a fire being outlined below.

Hydrogen Leak

In case of a hydrogen leak in flight, the sensor should give a warning to the pilot when the concentration reaches 10% of the concentration level where the hydrogen might catch fire, which is at 4% of the total concentration of air within the fuselage. Therefore, an alarm will go off when the concentration of the hydrogen is 0.4%. This gives the pilot time to cross-check the warning between the three sensors and speed up the ventilation fans. If the concentration continues to rise with the fan speed increased and passes 1%, the pilot should shut off the hydrogen system and close all valves. If the hydrogen level does not decrease the pilot should find a safe space to land as quickly as possible. An increasing hydrogen percentage in the aircraft with the valves closed means the pilot will move on to decreasing the altitude and speed of the aircraft as much as possible and try to land before a concentration of 1.2% is reached. If this is not possible the pilot should start the evacuation procedure, which is discussed below. Furthermore, all procedures for a hydrogen leak are summarised in Figure 14.1 below.

Pilot evacuation

Following the procedures mentioned above, a sensor reading of more than 1.2 % hydrogen means the leak is non-fixable at this point. This forces the pilot to evacuate the plane. As previously discussed evacuation at the cruise altitude of 12.5 [km] is not straightforward. Figure 14.1 shows the procedure to be followed by the pilot in case of evacuation.

[9] https://www.eaa.org/eaa/aircraft-building/builderresources/while-youre-building/building-articles/engines-and-firewalls/firewalls [Accessed on 11-06-2024]

[10] https://www.gabrian.com/melting-point-of-aluminum/ [Accessed on 11-06-2024]

Figure 14.1: Hydrogen safety procedures during flight

15. Final Design

With all subsystems designed, the final design is also ready to be presented. However, before showing the major design parameters, the high-level iterations performed throughout the design will be explained in more detail in Section 15.1. Then, the final design parameters will be shown in Section 15.2. Next, the mass of the individual components of the aircraft will be discussed in Section 15.3. Finally, the resource allocation of the aircraft is discussed in Section 15.4.

15.1. Iterative process

Up to this point, the functioning of the different departments was discussed individually, with very little being explained about their interactions. This was done for clarity, however these were a crucial part of the project. Hence, these will be presented here to get a general overview of the design process for this aircraft.

The preliminary design of the aircraft was used as a starting point for the detailed design. With these parameters, each department investigated methods to further design their subsystems. Then each department implemented this method to get an initial design for their respective subsystems. This gave new values with respect to weight, power required, loads, and aerodynamic performance. This also provided insight into how certain aspects of the aircraft might change during future iterations.

After this first subsystem sizing iteration, the task was to create a design that was satisfactory with regard to all subsystems. The main problem encountered after the first iteration was that the mass of the aircraft had significantly increased. Thus, an iteration process was determined that would work towards the convergence of the aircraft. This process is shown in Figure 15.1.

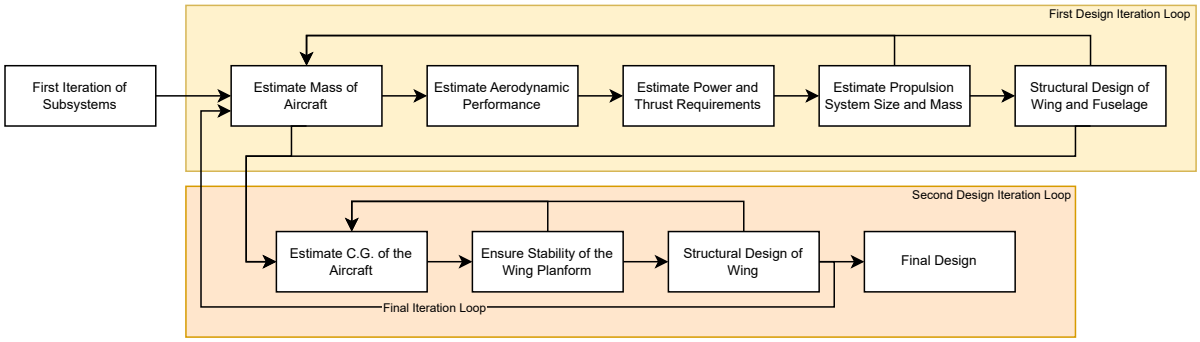

Figure 15.1: Diagram of design iterations

In Figure 15.1 the major iteration loops for the project are shown. These will be explained in more detail in the following paragraphs.

The first iteration loop mainly considers the mass of the aircraft. After the first subsystem design iteration, the mass of the aircraft significantly increased to about 1000 [kg]. This meant that the different subsystems needed to be redesigned based on the newly determined weight. Some margin was used to ensure convergence would occur sooner. After multiple iterations convergence was reached to an aircraft mass of around 1200 [kg]

The second iteration loop concerned the stability of the aircraft as it was found that the Prandlt plane configuration was inherently hard to make stable. With the determined weights of the components, the CG of the aircraft was determined, after which the wing platform was adjusted to ensure stability. For the changed wing platform the new structure for the wing needed to be determined, as well as checking that the wing placement would be possible structurally. Then the new CG was determined which led to more iterations as the margins were generally small. Eventually, this led to convergence. Then a final iteration back to the first iteration loop was required as some of the aircraft masses had changed as well as the aerodynamic parameters. Once this was all checked, adjusted, and converged, a final design was reached which will be presented in Section 15.2.

15.2. Final Design Parameters

With all departments converged, a final design was reached. The main parameters of the design are summarised in Table 15.1 and Table 15.2. In Table 15.3-15.6, more parameters of the final design are presented, and a final detailed drawing of the aircraft is presented in Figure 15.2. Additionally, a render of the final design is shown in Figure 15.3

Table 15.1: Final geometric parameters of the wings

Front Wing		Rear Wing	
Surface Area	4.29 [m^2]	Surface Area	4.29 [m^2]
Aspect Ratio	12.96	Aspect Ratio	12.96
Wingspan	7.46 [m]	Wingspan	7.46 [m]
MAC	0.58 [m]	MAC	0.58 [m]
Quarter Chord Sweep	33.50 [°]	Quarter Chord Sweep	-8.10 [°]
Taper Ratio	0.80	Taper Ratio	0.80
Dihedral	4.00 [°]	Dihedral	0.00 [°]
Incidence	2.3 [°]	Incidence	0.00 [°]
Airfoil	OAF128	Airfoil	OAF128

Table 15.2: Final geometric parameters of the fuselage and propeller

Fuselage		Propeller	
Length	4.7 [m]	No. Propellers	2
Height	1.2 [m]	No. Blades	5
Width	1.1 [m]	Diameter	1.8 [m]

Table 15.3: Main aerodynamic parameters of design

Aerodynamics		
Parameter	**Value**	**Unit**
$C_{L_{cruise}}$	0.358	$-$
$C_{L_{TO}}$	1.03	$-$
$C_{L_{land}}$	1.24	$-$
$C_{D_{cruise}}$	0.02155	$-$
L/D_{cruise}	16.612529	$-$
L/D_{max}	19	$-$
Stability margin	5	cm

Table 15.4: Main structural parameters of design

Structures		
Parameter	**Value**	**Unit**
Fuselage skin thickness	0.4	mm
Amount of stringers fuselage	16	$-$
Amount of frames	13	$-$
Wing box skin thickness	top: 1.9 bot: 1.5	mm
Wing stringers	top: 9 bot: 6	$-$
Wing ribs	88	$-$
Wing and Fuselage material	7075 T6 AL	$-$
Canopy thickness	0.4	mm
Canopy material	Polycarbonate	$-$

Table 15.5: Main performance parameters of design

Performance		
Parameter	**Value**	**Unit**
Range	2291	km
Cruise speed	163	m/s
Cruise altitude	12500	m
Race Time	206.41	min
Service Ceiling	12500	m
Take-off Distance	1544	m
Landing Distance	654.018	m
Max ROC	7.36	m/s
Max climb angle	11	°

Table 15.6: Main propulsion parameters of design

Propulsion		
Parameter	**Value**	**Unit**
Battery Capacity	14.45	kWh
Battery Power	43.35	kW
Fuel Cell Power	238	kW
Hydrogen Mass	30	kg
Hydrogen Tank Mass	70	kg
Peak Power	149	kW
Continuous Power	113.1	kWh
High-voltage	600	V
Low-voltage	12 & 24 & 48	V
Power train efficiency	0.56	$-$
Max Motor RPM	2500	rpm

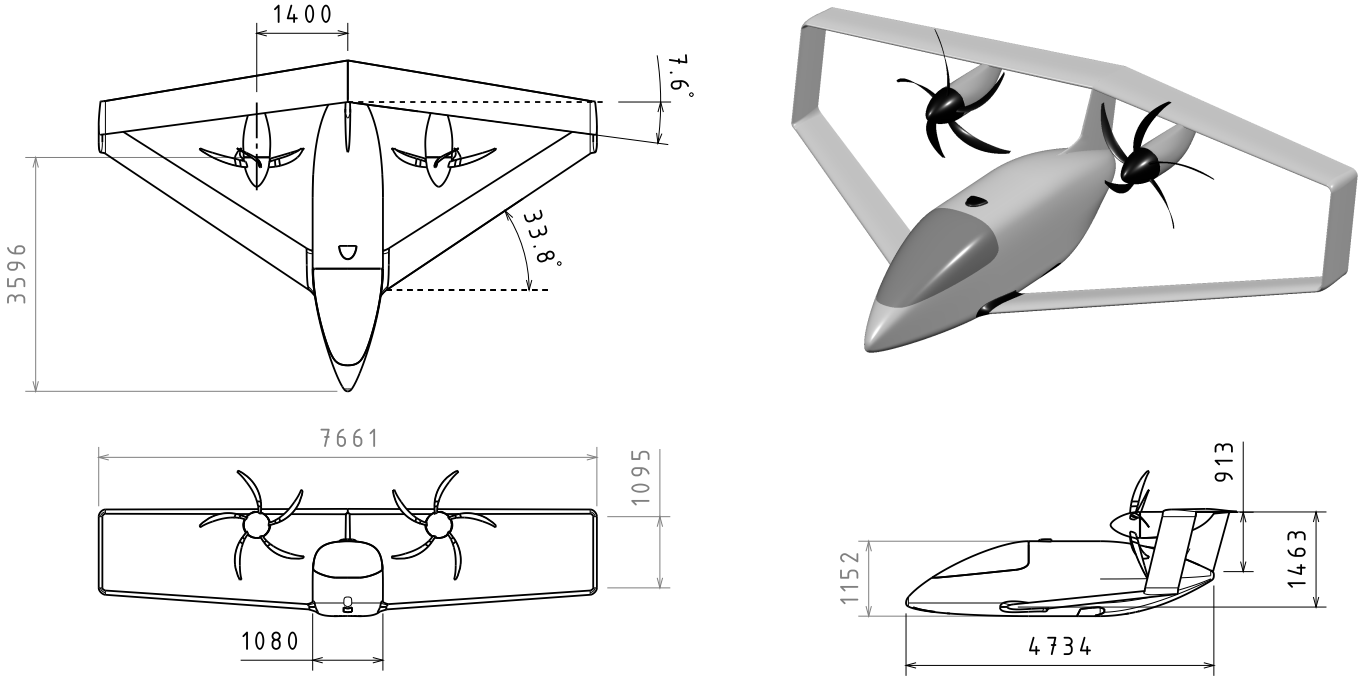

Figure 15.2: General dimensions of the Prandtl plane

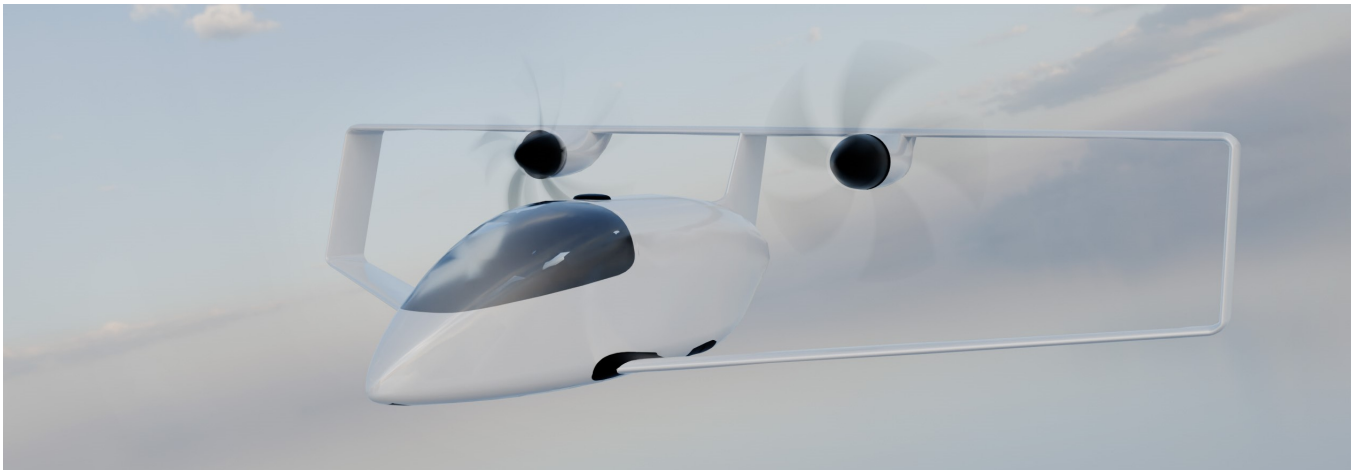

Figure 15.3: Final Design Render

15.3. Mass of Components

The masses for all aircraft components are presented in Table 15.7. The total mass of the E-Racer is equal to 1,162.51 [kg], with a margin of 37.49 [kg] with respect to the mass of 1,200 [kg] stated in ER-NLR-TECH-PPR-3.

For various components, the mass has been estimated and some assumptions have been made as it was not possible to find a specific value in the available literature. In the following paragraphs, these estimations will be discussed. It should be noted that all weights that have been previously discussed in the report will not be explained in this section.

The cockpit mass can be broken down into different subcomponents; for these, assumptions were made as little information could be found. The mass of 50 [kg] for the cockpit includes the pilot seat (10 [kg]), flight controls (10 [kg]), instruments and avionics (15 [kg]), and structural components (15 [kg]).

The mass of the pilot is assumed to be 85 [kg]; this is a design choice made by the team. A constraint of 75 [kg] will be imposed on the pilot since they will be wearing a flight suit and a helmet that add an extra 10 [kg] to this value.

The mass of the pressure regulators was estimated by looking at COTS alternatives[1]. Although pressure regulators do not have a high weight, a conservative estimate was made for the mass of this component to account for any valves and pressure relief devices that have not been taken into account but that still contribute to the overall weight, equal to 20 [kg]. Similarly, a mass of 11 [kg] for the hydrogen tubing[2] and 9 [kg] for the vacuum insulated tubing[3] was decided based on the mass per length of COTS alternatives.

After an extensive literature review on cooling and heating systems, no mass value could be determined. A low confidence estimate of the mass of the liquid coolant was made, equal to about 30 [kg], and an additional 30 [kg] was added for other subcomponents involved in the cooling and heating process, giving a total mass of 60 [kg].

The exact power box and relays necessary for this mission have not been found. Consequently, after researching similar COTS alternatives for relays[4], an estimated mass of 10 [kg] was assumed. As explained in Section 10.4, the mass of the low-voltage battery is equal to 4.12 [kg]. The low-voltage system has a mass of 15 [kg] has been assumed, which includes the low-voltage battery mass.

Table 15.7: Mass of all components of the E-Racer

System	Component	Mass [kg]
Landing gear	Front	15.00
	Main	35.00
Fuselage	Structure	120.00
	Cockpit	50.00
	Pilot	85.00
Wing	Front	77.07
	Rear	69.72
	Skin	24.00
	Side stabilisers	10.00
	Tail	5.00
Propulsion	Hydrogen tank mass	70.00
	Hydrogen mass	30.00
	Pressure regulators	20.00
	Hydrogen tubing mass	11.00
	High power cable mass	25.40
	Vacuum insulated tubing	9.00
	Air compressor and controller	68.60
	Fuel cell mass	115.00
	Cooling system mass	60.00
	Battery mass	53.52
	Power box / relays	10.00
	High low DC-DC converter	1.80
	Capacitor	16.30
	Motor mass	88.00
	Motor Controller	5.00
	Propeller	40.00
	Feathering system	14.80
Safety	Firewall	10.10
	Parachute	3.20
	Oxygen tank	5.00
Guidance & Navigation	Low-voltage system mass	15.00
	Total:	**1,162.51**

15.4. Resource Allocation Plan

To be able to realise the aircraft design, several resources are needed. To ensure that the required resources are used as efficiently as possible, several resource budgets have been made. In this chapter, the allocation of resources is discussed. First, a discussion on the difference between the estimated resources before the detailed design and the actual calculated resources after the detailed design is made in Section 15.4.1. After that, the allocation budgets after detailed design are elaborated upon in Section 15.4.2.

15.4.1. Baseline & final Budgets

In the first stages of the design process, estimations were made for various technical budgets. These previously defined budgets will be compared to the results of the detailed design. In addition, a contingency for each design phase has been formulated which indicates the change of the design parameters within that specific design phase. These contingencies are tabulated in Table 15.8.

Table 15.8: Contingency evolution across design phases

Phase	Contingency as percentage of initial
First Estimate	-
Preliminary Design	50%
Detailed Design I	25%
Detailed Design II	15%
Prototyping	5%
Production	1%

[1] https://www.swagelok.com/downloads/webcatalogs/en/ms-02-230.pdf [Accessed on 19-06-2024]

[2] https://www.swagelok.com/downloads/webcatalogs/en/ms-01-181.pdf [Accessed on 19-06-2024]

[3] https://directories.gasworld.com/files/a81855a8ca/4429/documents/4429-Demaco-Product-Sheet-combined.pdf [Accessed on 19-06-2024]

[4] https://new.abb.com/products/nl/1SFL467001R1411/af146-30-11-14 [Accessed on 19-06-2024]

Table 15.8 shows the contingency margin for each design phase output. This means that the output of a particular phase is allowed to change as a maximum with the respective contingency during the next phase. For example, the output of the preliminary design phase may change by 50% at most during the detailed design phase. This approach is used to ensure that the design will converge after all iterations.

To be able to compare the evolution of the resources between the preliminary phase and the first detailed design phase, a margin of 25% will be used as a reference. This margin is used as an indicator to monitor the obtained growth of the resources. If the change in resource is larger than 25% then that resource has grown above expectations.

Cost budget

The most limited resource in this project is the monetary budget of €900,000. This budget is imposed by the NLR. A detailed cost breakdown analysis will be presented in Chapter 22. Here the difference in the cost estimation in the preliminary design and the detailed design phase will be investigated.

To compare the cost estimations from the preliminary phase with the current cost breakdown, Table 15.9 is used. Most of the items are above the 50% margin set for the preliminary design. This can be explained due to the fact that the type of aircraft at the time of the estimation was not determined, making for example the propulsion systems underestimated as a hydrogen system proved to be way more expensive than the conventional option. However, the total cost differs only 2% from the initial estimate. In the end, the initial estimation has not been proven useful as the allocation of the different items was not accurate.

Table 15.9: Cost budget comparison

Item	First Estimate [Euro 2024]	New [Euro 2024]	Contingency
Fuselage	219,500	9,091	-96 %
Wings	85,000	2,727	- 97 %
Landing	34,500	18,182	- 47 %
Propulsion	40,500	354,209	776 %
Electrical	34,000	14,782	-57 %
Equipment	42,000	46,827	11 %
Total	455,500	444,455	2%

Mass Budget

For the mass budget, the same approach has been taken. Table 15.10 shows the initial estimate for various components. Most components are in the 50 % contingency range. However, both the wing and fuselage

Table 15.10: Mass budget comparison

Component	First Estimate [kg]	Current Design [kg]	Change
Wing	85	185.8	119%
Fuselage	111	170	53%
Landing	42.5	50	18 %
Propulsion	452.2	633.4	41 %
Pilot	100	85	-15 %
Safety Systems	51	33.3	-64%
Total	841.7	1166.5	38 %

Drag Budget

The comparison of the drag budget has been made and is visualised in Table 15.11.

Table 15.11: Drag budget, during cruise, comparison

Drag component	Total Drag fraction [%]	Preliminary drag component [N]	Current drag component [N]	% change
Skin Friction Wing + Fuselage	35	174.3	242.998	39.41
Skin Friction hor. tail + ver. tail + Propeller	15	74.7	104.142	39.41
Lift-induced drag	33.3	166	231.195	39.27
Parasite + wave drag	16.7	83	115.945	39.69
Total drag	100	498	694.28	39.41

In Table 15.11, it can be seen that the total drag has grown by 39.41%. This indicates that the drag has grown beyond expectations. A reason for this is that the preliminary value is based on statistics from ”comparable aircraft”. These aircraft are in reality not as closely related to the E-Racer design as initially thought and therefore the deviation is not unexpected. Specifically, as the weight of the aircraft increased during the detailed design process, the surface area was also increased to maintain the same wing loading value, thus increasing drag. Nevertheless, the change is still within the 50% limit which has proved the estimate to be useful.

15.4.2. Budget Contingencies for Future Steps

Going forward from this point in the design process future steps will have to be taken to arrive at a final design, as discussed in Chapter 21. For this reason, contingencies for the technical resources have been established. The resources that will be taken into account are mass, cost, power, and drag. Therefore, a contingency for each design phase has been formulated which indicates the change of the design parameters within that specific design phase. These contingencies are tabulated in Table 15.8. At this stage, 'Detailed Design I' has been completed, with 'Detailed Design II' and 'Prototyping' remaining as the next steps. These next steps are also expanded upon in Chapter 21.

Mass Allocation

The mass budget established in Section 15.3 is again tabulated in Table 15.12. For each mass, the contingency for 'detailed design phase II' is applied giving both an upper and lower limit for the mass of various components.

Table 15.12: Mass allocation budget 'Detailed Design II'

Component	Mass [kg]	Contingency	Upper [kg]	Lower [kg]
Wing	185.9	15%	213.79	158.02
Fuselage	170	15%	195.50	144.50
Landing	50	15%	57.50	42.50
Propulsion	657.42	15%	756.03	558.81
Pilot	85	15%	97.75	72.25
Safety Systems	28.2	15%	32.43	23.97
Total	1166.519	-	1341.5	991.55

Power Allocations

The power allocation might have a significant impact on the mass of the aircraft, as an increase in power will increase the fuel cell size which adds a large amount of weight. For this reason, the power budget might be limited by the weight margin defined earlier. Therefore, the power increase limited by weight will be researched to see whether the contingency is below the 15% from Table 15.8. A power density of 2 [kW/kg] is defined in Chapter 10 for the fuel cell mass. However, the fuel cell mass makes up 21% of the total mass, when scaling the power. Therefore, a power density of 0.42 [kW/kg] will be used. From the contingency applied to the propulsion mass budget, a maximum change of 98.6 [kg] is allowed during 'Detailed Design phase II'. This results in a power margin of 41.4 [kW].

However, this only applies to the cruise power, which is continuous power delivered by the fuel cell and scales the entire propulsion system. Power available used in climb also is provided by the batteries. Scaling peak power proves to be less impact-full on the mass of the propulsion system as the power density has been determined to be 0.68 [kW/kg]. The components considered to scale with increasing peak power are listed below, these components can also be found in Table 15.7.

- Battery mass
- High power cable mass
- Controller mass
- Power box
- High low DC-DC converter
- Capacitors
- Cooling system

With the mass budget of 98.6 [kg] peak power is allowed to be scaled with 67.0 [kW].

In Table 15.13 the results are tabulated with the contingency for the given power change. Both contingencies are higher than 15% which means the mass budget is not limiting the allowable 15% contingency for the second detailed design phase. Therefore, the 15% contingency is applied and shown in the last two columns of Table 15.13.

Table 15.13: Power budget

Component	Power density [kW/kg]	Change [kW]	Contingency	Upper [kW]	Lower [kW]
Continuous Power	0.42	41.4	23.5 %	202.4	149.6
Peak Power	0.76	67.0	37.4 %	205.9	152.2

Drag Allocation

The drag budget is connected to the continuous power budget. To determine the drag budget, the following formula will be used as defined in Section 12.2:

$$P_{req} = D \cdot V_{cruise} = C_D \frac{1}{2} \rho V^3 S \tag{15.1}$$

This gives upper and lower limits for the drag, D, and drag coefficient, C_D. It should be noted the power required is after propeller efficiency, this efficiency is determined using the 113 [kW] from Chapter 10 divided by the 176 [kW] continuous power delivered to the motor, and the results is an efficiency of 64.2 %. With a drag coefficient of C_D = 0.02151 from Chapter 8 the upper limit for C_D is 0.0249 which is a contingency of 12.9% could be determined using the power budget. However, the lower limit of 0.01796 was obtained which is a contingency of 16.5%, exceeding the 15% limit. Therefore, the upper limit is set by the power budget at 12.9% and the lower limit is set by the second design phase of 15%. The final contingency values are listed below.

- $C_{D,cruise}$ **upper limit**: 0.02490 (12.9%)
- $C_{D,cruise}$ **lower limit**: 0.01828 (15%)

16. Verification & Validation

Verification and validation of the entire aircraft are crucial to determining if the aircraft meets the previously set requirements, as well as if it can complete its intended goal. Verification and validation of the subsystems have also been considered and are discussed in their respective dedicated chapters. This chapter aims to elaborate on the verification and validation procedures for the aircraft as a whole. Firstly, the testing and certification will be performed in Section 16.1. Next, validation will be discussed in Section 16.2. Required resources will be elaborated on in Section 16.3. Following this, a sensitivity analysis was performed for every subsystem and flight performance, which are discussed in Section 16.4. Finally, a reliability analysis was performed in Section 16.5.

16.1. Test & Certify

The aircraft must be tested and certified to allow it to be legal to fly, and in turn, make it eligible for the race. ER-MIS-NAA-01.05 is therefore in need of further explanation. After a thorough discussion with the client, it was decided that a Special Airworthiness Certificate in the experimental category would satisfy the type of certification required.

Therefore, the initial requirement ER-MIS-NAA-01.05 previously reported has been updated in Table 5.1 to a more clear definition. This type of certification is a special type of permit that allows non-certified aircraft to fly legally and has a special category for racing purposes. In general terms, with this type of certification, you must have proof of the aircraft's safety by means of tests. It also restricts operations and does not allow you to fly over populated areas. Thus, this puts the responsibility on the designer to determine what is safe and how to prove it[1].

16.1.1. Requirement Verification

For every requirement, there should be a method in place that will be used to verify compliance. This can then be put into a compliance matrix at the end of the project that shows if and how the product complies with all the requirements. There is a distinction made between five different types of verification.

1. Inspection (I): The physical inspection of the product.
2. Demonstration (D): Demonstrating the capabilities of a product.
3. Analysis (A): Mathematically analysing the properties and performance of the product.
4. Testing (T): Testing the properties and performance of the product while gathering measurements.
5. Review of Design (RD): The inspection of design process and documents.

In Table 16.1 and Table 16.2, all mission and system requirements and their associated verification method are shown. For the design stage, only analysis or review of design was an available method. Therefore, all requirements show one of these verification methods. The methods of inspection, demonstration, and testing can only be done when the product has been manufactured but are included to show which method will be used in future stages of the project. Furthermore, some requirements have not been analysed at this stage of the design which is indicated with NA in the tables.

Table 16.1: Mission requirement compliance matrix

ID	Requirement	Method	Compliance
ER-MIS-NLR-01.01	The aircaft shall be able to win the Pulitzer Electric Aircraft Air Race.	A, T	✓
ER-MIS-NLR-01.02	The aircraft shall be able to travel 1,000 nautical miles in four days.	A, T	✓
ER-MIS-NLR-02.01	The technology involved with the aircraft shall be available by the year 2023.	A	✓
ER-MIS-NLR-03.01	The aircraft shall be producible with a budget of €900,000.	A	✓

[1] https://www.faa.gov/documentLibrary/media/Order/8130.2H.pdf[Accessed on 31-05-2024]

ER-MIS-NLR-06.01	The aircraft shall be equipped with at least one additional safety system.	RD, I	✓
ER-MIS-NAA-01.01	The aircraft shall be heavier than air.	RD, I	✓
ER-MIS-NAA-01.02	The aircraft shall be zero-emission.	RD, T	✓
ER-MIS-NAA-01.05	The aircraft shall be able to obtain a special airworthiness certificate in the experimental category with the purpose of air racing.	A	✓
ER-MIS-NAA-01.06	The aircraft shall be operated by a human pilot.	RD, I	✓
ER-MIS-AIRP-01.01	The aircraft shall be able to use the County Regional Airport, Manteo, North Carolina, US.	A, D	✓
ER-MIS-AIRP-01.02	The aircraft shall be able to use the Eppley Airfield, Omaha, Nebraska, US	A, D	✓
ER-MIS-SOC-01.01	The aircraft shall provide test data for electrical propulsion aviation.	RD	✓

In Table 16.1, it can be seen that the design does not comply with the budget requirement. This will be further discussed in Chapter 22.

Table 16.2: Compliance matrix

Indicator	System Requirement	Method	Compliance	Value	Chapter
ER-SOC-CON-SUS-1.1	The aircraft shall have a maximum fly-over perceived noise level of 89 dB.	A,T	✓	87 [dB]	19
ER-SOC-CON-SUS-1.2.1	The aircraft shall not emit harmful compounds.	A, T	✓	-	19
ER-SOC-CON-SUS-1.2.2	Damaging compounds that are part of the aircraft shall be clearly indicated.	RD	✓	-	17
ER-TUD-CON-SUS-2.1	A partnership shall be used to develop the powertrain.	RD	NA	-	22
ER-NLR-CON-SAF-1	The aircraft shall have a reliability of 99% to successfully complete the race.	A	NA	-	16
ER-NLR-CON-SAF-2.1	The aircraft shall protect the pilot against a fire for 4 minutes.	A, D	✓	-	14
ER-NLR-CON-SAF-2.2	The aircraft shall prevent crashing into populated areas.	A, D	✓	-	14
ER-NAA-CON-REG-1.1.1	The aircraft shall derive its lift mainly from aerodynamic forces.	RD	✓	-	8
ER-NAA-CON-REG-1.2	The aircraft shall not emit carbon dioxide.	RD	✓	-	19
ER-NAA-CON-REG-1.3	The aircraft shall use an electrical propulsion system.	RD	✓	-	10
ER-NAA-CON-REG-1.5.1	The aircraft shall provide breathable air to the pilot.	RD, D	✓	-	14
ER-NAA-CON-REG-1.6	The aircraft shall be equipped with a GPS sensor.	RD	✓	-	13
ER-NAA-CON-REG-1.7	The aircraft shall fly in day Visual Meteorological Conditions.	RD, D	✓	-	13
ER-NLR-CON-RES-1.2.1	The design shall use a COTS engine.	RD	✓	-	10
ER-NLR-CON-RES-1.2.2	The design shall use COTS battery cells.	RD	✓	-	10
ER-NLR-CON-RES-1.2.3	The design shall be producible between 2025 and 2030.	A	✓	-	21
ER-PIL-TECH-NAV-1.1	The aircraft shall be able to measure altitude.	RD, D	✓	-	13
ER-PIL-TECH-NAV-1.2	The aircraft shall be able to measure airspeed.	RD, D	✓	-	13
ER-PIL-TECH-NAV-1.3	The aircraft shall be able to determine its location.	RD, D	✓	-	13
ER-PIL-TECH-NAV-1.4	The aircraft shall be able to measure internal vehicle states.	RD, D	✓	-	13
ER-PIL-TECH-NAV-1.4.1	The aircraft shall be able to measure energy storage levels.	RD, D	✓	-	13

ER-PIL-TECH-NAV-1.4.2	The aircraft shall be able to measure power output levels.	RD, D	✓	-	13
ER-PIL-TECH-NAV-1.4.3	The aircraft shall be able to measure temperature of powertrain.	RD, D	✓	-	14
ER-PIL-TECH-NAV-2.1	The aircraft shall be able to display the determined flight route.	RD, D	✓	-	13
ER-PIL-TECH-NAV-2.2	The aircraft shall be able to display the measured data.	RD, D	✓	-	13
ER-SOC-TECH-NAV-3	The aircraft shall be able to store the measurements taken during flight.	RD, D	✓	-	13
ER-NLR-TECH-GOP-1.1	The aircraft shall be able to be refuelled at all landing sites.	A, D	✓	-	18
ER-NLR-TECH-GOP-1.2	The aircraft shall be able to be refuelled in 7 hours and 10 minutes or less.	A, D	✓	1 hour	18
ER-PIL-TECH-GOP-2.1	The aircraft shall provide an entrance for the pilot.	RD, I	✓	-	11
ER-NLR-TECH-GOP-2.2	The aircraft shall enable access for regular maintenance.	RD, I	✓	-	17
ER-NLR-TECH-GOP-2.2.1	The aircraft shall enable access to check the landing gear.	RD, I	✓	-	17
ER-NLR-TECH-GOP-2.2.2	The aircraft shall enable access to check the powertrain.	RD, I	✓	-	17
ER-NLR-TECH-GOP-2.2.3	The aircraft shall enable access to check the control actuators.	RD, I	✓	-	17
ER-NLR-TECH-GOP-3.1	The aircraft shall be able to manoeuvre on the ground without tipping over.	A, D	✓	-	11
ER-NLR-TECH-GOP-3.2	The aircraft shall be able to move from the hangar to the take-off location.	A, D	✓	-	11
ER-PIL-TECH-COM-1	The aircraft shall enable the pilot to communicate with the ground team.	RD, D	✓	-	13
ER-PIL-TECH-COM-2	The aircraft shall enable the pilot to communicate with air traffic management.	RD, D	✓	-	13
ER-PIL-TECH-COM-3	The aircraft shall enable the pilot to communicate with other planes.	RD, D	✓	-	13
ER-NLR-TECH-CRU-1	The aircraft shall have a minimum average speed of 145 [m/s].	A, T	✓	149 [m/s]	12
ER-NLR-TECH-CRU-1.1	The aircraft shall have a continuous power-to-weight ratio of at least 8.1 [W/N].	A	✓	9.6 [W/N]	10
ER-FAA-TECH-CRU-1.2	The aircraft shall have a minimum cruise altitude of 10,000 [ft].	A, T	✓	41,000 [ft]	12
ER-NAA-TECH-CRU-2	The aircraft shall have a minimum range of 200 [km].	A, T	✓	2286 [km]	12
ER-NLR-TECH-CRU-2.1	The aircraft shall have a maximum lift-to-drag ratio of at least 18:1.	A, T	✓	19:1	8
ER-FAA-TECH-FLM-1.1	The aircraft shall be able to withstand a load factor of 3.8.	A, T	✓	3.8	11
ER-NLR-TECH-FLM-2.1	The aircraft shall have a peak power-to-weight ratio of 10 [W/N].	A	✓	12.6 [W/N]	10
ER-AIRP-TECH-FLM-2.2	The aircraft shall have a maximum take-off distance of 2000 [m].	A, T	✓	1544 [m]	12
ER-AIRP-TECH-FLM-3.1	The aircraft shall have a maximum landing distance of 1000 [m].	A, T	✓	654 [m]	12
ER-NLR-TECH-FLM-4.1	The aircraft shall be able to achieve a minimum climb rate of 5 [m/s].	A, T	✓	7.36 [m/s]	12
ER-FAA-TECH-FLM-4.2	The aircraft shall be able to achieve a minimum climb angle of 4 degrees.	A, T	✓	6 degrees	12
ER-PIL-TECH-CON-1.1.1	The aircraft shall be trimmable.	RD, D	✓	-	9
ER-PIL-TECH-CON-1.1.2	The lateral stick forces shall be at most 140 [N].	A, T	NA	-	-

ER-PIL-TECH-CON-1.1.3	The longitudinal stick forces shall be at most 400 [N].	A, T	NA	-	-
ER-PIL-TECH-CON-1.1.4	The pedal forces shall be at most 1500 [N].	A, T	NA	-	-
ER-PIL-TECH-CON-1.2.1	The stick deflection angle shall be at most 45 degrees.	A	NA	-	-
ER-PIL-TECH-CON-1.2.2	The stick deflection travel shall be at most 30 [cm].	A	NA	-	-
ER-FAA-TECH-CON-2.1.1	The control accelerations shall not be larger than 1.1799 [rad/s^2] in pitch.	A	NA	-	-
ER-FAA-TECH-CON-2.2.1	The aircraft shall be statically stable.	A, T	✓	-	9
ER-FAA-TECH-CON-2.2.2	The aircraft shall be dynamically stable in the short period.	A, T	✓	-	9
ER-FAA-TECH-CON-2.2.3	The aircraft shall be dynamically stable in the Dutch roll.	A, T	✓	-	9
ER-NLR-TECH-PPR-1.1	The aircraft shall structurally support the pilot.	A	✓	-	11
ER-NLR-TECH-PPR-1.2	The aircraft shall maintain its aerodynamic shape.	A	✓	-	11
ER-FAA-TECH-PPR-1.3	The structure shall not be damaged under ultimate loads.	A, T	✓	-	11
ER-AIRP-TECH-PPR-2	The aircraft shall have a maximum wingspan of 40 [m].	RD, I	✓	7.46 [m]	8
ER-NLR-TECH-PPR-3	The aircraft shall have a maximum mass of 1,200 [kg].	RD, I	✓	1,162.5 [kg]	15

In Table 16.2, multiple requirements have not been analysed yet. There are a number of reasons for that. For ER-TUD-CON-SUS-2.1, companies have been approached as For ER-NLR-CON-SAF-1, it was found that estimating the reliability of the design at this stage is not possible as detailed information on the components used would be required as discussed in Section 16.5. However, it was found that the reliability can both be analysed and increased by sufficient testing and therefore, the time has been allocated for that in the future steps of the project as is discussed in Chapter 21. Lastly, ER-PIL-TECH-CON-1.1.1-2.1.1 were not analysed as again a more detailed design is required for this. This is highly dependent on the high point for the different control surfaces as well as the gear ratio of the controls which have not been established yet.

16.1.2. Subsystem Verification

The aircraft consists of multiple different subsystems that all have their purpose, and therefore the working of the subsystem can be verified. For this aircraft, the following subsystems were considered: powertrain, structures, avionics & control, and the safety system.

Propulsion

For the propulsion system, a number of tests are required for validation. These are shown in Table 16.3.

Table 16.3: Propulsion system verification tests

Test	Explanation	Resources
Cooling Test	The cooling system is tested independently to determine if the cooling capabilities are sufficient.	Assembled cooling loop, flow and temperature sensors
Electric Motor Test	The electric motor is tested on its own over a range of rpms to check the capabilities and efficiency of the motor	Electric motor, power supply, dynamometer
Propeller Test	The propeller is tested independently over a range of rpms. The power output and the functioning of the pitch control are checked.	Propeller, motor, test bench, wind tunnel
Test	The wires are connected together. Then the layout is checked according to design schematics as well as determining power losses.	Connected wiring, multimeter
Battery Charge Test	The battery is charged using the determined charge settings. The time and efficiency of charging is determined.	Battery, power supply, charger
Battery Output Test	The battery is discharged at the desired power setting. The discharge efficiency, voltage and current are determined.	Battery, discharge tester
Maximum Power Test	The powertrain unit is throttled up to maximum power to check its capabilities and proper operation.	Assembled powertrain, dynamometer

Long Duration Cruise Test	The powertrain unit is tested over a long duration at cruise power setting. This is done multiple times to check reliability and cruise capability.	Assembled powertrain, dynamometer
Hydrogen Tank Pressurisation Test	The hydrogen tank is pressurised until ultimate pressure. The tank is checked for leaks and damage.	Assembled tank, compressor, test bench
Hydrogen Tank Refuelling Test	The hydrogen tank is filled with hydrogen and is checked for leaks and insulation performance.	Assembled tank, hydrogen supply, fuelling device
Hydrogen Fuel Cell Test	The hydrogen fuel cell is supplied with hydrogen and run at cruise output power. The system is checked for any leaks and the efficiency is determined.	Assembled fuel cell, hydrogen supply, test bench, power output measuring device
Long Duration Hydrogen System Test	The full hydrogen system including tank, tubes and fuel cell is run continuously for designed cruise duration. The reliability of the system and the boil-off of hydrogen is determined.	Assembled hydrogen subsystem, power output measuring device

Structures

Another test campaign is set up for the structures subsystem. The tests involved are presented in Table 16.4.

Table 16.4: Structures subsystem verification tests

Test	**Explanation**	**Resources**
Wing Bending Test	The total wing structure is subjected to the ultimate bending load. The wing is then checked for damage using Non-Destructive Testing (NDT).	Assembled wing, bending test machine, NDT equipment
Wing Fatigue Test	The wing is subjected to a nominal bending moment for at least 1000 cycles. The wing is checked using non-destructive testing.	Assembled wing, bending test machine, NDT equipment.
Fuselage Ultimate Load Test	The fuselage is subjected to the ultimate loads. This includes bending, normal and torsional loads. Then the fuselage is checked for damage using non-destructive testing.	Assembled fuselage, fuselage testing machine, NDT equipment.
Fuselage Fatigue Test	The fuselage is subjected to nominal loads for at least 1000 cycles. Damage is checked using non-destructive testing.	Assembled fuselage, fuselage testing machine, NDT equipment.
Structure Impact Test	Both wing and fuselage are subjected to impact representing a bird strike and are checked for damage afterwards. Most important is the cockpit as it should protect the pilot from a bird strike.	Assembled fuselage and wing, impact test equipment, NDT equipment
Landing Gear Test	The landing gear is subjected to ultimate normal and bending loads. The landing gear is checked for damage using non-destructive testing.	Assembled landing gear, load testing machine, NDT equipment
Landing Gear Fatigue Test	The landing gear is subjected to nominal loads for at least 1000 cycles. Damage is checked using non-destructive testing.	Assembled landing gear, load testing machine, NDT equipment

Avionics and Control System

The next set of tests is planned for the aircraft's avionics system and control system. It is shown in Table 16.5.

Table 16.5: Avionics and control subsystem verification tests

Test	**Explanation**	**Resources**
Software testing	All software used in the aircraft is tested thoroughly. Starting with unit tests and ending at full system tests.	Computing resources and time.
Electronics stress testing	All electronic systems of the aircraft are pushed to their operational limits to see whether they still perform as they should under those conditions.	Assembled electronics, power supply, multimeter.

Measurement accuracy tests	Measurement devices are tested and their output is inspected to determine the correctness and accuracy of measurements.	Measurement devices connected to the onboard computer, environment simulating test bench, reference measuring devices
Display and telemetry testing	It is tested whether the telemetry is correctly shown on the displaying instruments.	Assembled onboard computer and displays, telemetry simulating signals equipment
Control surfaces deflection tests	Control surfaces are checked and their deflection is measured for a given pilot input. The results are then compared with the specifications.	Assembled control subsystem, measuring devices.

Safety System

Finally, the client requires an additional safety system to be in place such that both pilot and aircraft survivability is increased. At this stage, the type of safety systems used are still unknown and therefore the tests are very high level. However, for the sake of completeness, the tests are shown in Table 16.6.

Table 16.6: Safety system verification tests

Test	Explanation	Resources
Pilot Safety Analysis	The safety system that protects and saves the pilot is analysed and its performance is checked.	Computing resources and time.
Aircraft Safety Test	The aircraft safety system is tested for both duration it can extend aircraft flyability as well as the severity of accident it can contain.	Assembled safety system, safe test location

16.1.3. Aircraft Verification

Having performed subsystem verification, it is then possible to perform tests on the whole aircraft. Those can confirm whether the real product has been up to the design specifications. The full campaign of those tests has been established and is presented in Table 16.7.

Table 16.7: Aircraft verification tests

Test	Explanation
Static Full Power	The brakes are applied to the aircraft and then full power is applied. The aircraft is checked for damage and everything should be the same as the subsystem propulsion test.
Ground Manoeuvres	The predetermined ground manoeuvres such as taxis and turns are performed. The manoeuvring performance and tip-over criteria are checked.
Take-Off	Multiple take-offs are performed to determine the minimum take-off distance required for configurations both with and without high-lift devices.
Landing	Multiple landings are performed to determine the minimum landing distance for configurations both with and without high-lift devices.
Communication	The functioning of the communication system at different required frequencies is tested.
Maximum Climb Rate	The aircraft is flown at the angle of attack and speed of theoretical maximum climb rate. The climb rate is measured and compared to requirements.
Maximum Climb Angle	The aircraft is flown at the angle of attack and speed of theoretical maximum climb angle. The climb angle is measured and compared to requirements.
Maximum Level Flight Speed at Cruise Altitude	The aircraft climbs to cruise altitude and applies maximum continuous power. The resulting speed is measured and compared to requirements.
Maximum Descent Speed	The aircraft is pitched down and accelerated until it reaches its specified maximum Mach number to confirm it is able to reach that speed.
Maximum Glide Ratio	The aircraft is flown at angle of attack and speed of theoretical maximum glide ratio. The glide ratio is then determined and compared to requirements.
Stall Speed at Sea-Level	The aircraft is flown at lower speeds and higher angles of attack until early indications of stall occur. Then control characteristics close to the stall are measured as well as the stall speed.
Service Ceiling	Aircraft is flown at its maximum climb rate configuration until it reaches a certain altitude at which it does not increase its altitude anymore.

Maximum Range	The aircraft is fully charged and fueled and is flown at cruise altitude until all fuel except reserves is used. This will determine the maximum range which is compared with requirements.
Maximum Turn Rate	The aircraft is flown at maximum required turn rate. The performance during the turn and the effect on the subsystems is tested.
Flight Envelope	Aircraft is flown at its operational limits and all its subsystems are checked for proper operation.
Control Characteristics	Aerodynamic control derivatives and stick forces are measured or derived from flight measurements.
Stability Characteristics	Aerodynamic stability derivatives and eigenmotion characteristics are derived from a flight test.
Emergency Scenarios	All of the emergency scenarios that are required by the aircraft to handle are simulated during flight.
Noise	The noise that the full aircraft emits during various flight phases is measured and compared against its requirements.

The resources for the flight test also should be considered. Firstly, a full working prototype is needed as well as a pilot and ground team to ensure that the aircraft is operational. For the experimental certification, a minimum of 10 hours of flight tests are required. However, considering the extensive testing it was estimated that at least 20 hours of flight testing will be required. Furthermore, an airfield in a scarcely populated area is required. It is preferred that this is a relatively small airfield but still with a runway at least twice as long as the designed runway length of 1000 [m].

16.2. Validation

Validation of a product is about relating back to the intended purpose of the product. The question to be answered is as follows: does the product fulfil the intended purpose? For this project, the intended purpose is reflected by the mission need statement: The design of an aircraft that can win the Pulitzer Electric Aircraft Air Race. To validate that this purpose is being fulfilled, action can be taken both during the design phase and when the product has been realised. The validation can be split up between validation of the aircraft which will be discussed in Section 16.2.1 and validation of the support team which is explained in Section 16.2.2.

16.2.1. Aircraft Validation

During verification, a large number of flight tests were conducted to determine the aircraft's performance characteristics. This leaves only one test to be conducted for validation. To validate the ability of the aircraft to win the Pulitzer Electric Aircraft Air Race, a practice run of the race needs to take place. This includes flying the full distance within the specified time limits and determining the time the aircraft takes to fulfil the flight. During the practice run the aircraft is monitored for in-flight performance measurements. While a successful practice run does not guarantee that the product has fulfilled its mission, this provides the most amount of evidence of its winning capabilities.

16.2.2. Support Team Validation

Apart from the aircraft itself, a support team is an integral part of the race and is needed to ensure victory. Therefore, it also needs to be validated against its functions. This validation consists of the tests presented in Table 16.8.

Table 16.8: Support team validation tests

Test	Explanation
Hydrogen equipment test	All hydrogen related equipment (eg. tanks, lines, dispensers, etc.) that is not part of the aircraft is tested for proper operation to ensure its reliability.
Charger test	The electric charger for the aircraft's battery is tested for proper working.
Strategy software test	Potential software that might be used for race strategy is checked and tested for accuracy and reliability.
Communication test	Communication equipment used for a relay with the pilot is tested to ensure stable communication throughout the whole flight.

16.3. Required Resources

To perform the verification and validation procedures outlined in this chapter a number of resources are required. The labour cost concerning these tests are already discussed in Chapter 22. However, the facilities required for the test are also of importance.

16.4. Sensitivity Analysis

To assess the robustness of the design, the effect of changing initial parameters on the final design can be investigated. This can create multiple different insights. Firstly, it can show how much variance can be expected in certain parameters in future stages. Secondly, it shows which input parameters are particularly influential on the design and thus, these need to be designed with more detail. Finally, it can also create insight into potential ways the designs can be improved and how much. The sensitivity analysis for the different subsystems and the flight performance are presented in the paragraphs below.

16.4.1. Aerodynamics

In order to determine the effects of some of the aircraft parameters on the aerodynamics of the aircraft, a sensitivity analysis on these was performed. It was decided that five parameters were relevant to be changed. These were the weight, the wing surface area, the sweep of the front wing, the dihedral of the front wing and the taper ratio of both wings. The results of this can be seen in Figure 16.1.

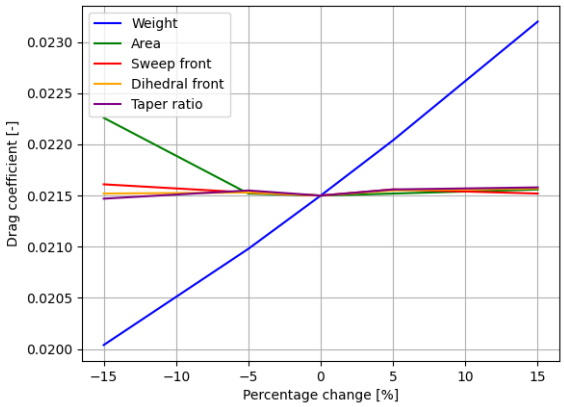

Figure 16.1: Drag coefficient based on a percentage change of given input parameters

From this graph, it can be seen that the parameter with the largest effect on the drag is the weight. The lift coefficient of the aircraft during the cruise increases proportionally with the weight of the aircraft, which leads to such a change. This parameter is considered to be heavily sensitive. After this, the surface area of the wing causes a severe increase in drag coefficient when too low. However, overall drag would not change as much as it would appear on this graph as the surface area of the wing is also used in the calculation for drag based on the drag coefficient. Finally, the last three parameters have very little variation and are hence considered not sensitive.

16.4.2. Stability

To gain a greater idea of the impact of changing the variables mentioned in Section 16.4.1, a brief stability analysis was performed. From this, the stability margin of the aircraft assuming the centre of gravity of the aircraft doesn't change. It should be noted that the centre of gravity would change, especially in some parameters such as wing sweep and weight, so this assumption may not hold, however this can still be used to indicate how the maximum allowed centre of gravity for stability changes. The results can be found in Figure 16.2.

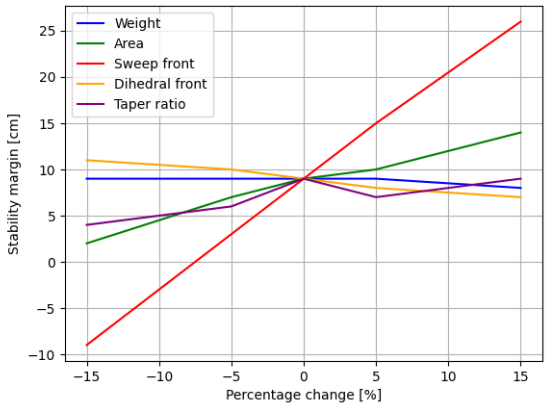

Figure 16.2: Centre of gravity based on a percentage change of input parameters

Here, the sweep of the front wing can be seen to have the greatest impact on the centre of gravity of the aircraft. It should be noted, however, that having a greater sweep in the wing causes the centre of gravity to move further aft, diminishing the effects of this parameter. It is still considered to be very sensitive. Surface area and taper ratio can also be seen to be quite sensitive, with some variation seen at lower values in particular. Finally, weight and dihedral of the front wing are considered to not be sensitive as the variation of the centre of gravity with a change of either of these parameters is minimal.

16.4.3. Fuselage Structure

For the fuselage, the main input parameters that will be investigated are the total aircraft weight and the volume occupied by the aircraft. Here it is assumed that with a changing volume the design in terms of the amount of stringers and skin thickness does not change. This results in the relation shown in Figure 16.3, which shows the effect of these parameters on the weight of the fuselage structure.

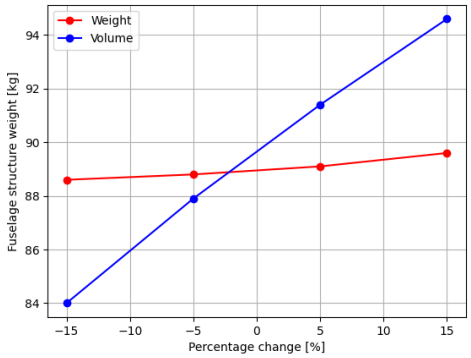

Figure 16.3: Fuselage structure sensitivity

It can be seen that the fuselage weight is not very sensitive with respect to aircraft weight. This is because the limiting failure mode is buckling and therefore only the amount of stringers changes, which is a relatively small part of the fuselage structure. It is more sensitive to changes in volume as this influences the total skin area as well as the size of the frames resulting in a stronger influence on structural weight of the fuselage.

16.4.4. Wingbox structure

The wingbox is dependent on output of the VLM analysis of the aerodynamics department. For 5 combinations of various Maximum Take-off Mass ($MTOM$) and 5 combinations of different (AR) a VLM analysis is performed providing data for the wingbox design. The results of the wingbox mass are plotted in Figure 16.4. In general, a higher MTOM results in a higher wingbox mass which can be expected as the wing is required to produce more

lift, and therefore apply more loading on the wingbox. Also, the aspect ratio increase correlates with an increase in wingbox mass, except for a change of -5% to -15%, where it slightly decreases.

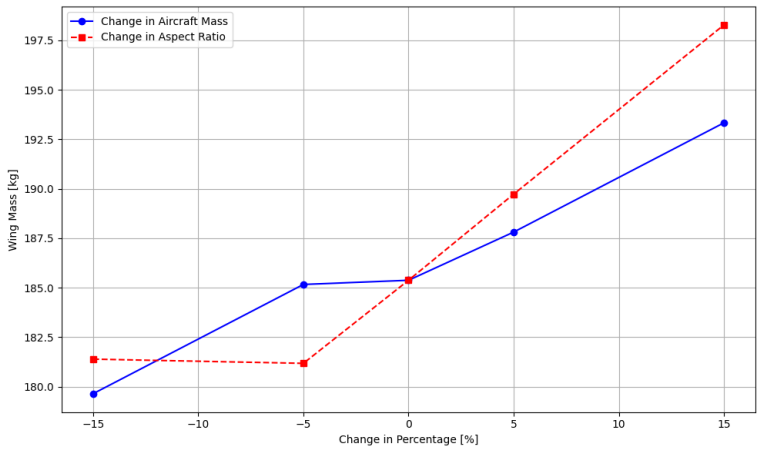

Figure 16.4: Wing structure sensitivity

16.4.5. Power & Propulsion

In order to understand the impact of parameters related to the power and propulsion system of the aircraft, a sensitivity analysis has been performed. The parameters that were deemed relevant for the sensitivity analysis, were those that have a higher uncertainty. These six parameters are the fuel cell specific power in [kW/kg], battery discharge efficiency [-], tank gravimetric density [-], battery energy density [kWh/kg], propeller efficiency [-] and the fuel cell efficiency [-]. These parameters were chosen since they are based on future developments or not tested in reality such as the propeller, increasing the uncertainty. These parameters were increased and decreased with 5% and 15%. The parameters were related to a relevant parameter which they affect. The four parameters with a main influence on mass are presented in Figure 16.5.

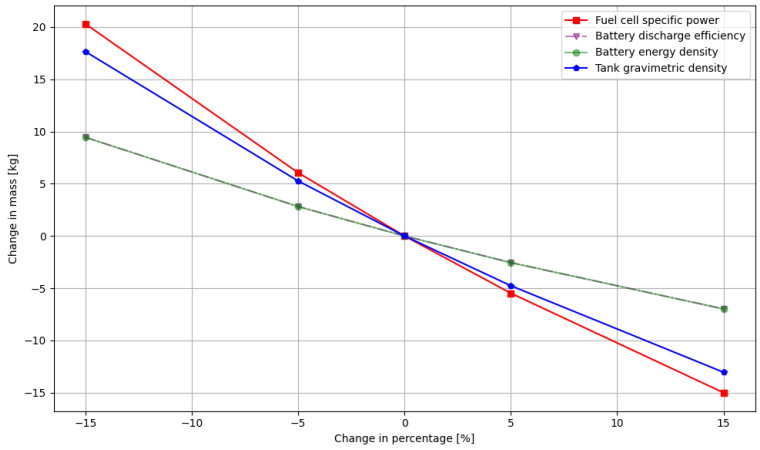

Figure 16.5: Change in mass due to percentage change in input parameters

In Figure 16.5, it can be seen that the fuel cell specific power has the largest impact on the mass. A decrease of 15% from the current fuel cell specific power of 2 [kW/kg], results in an increase of 20.3 [kg]. The changes in battery discharge efficiency and battery energy density have a similar effect and have the smallest effect on the mass. Decreasing the battery energy density with 15% results in a mass increase of 9.4 [kg]. The remaining two parameters, the propeller efficiency and the fuel cell efficiency were deemed to not directly affect the mass. A change in propeller efficiency is related to the required power outputted, which could eventually influence the mass of the fuel cell, the hydrogen mass, and the hydrogen tank mass. A change in the fuel cell efficiency affects the amount of hydrogen inputted into the fuel cell, therefore a change in hydrogen flow rate is observed. Table 16.9 presents the

changes in power and hydrogen flow rate due to a percentage change. It can be seen that a decrease in propeller efficiency of 15% would result in an increase of power of almost 30 [kW]. With the current output power of the fuel cell of 230 [kW], this would be an increase of power of almost 13%.

Table 16.9: Change in power and hydrogen flow rate due to percentage change in input parameters

Changed parameters	-15%	-5%	0%	5%	15%	Unit
Propeller efficiency change in power	29.74	8.87	0.00	-8.02	-21.98	kW
Fuel cell efficiency change hydrogen flow rate	0.48	0.14	0.00	-0.13	-0.35	g/s

16.4.6. Flight Performance

To ensure that optimal performance has been achieved, a study has been done to examine the change in flight performance with changes in crucial parameters. The input parameters that have been examined are mass and power. These parameters have been selected because the power is the most limiting on the flight performance, while the mass is a driving variable for the lift performance.

A change of 5% and 10% have been applied in both directions for this analysis. Only the impact of 1 input variable is inspected at a time. The impact on the flight performance is summarised in Table 16.10.

Table 16.10: Sensitivity analysis for flight performance

Mass [kg]	Power [kW]	Range [km]	Time [minutes]	Average Velocity [m/s]
1200	179	2286.66	205.69	149.89
1200	171.05	2293.58	208,97	147,54
1200	161.1	2303,78	209,95	146,85
1200	187.95	2259,6	201,77	152,8
1200	196.9	2234,32	198,33	155,45
1140	179	2348,97	205,27	150,2
1080	179	2404,19	203,94	151,18
1260	179	1818,7	222,7	136,1
1320	179	1808	223	135,1

From Table 16.10 it can be seen that increased power and lower mass both decrease the race time. From these 2, it seems that increasing the power has a more dominant effect on the performance than reducing the weight. In the case where mass is increased or the power is lowered, it is concluded that the race time will increase. The increase in weight has a larger effect in this scenario than the decrease in power. From this analysis, it can be concluded that power has a dominant effect on performance increase, while weight predominantly decreases performance.

16.4.7. Overall sensitivity conclusion

Every subsystem has been investigated during the sensitivity analysis, as is the performance. The weight of the aircraft is found to influence the most subsystems, the aerodynamic performance, the wingbox, and flight performance are the most affected by this parameter, while the sweep of the front wing affects the stability the most, and specific power affects the power unit the most. Therefore in future design steps, extra attention should be put on these parameters such that any variation is closely monitored since these affect the design the most.

It is advised to use a larger margin for the aircraft mass and the specific power since these 2 parameters will have the most effect on the overall design. This is done to ensure that the design does not drastically change over future iterations.

16.5. Reliability Analysis

The E-Racer has been designed with the intention of winning the race. In the initial stages of the project when the requirements and constraints were being determined, the client was contacted. During these discussions, ER-NLR-CON-SAF-1 was defined. This requirement states that the aircraft should have a reliability of 99%. For this mission, reliability has been defined as the probability of starting and finishing the race with the same undamaged airframe and the same flawless propulsion system.

Due to time constraints and the lack of information available on the components chosen to manufacture this aircraft, an accurate estimation of the reliability is not possible at this stage. However, to meet this requirement, a high-level

improvement strategy has been drawn up. The impact on the reliability of the verification and validation tests that have already been suggested in this chapter will now be discussed, as well as additional steps and ideas that can be implemented for aircraft reliability improvement.

The verification and validation tests for the propulsion and structure subsystems that have already been discussed in this chapter have a direct contribution towards the level of reliability due to the way in which this term has been defined for this specific mission. Tests such as hydrogen tank pressurisation tests and wing bending tests, amongst others, are carried out to check that the system works properly and hence the system can be verified, but, although they help improve the reliability of the subsystem itself, these tests do not guarantee that the requirement can be met.

Verification and validation tests performed on other subsystems such as the avionics and control subsystem, as well as tests performed on the whole aircraft or even support team validation tests, have an impact on the performance of the aircraft which then also affects reliability. For example, the control surface deflection tests, although part of the avionics and control subsystem, can have a direct impact on the airframe and propulsion subsystems in case there is any malfunction that could cause the aircraft to crash.

In essence, all verification and validation procedures must be performed to ensure that the E-Racer works correctly; nevertheless, in order to improve the reliability of the aircraft and guarantee that the E-Racer can reach the finish line with an airframe and propulsion subsystems with no defects, other strategies should be put into place. These are discussed in the following chapters.

Ensuring quality throughout the manufacturing process is important for better reliability. Therefore, skilled workers led by a person overseeing this process by making sure that all manufacturing procedures are followed and all parts and components are handled correctly would increase the quality of the process.

As the Prandtl plane is an unconventional design, pilot training could be a good way to increase reliability. This is mainly because control of the aircraft would differ from typical aircraft flown by average pilots. Also, even if the aircraft is structurally reliable, placing an unskilled pilot on Prandtl planes could have detrimental effects on the mission. Therefore, programming a flight simulator to behave similarly to the designed aircraft and training the pilot on that configuration would be a good strategy for recording significant flight hours with no considerable budget. Training the pilot on the aircraft itself would be more cost-intensive.

Another way to improve reliability would be to carry out regular routine checks on the aircraft, especially after each flight, focusing on the propulsion system. This would mean that most obvious problems would be detected at an early stage, ensuring no further damage to the system and a safe environment for the pilot. Easy access to aircraft subsystems is important to facilitate the maintenance process.

17. Manufacturing & Maintenance

In order to eventually participate the aircraft needs to be manufactured. Furthermore, maintenance procedures will also be required to keep the aircraft running smoothly for multiple flights. It is important to already consider these aspects of the product during the design phase as they can have a significant impact on the design. It was decided to manufacture the aircraft in the United States, as this makes the test and certification process easier. The manufacturing of the custom parts is discussed in Section 17.1. Then the acquirement of COTS parts is discussed in Section 17.2. Assembly is the topic of Section 17.3. Lastly, quality control is explained in Section 17.4.

17.1. Manufacturing of Custom Parts

The aircraft will make use of as many COTS parts as possible, however, a substantial amount of parts still need to be made custom. This can be done either in-house at the NLR, or it can be delegated to a third-party manufacturer. Either way, a manufacturing plan will be required. An important part of the aircraft that needs to be manufactured custom is the aircraft structure, as this has been designed tailor-made to the different subsystems in the aircraft. For each main structural element, a manufacturing method is chosen. The chosen manufacturing method is based on consideration of cost and shape.

Table 17.1: Structural components and their associated manufacturing methods

Component	Manufacturing Method
Skin	Rolling, Laser Cutting Roll Bending, Stretch Forming
Stringers	Extrusion, Bending
Beams	Extrusion
Ribs	Laser Cutting, Rubber Forming
Frames	Extrusion, Bending
Canopy	Thermoforming

The different types of elements in Table 17.1 can be discussed shortly. Firstly, the stringers and the structural beams will be manufactured using extrusion. This creates the desired profile and can be used to create long slender elements. These stringers are then cut to length using a saw. Some of the stringers might require slight bending to conform to the shape of the aircraft. The choice was made to drill the holes for the rivets during assembly as drilling during this stage would require low tolerances and perfect alignment

Secondly, the skin for the fuselage, wing, and wing box will be created by rolling the aluminium to the desired thickness. The aluminium sheets can then be cut to the correct size using laser cutting. Laser cutting is used for the cutting of all sheets as it does not require any part-specific tools, which makes it cost-effective for a one-off aircraft. Furthermore, laser cutting creates the best edge quality compared to other universal cutting processes. Finally, some parts of the aircraft skin are curved. Then the sheets need to be bent. This can be done by either roll bending or by stretch forming depending on whether the panel is single or double-curved. A similar process will be used for the bulkheads/firewall. However, this will be made of 300M steel and only needs to be rolled to the required thickness and then laser cut as they are straight panels.

Thirdly, the ribs of the skin will manufactured using rubber forming. This requires only one part specific die, reducing cost. Furthermore, machining was not chosen as it generates a lot of waste, and the thickness of the ribs comes close to the minimum wall thickness that can be achieved using machining, further complicating this method. Furthermore, the initial sheets for the ribs need to be rolled and laser cut beforehand as well.

The frames are made first by extruding aluminium in the desired profile. Then the frame needs to be bent to the correct shape.

Finally, the canopy will be made custom as well as it is specific to the shape of the aircraft. Firstly, a sheet of polycarbonate of the right size and thickness needs to be obtained. Then thermoforming will be used to create the desired shape. This includes creating a mould where the sheet is placed inside. The mould with the polycarbonate is then heated in an oven to make the polycarbonate form to the mould.

17.2. Acquiring COTS parts

The parts that will not be made custom, will be COTS and thus, be bought from a company. There are several considerations that need to be taken into account when picking the right COTS part. These considerations are listed below.

1. Correct specifications
2. Sustainability
3. Interface with other parts or systems
4. Reputation of the supplier
5. Cost

These will ensure that the best product is chosen.

It should be noted that the fuel cell, battery cell and hydrogen tank are not based on future expected COTS parts. This means that a COTS component with the exact specifications set might not be possible. However, it is expected that the supply and diversity of these components will increase in the near future, as they are these components are part of a growing market.

17.3. Assembly

When all parts have been manufactured the structural assembly can take place. This will be divided into two main parts: the assembly of the fuselage and the assembly of the wings. In general steps, the stiffening elements will be attached to the skin using rivets. Furthermore, the different skin panels are also connected using rivets. This was done, as it is the most cost-effective option while creating a strong connection between the different structural elements. The flow of the assembly is shown in Figure 17.1.

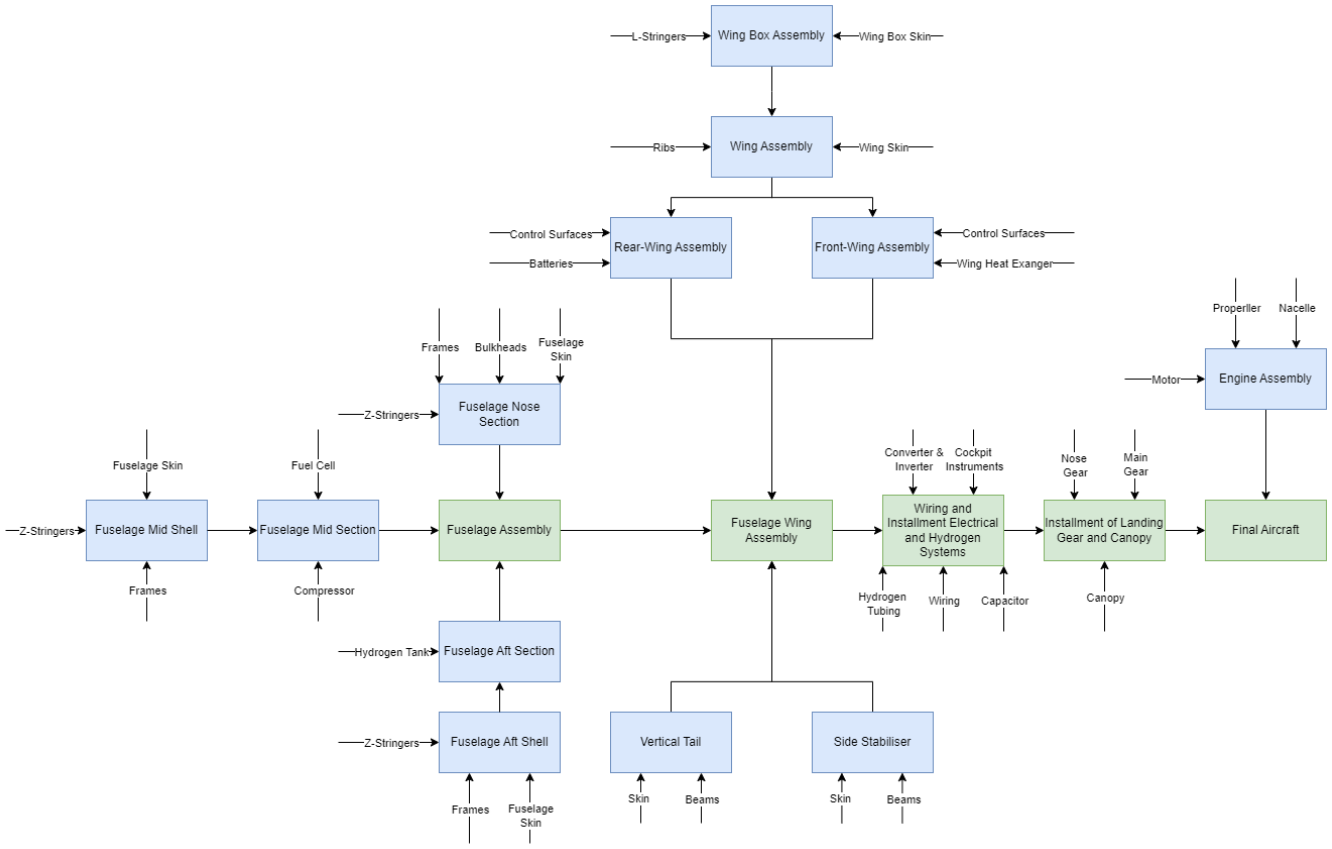

Figure 17.1: Diagram of the assembly process

It is important to note that for the assembly process, different assembly jigs will be required. This is to ensure the correct alignment of the different parts that will be assembled. The jigs will also hold the different parts while holes can be drilled and fasteners are attached. Lastly, the wings need to be able to be dismantled from the main fuselage as the aircraft needs to be able to be transported, otherwise, it would be too big. Finally, the decision was made to manufacture and test the aircraft near the start of the race and therefore, this will happen in the US.

17.4. Quality Control

An important part of the manufacturing process will be quality control. Generally, this can be subdivided in quality control of COTS components and quality control of custom-manufactured components.

For the COTS components, the correct paperwork needs to be checked upon arrival. Then the performance of the components needs to be tested. How this is done, depends on the components. For example, for rivets one or multiple rivets can be tested for their strength and durability, for the fuel cell the output and efficiency can be tested. If the tested component is found to be not up to specification then an official report needs to be sent to the supplier. This shows that documentation and full traceability is a crucial part of quality control. For the custom parts, a continuous quality control process is used. This means that during every step of the manufacturing process, quality control will be performed. This includes checking dimensions and correct tool settings as well as ensuring traceability of the parts. Finally, during the assembly quality control will also be performed on the connections and interfaces between the different parts and subsystems.

Maintenance is important for keeping the aircraft in good condition. Therefore, this part of the operational procedure of the aircraft has to be taken into account when designing the aircraft. The aircraft must be designed so that it is easy to set up inspection procedures for important parts of the aircraft that are more susceptible to damage, such as the propulsion system, sensors, instruments, or structural parts. The aircraft must allow for fast, easy, and cheap maintenance procedures and replacement of parts in case a fault is detected. Therefore, easy accessibility is a priority for the design. Also, COTS parts are extremely helpful for saving time and costs in case one of those parts breaks, as custom parts require a new part to be manufactured after the broken part has been identified. The design must allow for easy detection of damaged components. In addition, the software of the aircraft must also be reliable and easy to fix in case bugs are detected. Some additional more detailed maintenance considerations are outlined in the paragraphs below. Generally, preventive maintenance will take place every 25 flight hours, while minor maintenance will take place every 100 flight hours[1]. It should also be noted that the expected maintenance for the aircraft is generally low as it will be used for a short amount of flight hours. Therefore, the maintenance procedure outlined focuses on preventative maintenance. Lastly, to ensure safety during maintenance work, harmful or damaging compounds of the aircraft shall be labelled.

Firstly, the electric motor has few moving parts and therefore does not require a lot of maintenance. Still, several inspections need to be performed at regular intervals. These include inspections of the high-speed bearings, the condition of the windings, and the insulating components [114].

Secondly, the high-voltage batteries require their own inspections as well. This is to ensure safety. Any damage to the cells or the connectors will increase the risk of thermal runaway and therefore the batteries need to be checked regularly. These checks will include inspecting the connectors and the cells themselves as well as the protection material of the battery pack. To allow for the inspections of the batteries, access holes should be present as they are located in the wings. Then a small camera can be used to inspect the batteries.

Thirdly, the hydrogen system requires specific maintenance. As hydrogen aircraft are a novel concept, this is still partially unknown, however, studies have been performed on the matter. Meissner et al. investigated the maintenance required for an aircraft hydrogen system [115]. They outlined a large number of maintenance procedures but they can be grouped into the following main maintenance tasks:

1. Inspection of the fuel tank
2. Inspection of valves and connectors
3. Inspection of the piping
4. Operational check of valves and connectors
5. Functional check of safety devices
6. Replacement of filter for tank and fuel cell
7. Inspection of fuel cell[2]

Finally, the airframe and the other conventional components need maintenance as well. The preventive maintenance checks for these components are listed below[3].

[1] https://www.lycoming.com/content/basics-maintenance-general-aviation [Accessed on 13-06-2024]

[2] https://fuelcellsworks.com/news/what-everyone-needs-to-know-about-fuel-cell-care-and-maintenance/ [Accessed on 13-06-2024]

[3] https://limblecmms.com/blog/aircraft-preventive-maintenance-checklist/ [Accessed on 13-06-2024]

1. Check exterior lights
2. Inspect wings for damage
3. Inspect canopy for damage
4. Check oxygen and pressurisation system works properly
5. Inspect engine nacelles for damage or faults
6. Check if propeller blades are not loose and rotating freely
7. Check tyre pressure
8. Check lubrication of landing gear struts
9. Check wheel bearings of landing gear
10. Inspect control surfaces for damage
11. Check control surfaces move properly

18. Operations & Logistics

This chapter aims to elaborate on the operations that have to be carried out from preparation for the race up until the post-flight operation procedures. First, the operations during the mission are discussed in Section 18.1. Then the required facilities and staff for the operations are briefly mentioned in Section 18.2. Lastly, procedures for special circumstances are explained in Section 18.3.

18.1. Operations During the Mission

In order to be able to complete the mission, the operational and logistical aspects have to be correctly planned for in advance. The aircraft must first be transported to Eppley Airfield in Omaha, Nebraska, in order to start the race. From there, ground operations will need to be performed before the aircraft is ready to take off. The aircraft will then climb to its designated cruise altitude and eventually descend to land at Dare County Regional Airport in Manteo, North Carolina, flying the whole distance of the race without making any intermediate stops. During the flight, manoeuvres will be performed and communications with Air Traffic Management (ATM) and the ground team will occur.

18.1.1. Transportation

In order to transport the aircraft to the required location where the race begins, a secondary vehicle will be made use of. The aircraft can be easily disassembled for road transport by truck. This transportation service has an approximate cost of $1,500 for a small propeller aircraft, directly dependent on the travel distance[1]. Finally, upon delivery, the aircraft will require re-assembly, and it will be checked for potential damage caused during transportation. Air freight is not preferred over road freight due to increased costs; although the former is indeed a safer[2] and faster transportation method, the cost is most limiting in this case[3]. Another option could involve flying the aircraft from the place where it is manufactured to Eppley Airfield. However, making this trip could impact the chances of winning the race, as the aircraft could suffer unnecessary damage as a result of this flight. Moreover, depending on where the aircraft is manufactured, the travel distance may be greater than the range of the aircraft, forcing one or more stops along the way. Additionally, because the aircraft has an experimental licence, it is not allowed to fly routes that are not approved by the FAA. Regardless of this, hydrogen will have to be purchased in order to make the trip, as well as a way of refuelling the aircraft at any take-off points.

18.1.2. Pre-Flight Operations

Once the aircraft is re-assembled, the ground operations can begin before the race. This involves checking hydrogen and energy levels, recharging batteries and refuelling the aircraft. Very few airfields have the facilities for recharging and none have facilities for refuelling hydrogen. For this reason, liquid hydrogen will be provided by an external company[4] due to the fact that designing a truck that can carry the necessary liquid hydrogen poses many different issues; for example, the necessary equipment to ensure that the hydrogen is carried correctly and safely is a very complex system and consequently very expensive. The charging of the batteries can be easily performed using power outlets located at the hangar, as the battery will not be fully charged on the ground, as excess energy from the flight will be used instead.

An important part of the pre-flight operations that can be elaborated upon is the fuelling of the aircraft. To start the fuelling process, the correct safety measures need to be taken. As the fuelling will take place outside the risk caused by leakage is relatively small, as the hydrogen has a high dispersion rate. However, any spark could still light a potential hydrogen leak; therefore, a spark-free zone of 27 [m] will be established [112]. Furthermore, any air compressors, ventilation equipment, and air conditioning intakes should be located 23 [m] away from the liquid hydrogen storage as well [112]. The aircraft can then be connected to the fuelling truck with insulated tubing. All the required valves can then be opened which starts the fuelling process. It should be noted that for this process all hoses and connectors should be equipped with hydrogen sensors to detect leaks as soon as possible [112]. Throughout the fuelling process, the sensors on the fuelling equipment and on the vehicle itself will be monitored by the ground team to ensure safety. This way the fuelling can be stopped when the temperature, pressure, or hydrogen content in the air increases above safe values. Furthermore, during ground operations either before or after flight, the pressure

[1] https://www.heavyhaulers.com/blog/how-do-you-transport-an-airplane/ [Accessed on 22-05-2024]

[2] https://kingtriallaw.com/blog/is-flying-safer-than-driving/ [Accessed on 24-06-2024]

[3] https://www.cannonlogistics.com.au/blog/road-vs-air-freight/ [Accessed on 13-06-2024]

[4] https://airportindustry-news.com/zeroavia-to-develop-liquid-hydrogen-refuelling-trucks-for-airports/ [Accessed on 13-06-2024]

of the hydrogen tank of the aircraft should be monitored as boil-off will increase the pressure. If the pressure gets too high, venting will be required which means that again a spark-free zone needs to be created to ensure safe venting.

Once ready for flight, the electrical and propulsion system can be started, and all avionics can be set. From this point, the aircraft should be capable of providing necessary flight information such as airspeed, location, turn rate, etc. This needs to be provided constantly throughout the flight, until the point the aircraft is shut down. At this point, the aircraft will be ready to take off.

The aircraft must then be moved to the take-off location. This will require the aircraft to taxi to its take-off location or to be towed by the services provided by the personnel working in the airfield. The aircraft will subsequently accelerate, take flight and climb to cruise conditions. When reaching a cruise altitude of 12.5 [km], the cruise settings will be applied. At this point, the aircraft will maintain altitude, attitude, airspeed, heading, vertical speed, and turn profile.

18.1.3. Flight Operations

During the flight, the aircraft will perform certain manoeuvres to ensure the correct flight path is being followed. For this, inputs from the controls in the cockpit will be acted upon by control surfaces or other relevant systems, enabling the aircraft to change its airspeed, altitude, attitude, heading, vertical speed, and turn rate.

Once approaching the destination, the aircraft will perform a descent phase, where it will decrease its altitude, apply its landing settings and decrease its airspeed to the necessary approach speed. Once the aircraft lands, it will taxi to its hangar. Here, all avionics, the propulsion system, and the electrical system will be shut down and a post-flight check will be performed.

Throughout the flight, from engine start to shut down of all systems, the aircraft will require communication capabilities. Allowing the pilot to communicate with the ground team is essential, enabling an exchange of information on the race status of the aircraft as well as the reporting of any problems that may occur or even a change in flight strategy. Besides, the aircraft shall allow communication with ATM, as this is required to obtain take-off and landing clearances, cruise directions, and any other vital information that is necessary to ensure a safe flight for the pilot and the other aircraft in the same airspace. As mentioned in Section 13.1.4, data will be continuously sent to the ground team to enable them to monitor the safety of the system as well as to determine possible strategy changes depending on the circumstances and aircraft state.

Finally, the aircraft may need to perform some flight operations for some unexpected flight conditions. For instance, if the landing runway is occupied, the aircraft may need to loiter, requiring additional energy from what is required for the total flight. In addition, in case of a disaster on the runway of a small intermediate airport, the aircraft may need to travel to the next closest airport to land there, which would emphasise the need for communication and additional energy.

18.1.4. Concept Operation Diagram

In order to visualise the mission of the E-Racer, a concept operations diagram (ConOps) has been created in accordance with the functional diagrams in section Chapter 4. This shows the different mission phases along with the necessary communications to be performed. As can be seen in Figure 18.1, communication is performed with ATM and the ground team at various points throughout the mission.

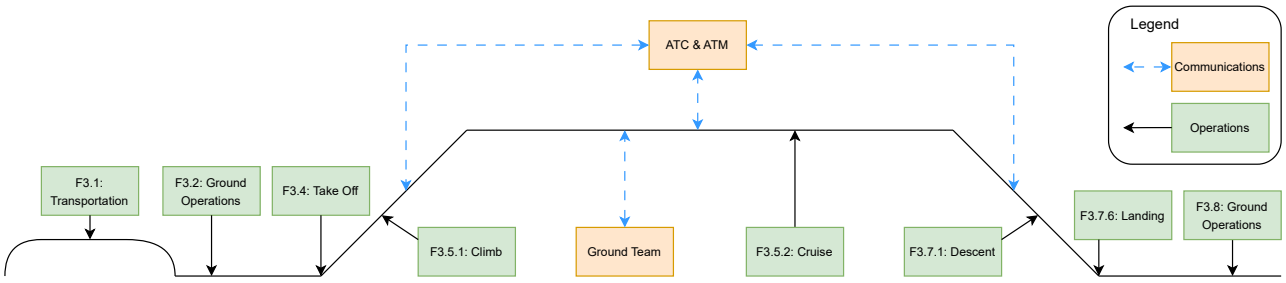

Figure 18.1: Concept operations diagram for E-Racer

18.2. Required Facilities & Personnel

Now the required facilities and personnel will be discussed that are required to perform the aforementioned mission. An analysis on the required facilities is given in Section 18.2.1. Next, an analysis on the necessary personnel is done

in Section 18.2.2.

18.2.1. Required Facilities

To be able to perform the necessary operational activities to prepare the aircraft for the race and to protect it from possible bad weather conditions, a hangar facility will be required at Eppley Airfield. Two days before the race starts, the aircraft will arrive at this location. At the hangar, the re-assembly of the aircraft will take place, as well as the charging of batteries, refuelling of the hydrogen tank, and the necessary checks before starting the race.

Once the race is concluded, another hangar will be required in Dare County Regional Airport to dismantle the aircraft to be able to transport it back to where it was first manufactured in order to commence the end-of-life procedures of the aircraft. In case unplanned stops need to be performed during the duration of the race, the use of other hangars in the intermediate airport will have to be arranged.

Finally, a control room will be set up at Eppley Airfield to allow the ground team to monitor the performance of the aircraft during the race. Besides the ones previously discussed, no other facilities will be required during the operations of the aircraft.

18.2.2. Necessary Personnel

The personnel required for the smooth running of this mission can be divided into 4 different professions: aerospace engineers, aircraft mechanics, electrical engineers, and a pilot. These are discussed below.

Transport Team

This team is in charge of transporting the dismantled aircraft to its required destination. In addition, the members of this team are also responsible for the carrying of all tools, equipment, and replacement parts needed during the period of operations. This team will be composed of two aircraft mechanics and one electrical engineer.

Monitoring Team

This team is concerned with planning the best flight strategy and monitoring the status of the aircraft during the race. They will have to consider the weather conditions and analyse them closely to select the best day to fly through the use of flight simulations, considering that the race spans over a 4-day period. The team will be composed of two aerospace engineers, who will work together from a control room in Eppley Airfield and who will communicate directly with the aircraft during the duration of the race.

Mechanics Team

A team of two mechanics and one electrical engineer is responsible for the following tasks: assembly, repairs, maintenance and disassembly of the aircraft. Their workspace will be the hangar of the airfield in question. Together, they ensure that all parts of the aircraft work flawlessly. It is worth mentioning that all 3 employees will have expertise in the handling of hydrogen to ensure that the setting up of the technology and the refuelling procedures are performed correctly and safely.

18.3. Procedures for Unexpected Mission Scenarios

The ideal flight strategy to win the race would be to complete the whole journey without making any intermediate stops. However, there is a slight chance that this will not happen, mainly because of 2 reasons: the effect of adverse weather conditions and damage to the aircraft. For both of these cases, extensive communication will occur between the pilot, the monitoring team, and the ATM. Together they will locate an airfield that allows the aircraft to land.

If one of these scenarios were to happen, the race would have to be completed in one or even more intermediate stops. Consequently, it is crucial that the transport and mechanics team also travel by road from the start to the end location of the race. This way they can quickly get to the aircraft in the event that it makes an extra stop. The personnel that travels by road will of course still take longer to reach the location of the halted aircraft. Therefore, the possibility of flying on the same day would have to be reconsidered, as it might be more advantageous to wait until the next day. This is depending on the weather conditions or how long the repair of the aircraft is going to take. During this intermediate stop, the best flight strategy would need to be reconsidered by the monitoring team.

In case of aircraft loss, the exact location of the aircraft and pilot will be determined by the monitoring team, which would then inform the local emergency services, rescue services, and the transportation team. A retrieval procedure would then take place to gather the aircraft parts and the black box to be able to determine the cause of the problem.

19. Sustainable Development Strategy & Analysis

Sustainability can be divided into three pillars: environmental, social, and economic. This chapter aims to elaborate upon all three. To incorporate sustainability in the design of the hydrogen Prandtl plane, it is important to establish a sustainable development strategy. This will ensure that the design process and the operation of the aircraft itself contribute to sustainability in aviation. In Section 19.1, the approach to environmental sustainability is discussed. Subsequently, social sustainability is touched upon in Section 19.2. Next, Section 19.3 elaborates on economic sustainability. Finally, the end of life procedures will be performed Section 19.4.

19.1. Environmental Sustainability

Environmental sustainability is the ability to restore and preserve natural resources and protect the natural environment over time. This can be done according to policies and appropriate practices. Environmental sustainability is influenced by several factors such as resource management and technological innovations. For the hydrogen Prandtl plane, environmental sustainability mainly involves keeping track of the materials used in the hydrogen fuel cell, batteries, and airframe. Additionally, the production of hydrogen should be taken into account.

19.1.1. Hydrogen

An important aspect of the design is the hydrogen propulsion system that will be used. This system will influence the sustainability of the aircraft in several ways. Firstly, hydrogen will be converted into water vapour in the fuel cell. This water vapour then exits the aircraft via the exhaust. This water vapour will then condense and form contrails. Contrails also form from combustion aircraft as water vapour is created as well. The effect of the contrail formation is hard to estimate, however, in general, it will have a warming effect on the climate. Even though that contrails will still be formed it is expected that the total warming of hydrogen aircraft will drop by 71% compared to conventional aircraft [111]. The contrail formation is highly dependent on a number of factors. Firstly, flying through Ice Super Saturated Regions (ISSR) increases the chance of creating contrails and should therefore be avoided [116]. This can be done by either going around them or going over or under them. It was found that the chance of ISSR being present at the cruise altitude is almost 0% meaning that greatly reduces contrail formation during cruise. Further estimating the effect of contrail formation from hydrogen aircraft is a developing research area and therefore no proven tools are available. This is because there are large differences between conventional and hydrogen aircraft regarding contrail formation, as no additional particles will be emitted from hydrogen aircraft and the respective amount of water vapour in the exhaust is much higher [117].

Secondly, the production of hydrogen itself can also cause emissions. Hydrogen can be produced without creating additional CO_2 emissions when it is produced via electrolysis. But, then the energy for the electrolysis also needs to originate from green energy sources. Currently, investments are being made towards increasing the production of green hydrogen in the US[1], however, it is hard to estimate at what stage the facilities will be near 2030. Green hydrogen will be available in the US at that time, however, if it will be near the starting point of the race is uncertain. Then the trade-off has to be made between transporting green hydrogen or using less sustainable hydrogen. Generally, this means that the estimated emissions due to the hydrogen production lie between 11.1 and 359 [$kgCO_2 - eq$] per full tank [118]. Depending on whether the hydrogen is produced through electrolysis or methane steam reforming.

As mentioned before, the transport of hydrogen causes significant emissions as well. Generally, insulated trucks are used to transport liquid hydrogen from the electrolysis plant to the destination. These trucks carry much more hydrogen than what would be required for the aircraft. Therefore, coordination with other teams that might also require liquid hydrogen will be used such that only one truck will be required. The distance for transportation is estimated to be 140 [km] for grey hydrogen[2] and currently up to 700 [km] for green hydrogen.

19.1.2. Battery

Another important source of emissions is the production and charging of the batteries. Firstly, the emissions due to the production of the batteries were taken into account for the battery trade-off and it was found that for Li-S batteries,

[1] https://www.cleanegroup.org/initiatives/hydrogen/projects-in-the-us/ [Accessed on 17-06-2024]
[2] https://energynews.biz/monolith-to-expand-turquoise-hydrogen-plant/ [Accessed on 17-06-2024]

the life cycle emissions were 89.8 [$kgCO_2 - eq/kWh$]. Thus, the total battery leads to 1297.6 [$kgCO_2 - eq$] life-cycle emissions. Furthermore, the batteries need to be charged as well which requires 17.2 [kWh] of electricity, which includes the low and high-voltage batteries as well as the charging efficiency. This can cause the emissions from charging the batteries to be between 0.7[3] and 6.64[4] [$kgCO_2 - eq$]. This again depends on whether solar energy or the US grid electricity is used.

19.1.3. Structures

A large part of the structures of the aircraft will be made custom as explained in Section 17.1. The materials used for the production of the aircraft have life cycle emissions related to them. During the design process sustainability was kept in mind for the material selection, which led to the choice for aluminium 7075. Aluminium 7075 has an associated life cycle emissions of 12.7 [$kgCO_2 - eq/kg$]. Thus, this results in a total of 3883.5 [$kgCO_2 - eq$]. Furthermore, 300M steel was used for the bulkheads which resulted in 20.2 [$kgCO_2 - eq$] emissions. Lastly, an estimation of the emissions during manufacturing can be made. For aluminium aircraft, it was found that the emissions from the manufacturing is estimated to be 14% of the material emissions [119]. Thus, the emissions from manufacturing can be estimated to be 546.6 [$kgCO_2 - eq$] It should be noted that these values are for conventional production processes. Both the materials and the structure itself could be manufactured using sustainable energy sources. Thus, these values reflect the worst-case scenario and actual emissions for the structure of the aircraft could be reduced if the choice was made to use sustainable energy for the production of the aircraft.

19.1.4. End-Of-Life

An important aspect of environmental sustainability is the End-of-Life (EoL) of the product. The end-of-life of a product can both increase or decrease the life cycle emissions of the product. Different components of the aircraft have different possibilities regarding end-of-life and therefore will be discussed individually in the following paragraphs.

In general, the effort will be made to reuse as many of the components as possible. The mission has a relatively short duration and therefore, it is expected that after the race most components will still be in good condition. Then a choice is to be made whether the aircraft will be used for future research applications on sustainable aviation or whether the aircraft will not be used anymore. If the choice is made to not use that aircraft after the race, the aircraft will be dismantled, and the components will be inspected for re-use. This mainly concerns the engines, fuel cell, batteries, compressors, and other electronic equipment. If reuse is not possible, then the following EoL procedures will be used to recycle the components.

Firstly, the fuel cell can be considered. For the fuel cell EoL procedures, the recovery of rare earth elements such as platinum, iridium, and ruthenium is the main objective [121]. Generally, hydrometallurgical treatment is used to recover these elements. However, this method involves pre-treatment of the fuel cell, using large amounts of solvents, and the generation of wastewater, which means this method is far from ideal. Therefore, the aim is to use selective electrochemical dissolution, which is an EoL procedure currently researched for fuel cells. This method can recover a high-purity catalyst and has more favorable conditions in terms of temperature, voltage, and pH compared to hydrometallurgical treatment. Furthermore, more elements of the fuel cell can be recovered using this method [121].

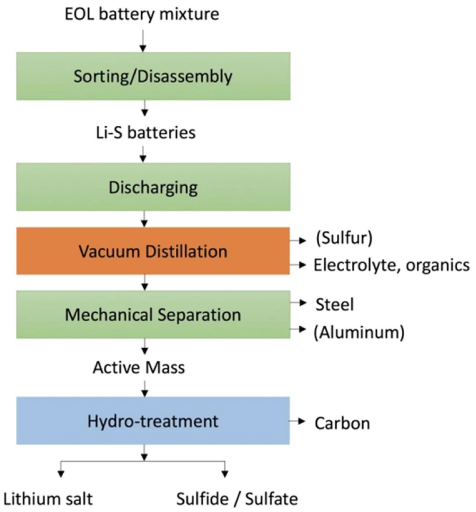

Figure 19.1: EoL process for Li-S batteries [120]

Secondly, the EoL procedures for the battery should be considered. The general EoL process for the batteries is shown in Figure 19.1.

From Figure 19.1 some of the steps can be discussed in more detail. The most important steps regarding actually recovering some of the materials in the battery is the separation and the hydro-treatment steps [122]. In the separation step, the battery is shredded and the pieces are sorted. The electrode fractions will be processed further using the hydro-treatment. This consists of a series of subprocesses including filtration, precipitation, and solvent extraction, which are used to extract lithium and other valuable materials from the powder. It should be noted that Li-S batteries have less valuable metals than comparable Li-ion batteries, for example, no cobalt is present.

The structure also has specific EoL procedures. This starts of with decommissioning the aircraft. In this step all the

[3] https://www.solar.com/learn/what-is-the-carbon-footprint-of-solar-panels/ [Accessed on 17-06-2024]
[4] https://news.mit.edu/2024/cutting-carbon-emissions-us-power-grid-0311 [Accessed on 17-06-2024]

fluids are removed from the aircraft and the aircraft is cleaned and decontaminated. Then the aircraft is disassembled, in this process, the parts and components are detached from the aircraft. It is important that proper documentation of the different parts, their materials, and their connections is present as this can greatly increase the disassembly process. Then the empty structure should be left, which consists of aluminium 7075, 300M steel, and polycarbonate. Firstly, the airframe will be reduced into smaller parts using several different tools such as angle grinders, plasma cutters, saws, and hydraulic scissors. This is done such that every chunk of structure is made primarily of one material. The chucks are then sorted per material and the metals are shredded and remelted to be used in different products. It should be noted that often these recycled metals can not be cost-effectively recycled to the quality required for aerospace applications and are therefore used in other sectors. The polycarbonate is also shredded and remelted as it can be reused effectively.

19.2. Social Sustainability

Social Sustainability is also an important aspect of this project. This element of sustainability involves the effect that businesses have on people[5]. The social sustainability of this project leads to numerous aspects that have to be taken into account.

Firstly, air pollution can be considered as a social sustainability aspect. During the production of materials, the production of hydrogen, and the assembly processes, the air around the production site is polluted with particulate matter emissions. The emission of particulate matter is detrimental to the health of the people living in the surrounding areas [123]. Several components and the raw materials for the structure will be sourced from COTS. Therefore, the team does not have a direct influence on the emissions during this production process. Nevertheless, the team will make a great effort to select COTS products provided by suppliers who implement sustainability methods in their operations. Such as recyclable materials in their products and suppliers who ensure materials come from responsibly managed sources, like raw materials that come from sustainable mining[6]. The team is expecting to make a positive contribution to changing air pollution levels by using electric propulsion in combination with a hydrogen fuel cell [124]. Therefore, this design shall produce minimal particulate matter emissions. When producing and operating the aircraft, energy usage should be taken into account. Using more energy than necessary would be wasteful and could take away energy that would otherwise be available for households.

Additionally, the Pulitzer Air Race is partially organised to educate people about the capabilities and advantages of flying with electric propulsion. Therefore, it is important to consider that the design is also about educating society about what is possible. Therefore, the choice was made that the data generated should be used for research and that the public should be informed about the progress and development in the aviation sector. Besides, it is important to educate the public on hydrogen. Currently, society is not convinced that the safety levels of hydrogen are adequate [125]. This is not helped by the fact that knowledge about hydrogen is generally low. Participating in the Pulitzer Air Race could improve this, and show the public a future of hydrogen in aviation is possible. This further increases the focus on the safety of the aircraft. An accident regarding hydrogen with the aircraft would not only be detrimental to the project but would also affect the reputation of hydrogen aircraft in general. Therefore, the safety system got additional attention as this was perceived as a crucial part of the design.

Moreover, noise is considered during the design phase (SUS-05, Table 20.2). Aircraft noise is bothersome for many people, especially for people living close to an airport. While it is true that electric aircraft make less noise than conventional aircraft [126], this could still be an issue. For this design, the main source of noise during flyover was determined to be the propellers as the external compressors, another source of noise are not running at that altitude. However, creating an accurate estimation of the noise generated by the propeller is a difficult task as multiple different noise generation processes occur at the same time.

Still, an analysis was made of the noise footprint on the ground at screen height during take-off, as this was perceived to be the most critical condition. XROTOR, a propeller analysis program was used which resulted in the nose footprint as shown in Figure 19.2.

[5] `https://unglobalcompact.org/what-is-gc/our-work/social` [Accessed on 21-05-2024]

[6] `https://www.ief.org/news/how-to-make-mining-more-sustainable?` [Accessed on 21-5-2024]

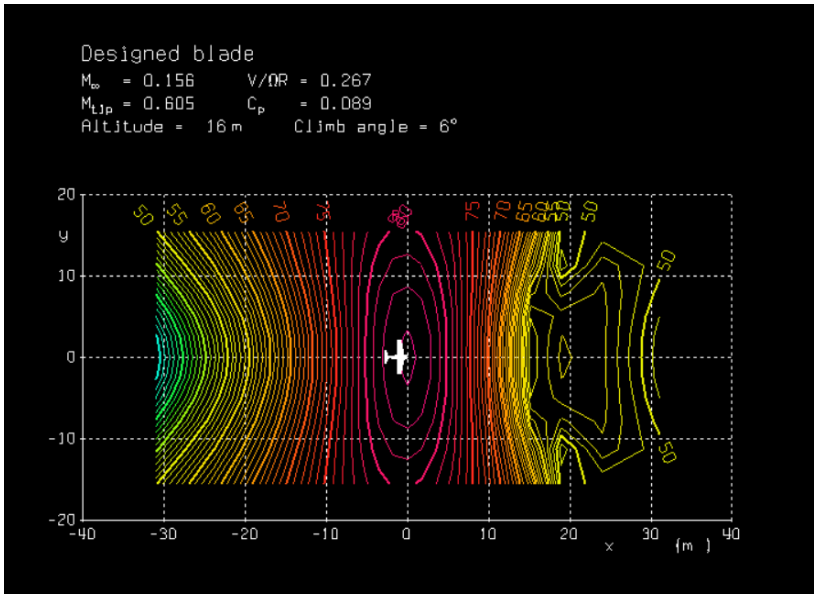

Figure 19.2: Noise ground footprint at screen height during take-off

The result is shown in Figure 19.2 is only valid for one propeller and the highest noise level is equal to 84 [dB], just below the aircraft. To determine the noise generated by two propellers, noise levels from both of them need to be summed. That accounts for a total noise level emitted by the aircraft to 87 [dB].

Lastly, Third Party Risk (TPR) has to be considered. TPR is the risk of people on the ground being injured in an aviation-related accident. The TPR is mostly elevated in the vicinity of airports. The aircraft design should limit TPR as much as possible, this is again related to the safety systems of the aircraft and that is one of the reasons why systems such as firewalls, proper ventilation, thermal runaway protection systems, and a double-walled hydrogen tank are in place.

19.3. Economic Sustainability

In terms of economic sustainability, advances in aircraft design could be the main driver for the normalisation of electric propulsion in the aviation industry. The possibility of using concepts from the E-Racer in commercial aviation will ideally be kept in mind during the design phase. As of now, electric aircraft have not yet been able to achieve performance levels ready for the commercial market. This project aims to improve electric-driven aircraft performance, which in turn can be valuable to commercial electric aircraft. Some solutions may be easier and more beneficial to implement in civil aviation than others, and could potentially lead to a more sustainable aviation industry which is also economically viable.

In addition, recyclable materials need to be taken into account. If parts of the aircraft are recyclable, it could mean that these materials can be sold in the disposal stage of the aircraft's life cycle, making them more economically viable. Hence, when making the design, recyclable materials are preferred for economic sustainability. A recommended end-of-life procedure should also be included for the customer to follow at the end of the product's life.

Finally, to achieve economic sustainability, the team intends to establish a partnership with one or more companies. An attempt has been made to establish a partnership before the end of the DSE. This, however, did not succeed. No companies have responded to an email that was sent out to establish initial contact. The companies that have been contacted are summarised in Section 22.7. It must be stated that more companies can be approached to increase the chances of establishing a partnership that will reduce the economic strain of the project.

19.4. Perform End-of-Life Procedure

Once the aircraft has reached the end of its life based on either regulation or is no longer useful, the end-of-life procedures may begin. These ensure that the aircraft is safely and sustainably decommissioned, dismantled, and recycled.

Firstly, the aircraft is decommissioned. To this end, disassembly of the aircraft is planned, which will require the

establishment of documentation and procedures; the aircraft should also be designed with ease of disassembly in mind. Further, the electrical systems of the aircraft must be dismantled, with the power unit being discharged and the electrical system disconnected.

Following this, the aircraft must be prepared for dismantling. Once it is ready, the components must be separated. Reusable components must be identified and removed, while the structural components may be disassembled. From this, the materials of non-reusable parts are sorted based on whether they are recyclable, with recyclable material being isolated. Non-recyclable material is then disposed of according to waste management.

For recyclable materials, they must be processed and dealt with according to procedures. Reusable components must be dealt with in a similar fashion. In order to maximise the sustainability of the aircraft, it should use as much recyclable material and components as possible.

20. Technical Risk Assessment

In Chapter 5, it is mentioned that the aircraft shall have a reliability of 99%. To ensure this requirement is met, a risk assessment is done. This is done to identify and mitigate risks that may interfere with the success of the mission. This chapter aims to elaborate on the technical risk assessment. The technical risk assessment is started by doing a SWOT analysis of the design and is discussed in Section 20.1. Following this SWOT analysis, a risk assessment has been performed and is the topic of Section 20.2. After the risks were identified, mitigation strategies were created to decrease the likelihood and impact of the risks, this is discussed in Section 20.3.

20.1. SWOT Analysis

In this section, an analysis of the project's associated risks is discussed. The analysis is done with the SWOT approach, which identifies weaknesses and threats to the project as well as strengths and opportunities. Then, from this SWOT analysis, risks can be identified.

To have a better understanding of the potential risks that might occur, a SWOT analysis has been performed. In Table 20.1, the strengths, which are considered to be helpful and internal, weaknesses, which are harmful and external, opportunities, which are viewed as helpful and external, and the threats, which are seen as harmful and external items, are visualised.

Table 20.1: Risk SWOT

	Helpful	**Harmful**
Internal	• Use of innovative technology • Zero-emission propulsion system • Use of backup systems • Flexible design • COTS as much as possible • Flexible flight strategy	• Fixed budget • Sensitivity to weather • Immature technology • Minimum range requirement • Less comfortable • Limited time / Strict deadlines • Limited energy storage options • New design • Battery life
External	• Advancing technology • New experimental data • Promotion opportunities	• Limited availability of special parts • Limited access to unconventional fuel sources • Limited (commercial) use of aircraft • Changes in Pulitzer Race rules • Budget cuts from client • Component failure leading to malfunction • Unsustainable production of parts • Unpredictable weather • Non-recyclable aircraft • Assembly mistakes • External damage to aircraft • Production of batteries • Waste of materials • Competitive race • Limited airport options

20.2. Risk Assessment

From the weaknesses and threats found in the SWOT analysis performed in Section 20.1, risks have been identified. To identify which risks are the most detrimental to the design, a risk assessment has been performed. This section elaborates on this assessment. In this assessment of risks, 2 factors are taken into account, which are the likelihood of occurring and their impact on the project.

To order the risks, six categories are used: Technical (TEC), Financial (FIN), Organisational (ORG), Sustainability (SUS), Safety (SAF), and Race (RAC). The given abbreviations are used in the risk IDs. In addition, the technical

risks are provided with an extension in their risk ID, identifying the engineering discipline. The distinct disciplines are Aerodynamics (AE) Chapter 8 and Chapter 9, Propulsion (PR) Chapter 10, structures (ST) Chapter 11, and Flight Performance (FP) Chapter 12. Where most of the risks are touched upon in the chapters referenced above.

All the risks are presented in the risk register (see Table 20.2) where each risk is given a unique identifier, likelihood score, and impact score. The likelihood is defined by the probability or frequency at which a specific risk might occur, impacting the project or operation negatively. It is quantified on a scale of 1 to 5. The impact of a risk refers to the extent of the damage, disruption, or negative consequences that could result if the risk materialises; the impact is also rated on a scale of 1 to 5. The likelihood and impact scales are defined as such:

Likelihood

- **1 - Very unlikely**: Chance of occurring lower than 1%
- **2 - Unlikely**: Chance of occurring between 1% and 20%
- **3 - Likely**: Chance of occurring between 20% and 50%
- **4 - Very likely**: Chance of occurring between 50% and 80%
- **5 - Almost certain**: Chance of occurring higher than 80%

Impact

- **1 - Negligible**: No mission objectives are affected
- **2 - Minor**: Non-critical mission objectives might be affected
- **3 - Severe**: Some mission objectives might be affected
- **4 - Critical**: Mission objectives are endangered
- **5 - Catastrophic**: The mission objectives are no longer achievable

The total risk, which is a multiplication of the likelihood and impact, is shown in the last column, using a colour scale to quickly identify the most critical risks.

Table 20.2: Risk register

ID	Risk	Likelihood	Impact	Score
TEC-01-AE	Assumptions in VLM model causes overestimation of performance	3	3	9
TEC-02-AE	Stability Coefficients are not accurate causing an unstable aircraft	2	4	8
TEC-03-AE	Sizing of control surfaces inaccurate resulting in an uncontrollable aircraft	2	4	8
TEC-04-AE	Inaccurate CG estimation causes unstable aircraft design	2	4	8
TEC-05-AE	Angle of Attack margin not sufficient causing unexpected stall	2	3	8
TEC-06-PR	Failure of hydrogen tank causes large leak	2	4	8
TEC-07-PR	Due to motor failure an overproduction of power	2	3	6
TEC-08-PR	Leak in cooling system causes overheating, or short circuit from cooling liquid	2	4	8
TEC-09-PR	Torque overload on motor due to failure of feathering mechanism	2	4	8
TEC-10-PR	Failure of fuel cell results in no power	2	4	8
TEC-11-PR	Compressor failure chokes air supply fuel cell	2	4	8
TEC-12-PR	Failure of cooling pump	2	4	8
TEC-13-PR	Failure of motor controller stops the motor	2	4	8
TEC-14-PR	Battery catches fire due to overheating	1	5	5
TEC-15-PR	Over-pressurised hydrogen systems causes leak	2	4	8
TEC-16-ST	Inconsistent material properties decrease structural safety	3	3	9
TEC-17-ST	External damage such as corrosion causes decrease in structure strength	3	3	9
TEC-18-ST	Invalid assumptions lead to under-designed structure	3	3	9
TEC-19-FP	Assumptions cause inaccurate flight simulation	3	3	9
SUS-01	Production of batteries causes an impact on the environment	4	1	4
SUS-02	Waste of materials after completion of the race	3	1	3
SUS-03	Chemical leaks caused by crash/accident	2	2	4
SUS-04	Spillage or leaks during maintenance, assembly or production	3	2	3
SUS-05	The aircraft produces excessive amount of noise	3	2	6

SAF-01	Aircraft damaged by hail or other extreme weather	2	3	8
SAF-02	Rough landing causes damage to aircraft	3	3	9
SAF-03	Aircraft faces bird strikes	1	4	4
SAF-04	Collision with other aircraft	1	5	5
SAF-05	Accidents during ground handling	2	3	6
SAF-06	Structural failure results in unflyable aircraft	2	5	10
SAF-07	Hydrogen build-up causes fire/explosion in aircraft	2	5	10
RAC-01	Weather conditions ground the aircraft	3	3	9
RAC-02	Competition has access to better technology making the aircraft less competitive	4	4	16
RAC-03	Change in race regulations makes aircraft not able to participate in the race	1	4	4
RAC-04	Due to headwind, zero-stop strategy will not be achievable	2	3	8
RAC-05	Battery system failure causes decrease in climb performance	2	3	6
RAC-06	Inaccurate simulation of performance results in sub-optimal race strategy	2	3	6
FIN-01	Budget cuts from stakeholders strain the budget	1	4	4
FIN-02	Expensive fuel due to limited supply of unconventional fuels	4	2	8
FIN-03	Inaccurate cost-breakdown results in budget overshoot	3	4	12
FIN-04	Delays in the procurement of materials or parts cause costs increases	3	2	6
FIN-05	Unforeseen challenges in integration of subsystems strains budget	3	2	6
FIN-06	Due to location of the race transportation costs rise unexpectedly	3	2	6
FIN-07	Unexpected maintenance costs during testing	2	2	4
FIN-08	Unexpected sponsorships shortfalls (in case of future sponsorship)	2	4	8
FIN-09	Providing refuelling option in case of unexpected one-stop strategy	2	4	8
FIN-10	Unexpected underperforming batteries demand battery replacement	2	2	4
ORG-01	Getting unconventional fuels takes more time resulting in delays	3	2	6
ORG-02	Delays in assembly/production due mistakes	3	2	6
ORG-03	Foreign regulations cause delays in procurement of fuels and parts	3	2	6
ORG-04	Due to unexpected one-stop strategy refueling has to take place	2	4	8
ORG-05	Limited availability of parts cause delays	2	2	4

20.3. Risk Mitigation

The risks identified in the previous section will be mitigated by either reducing impact or reducing likelihood. Some risks will be accepted due to their extremely low likelihood or impact or because they cannot be mitigated. For each mitigation, a responsible organisational role is appointed within the team to ensure the mitigation strategies will be applied properly. The mitigation strategies are summarised in Table 20.3. Furthermore, risk maps are also produced showing the total risk before and after mitigation.

Table 20.3: Mitigation strategies

ID	Strat.	Mitigation 1	Mitigation 2	Likelihood Change	Impact Change	Responsible
TEC-01-AE	RI	Clearly state assumptions made and analyse their impact	-	0	-1	Aero. Dep.
TEC-02-AE	RL	Perform additional in-depth aerodynamic analysis to cross-check	-	-1	0	Aero. Dep.
TEC-03-AE	RL	Perform additional in-depth aerodynamic analysis to cross-check	-	-1		Aero. Dep.
TEC-04-AE	RL	Provide a CG range margin	-	-1	0	Aero. Dep.

TEC-05-AE	RL	Perform scaled windtunnel testing	Perform additional in-depth aerodynamic analysis	-1	0	Aero. Dep.
TEC-06-PR	RL	Use of double walled hydrogen tank	-	-1	0	Prop. Dep.
TEC-07-PR	RI	Excess power can be stored in capacitors and battery before fuel cell lowers its power	-	0	-1	Prop. Dep.
TEC-08-PR	RL	Valves in cooling system	-	-1	0	Prop. Dep.
TEC-09-PR	RI	Ensure motorcontroller regulates allowable torque	-	0	-3	Prop. Dep.
TEC-10-PR	RI	Windmilling propellers charging battery while descending	Provide battery system on which aircraft can fly	0	-1	Prop. Dep.
TEC-11-PR	RI	Second compressor		0	-1	Prop. Dep.
TEC-12-PR	RI	Use of two cooling pumps	-	0	-2	Prop. Dep.
TEC-13-PR	RI	Propeller feathering, excess power stored in capacitors and battery before fuel cell lowers its power	-	0	-1	Prop. Dep.
TEC-14-PR	RI	Provide evacuation plan for pilot	-	0	0	Project Man.
TEC-15-PR	RL, RI	Use of double walled hydrogen tank	Provide proper ventilation strategies for hydrogen build-up	-1	-1	Chief Eng.
TEC-16-ST	RL	Sample testing of materials used in production and assembly	-	-1	0	Quality Cont.
TEC-17-ST	RL	Plan inspection routines	-	-1	0	Quality Cont.
TEC-18-ST	RL	Clearly state assumptions made and analyse their impact	-	-1	0	Struct. Dep.
TEC-19-FP	RL ,RI	Clearly state assumptions made and analyse their impact	Perform flight test to validate performance models	-1	-1	Flight. Dep.
SUS-01	RL	Incorporate sustainability in battery trade-off	-	-1	0	Sust. Man.
SUS-02	RL	Setup proper waste management strategy	-	-1	0	Sust. Man.
SUS-03	RI	Identify harmful materials and set up procedures accordingly	-	0	-1	Sust. Man.
SUS-04	RI	Identify harmful materials and set up procedures accordingly	-	0	-1	Sust. Man.
SUS-05	RL	Perform noise analysis	-	-1	0	Chief Eng.
SAF-01	RL	Park in hangar while grounded	Make use of advanced weather forecast systems	-1	0	Project Man.
SAF-02	RL	Find an experienced pilot	Include more forgiving suspension in the landing gear	-1	0	Chief Eng.
SAF-03	AC	-	-	0	0	-
SAF-04	AC	-	-	0	0	-

SAF-05	RL	Implement procedures and safety measures for ground handling	-	-1	0	Project Man.
SAF-06	RL, RI	Implement safety factors in structure design	Provide evacuation plan for pilot	-1	-1	Struct. Dep.
SAF-07	RL	Provide proper ventilation strategies for hydrogen build-up	-	-1	0	Chief Eng.
RAC-01	RL	Implement weather forecasting tool in strategy	-	-1	0	Project Man.
RAC-02	AC	-	-	0	0	Project Man.
RAC-03	RI	Setup regular check-ups with regulation to increase response time	-	0	-1	Chair
RAC-04	RL, RI	Provide strategy for choosing optimal flight window	Provide strategy for one-stop flight	-1	-1	Project Man.
RAC-05	RI	Analyse climb without battery and implement strategy	-	0	-1	Flight. Dep.
RAC-06	RL, RI	Verify flight performance models	Design for more performance than set by requirements	-1	-1	Flight. Dep.
FIN-01	RI	Introduce safety margin in design budget	-	0	-1	Business Man.
FIN-02	RI	Minimise runtime of propulsion by properly planning test phase	-	0	-1	Business Man.
FIN-03	RI	Apply a safety margin in the cost breakdown		0	-1	Business Man.
FIN-04	RL, RI	Setup register for parts and materials which have to be ordered beforehand	Plan the procurement of materials and parts in advance	-1	-1	Project Man.
FIN-05	RL	Make use of prototyping and incremental integration	-	-1	0	Chief Eng.
FIN-06	RL	Setup transportation plan in advance for efficient transport	-	-1	0	Business Man.
FIN-07	RL, RI	Setup preventive maintenance schedule	Allocate contingency maintenance budget	-1	-1	Business Man.
FIN-08	RL	Sign contract with sponsors	-	-1	0	Business Man.
FIN-09	RI	Allocate contingency budget	-	0	-1	Business Man.
FIN-10	RL	Perform battery tests beforehand	-	-1	0	Chief Eng.
ORG-01	RL	Implement margins in fuel ordering timeline	Minimise runtime of propulsion by properly planning test phase	-1	0	Chair
ORG-02	RL	Appoint responsible person for assembly planning	Ensure clear and complete design drawings	-2	0	Project Man.

ORG-03	RL	Appoint responsible person in charge of regulatory affairs	-	-2	0	Secretary
ORG-04	RI	Plan for one-stop strategy in advance	-	0	-1	Project Man.
ORG-05	RI	Setup register for parts and materials which have to be ordered beforehand	Plan the procurement of materials and parts in advance	-1	-1	Business Man.

In Figure 20.1, the unmitigated risks can be seen with their likelihood and impact. In Figure 20.2, it can be seen how the mitigation strategies effectively lower the likelihood and impact of most risks as much as possible. It also shows the risks with the most impact and likelihood to happen, which is RAC-02, related to the technical edge of the competition. No effective mitigation strategy is possible for this risk, except for having the best design possible and monitoring the competition when possible.

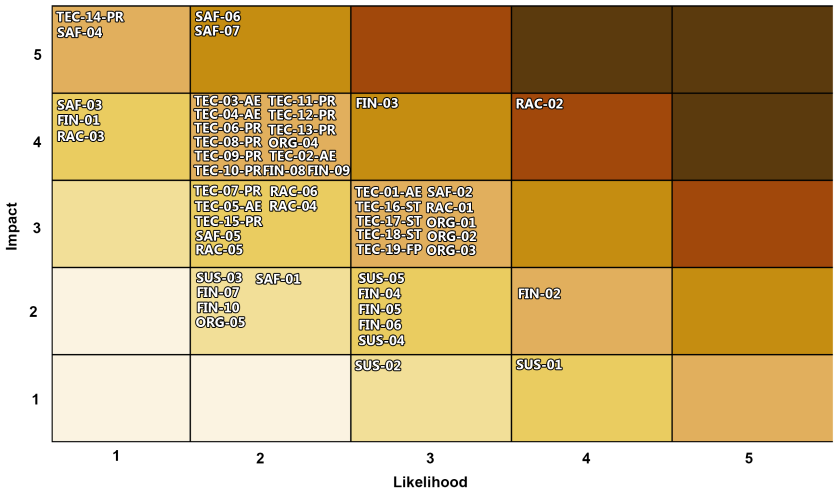

Figure 20.1: Riskmap before mitigation

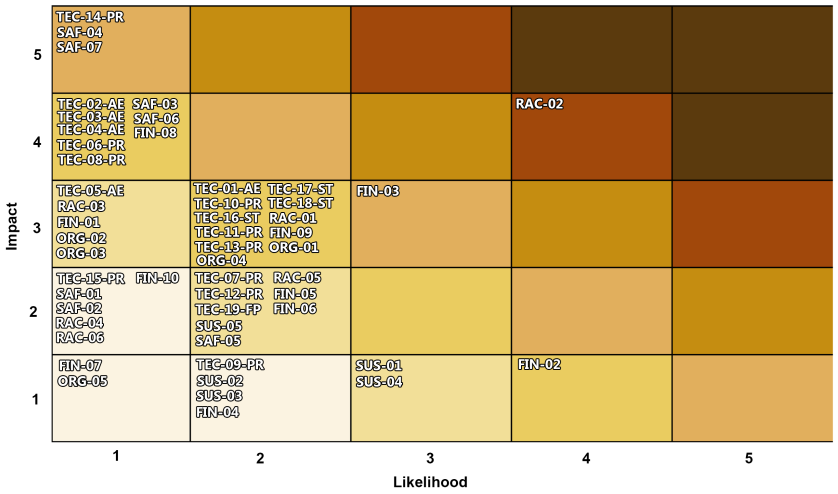

Figure 20.2: Riskmap after mitigation

21. Project Organisation

In this chapter, the Project Design & Development Logic Diagram is presented in Section 21.1 by explaining the main items included in it. Also, the Post-DSE Gantt chart is explained and shown in Section 21.2.

21.1. Project Design & Development Logic Diagram

In order to have a good overview of what the post-DSE steps are with this project, it is important to construct a Project Design & Development Logic Diagram. This diagram incorporates all the tasks that will have to be performed after the finalisation of the DSE.

The first step would be finalising the design by improving the accuracy of the analysis performed by all separate departments followed by verifying and validating the methods. Iterations are then performed in order to obtain a design that is afterwards scaled to a prototype that would be tested in a wind tunnel. This will help in gathering more data for improving the design.

The next step would be represented by the manufacturing of the aircraft. This is done by first ordering or producing the required parts and components and then testing those parts for any production damage. Finally, the aircraft is assembled.

After the construction of the Prandtl plane, ground and flight testing can be performed. Using the data obtained from the tests, certification can be done, followed by the registration of the aircraft with the responsible authorities.

As the aircraft is not assembled at the starting location of the aircraft, transportation has to be arranged and performed when the race is approaching. Afterwards, operations are prepared in order to ensure that the aircraft is not damaged during transportation. Finally, ground operations are done during the race day to analyse and monitor the optimal strategy.

Maintenance is performed multiple times throughout the life-cycle of the aircraft, mainly after each flight, whether it is after the race or after the test flights. Routine inspections are included in the maintenance procedure, aircraft repair, and software management.

The last part of the life cycle of the aircraft corresponds to carrying out the end-of-life procedure, which incorporates disassembling the aircraft and recycling the parts or components.

21.2. Post-DSE Gantt Chart

Once the duration of each of the tasks has been determined, a Gantt Chart can be constructed. These activities take place after the DSE, with a total duration of approximately 4 years (1455 days).

The E-Racer will be prepared to participate in the Pulitzer Air Race by mid-2027. Given that the race was planned to take place between May 22 and May 25 in 2023 (before it was cancelled), this same date has been assumed for 2028. It is worth noting that the start and end dates are date-inclusive, and that the interval between August 2027 and March 2028 allows for any potential delays in the development of the Prandtl plane, ensuring the aircraft can still compete in May 2028.

Project Design & Development Logic Diagram

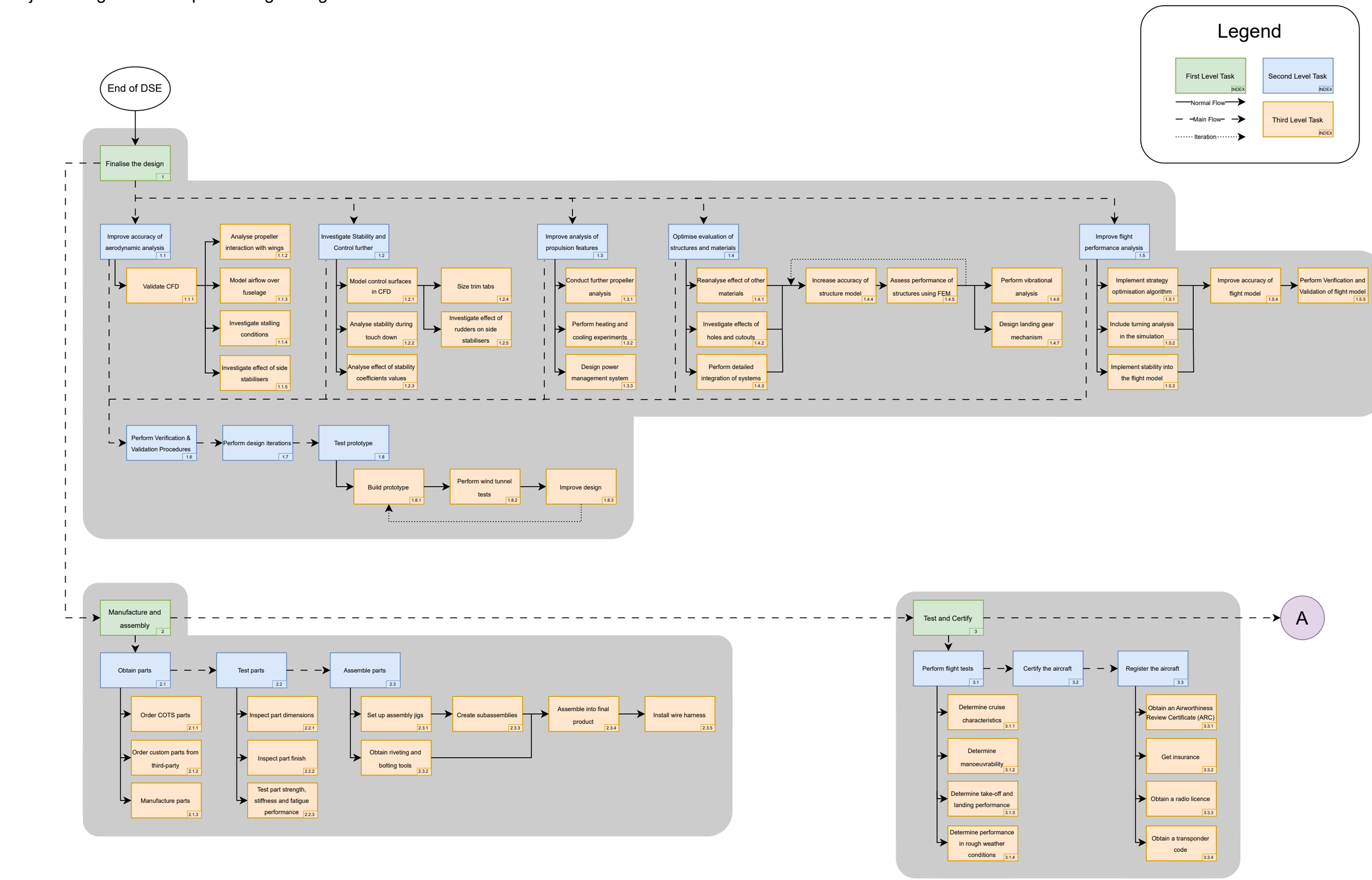

Project Design & Development Logic Diagram (continued)

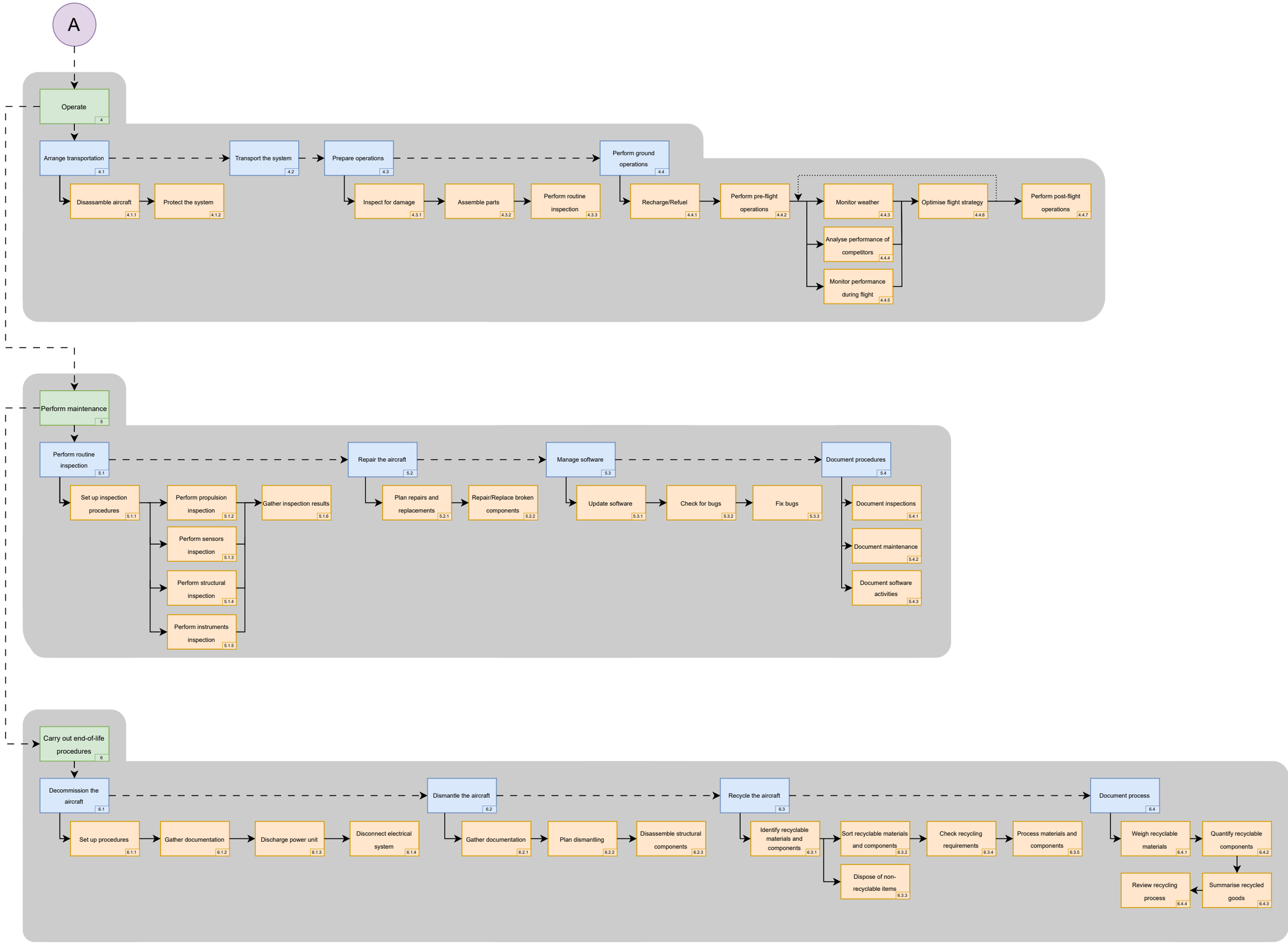

Post-DSE Gantt Chart

	First Level Task	Duration (Days)		Second Level Task	Duration (Days)	Start (Day/Month/Year)	Finish (Day/Month/Year)
1	Finalise the design	730	1.1	Improve accuracy of aerodynamic analysis	92	01/07/2024	30/09/2024
			1.2	Investigate stability and control further	92	01/07/2024	30/09/2024
			1.3	Improve analysis of propulsion features	92	01/07/2024	30/09/2024
			1.4	Optimise evaluation of structures and materials	92	01/07/2024	30/09/2024
			1.5	Improve flight performance analysis	92	01/07/2024	30/09/2024
			1.6	Perform verification &validation procedures	92	01/10/2024	31/12/2024
			1.7	Perform design iterations	365	01/01/2025	31/12/2025
			1.8	Test prototype	181	01/01/2026	30/06/2026
2	Manufacture and assembly	184	2.1	Obtain parts	123	01/07/2026	31/10/2026
			2.2	Test parts	122	01/08/2026	30/11/2026
			2.3	Assemble parts	122	01/09/2026	31/12/2026
3	Test and certify	212	3.1	Perform flight tests	90	01/01/2027	31/03/2027
			3.2	Certify the aircraft	91	01/04/2027	30/06/2027
			3.3	Register the aircraft	31	01/07/2027	31/07/2027
4	Operate	8	4.1	Arrange transportation	2	18/05/2028	19/05/2028
			4.2	Transport the system	1	20/05/2028	20/05/2028
			4.3	Prepare operations	2	20/05/2028	21/05/2028
			4.4	Perform ground operations	4	22/05/2028	25/05/2028
5	Perform maintenance	5	5.1	Perform routine inspection	1	-	-
			5.2	Repair the aircraft	1	-	-
			5.3	Manage software	1	-	-
			5.4	Document procedures	2	-	-
6	Carry out end-of-life procedures	24	6.1	Decommission the aircraft	7	01/06/2028	07/06/2028
			6.2	Dismantle the aircraft	7	08/06/2028	14/06/2028
			6.3	Recycle the aircraft	3	15/06/2028	17/06/2028
			6.4	Document process	7	18/06/2028	24/06/2028

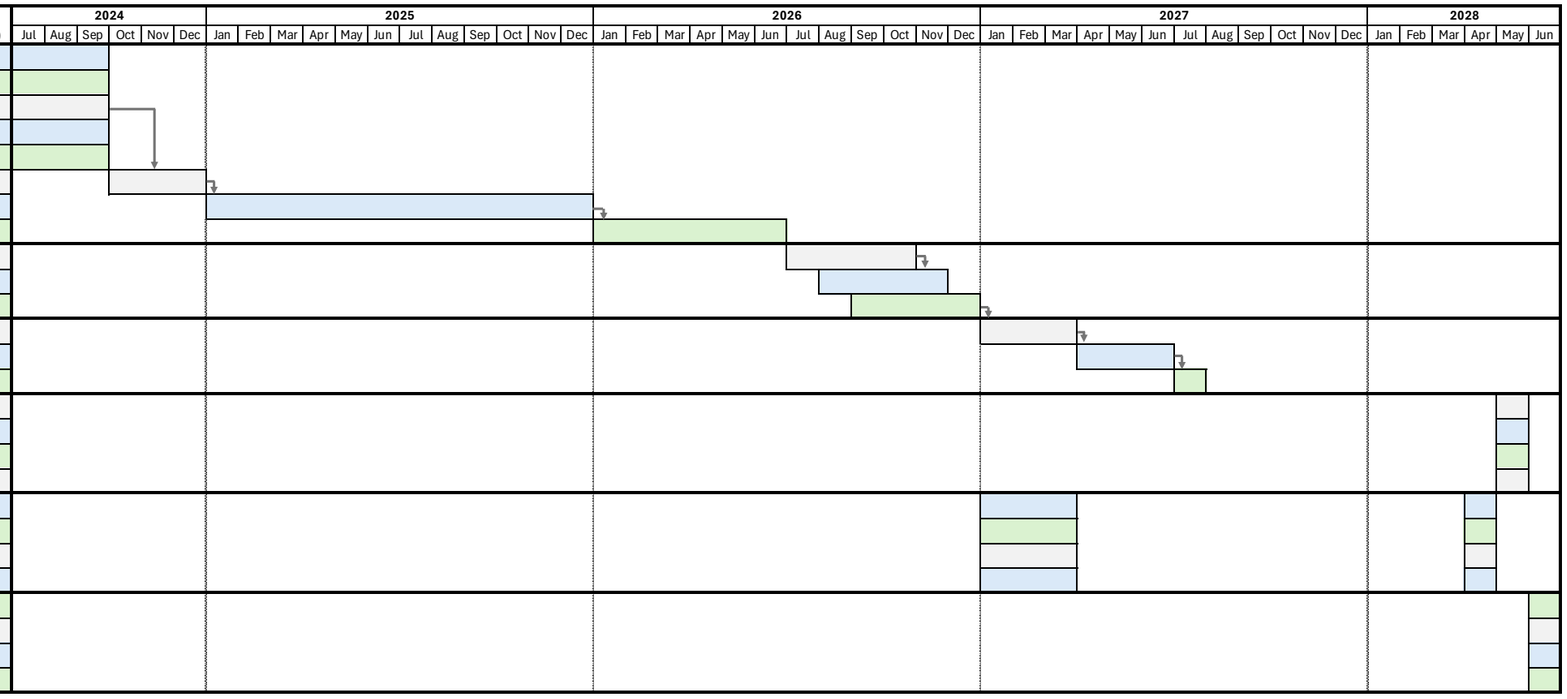

22. Cost Breakdown

In order to estimate costs for the aircraft, three mission phases are identified as having important costs. All costs are taken in dollars, and a conversion rate of 1.1 is taken to convert costs to euros[1]. This would result in a budget of $990,000. Firstly, the design is discussed, and a cost estimate is shown in Section 22.1. Secondly, there is production, which is further split into two major sections: the cost of components and the cost of labour and equipment. These are presented in Section 22.3, together with the costs of aircraft testing and certification. Lastly, the cost of the operations is considered, this includes everything that would involve the aircraft completing the race. This is shown in Section 22.4. All the final values discussed in this chapter will then be discussed in Section 22.5. Possibilities for cost reduction will be discussed in Section 22.6. Finally, potential sponsorships will be discussed in Section 22.7.

22.1. Design

The first phase of the E-Racer project is to design the aircraft. As already mentioned previously, no costs were considered for the design work done by students. However, after this project, it is expected that the design has to be finalised and designed in more detail. It is estimated that this will take a total of 500 days and will be performed by 4 aerospace engineers, working 8 hours per day. See 'Post-DSE Gantt Chart' in Section 21.2. Therefore, this would cost $688,000[2]. The further design of the aircraft was not considered in the budget given by the client, and will therefore not be added to the final cost discussed in Section 22.5.

22.2. Components

In this section the component costs are considered, these are also a large part of the costs. Some of these components have the largest individual cost such as the fuel cell and the propellers. This also contains the most costs, as this is the area with the most detail.

Many of the components presented in Table 22.1 are chosen as COTS, and hence the price can be easily found. However, some other components are more complicated and hence are explained in more detail.

Firstly, the fuselage and wings are considered to be the price of the sheets required to build the airframe based on mass. The aluminium sheets are found to be €14.52 per [kg][3]. Next, the budget given for the landing gear is €20,000. This also includes the hydraulics needed for the landing gear. Pilot equipment includes an oxygen mask[4] and an oxygen tank[5]. For the cockpit equipment, two elements are considered: the primary flight display[6] and the navigation display display[7]. For the fuel cell, the price in the near future is considered as this is a considerable amount of the aircraft costs and a price reduction is considered heavily beneficial. The price of near future fuel cells per [kWh] is used [127]. A usable hydrogen tank was found as a basis for the price[8]. For the pressure regulator[9] and pressure relief valve[10] COTS components were found. A version of stainless steel tubing was found and used to estimate the price[11]and the same was done for vacuum insulated tubing[12].

For the battery, a similar process was followed as for the fuel cell with a price per [kg] was found [128]. Many cables

[1] https://www.jpmorgan.com/insights/global-research/currencies/currency-volatility-dollar-strength [Accessed on 17-06-2024]

[2] https://www.indeed.com/career/aeronautical-engineer/salaries?from=top_sb [Accessed on 17-06-2024]

[3] https://onlinealuminium.nl/en-aw-7075-t651/ [Accessed on 17-06-2024]

[4] https://en.raptorsupplies.nl/pd/allegro/9901 [Accessed on 17-06-2024]

[5] https://www.heelgoedgereedschap.nl/gasfles-zuurstof-1-liter-110-bar-m10x1rh/ [Accessed on 17-06-2024]

[6] https://www.aircraftspruce.com/pages/av/pfd/garmin-g5-cert.php [Accessed on 17-06-2024]

[7] https://www.aircraftspruce.com/catalog/avpages/garminaera600.php?clickkey=124821 [Accessed on 17-06-2024]

[8] https://www.alibaba.com/product-detail/DPL-450-Liquid-Nitrogen-Oxygen-Gas_1600868180249.html [Accessed on 17/06/2024]

[9] https://products.swagelok.com/en/c/back-pressure-regulators/p/KBP1E0A4A5A20000 [Accessed on 17-06-2024]

[10] https://www.diveavenue.com/en/high-pressure-high-pressure-relief-valve/307-stainless-steel-high-pressure-relief-va.html [Accessed on 17-06-2024]

[11] https://www.wildkamp.nl/product/gelaste-buis-rvs-316l-gegloeid-l-6-m-42-x-1-5-mm/15437957 [Accessed on 17-06-2024]

[12] https://www.goldleaflabs.com/3-4-stainless-steel-vacuum-insulated-tubing.html [Accessed on 17-06-2024]

are required and the costs are found based on their length[13][14][15][16]. Five relays are required for the power box[17]. The budget for a high low DC-DC converter is estimated with little information available about the component. The low-voltage system includes most of the sensors, being the heated pitot tube[18], a static port[19] and an ADS-B[20], with a margin left for other sensors. The last part of the battery system are the capacitors, the cost of these was also estimated using COTS components[21].

Two motors and motor controllers[22] are required for the propeller. In order to find the price of the motors, Emrax had to be contacted to get a price. The price of the two propellers is estimated based on an average of a list of propellers[23].

For the air compressor and its controllers, estimations were made as little information was available. Two pumps are required for the cooling system[24]. As the final component, a parachute is used as a safety system[25]. A conversion rate of 1.1 was used to convert dollars to euros.

Table 22.1: Cost breakdown of all aircraft components

Category	Component	Cost (dollar)	Cost (euro)
Airframe	Fuselage + window	10,000	9,091
	Wings	3,000	2,727
	Landing gear	20,000	18,182
Cockpit	Pilot equipment	540	491
	Cockpit equipment	3,600	3,273
Hydrogen system	Fuel cell	253,000	230,000
	Hydrogen tank	2,200	2,000
	Pressure regulator and relief	1,000	909
	Hydrogen tubing	220	2,000
	Vacuum insulated tubing	570	518
Electrical system	Battery	1,380	1,255
	High volt cable 20A and 75 A	50	45
	High volt cable 260A	400	364
	High volt cable 430A	90	82
	PDU / relays	6,390	5,809
	High low DC-DC converter	2,000	1818
	Low-voltage system	4,500	4,091
	Capacitors	1,450	1,318
Motor and propeller	Motor	24,660	22,418
	Motor controller	9,000	8,182
	Propeller	97,000	88,182
Air compressor	Compressor	36,000	32,727
	Converter	10,000	9,091
Cooling system	Pumps	480	436
Safety System	Parachute	1,370	1,245
	Total	**488,900**	**444,455**

[13] https://www.wireandcableyourway.com/12-awg-xlp-use-2-rhh-rhw-2-building-wire [Accessed on 17-06-2024]
[14] https://www.wireandcableyourway.com/6-awg-xlp-use-2-rhh-rhw-2-building-wire [Accessed on 17-06-2024]
[15] https://www.wireandcableyourway.com/4-0-awg-xlp-use-2-rhh-rhw-2-building-wire [Accessed on 17-06-2024]
[16] https://nassaunationalcable.com/products/500-mcm-thhn-thwn-2-stranded-copper-building-wire [Accessed on 17-06-2024]
[17] https://portal.vanegmond.nl/producten/abb-componenten-magneetschakelaar-af-146-30-11-14-250-500vac-dc/1208631 [Accessed on 17-06-2024]
[18] https://www.aircraftspruce.com/catalog/inpages/heatedptubes2.php?clickkey=5714 [Accessed on 17-06-2024]
[19] https://www.aircraftspruce.com/pages/in/staticports/alumstaticports.php [Accessed on 17-06-2024]
[20] https://www.aircraftspruce.com/catalog/avpages/skybeacon11-16531.php [Accessed on 17-06-2024]
[21] https://nl.mouser.com/ProductDetail/EPCOS-TDK/B43720B8688M000?qs=W0yvOO0ixfFeZU0c%252BNhmrA%3D%3D [Accessed on 19-06-2024]
[22] https://www.embention.com/en/product/mc110/ [Accessed on 17-06-2024]
[23] https://hartzellprop.com/wp-content/uploads/2023-Price-List-for-Distribution-.pdf [Accessed on 17-06-2024]
[24] https://races-shop.com/water-pumps/88339-davies-craig-universal-electric-water-pump-150l-min-10a.html [Accessed on 17-06-2024]
[25] https://www.aircraftspruce.com/catalog/pspages/paracushion-midlitecanopy.php [Accessed on 17-06-2024]

22.3. Manufacturing, Testing and Certification

The manufacturing, testing and certification mostly involve working hours. As the aircraft is being built in the United States, the salary in the United States is used for calculations. The number of hours for the construction of the aircraft is taken to be 125 working days, following the Gantt Chart presented in Chapter 21. Six people will be employed, of which 2 aerospace engineers, 3 aircraft mechanics and 1 electrical engineer, for who the hourly rate is $33, $43 and $43, respectively[26][27][28]. Next, for manufacturing equipment, a cost budget of $30,000 is assigned.

For testing, three aerospace engineers taking 63 working days are used. Meanwhile, one high-end pilot, considered a test flight pilot, is paid $70 per hour for seven working days[29]. The price of any equipment needed for testing, including spare parts, is said to cost $50,000. For certification, a designated airworthiness representative and a designated employer representative would be required, so a budget is set aside for this. To certify the aircraft, only one aerospace engineer is employed for 2 days a week for 12 weeks to certify the aircraft and obtain registration. The cost breakdown can be seen in Table 22.2.

Table 22.2: Cost breakdown of manufacturing cost

Category	Component	Cost (dollar, 2024)	Cost (euro, 2024)
Manufacturing	Manufacturing labour	228,000	207,273
	Manufacturing equipment	30,000	27,273
Testing and Certification	Testing labour	69,160	62,869
	Testing equipment	50,000	45,455
	Certification	1,000	909
	Total	**378,160**	**343,779**

At this point of the cost breakdown, the aircraft is now over budget when costs in this section and Section 22.2 are combined. As more costs will further be added, ways to reduce the price of the aircraft will be discussed in Section 22.6.

22.4. Operations

The costs associated with the operation of the aircraft are presented in Table 22.3. These are all costs that have to be taken into account in order to participate in the Pulitzer race, and the cost of maintenance. The first cost is the transportation of the aircraft to Eppley Airfield, $2,580 has been assigned to this[30]. This cost is based on the assumption that the aircraft will be produced relatively close to the airport, such as in Nebraska or a neighbouring state. Additionally, 2 aircraft mechanics are paid to dismantle the aircraft for transportation. The pilot will be paid for four days to fly the aircraft during the race. Next, a ground team consisting of 3 aircraft mechanics, 2 aerospace engineers and 1 electrical technician will be present at the race. They will ensure that any small maintenance on the aircraft will be done and that the optimal strategy for the race is determined depending on the weather. For any tools to do maintenance on the aircraft, $3,000 has been allocated. Because the aircraft has to be reassembled after transport, a hanger should also be rented at the airport, which will cost around $600 for a month[31].

Additionally, the hydrogen has to be bought and transported. The aircraft has to be fuelled at the start of the race, but hydrogen should also be available at other airports in case the aircraft is forced to land due to weather or technical problems. Therefore, a specialised truck for transporting hydrogen will be rented. According to Jimmy Li et al., it would cost 6.85 [$\$/kg$] for delivered liquid hydrogen [129]. Since only 30 [kg] is needed, this would cost around €210. However, since the truck is not fully filled, is driving a large distance, and also has to drive back, $1,000 is estimated for this. Next, a race fee has to be paid, as well as the insurance for the aircraft.

[26] https://www.indeed.com/career/aircraft-mechanic/salaries?from=top_sb [Accessed on 18-06-2024]
[27] https://www.indeed.com/career/aeronautical-engineer/salaries?from=top_sb[Accessed on 18-06-2024]
[28] https://www.indeed.com/career/electrical-engineer/salaries[Accessed on 18-06-2024]
[29] https://www.indeed.com/career/pilot/salaries [Accessed on 18-06-2024]
[30] https://www.heavyhaulers.com/blog/how-do-you-transport-an-airplane/ [Accessed on 18-06-2024]
[31] https://republicjetcenter.com/hangar-space-for-rent-everything-you-need-to-know/[Accessed on 18-06-2024]

Table 22.3: Cost breakdown of the aircraft operation

Component	Cost (dollar)	Cost (euro)
Transport aircraft	2,580	2,345
Pay pilot	2,240	2,036
Pay ground team	14,040	12,764
Hydrogen	180	164
Hydrogen transport	1,000	909
Race fee	1,500	1,364
Insurance	750	682
Hangar	600	545
Maintenance Labour	4,760	4,327
Maintenance	3,000	2,727
Total	**30,650**	**27,863**

22.5. Total Cost

The total cost of the aircraft is presented in Table 22.4. The next biggest cost is the cost of the components of the aircraft, which stays within the budget. However, the manufacturing, testing and certification, and operation are also considered to be part of the budget. Additionally, a margin of 10% is added to account for unexpected costs. Initially, a budget of €500,000 was provided by the NLR, however, this budget was found to be too optimistic. Therefore, the budget was renegotiated with the client and increased to €900,000, which means that the aircraft is within budget.

Table 22.4: Cost breakdown of all aircraft cost

	Cost (dollar)	Cost (euro)
Components	488,900	444,455
Manufacturing	258,000	234,545
Testing and certification	120,160	109,236
Operations	30,650	27,863
Total	**897,709**	**816,099**
Margin (+10%)	**89,770**	**81,610**
Total + Margin	**987,480**	**897,709**

22.6. Cost Reduction

The budget that the NLR provides to build the aircraft is €900,000. Even though this budget has not been surpassed, it is still interesting to look at potential ways to reduce costs. The most expensive parts are the expensive fuel cell and propeller, and the expensive labour costs of manufacturing and testing. These are all vital components and are necessary to win the Pulitzer race. It could be possible to find cheaper components that also satisfy the requirements. Next, it could be possible to reduce manufacturing costs by choosing to manufacture the aircraft in a state where labour is cheaper. For example, in Wyoming, the average hourly rate of an aerospace engineer and aircraft mechanic is only \$37 and \$25[32],[33] compared to \$43 and \$33, reducing the manufacturing costs by \$72,000. The same can be done for the hourly rate paid during testing and operation.

Additionally, it is also possible to lower the testing time needed for the aircraft to, for example, 40 working days. Testing could be done more efficiently and less testing can be done. This might lower the reliability of the design, but it would decrease costs by \$47,360 when also considering the reduction of labour costs.

Finally, the performance of the aircraft can also be sacrificed. By lowering the power provided by the fuel cell, the cost can be lowered significantly. If the fuel cell were to be reduced to the minimum, 119 [kW], this would result in a reduction of €111,000. Implementing this new fuel cell into the aircraft without doing a new iteration, would result in a race time of 395 minutes, at an average velocity of 78 [m/s]. Any reduction of the fuel cell power would result in the speed requirement not being met.

[32] `https://indeed.com/career/aeronautical-engineer/salaries/WY`[Accessed on 19-06-2024]
[33] `https://www.indeed.com/career/aircraft-mechanic/salaries/WY?from=top_sb` [Accessed on 17-06-2024]

For this new fuel cell, the aircraft would need a new iteration, as the hydrogen consumption would be less, allowing for a smaller tank. This would reduce the overall size of the aircraft, as the fuselage can be smaller. Therefore, doing this iteration could increase the performance of the reduced-cost design. However, during the detailed design, it was found that with this lower power, the aircraft could not climb at the same rate. Therefore, this design could not reach the required 145 [m/s], lowering the chances of winning the race.

The reduction of cost is shown in Table 22.5. If all these reductions except for the fuel cell are implemented, the aircraft cost can be lowered by €123,730. This can be increased to €234,730 if the fuel cell power is lowered. However, this can only be reached with a significant decrease in quality and performance. Therefore, it would be good to consider sponsorships with other companies in order to increase the budget or decrease the cost of some components, in case the NLR wants to lower the cost of the aircraft.

Table 22.5: Cost breakdown of all aircraft cost after reduction with original fuel cell

	Cost (dollar)	Cost (euro)
Components	488,900	444,455
Manufacturing	186,000	169,091
Testing and certification	72,800	66,182
Operations	26,280	23,893
Total	**733,980**	**703,621**
Margin (+10%)	**73,390**	**70,362**
Total + Margin	**807,378**	**773,983**

22.7. Potential Sponsorships

Another possible strategy is to establish partnerships with companies and thus increase the budget. In these partnerships, it is envisioned that the company would contribute with either a direct financial budget or with parts/components that can be used in the aircraft.

An attempt has been made to make contact with various companies with the goal of establishing partnerships. A list of companies that have been contacted is given below.

1. GKN Aerospace
2. Rolls-Royce Power Systems
3. Hartzell Propellers
4. The Royal Dutch Airlines, KLM
5. Evolito LTD
6. EMRAX
7. Siemens
8. Red Bull Air Racing
9. Aeronamic

These companies have been carefully chosen, based on their particular expertise, the products/solutions that are produced by the company, the reputation of the company, the needs of the project, and past contributions to aviation projects made by the companies.

Due to the timeframe of the detailed design phase, sponsorship emails could only be sent out from week 6 of the DSE. The reason for this is that only at this stage, the final concept is known and specific requests could be made. At the time of writing, no companies have answered the sent-out sponsorship emails. The reason for this may lie in the email that has been sent out. To increase the chances of receiving a response, more ways to establish contact can be used such as phone calls, in-person visits, or revising the ”sponsorship” email. A possibility exists that companies may respond after the DSE has ended since the attempt to connect is made close to the end of the DSE.

This still serves as a viable strategy to increase the budget or decrease the cost, since other companies can be approached if the current ones do not respond. This can be done many times until a company is found that is willing to contribute. A list of companies that can be approached in addition to the ones that already have been approached is given below.

- Other airliners: Transavia, Emirates, and TUI
- Suppliers: companies from which components are bought for the aircraft
- Government Institutions: Department of Defence

23. Conclusion

The goal of this report is to elaborate on the detailed design procedure of the E-Racer. The E-Racer is a box-wing aircraft that utilises an electric propulsion unit which is driven primarily by a hydrogen-based power train. Some concluding remarks will be given in Section 23.1, and afterward, future recommendations are given in Section 23.2.

23.1. Concluding Remarks

The detailed design of the E-Racer consists of different aspects, each aspect concerns a crucial subsystem in the aircraft. These subsystems have been analysed and sized. The different procedures are summarised below.

1. Aerodynamic Analysis and wing sizing
2. Stability and control analysis
3. Propulsion & power analysis and sizing
4. Stability & control analysis and sizing
5. Structural analysis and sizing
6. Flight performance analysis

First, the aerodynamic analysis was performed. Using a VLM analysis software called Athena Vortex Lattice, different kinds of wing planforms have been analysed together with a variety of different airfoils. The result of this analysis is a final wing planform that minimises drag and provides the required lift capabilities. Stability has also been considered during this process. Using stability parameters outputted from the same VLM software, stability was estimated. The final wing planform is therefore both statically & dynamically stable.

Next, the propulsion & power analysis was concerned with sizing the power train including the propulsion unit. The propulsion unit was determined to consist of 2 propellers with 5 blades. The unit is powered by a hydrogen-based fuel cell that also provides power for the smaller electronics in the aircraft.

The flight performance was estimated using an in-house developed flight path simulation model. This model provides the performance over a flight profile that follows an optimised flight strategy. The strategy has been determined by an energy model and the flight path simulation together. The output of the combined effort of the aerodynamic, power & propulsion, and flight performance analyses is shown in Table 23.1.

Table 23.1: Output parameters of flight path model

Output parameter	Value	Unit	Description
Total possible range	221	km	This range represents the total potential distance the aircraft can fly with the implemented fly strategy
Average Velocity	149.38	m/s	The average velocity that the aircraft completes the race.
Race time	206.41	$minutes$	The race time represents the amount of time the aircraft takes to complete 1850 [km]
Cruise Altitude	12.5	km	The altitude the aircraft cruises at
Take-Off distance (dry)	1,544	m	The required length of the take-off runway in dry conditions
Take-off distance (wet)	1,689	m	The required length of the take-off runway in wet conditions
Landing distance (dry)	763	m	The required length of the landing runway in dry conditions
Landing distance (wet)	1,364	m	The required length of the landing runway in wet conditions
Cruise velocity	163.11	m/s	The velocity during cruise

The structure of the aircraft also needed to be determined which was done in the structural analysis. A comprehensive weight analysis for each component was performed in order to determine the total mass of the aircraft. This led to the final aircraft design having a mass of 1,162.51 kg.

After all the different subsystems were sized and analysed, follow-up procedures were determined for the manufacturing, assembly, testing and certification, operations, maintenance, and end-of-life procedures, which included the time it would take, as well as the number of people required to perform each of these procedures.

For all the subsystems and procedures, a cost analysis has been performed to ensure that the E-Racer remains within budget. In this analysis, the cost of each component was found, as well as costs for all manufacturing, testing,

and all other labour that would be required. The components alone, add up to €444,455. All costs combined for design, components, manufacturing, testing, certification, and operations lead to a total cost of €897,709, including a margin of %10 that is added as a contingency. The budget provided by the client, the NLR, is €900,000, which means that the project is within the budget. Nevertheless, various methods to reduce costs were explored, which could reduce the total cost to €773,983, or €663,983 when reducing the fuel cell power to the minimum. Sponsorships with other companies to obtain parts or a higher budget can also be considered.

23.2. Recommendations

Throughout the report there are some knowledge gaps or areas that should be further investigated, some of these will be discussed below.

Firstly, the possible gains for the structural efficiency of Prandtl planes will be discussed. As mentioned in Chapter 11, it should be possible to save structural weight in the wing structure when using a Prandtl plane. However, knowledge about this is very limited, which makes it very difficult to estimate how big these effects will be. This should be further investigated to allow for more accurate weight estimation and structural load paths.

Secondly, the use of wing heat exchangers for small aircraft is still poorly analysed, this entails two separate subjects: aerodynamic effects and heat exchanger sizing. The aerodynamic effects of heating the flow should be more accurately analysed in experiments. The same is true for the heat exchanger sizing; it is stated in Chapter 10 that the current calculation is optimistic. However, there was very limited information to be found, so this might be best analysed with experiments.

Another point from Chapter 10 is the possibility of windmilling the propellers to generate electricity. How effectively that is and how that should be incorporated into the power management system is still poorly understood. This is purely a knowledge issue since current electric motors and motor controllers are capable of generating electricity as well. However, how this would affect the structural design of the propeller, the aerodynamic performance of the wings or the power management system is still unknown.

Finally, the aerodynamic interaction between the 2 wings should be further investigated. There has already been some research done in this area, but the results seem to be inconclusive since different papers contradict each other, so a more comprehensible approach is necessary. This should investigate the optimum wing planform configuration and downwash effects between the two wings with the propeller in between.

Bibliography

[1] Ritchie, H., "What share of global CO2 emissions come from aviation?" *Our World in Data*, 2024.

[2] Adu-Gyamfi, B. A., and Good, C., "Electric aviation: A review of concepts and enabling technologies," *Transportation Engineering*, Vol. 9, 2022, pp. 100–134. doi:10.1016/j.treng.2022.100134.

[3] Rankin, R. H., "The Pulitzer Races, 1920-1925," *Transportation Engineering*, Vol. 85/9/679, 1959.

[4] in 't Veld, A., *Project Guide Design Synthesis Exercise Pulitzer E-Racer*, Delft University of Technology, 2024.

[5] Wolleswinkel, R. E., de Vries, R., Hoogreef, M., and Vos, R., "A New Perspective on Battery-Electric Aviation, Part I: Reassessment of Achievable Range," *AIAA SCITECH 2024 Forum*, 2024, p. 1489.

[6] Corporation, P., *The Human Factor in the Design of Stick and Rudder Controls for Aircraft*, Psychological Corporation, 1948.

[7] Paul Jemitola, P. O., "Review of Structural Issues in the Design of a Box Wing Aircraft," *Journal of Aerospace Engineering and Mechanics*, 2019.

[8] Alberto, V., "Structural design of a ULM PrandtlPlane wing system," , 2011.

[9] Schiktanz, D., and Scholz, D., "Box wing fundamentals–An aircraft design perspective," *DGLR Dtsch. Luft-und*, 2011, pp. 601–615.

[10] Carnini, M., Méheut, M., Kanellopoulos, S., Cipolla, V., and Salem, K. A., "Aerodynamic analysis and optimization of a boxwing architecture for commercial airplanes," *AIAA SCITECH*, 2020.

[11] Zohlandt, C., "Conceptual Design of High Subsonic Prandtl Planes," , 2016.

[12] Gur, O., "Maximum Propeller Efficiency Estimation," *Journal of Aircraft*, Vol. 51, No. 6, 2014, pp. 2035–2038. doi:10.2514/1.C032557.

[13] Thomas Kadyk, C. W., "Analysis and Design of Fuel Cell Systems for Aviation," *Energies*, 2018.

[14] P.O. Jemitola, J. F., G. Monterzino, "Wing mass estimation algorithm for medium range box wing aircraft," *The Aeronautical Journal*, 2013.

[15] Raymer, D.P., *Aircraft Design: A Conceptual Approach*, 2nd ed., American Institute of Aeronautics and Astronautics, Inc., Washington, DC, 1992.

[16] Vittorio, C., and Stefano, G., "Utilizzo di codici a pannelli nel progetto preliminare di velivoli PrandtlPlane ultraleggeri; applicazione a nuove configurazioni," , 2006.

[17] Cipolla, V., Frediani, A., Oliviero, F., Rossi, R., Rizzo, E., and Pinucci, M., "Ultralight amphibious PrandtlPlane: the final design," Tech. rep., University of Pisa, 2015. doi:10.1007/BF03404701.

[18] Frediani, A., Cipolla, V., and Oliviero, F., "IDINTOS: the first prototype of an amphibious PrandtlPlane-shaped aircraft," Tech. rep., University of Pisa, 2011.

[19] Caja, R., and Scholz, D., "Box Wing Flight Dynamics in the Stage of Conceptual Aircraft Design," Tech. rep., Hamburg University of Applied Sciences, 2012.

[20] Jemitola, P., and Okonkwo, P., "An Analysis of Aerodynamic Design Issues of Box-Wing Aircraft," *Journal of Aviation Technology and Engineering*, Vol. 12, 2023. doi:10.7771/2159-6670.1253.

[21] Paul Olugbeji, J., Ekene Gabriel, O., and Abbe, G., "Wing area optimization for box wing aircraft," *International Journal of Engineering & Technology*, Vol. 7, No. 4, 2019, p. 5679–5682. doi:10.14419/ijet.v7i4.17147.

[22] Torenbeek, E., *Synthesis of Subsonic Airplane Design*, 9th ed., Delft University Press & Kluwer Academic Publishers, Delft & Dordrecht, The Netherlands, 1982.

[23] Pereira, R. L., "Validation of software for the calculation of aerodynamic coefficients aerodynamic coefficients with a focus on the software package th a focus on the software package with a focus on the software package Tornado," , 2010.

[24] Mulder, J. A., van Staveren, W. H. J. J., van der Vaart, J. C., de Weert, E., de Vissed, C. C., in't Veld, A. C., and Mooij, E., "Flight Dynamics Lecture Notes," , 2013.

[25] Roth, B., "Control Power Design Requirements for Aircraft Flying Qualities," , 2009.

[26] Oliviero, F., *Aircraft aerodynamic analysis: Mobile surfaces of the wing*, Delft University of Technology, 2021.

[27] Al-Shamma1, O., Ali, R., and Hasan, H. S., "An Instructive Algorithm for Aircraft Elevator Sizing to be Used in Preliminary Aircraft Design Software," *Journal of Applied Engineering Science*, Vol. 15, No. 4, 2017, pp. 489 – 494. doi:10.5937/jaes15-14829.

[28] Al-Shamma1, O., Ali, R., and Hasan, H. S., "An Educational Rudder Sizing Algorithm for Utilization in Aircraft

Design Software," *International Journal of Applied Engineering Research*, Vol. 13, No. 10, 2018, pp. 7889 – 7894.

[29] van Es, G., "Crosswind Certification - How does it affect you?" , 2006.

[30] Sadraey, M., *Aircraft Design: A Systems Engineering Approach*, Wiley Publications, 2012.

[31] Scholz, D., *Aircraft Design*, Hamburg University of Applied Science, 2005.

[32] Chaitanyaa, K. K., Patil, C. R., Pal, B., and Dandotiya, D., "Aerodynamic Analysis and Optimization of Airfoils Using Vortex Lattice Method," *IOP Conference Series: Materials Science and Engineering*, Vol. 1013, No. 1, 2021. doi:10.1088/1757-899X/1013/1/012023.

[33] Sheridan, C. N., Pham, D. D., and Whiteside, S., "Evaluation of VSPAERO Analysis Capabilities for Conceptual Design of Aircraft with Propeller-Blown Wings," *AIAA Aviation 2021 Forum*, 2021. doi:10.2514/6.2021-2510.

[34] Conlan-Smith, C., Ramos-García, N., Sigmund, O., and Andreasen, C., "Aerodynamic Shape Optimization of Aircraft Wings Using Panel Methods," *AIAA Journal*, Vol. 58, 2020. doi:10.2514/1.J058979.

[35] Epps, B., "OpenProp v2.4 Theory Document," 2010.

[36] McDonald, R. A., and Gloudemans, J. R., "Open Vehicle Sketch Pad: An Open Source Parametric Geometry and Analysis Tool for Conceptual Aircraft Design," *AIAA SciTech*, 2022. doi:10.2514/6.2022-0004.

[37] Anderson, J., *Aircraft Performance and Design*, McGraw-Hill Education, 1999.

[38] Dubs, F., *Aerodynamik der reinen Unterschallströmung*, Springer Basel AG, 1979.

[39] Johanning, A., and Scholz, D., "Propeller Efficiency Calculation in Conceptual Aircraft Design," *Hamburg University of Applied Sciences*, 2013.

[40] European Aviation Safety Agency, "Type-Certificate Data Sheet EASA P.087," Vol. 3, 2018.

[41] Piaggio Aero Industries, *Avanti P-180 II Specification and Description*, 5th ed., 2005.

[42] Air Ministry, *Pilot's Notes for Spitfire XIV & XIX*, 2nd ed., Air Publication, 1946.

[43] Air Ministry, *Pilot's Notes for Mustang III*, 1st ed., Air Publication, 1944.

[44] Federal Aviation Administration, *Pilot's Handbook of Aeronautical Knowledge*, 2023.

[45] Veldhuis, L., "Review of propeller-wing aerodynamic interference," *ICAS*, 2004.

[46] EMRAX Innovative E-Motors, *Technical Data and Manual for EMRAX Motors / Generators*, 2018.

[47] European Aviation Safety Agency, "Type-Certificate Data Sheet EASANo. IM.P.137," Vol. 3, 2023.

[48] Yokota, K., Fujimoto, H., and Hori, Y., "Pitch Angle Control by Regenerative Air Brake for Electric Aircraft," *2020 AIAA/IEEE Electric Aircraft Technologies Symposium (EATS)*, Vol. 11, No. 2, 2022, pp. 308–316. doi:10.1541/ieejjia.21005706.

[49] Yokota, K., Fujimoto, H., and Hori, Y., "Basic Study on Regenerative Air Brake Using Observer-based Thrust Control for Electric Airplane," *2020 IEEE 16th International Workshop on Advanced Motion Control (AMC)*, 2020, pp. 34–39. doi:10.1109/AMC44022.2020.9244329.

[50] Yadlapalli, R. T., Alla, R. R., Kandipati, R., and Kotapati, A., "Super capacitors for energy storage: Progress, applications and challenges," *Journal of Energy Storage*, Vol. 49, 2022, p. 104194. doi:10.1016/j.est.2022.104194.

[51] Marin-Garcia, G., Vazquez-Guzman, G., Sosa, J., Lopez, A. R., Martinez-Rodriguez, P., and Langarica, D., "Battery Types and Electrical Models: A Review," *2020 IEEE International Autumn Meeting on Power, Electronics and Computing (ROPEC)*, Vol. 4, 2020, pp. 1–6. doi:10.1109/ROPEC50909.2020.9258711.

[52] Chen, A., and Sen, P. K., "Advancement in battery technology: A state-of-the-art review," *2016 IEEE Industry Applications Society Annual Meeting*, 2016, pp. 1–10. doi:10.1109/IAS.2016.7731812.

[53] Li, F., Wei, Z., Manthiram, A., Feng, Y., Ma, J., and Mai, L., "Sodium-based batteries: from critical materials to battery systems," *Journal of materials chemistry A*, Vol. 7, No. 16, 2019, pp. 9406–9431.

[54] Faegh, E., Ng, B., Hayman, D., and Mustain, W. E., "Practical assessment of the performance of aluminium battery technologies," *Nature Energy*, Vol. 6, No. 1, 2021, pp. 21–29.

[55] Capsoni, D., Bini, M., Ferrari, S., Quartarone, E., and Mustarelli, P., "Recent advances in the development of Li–air batteries," *Journal of Power Sources*, Vol. 220, 2012, pp. 253–263. doi:10.1016/j.jpowsour.2012.07.123.

[56] Šimić, Z., Topić, D., Knežević, G., and Pelin, D., "Battery energy storage technologies overview," *International journal of electrical and computer engineering systems*, Vol. 12, No. 1, 2021, pp. 53–65.

[57] Guo, Y., Wu, S., He, Y.-B., Kang, F., Chen, L., Li, H., and Yang, Q.-H., "Solid-state lithium batteries: Safety and prospects," *eScience*, Vol. 2, No. 2, 2022, pp. 138–163. doi:10.1016/j.esci.2022.02.008.

[58] Shen, X., Liu, H., Cheng, X.-B., Yan, C., and Huang, J.-Q., "Beyond lithium ion batteries: Higher energy density battery systems based on lithium metal anodes," *Energy Storage Materials*, Vol. 12, 2018, pp. 161–175. doi:10.1016/j.ensm.2017.12.002.

[59] Lampic, G., Gotovac, G., Geaney, H., and O'Dwyer, C., "Comparing the suitability of Lithium ion, Lithium Sulfur and Lithium air batteries for current and future vehicular applications," *arXiv preprint arXiv:1606.06347*, 2016.

[60] Zhou, G., Chen, H., and Cui, Y., "Formulating energy density for designing practical lithium–sulfur batteries," *Nature Energy*, Vol. 7, No. 4, 2022, pp. 312–319.

[61] Karpinski, A., Makovetski, B., Russell, S., Serenyi, J., and Williams, D., "Silver–zinc: status of technology and applications," *Journal of Power Sources*, Vol. 80, No. 1, 1999, pp. 53–60. doi:10.1016/S0378-7753(99)00164-0.

[62] Schismenos, S., Chalaris, M., and Stevens, G., "Battery hazards and safety: A scoping review for lead acid and silver-zinc batteries," *Safety Science*, Vol. 140, 2021, p. 105290. doi:10.1016/j.ssci.2021.105290.

[63] Zhao, E., Walker, P. D., Surawski, N. C., and Bennett, N. S., "Assessing the life cycle cumulative energy demand and greenhouse gas emissions of lithium-ion batteries," *Journal of Energy Storage*, Vol. 43, 2021, p. 103193. doi:10.1016/j.est.2021.103193.

[64] Vandepaer, L., Cloutier, J., and Amor, B., "Environmental impacts of Lithium Metal Polymer and Lithium-ion stationary batteries," *Renewable and Sustainable Energy Reviews*, Vol. 78, 2017, pp. 46–60. doi:10.1016/j.rser.2017.04.057.

[65] Benveniste, G., Sánchez, A., Rallo, H., Corchero, C., and Amante, B., "Comparative life cycle assessment of Li-Sulphur and Li-ion batteries for electric vehicles," *Resources, Conservation & Recycling Advances*, Vol. 15, 2022, p. 200086. doi:10.1016/j.rcradv.2022.200086.

[66] Shateri, N., Auger, D. J., Fotouhi, A., and Brighton, J., "An Experimental Study on Prototype Lithium–Sulfur Cells for Aging Analysis and State-of-Health Estimation," *IEEE Transactions on Transportation Electrification*, Vol. 7, No. 3, 2021, pp. 1324–1338. doi:10.1109/TTE.2021.3059738.

[67] Xu, B., Lee, J., Kwon, D., Kong, L., and Pecht, M., "Mitigation strategies for Li-ion battery thermal runaway: A review," *Renewable and Sustainable Energy Reviews*, Vol. 150, 2021, p. 111437. doi:10.1016/j.rser.2021.111437.

[68] Bingham, T., Moore, M., De Caux, T., and Pacino, M., "Design, build, test and flight of the world's fastest electric aircraft," *IET Electrical Systems in Transportation*, Vol. 12, No. 4, 2022, pp. 380–402. doi:10.1049/els2.12059.

[69] Neveling, S., Keimer, J., Nuño, M., Mayntz, J., Dahmann, P., and Schröder, K., "Analysis of Fire-Protected Load-Carrying Aircraft Structures for Electric Powertrains," 2021.

[70] European Aviation Safety Agency, *Easy Access Rules for Large Aeroplanes (CS25)*, 27th ed., 2023.

[71] Weydahl, H., "Dynamic behaviour of fuel cells," 2006.

[72] OpenStax, *University Physics Volume 2*, XanEdu Publishing Inc, 2016.

[73] Bhatti, W., Wu, W., Doyle, F., Llambrich, J., Webber, H., and Town, N., "Fuel Cells Roadmap Report," Tech. rep., Aerospace Technology Institute, 2022.

[74] de Boer, P., de Wit, A., and van Benthem, R., "Development of a Liquid Hydrogen-Based Fuel Cell System for the HYDRA-2 Drone," Tech. Rep. NLR-TP-2022-004, Royal NLR - Netherlands Aerospace Centre, 2022.

[75] Mills, A. F., *Basic Heat and Mass Transfer*, 2nd ed., Pearson, United Kingdom, 2013.

[76] Kellerman, H., Habermann, A. L., and Hornung, M., "Assessment of Aircraft Surface Heat Exchanger Potential," *Aerospace*, 2019. doi:10.3390/aerospace7010001.

[77] Habermann, A. L., Khot, A., Lampl, D. E., and Perren, C., "Aerodynamic Effects of a Wing Surface Heat Exchanger," *Aerospace*, 2023. doi:10.3390/aerospace10050407.

[78] Yan, L., Karnik, A., Pence, B., Waez, M. T. B., and Ozay, N., "Fuel Cell Thermal Management: Modeling, Specifications and Corrected-by-Construction Control Synthesis," *Amarican Control Conference*, 2017.

[79] Bahrami, M., *ENSC 388 Engineering Thermodynamics and Heat Transfer*, 2011. Forced Convection Heat Transfer.

[80] Incopera, F. P., and DeWitt, D. P., *Fundementals of heat transfer*, Wiley, 1981.

[81] Schlichting, H., *Boundary-Layer Theory*, 7th ed., McGraw Hill, 1905.

[82] National Fire Protection Association, *National Electrical Code*, 1st ed., International Electrical Code Series, Delmar Cengage Learning, 2017.

[83] Allan, G. M., and Kenny, D., "High-altitude decompression illness: case report and discussion," *CMAJ*, Vol. 169, No. 8, 2003, pp. 803–807.

[84] Annaratone, D., *Pressure vessel design*, Springer, 2007.

[85] MANIDEEP, B., and GUPTHA, M. S., "Factor of Safety and Stress Analysis of Fuselage Bulkhead using Composite Materials," 2015.

[86] Niu, C., and Niu, C., *Airframe Structural Design: Practical Design Information and Data on Aircraft Structures*,

Conmilit Press, 1988.

[87] Eremin, A., Burkov, M., Luybutin, P., and Kononova, A., "Mechanical behavior of carbon and aramid fiber reinforced composites with various layups under tension," *Procedia Structural Integrity*, Vol. 50, 2023, pp. 65–72. doi:10.1016/j.prostr.2023.10.023.

[88] Farag, M., and El-Magd, E., "An integrated approach to product design, materials selection and cost estimation," *Materials & Design*, Vol. 13, No. 6, 1992, pp. 323–327. doi:10.1016/0261-3069(92)90001-X.

[89] Bachmann, J., Hidalgo, C., and Bricout, S., "Environmental analysis of innovative sustainable composites with potential use in aviation sector—A life cycle assessment review," *Science China Technological Sciences*, Vol. 60, 2017, pp. 1301–1317.

[90] Das, S., "Life cycle assessment of carbon fiber-reinforced polymer composites," *The International Journal of Life Cycle Assessment*, Vol. 16, 2011, pp. 268–282.

[91] Iqbal, M. W., and Shaker, K., "13 - Life-cycle assessment of ballistic vest," *Composite Solutions for Ballistics*, edited by Y. Nawab, S. Sapuan, and K. Shaker, Woodhead Publishing Series in Composites Science and Engineering, Woodhead Publishing, 2021, pp. 341–358. doi:10.1016/B978-0-12-821984-3.00002-4.

[92] Priarone, P., Ingarao, G., Settineri, L., and Lorenzo, R., "On the Impact of Recycling Strategies on Energy Demand and CO2 Emissions When Manufacturing Al-based Components," *Procedia CIRP*, Vol. 48, 2016, pp. 194–199. doi:10.1016/j.procir.2016.03.044.

[93] Hallberg, L., and Sperle, J.-O., "Assessing the environmental advantages of high strength steel," *Towards Life Cycle Sustainability Management (LCM 2011)*, 2011, pp. 28–31.

[94] Rajemi, M. F., Mativenga, P., and Jaffery, S., "Energy and carbon footprint analysis for machiningtitanium Ti-6Al-4V alloy," *Journal of Machine Engineering*, Vol. 9, No. 1, 2009, pp. 103–112.

[95] Son, H.-G., Kumar, D., Park, Y.-B., Kweon, J.-H., and Choi, J.-H., "Structural design and analysis of composite aircraft fuselage used to develop AFP technology," *Hakone Pax Yoshino. Japan*, 2013.

[96] Krajangsawasdi, N., and Bunyawanichakul, P., "Structural Wing Sizing in Preliminary Aircraft Design," 2016.

[97] Rajendran, C., Srinivasan, K., Balasubramanian, V., Balaji, H., and Selvaraj, P., "Evaluation of load-carrying capabilities of friction stir welded, TIG welded and riveted joints of AA2014-T6 aluminium alloy," *Aircraft Engineering and Aerospace Technology*, Vol. 91, No. 9, 2019, pp. 1238–1244.

[98] Subramaniam, A., V, B., and Bhowmik, S., "Novel ultra high impact strength light weight transparent polycarbonate laminated composite for aviation and defence," *Journal of Polymer Research*, Vol. 30, No. 11, 2023, p. 413.

[99] Delprete, C., Dagna, A., and Brusa, E., "Model-Based Design of Aircraft Landing Gear System," *Applied Sciences*, Vol. 13, No. 20, 2023. doi:10.3390/app132011465.

[100] Ayaz, M., and Shah, S., "Comprehensive design of an oleo-pneumatic nose landing gear strut," *Proceedings of the Institution of Mechanical Engineers Part G Journal of Aerospace Engineering*, Vol. 235, 2020. doi: 10.1177/0954410020979378.

[101] Knowles, J. A., Krauskopf, B., and Coetzee, E. B., "Unlocking a nose landing gear in different flight conditions: folds, cusps and a swallowtail," *Nonlinear Dynamics*, Vol. 106, 2021, pp. 2943–2961.

[102] Megson, T. H. G., *Aircraft Structures for Engineering Students*, 4th ed., Elsevier, Linacre House, Jordan Hill, Oxford OX2 8DP, UK, 2007.

[103] Fisch, F., "Development of a Framework for the Solution of High-Fidelity Trajectory Optimization Problems and Bilevel Optimal Control Problems," Ph.D. thesis, Technical University of München, 2011.

[104] de Wringer, S. P., "Mission Performance Assessment of a Box-Wing Aircraft," Master's thesis, Delft University of Technology, 2020.

[105] Mooij, E., and Noomen, R., "Introduction, heritage, and trends," , 2023. Introduction to Aerospace 2, slide set 1.

[106] Sun, H., Zhang, G., Guo, L., and Liu, H., "A Study of dynamic characteristics of PEM fuel cells by measuring local currents," *International Journal of Hydrogen Energy*, Vol. 34, 2009, pp. 5529–5536. doi: 10.1016/J.IJHYDENE.2009.04.066.

[107] Ruijgrok, G., *Element of Airplane Performance*, Delft University Press, Delft, The Netherlands, 1996.

[108] Vinh, N. X., *Optimal trajectories in atmospheric flight*, Elsevier Scientific, 1981.

[109] Varriale, D. C., "Airfield Performance," , 2022. Flight & Orbital Mechanics, slide set 4.

[110] NASA, *Merra-2: File Specification*, National Aeronautics and Space Administration, 2016.

[111] Adler, E. J., and Martins, J. R., "Hydrogen-powered aircraft: Fundamental concepts, key technologies, and environmental impacts," *Progress in Aerospace Sciences*, Vol. 141, 2023, p. 100922. doi:10.1016/j.paerosci.

2023.100922, special Issue on Green Aviation.

[112] Mangold, J., "Economical assessment of hydrogen short-range aircraft with the focus on the turnaround procedure," Ph.D. thesis, University of Stuttgart, 2021.

[113] K. Brun, T. C. A., *Machinery and Energy Systems for the Hydrogen Economy*, 1st ed., Vol. 1, 2022.

[114] Naru, R., and German, B., "Maintenance considerations for electric aircraft and feedback from aircraft maintenance technicians," *2018 Aviation Technology, Integration, and Operations Conference*, 2018, p. 3053.

[115] Meissner, R., Sieb, P., Wollenhaupt, E., Haberkorn, S., Wicke, K., and Wende, G., "Towards climate-neutral aviation: Assessment of maintenance requirements for airborne hydrogen storage and distribution systems," *International Journal of Hydrogen Energy*, Vol. 48, No. 75, 2023, pp. 29367–29390. doi:10.1016/j.ijhydene.2023.04.058.

[116] Avila, D., Sherry, L., and Thompson, T., "Reducing global warming by airline contrail avoidance: A case study of annual benefits for the contiguous United States," *Transportation Research Interdisciplinary Perspectives*, Vol. 2, 2019, p. 100033. doi:10.1016/j.trip.2019.100033.

[117] Brookes-Gayton, E., "Contrails and Climate Change: Understanding Formation, Impact, and Mitigation Strategies for Aviation-Induced Clouds," 2022.

[118] Suleman, F., Dincer, I., and Agelin-Chaab, M., "Comparative impact assessment study of various hydrogen production methods in terms of emissions," *International Journal of Hydrogen Energy*, Vol. 41, No. 19, 2016, pp. 8364–8375. doi:10.1016/j.ijhydene.2015.12.225.

[119] Vieira, D. R., and Bravo, A., "Life cycle carbon emissions assessment using an eco-demonstrator aircraft: the case of an ecological wing design," *Journal of Cleaner Production*, Vol. 124, 2016, pp. 246–257. doi:10.1016/j.jclepro.2016.02.089.

[120] Velázquez-Martínez, O., Valio, J., Santasalo-Aarnio, A., Reuter, M., and Serna-Guerrero, R., "A Critical Review of Lithium-Ion Battery Recycling Processes from a Circular Economy Perspective," *Batteries*, Vol. 5, No. 4, 2019.

[121] Valente, A., Iribarren, D., and Dufour, J., "End of life of fuel cells and hydrogen products: From technologies to strategies," *International Journal of Hydrogen Energy*, Vol. 44, No. 38, 2019, pp. 20965–20977. doi:10.1016/j.ijhydene.2019.01.110, special Issue on HYPOTHESIS XIII.

[122] Ahmad, T., Sagir, M., Arif, M., and Tahir, M., "Recycling of Lithium Sulfur Batteries," *Lithium-Sulfur Batteries: Key Parameters, Recent Advances, Challenges and Applications*, Springer, 2024, pp. 203–216.

[123] TNO, "Particulate matter: standard achieved, problem unsolved," 2022.

[124] Mac Kinnon, M., Shaffer, B., Carreras-Sospedra, M., Dabdub, D., Samuelsen, G., and Brouwer, J., "Air quality impacts of fuel cell electric hydrogen vehicles with high levels of renewable power generation," *International Journal of Hydrogen Energy*, Vol. 41, No. 38, 2016, pp. 16592–16603. doi:10.1016/j.ijhydene.2016.07.054.

[125] Ingaldi, M., and Klimecka-Tatar, D., "People's Attitude to Energy from Hydrogen—From the Point of View of Modern Energy Technologies and Social Responsibility," *Energies*, Vol. 13, No. 24, 2020. doi:10.3390/en13246495.

[126] Hallez, R., Colanaeli, C., Cuenca, J., and De Ryck, L., "Impact of Electric Propulsion on Aircraft Noise - All-Electric Light Aircrafts Case Study," 2018, pp. 1–17.

[127] Bhatti, W., Wu, W., Doyle, F., Llambrich, J., Webber, D. H., and Town, N., "Fuel Cells Road Map Report," Tech. rep., Aerospace Technology Institute, 2022.

[128] Zhong, M., Guan, J., Sun, J., Shu, X., Ding, H., Chen, L., Zhou, N., and Xiao, Z., "A Cost- and Energy Density-Competitive Lithium-Sulfur Battery," *Energy Storage Materials*, Vol. 41, 2021, pp. 588–598. doi:10.1016/j.ensm.2021.06.037.

[129] Li, J., Allen, J. D., Stager, J. A., and Ku, A. Y., "Paths to low-cost hydrogen energy at a scale for transportation applications in the USA and China via liquid-hydrogen distribution networks," *Clean Energy*, Vol. 4, 2020. doi:10.1093/ce/zkz033.